Aromatic hydroxylation at a non-heme iron center: insights into the nature of the metal-based oxidant

A dissertation

submitted by

Olga V. Makhlynets

In partial fulfillment of the requirements

for the degree of

Doctor of Philosophy

in

Chemistry

May, 2011

Adviser:

Prof. Elena Rybak-Akimova

Abstract

Aromatic hydroxylation at non-heme iron model complexes. Development of regio- and stereoselective catalytic oxidation of organic substrates is of fundamental importance for organic synthesis. Biomimetic oxidations are particularly attractive, because they rely on cheap, non-toxic reactants (O_2 or H_2O_2 as oxidants, and Fe, Cu, or Mn complexes as catalysts). We have shown that regioselective hydroxylation of aromatic acids with hydrogen peroxide proceeds readily in the presence of iron(II) complexes with tetradentate aminopyridine ligands $[Fe^{II}BPMEN(CH_3CN)_2](ClO_4)_2$ (**1**) and $[Fe^{II}TPA(CH_3CN)_2](OTf)_2$ (**2**). The hydroxylation of the aromatic ring occurs exclusively in the vicinity of the anchoring carboxylate functional group: *ortho*-hydroxylation affords salicylates, while *ipso*-hydroxylation with concomitant decarboxylation yields phenolates. Through a series of studies **we have identified two distinct hydroxylation pathways** based on the electronic properties and the position of substituents in the substrates. Electron-withdrawing substituents on the aromatic ring of the carboxylic acids disfavor hydroxylation, indicating an electrophilic nature for the active oxidant. These two pathways are not mutually exclusive and likely proceed via a common intermediate. Complexes **1** and **2** exhibit very similar reactivity patterns, suggesting the generality of hydroxylation mechanism.

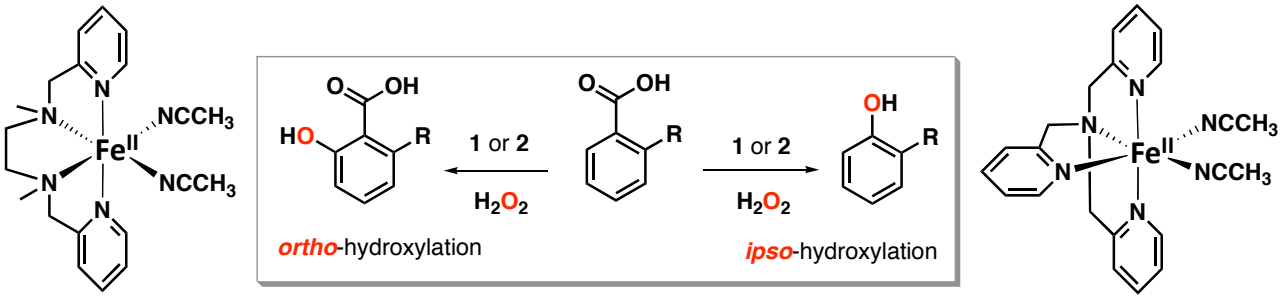

Insights into the nature of the active species. Synthetic non-heme Fe^{II}(BPMEN) has been shown to be an excellent catalyst for epoxidation and aromatic hydroxylation using H_2O_2. However, no intermediates were previously observed in these reactions and the exact mechanism remained unclear. **We have identified and experimentally characterized for the first time iron(III)-hydroperoxo (1a) and Fe(IV)-oxo (1c) intermediates formed by Fe^{II}(BPMEN) and H_2O_2. We have shown using detailed kinetic studies that iron(III)-hydroperoxo produces the reactive species in the rate-limiting step of the reaction.** The reactive species formation is facilitated by heterolytic cleavage of the O-O bond in the iron-hydroperoxide. Independently generated iron(IV)-oxo species proved to be inactive toward aromatic substrates. These results provide a detailed mechanistic picture of the Fe^{II}(BPMEN) catalyzed oxidation reaction based on direct characterization of the intermediates and the reaction products.

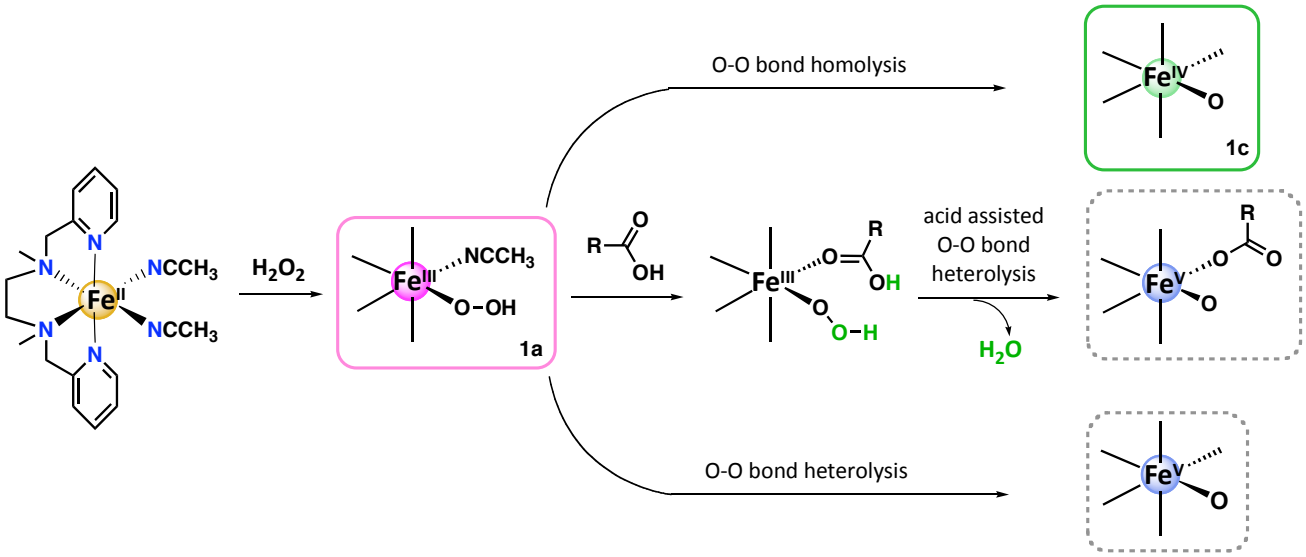

Development of novel catalysts. Our mechanistic studies demonstrate that aromatic hydroxylation is promoted by high-valent iron-oxo center, therefore **we have successfully designed a series of ligands to support a high-valent iron and showed that new complexes are more efficient at aromatic hydroxylation than the original Fe^{II}(BPMEN) compex.** Moreover, one of the modified complexes allowed us to observe a putative Fe(V)-oxo intermediate which is a reactive species in substrate oxidation. Detailed characterization of this important species is under current investigation.

TABLE OF CONTENTS

1. IRON-PROMOTED ORTHO- AND/OR IPSO-HYDROXYLATION OF BENZOIC ACIDS WITH H_2O_2 2

1.1 **Introduction 2**

1.2 **Results and discussion 4**

1.2.1 Ortho-hydroxylation 4

1.2.2 Oxidative decarboxylation leading to ipso-hydroxylation. 11

1.2.3 Mechanistic insights 16

1.3 **Experimental section 24**

1.3.1 Materials and methods 24

1.3.2 UV-vis studies of aromatic hydroxylation reactions 26

1.3.3 Identification of ortho-hydroxylation products by NMR 26

1.3.4 Identification of ipso-hydroxylation products by GCMS 27

1.3.5 Resonance Raman studies and labeling experiments 27

1.3.6 Crystallographic Studies 28

1.4 **References: 30**

2. AROMATIC HYDROXYLATION AT A NON-HEME IRON CENTER: OBSERVED INTERMEDIATES AND INSIGHTS INTO THE NATURE OF THE ACTIVE SPECIES 33

2.1 **Abstract 33**

2.2 **Introduction 34**

2.3 **Results and Discussion 37**

2.3.1 Hydroxylation of benzene by hydrogen peroxide in the presence of **1** 37

2.3.2 The scope of the hydroxylation reaction 39

2.3.3 Kinetic and mechanistic studies of benzene hydroxylation 41
2.3.4 Reaction of complex **1** with H_2O_2: formation of the Fe^{III}(OOH) intermediate. ... 41
2.3.5 Fe^{III}(OOH) reactivity pathways and effect of acetic acid. 45
2.3.6 Products of decomposition of Fe^{III}(OOH) and their role in hydroxylation reaction. 49
2.3.7 Mechanistic insights into O-O bond cleavage in Fe(III) peroxides supported by BPMEN..... 53
2.3.8 H/D Kinetic Isotope Effects in substrate oxidations with **1**/H_2O_2 56
2.3.9 Discussion..... 59

2.4 **Conclusions..... 65**

2.5 **Experimental section. 66**
2.5.1 General..... 66
2.5.2 Materials 66
2.5.3 Determination of phenol yield using GCMS..... 67
2.5.4 Stopped-flow experiments..... 67
2.5.5 Isotope-Labeling Studies..... 68
2.5.6 EPR studies 69
2.5.7 MPPH cleavage..... 69

2.6 **References: 70**

3. STUDIES OF THE MODIFIED COMPLEXES WITH LIGANDS STRUCTURALLY SIMILAR TO BPMEN..... 74

3.1 **Introduction..... 74**

3.2 **Experimental part..... 75**
3.2.1 General..... 75
3.2.2 Synthesis 76
3.2.3 EPR studies 80

3.2.4 Resonance Raman samples 80
3.2.5 Mössbauer samples 81
3.2.6 Electrochemical experiments 81

3.3 **Results and discussion 82**
3.3.1 New complexes 82
3.3.2 Hydroxylation of benzene 83
3.3.3 Formation of the Fe^{III}(OOH) intermediate, spectroscopic characterization 86
3.3.4 Cyclic voltammetry studies 91
3.3.5 CH_3COOH promotes decomposition of Fe^{III}(OOH) into reactive oxidant 92
3.3.6 Reactivity of the new intermediate 95
3.3.7 Identity of the new intermediate **SR-3X** 97
3.3.8 Studies with Fe^{II}(iPr-BPMEN)$(OTf)_2$ (**1-iPr**) 102

3.4 **Conclusions 103**

3.5 **References: 103**

4. REACTIVITY OF $[FE^{III}_2(\mu\text{-}O)(\mu\text{-}OH)(BPMEN)_2](CLO_4)_3$ IN AROMATIC HYDROXYLATION: DIMER VS. MONOMER 105

4.1 **Introduction 105**

4.2 **Experimental section 106**
4.2.1 General 106
4.2.2 Determination of phenol (ipso-hydroxylation product) yield using GCMS 107
4.2.3 Determination of Fe(III)-salicylate (ortho-hydroxylation product) yield using UV-vis 108

4.3 **Results 109**
4.3.1 ortho- and ipso- Hydroxylation promoted by diferric complex: one iron is better than two 109

4.3.2 Formation of $[Fe^{III}_2(\mu\text{-}O)(\mu\text{-}OOCPh)(BPMEN)_2]^{3+}$ 113
4.3.3 Reaction of $[Fe^{III}_2(\mu\text{-}O)(\mu\text{-}OH)(BPMEN)_2]^{3+}$ with H_2O_2 115
4.3.4 Protonation state of substrate is important 117

4.4 **Discussion 118**

4.5 **References 122**

5. ***IPSO*-HYDROXYLATION: EVIDENCE OF A RADICAL REACTION? 124**

5.1 **Introduction 124**

5.2 **Experimental section 124**
5.2.1 General 124
5.2.2 Identification of ortho-hydroxylation products by NMR 125
5.2.3 Identification of hydroxylation products by GCMS 125

5.3 **Results 126**
5.3.1 Branching in hydroxylation reaction 126
5.3.2 Subsequent oxidation of ipso-hydroxylated products 129

5.4 **Summary 135**

5.5 **References: 135**

6 **HYDROXYLATION OF BENZOIC ACIDS WITH H_2O_2 IN THE PRESENCE OF 1 ..... 136**

6.1 **Reaction between 1, benzoic acid and H_2O_2 ..... 136**
6.1.1 Kinetic studies with variable $[H_2O_2]$ 136
6.1.2 Kinetic studies with variable [**1**] 139
6.1.3 Discussion 142

6.2 **Effect of acids on hydroxylation rate 143**

6.3 **Self-hydroxylation of mCPBA..... 145**

6.4 **Kinetics with FeTPA 148**

6.5 **Conclusions..... 155**

6.6 **References 156**

7 APPENDIX A (CHAPTER 1)..... 157

8 APPENDIX B (CHAPTER 2)..... 173

8.1 **References: 201**

9 APPENDIX C (CHAPTER 3)..... 202

10 APPENDIX D (CHAPTER 4) 230

11 APPENDIX E (CHAPTER 5) 233

12 APPENDIX F (CHAPTER 6) 252

LIST OF FIGURES

Figure 1-1. Visible spectra of oxidation products derived from benzoic (•••), 3-methoxybenzoic (– –) and 2-methoxybenzoic acids (—) in the reactions of 1 (0.5 mM), the appropriate acid (1 mM), and H_2O_2 (1.5 mM) in CH_3CN at 20 °C. 7

Figure 1-2. ORTEP representation of $[Fe^{III}(TPA)(5\text{-MeO-salicylate})]^+$. Hydrogen atoms have been omitted for clarity. 7

Figure 1-3. Resonance Raman spectra of the green complexes generated in acetonitrile at -40 °C by mixing 1, 2-methoxybenzoic acid and hydrogen peroxide (above) and 1, 2,6-dimethylbenzoic acid and hydrogen peroxide (below). Spectra in blue were obtained with $H_2{}^{16}O_2$, while spectra in red were obtained with $H_2{}^{18}O_2$. Spectra were acquired on frozen samples at 77 K with 647 nm excitation. Solvent peaks were denoted with *. 13

Figure 1-4. Spectral changes observed in the reaction of **2** (1 mM) with 3 equiv H_2O_2 and 12 equiv 3-methoxybenzoic acid at -40 °C. Dashed lines represent spectra obtained immediately after mixing **2** and H_2O_2 and after 9 min. Solid lines correspond to spectra obtained subsequent to the addition of 3-methoxybenzoic acid (taken at 10, 20, 50, 90, 150 and 210 min after addition of the acid). 18

Figure 2-1. UV-vis spectral changes for the reaction of 1, benzene and H_2O_2 in acetonitrile at 20 °C ([1] = 0.5 mM, $[H_2O_2]$ = 5 mM, 200 equiv of benzene vs. 1). Solid lines represent spectra of 1 (red, time 0 s) and a product $[(BPMEN)Fe^{III}\text{-}OPh]^{2+}$ (blue, run time 90 s). Inset: kinetic trace at 650 nm showing accumulation of $[(BPMEN)Fe^{III}\text{-}OPh]$. 39

Figure 2-2. Time resolved UV-vis spectra of the $Fe^{III}(OOH)$ formation at 20 °C in acetonitrile ([1] = 1 mM, $[H_2O_2]$ = 10 mM). Inset: kinetic trace at 560 nm. Solid lines are spectra of 1 (red) and $Fe^{III}(OOH)$ (purple) at its maximum formation. 42

Figure 2-3. EPR spectrum (120 K) of $Fe^{III}(OOH)$ in acetonitrile. 25 % yield of $Fe^{III}(OOH)$ vs. initial concentration of iron was determined using $Cu(ClO_4)_2$ as an external standard.

Signals at 2.41 and 1.90 correspond to 1b that accompanies 1a at all temperatures. Red dotted line is a simulation of EPR spectrum with g values 2.21, 2.14, 1.96 (calculated using SimFonia). 44

Figure 2-4. Time resolved UV-vis spectra of the reaction of $Fe^{III}(OOH)$ with benzene in acetonitrile at 20 °C ([1] = 0.5 mM, $[H_2O_2]$ = 5 mM, 200 equiv of benzene vs. 1). Solid lines represent spectrum of 1a (λ_{max} = 560 nm) at its maximum formation (age time 7 s) and a spectrum of a product [(BPMEN)Fe^{III}-OPh] (λ_{max} = 650 nm, run time 80 s). 45

Figure 2-5**.** Rates of formation of phenol, $Fe^{III}(OOH)$ and decay of $Fe^{III}(OOH)$ in acetonitrile at 20 ˚C as a function of H_2O_2 concentration. Rate constant of hydroxylation was determined from a single mixing experiment, where **1** was mixed with benzene and H_2O_2 ([**1**]=0.5 mM, 300 equiv benzene vs. **1**). Kinetic traces at 650 nm were fitted in Kinetic Studio program using A→B→C model. Formation and decay of $Fe^{III}(OOH)$ was monitored at 560 nm after **1** (0.5 mM) was mixed with H_2O_2; kinetic traces at 560 nm were fitted using A→B→C model, where the first process represents formation of $Fe^{III}(OOH)$ and the second process is a decay of $Fe^{III}(OOH)$. 48

Figure 2-6. Rate constant of phenolate formation is directly proportional to $[CH_3COOH]$ ([1] = 0.5 mM, $[H_2O_2]$ = 5 mM, 560 equiv of benzene vs. 1, 20 ˚C, acetonitrile). 49

Figure 2-7. Stopped-flow time resolved UV-vis spectra of the reaction of $Fe^{III}(OOH)$ with 1 equiv of acetic acid. $Fe^{III}(OOH)$ was pre-generated by mixing **1** (0.5 mM) and H_2O_2 (5 mM) at 20 °C in acetonitrile over 10 s (solid line, λ_{max}=560 nm). $Fe^{III}(OOH)$ decays quickly (2 s) upon addition of acetic acid (1 equiv vs. iron, dashed line) followed by slow (over 80 s) accumulation of Fe^{IV}=O (solid line, λ_{max} = 740 nm).[35] Inset shows EPR spectra of $Fe^{III}(OOH)$ before (dotted line) and after (solid line) addition of acetic acid at room temperature. 51

Figure 2-8. Spectra of green species **1c** obtained upon mixing of **1** with IBX ester ([**1**]=1 mM; [IBX-ester]=3.8 mM, acetonitrile, 10 °C) and **1** with H_2O_2/ CH_3COOH ([**1**] = 1 mM, $[H_2O_2]$ = 10 mM, $[CH_3COOH]$ = 0.5 mM, acetonitrile, 20 ˚ C). 52

Figure 2-9. Product yields (in mol/1 mol Fe) and effects of acetic acid in aerobic reaction of benzene with 1/MPPH (Scheme 2-3): a) [1] = 2 mM, 280 equiv of benzene vs. 1, 1 equiv of MPPH; b) [1] = 2 mM, 280 equiv of benzene vs. 1, 1 equiv of MPPH, 0.5 equiv of acetic acid; control experiments:[46] c) MPPH in acetonitrile (same amount as in a and b); d) MPPH and acetic acid (same amounts as in b). All samples were stirred for 30 min, then acetylated, products extracted with dichloromethane and analyzed by GCMS. Error bars show standard deviation..... 56

Figure 3-1. X-Ray structure of the complex: left- $[Fe^{II}SR\text{-}BPMEN(CH_3CN)_2]^{2+}$ (SR-1) and right- $[Fe^{II}SR\text{-}BPBP(CH_3CN)_2]^{2+}$ (SR-3) with 50% probability thermal ellipsoids (hydrogen atoms omitted for clarity). Structure of SR-3 was acquired at room temperature (Albany, Dr. Alexander Filatov)..... 83

Figure 3-2. Kinetic traces at 650 nm represent formation of Fe(III)-phenolate product, complexes 1, 3, 4, SR-1, and SR-3 are capable of hydroxylating benzene. Experiment was performed in a single mixing mode: $[Fe^{II}L]$ = 0.5 mM, $[H_2O_2]$ = 5 mM, 300 equiv of benzene vs. iron..... 84

Figure 3-3. Kinetic traces at 560 nm show decomposition of $Fe^{III}(OOH)$ in the presence of variable amounts of water (left). Experiment was performed using stopped-flow in double mixing mode, $Fe^{III}(OOH)$ was pregenerated by reacting **3** and H_2O_2 in acetonitrile at 20 ˚C, at the maximum accumulation of this intermediate (5 s) water was added (0-200 equiv vs. **3**); [**3**] = 0.5 mM, $[H_2O_2]$ = 5 mM. Kinetic traces were fitted to two-exponential rate law and first observed rate constant was plotted against concentration of water (right)..... 87

Figure 3-4. Time resolved UV-vis spectra of the $Fe^{III}(OOH)$ formation at 20 °C in acetonitrile ([SR-3] = 1 mM, $[H_2O_2]$ = 10 mM). Maximum accumulation of $Fe^{III}(OOH)$ was seen in 2 s after mixing reagents (shown in the graph). Inset: EPR spectrum (120 K) of the $Fe^{III}(OOH)$, generated by mixing SR-3 and H_2O_2 in acetonitrile at 0 ˚C and frozen in 30 s after reagents were mixed ([SR-3] = 1 mM, $[H_2O_2]$ = 10 mM after mixing). G values 2.18, 1.99 and 1.95..... 89

Figure 3-5. Resonance Raman spectra of Fe^{III}(OOH) (SR-3a) and SR-3 in CD_3CN. Left: rRaman spectra acquired using 514.5 nm laser on samples containing ~ 5 mM Fe^{III}(OOH) (red) and ^{18}O labeled Fe^{III}(OOH) (black); right: rRaman spectra of Fe^{II}SR-BPBP using 568.2 (blue), 514.5 (red) and 406.7 (black) excitation wavelength. 91

Figure 3-6. Spectral changes upon addition of acetic acid to Fe^{III}(OOH) in acetonitrile at 20 ˚C. Left: Fe^{III}(OOH) was pregenerated from SR-3 and H_2O_2 and then acetic acid was added, time scale shown is 1 s. Right: Fe^{III}(OOH) was pre-generated by mixing SR-1 and H_2O_2 at 20 °C in acetonitrile over 5 s. Fe^{III}(OOH) decays quickly (~3 s) upon addition of acetic acid followed by slow (over 80 s) accumulation of Fe^{IV}=O (λ_{max} = 760 nm, see inset); ([Fe^{II}L] = 0.5 mM, [H_2O_2] = 5 mM, [CH_3COOH] = 0.5 mM after double mixing). 93

Figure 3-7. EPR spectra (120 K) of (SR-BPBP)Fe^{III}(OOH) and a product of its decay. Acetonitrile solutions of SR-3 and H_2O_2 were mixed in the EPR tube at 0 ˚C and incubated at 0 ˚C for 30 s, then acetic acid was added and reaction quenched in ~5 s (acetic 1) and ~7 s (acetic 2), ([SR-3] = 0.8 mM, [H_2O_2] = 8 mM, [CH_3COOH] = 0.4 mM). 94

Figure 3-8. Spectral changes after mixing **SR-3**, H_2O_2 and acetic acid in acetonitrile at -30 ˚C ([**SR-3**] = 1 mM, [H_2O_2] = 5 mM, [CH_3COOH] = 1 mM). Formation of **SR-3X** is shown on the left (0-62 s) and its decay (62-120 s) is on the right. 96

Figure 3-9. Spectral changes during the reaction between SR-3 and recrystallized mCPBA in acetonitrile at -10 ˚C. First, change in absorbance at 460 nm is observed (red) and then product accumulates (blue). [SR-3] = 1 mM, [mCPBA] = 1.8 mM, time scale shown 10 s. 97

Figure 3-10. EPR spectra of (SR-BPBP)Fe^{III}(OOH) (SR-3a) and SR-3X intermediate acquired at 2.4 K. Fe^{III}(OOH): SR-3 (0.2 mM, 2 mM) + H_2O_2 (0.2 mL, 20 mM); SR-3X : SR-3 (0.2 mL, 2 mM) and H_2O_2/HOAc (0.2 mL, [H_2O_2] = 10 mM, [HOAc] = 2 mM). 98

Figure 3-11. EPR spectra of SR-3X intermediate acquired at 2.4 K. 5 mM: SR-3 (0.2 mL, 10 mM) + HOAc/H_2O_2 (0.1 mL, [H_2O_2] = 50 mM, [HOAc] = 10 mM); 1 mM: SR-3 (0.2 mL, 2 mM) and H_2O_2/HOAc (0.2 mL, [H_2O_2] = 10 mM, [HOAc] = 2 mM). 99

Figure 3-12. EPR spectra of samples prepared by reacting SR-3 with H_2O_2/HOAc and incubating reaction mixture at -35 ˚C for 10, 20, 30, 50, 70 and 100 s; [SR-3] = 1 mM, [HOAc] = 1 mM, [H_2O_2] = 5 mM. 99

Figure 3-13. Resonance Raman spectra of [(SR-BPBP)Fe^{III}(OOH]$^{2+}$ in CD_3CN (black) and SR-3X in CH_3CN (red) acquired using 406.7 nm laser. 101

Figure 3-14. X-Ray structure of the complex Fe^{II}(iPr-BPMEN)$(OTf)_2$ with 50% probability thermal ellipsoids (hydrogen atoms omitted for clarity). 102

Figure 4-1. Spectral changes upon reaction of 5 (red), H_2O_2 and 3,5-dichlorobenzoic acid in acetonitrile at 20°C; [5] = 0.5 mM, [3,5-dichlorobenzoic acid] = 2 mM, [H_2O_2] = 10 mM after mixing) indicate formation of Fe(III)-salicylate complex (blue). Inset shows kinetic trace at 590 nm, hydroxylation reaction is complete in 800 s..... 109

Figure 4-2. Spectral changes upon reaction of 5 (red) with benzoic acid (BA) in acetonitrile at 20 ˚C; [5] = 0.5 mM, [BA] = 2 mM. Blue spectrum corresponds to the [Fe^{III}_2(μ-O)(μ-OOCPh)(BPMEN)$_2$]$^{3+}$. Inset: kinetic trace at 555 nm (red) was fitted to one exponential equation (fit in blue) , k_{obs} = 0.01 s^{-1} (average of three). 113

Figure 4-3. Spectral change upon addition of different amounts of hydrogen peroxide premixed with benzoic acid to **5** in acetonitrile (0 to 3 molar equivalents of H_2O_2 versus **5**, with 0.2 mM of **5** and 0.2 mM of benzoic acid). Yield of major products are indicated on the graph. 114

Figure 4-4. Spectral change upon reaction of **5** with H_2O_2 in acetonitrile at 20 ˚C; [**5**] = 0.5 mM, [H_2O_2] = 10 mM. Inset shows kinetic trace at 555 nm (black) and its double exponential fit (light green, dashed line); k_{1obs} = 0.022 s^{-1}, k_{2obs} = 0.002 s^{-1} 116

Figure 4-5. X-Ray structure of the complex [Fe^{II}_2(μ-OOCPh)$_2$(BPMEN)$_2$]$(ClO_4)_3$ (7) with 50% probability thermal ellipsoids (hydrogen atoms omitted for clarity). 117

Figure 4-6. Hydroxylation of benzoate by 1/H_2O_2 can occur only in the presence of triflic acid (equiv vs. iron content). A_{600} represent spectrophotometric yield of Fe^{III}-salicylate. 118

Figure 6-1. Spectral changes upon reaction of **1**, H_2O_2 and benzoic acid (BA) at 25 ˚C in acetonitrile; [**1**] = 0.25 mM, [H_2O_2] = 1 mM, [BA] = 1 mM. 136

Figure 6-2. Left: kinetic traces at 400 nm and 600 nm for reaction of 1 (0.5 mM), H_2O_2 and benzoic acid (1 mM) at 20 ˚C in acetonitrile. Right: observed rate constants as a function of [H_2O_2]. Kinetic traces at 600 nm were fitted to a double exponential equation (k1 600 nm and k2 600 nm); kinetic traces at 400 nm were fitted to a single exponential equation (k 400 nm). 137

Figure 6-3. Plot of the observed rate constant at 410 nm versus hydrogen peroxide concentration after mixing with **1** and benzoic acid acquired by stopped-flow technique at different temperatures (0.50 mM of **1** premixed with 1.5 equivalent of benzoic acid and 12-50 mM of hydrogen peroxide after mixing): T = -15 °C (□), -5 °C (Δ), 5 °C (□), 15 °C (□), 25 °C (□). 138

Figure 6-4. Arrhenius plot (A) and Eyring plot (B) for the first step of the reaction between **1**, benzoic acid and hydrogen peroxide. 138

Figure 6-5. Left: kinetic traces at 600 nm for the reaction between **1,** benzoic acid and H_2O_2 ; [**1**] = 0.125 mM, 0.25 mM, 0.375 mM and 0.5 mM, [BA] = 1 mM, [H_2O_2] = 1.5 mM. Right: kinetic traces at 600 nm (left) were fitted to a double exponential rate law and corresponding observed rate constants plotted against [**1**]. 140

Figure 6-6. Kinetic traces at 600 nm were acquired for the reaction of 1, benzoic acid and variable amounts of H_2O_2 and fitted to a second order rate law f(x) = Af-((Af-An)/(1+k*C*x)). Corresponding rate constant linearly increase with [H_2O_2]. 141

Figure 6-7. Rate constant of Fe(III)-salicylate formation increases with concentration of acetic acid. Fe^{III}(OOH) was pregenerated by mixing 1 (0.5 mM after DX) and H_2O_2 (10 equiv vs. iron) followed by addition of benzoic acid (2 equiv vs. iron) with variable amounts of acetic acid (0-7.5 equiv vs. iron) at 20 °C (V-14). Each kinetic trace at 700 nm was fitted using A→B→C model, first rate constants (k_{1obs}) were plotted against acetic acid concentration. Second rate constant (k_{2obs}) was much smaller compared to k_{1obs}. 144

Figure 6-8. Effect of triflic acid on the rate of hydrohylation. Left: kinetic traces at 650 nm acquired in the diode array mode using stopped-flow technique. Double mixing experiments: Fe^{III}(OOH) was generated by mixing 1 (0.5 mM) with H_2O_2 (5 mM) at

20 °C in acetonitrile and then benzene (560 equiv) and variable amounts of triflic acid (0-2 equiv vs. iron) were added. Age time: 8 s, run time 60 s. Right: all kinetic traces were fitted using A→B→C model and both k_{1obs} and k_{2obs} plotted against equiv of triflic acid. 145

Figure 6-9. Left: spectral changes upon reaction of 1, 3-chlorobenzoic (mClBA) acid and H_2O_2 in acetonitrile at 25 ˚C; [1] = 0.25 mM, [mClBA] = 1 mM, [H_2O_2] = 1 mM. Right: spectral changes upon reaction of 1 and mCPBA in acetonitrile at 25 ˚C; [1] = 0.25 mM, [mCPBA] = 1 mM. 146

Figure 6-10. Kinetic traces at 600 nm acquired for the reaction between **1** (0.25 mM), 3-chlorobenzoic acid (1 mM) and H_2O_2 (1 mM) and for the reaction between **1** (0.25 mM) and mCPBA (1 mM). Kinetic traces were fitted to one exponential (3-chlorobenzoic acid + H_2O_2) or double exponential (mCPBA) equation, corresponding observed rate constants are shown on the graph. 147

Figure 6-11. Kinetic traces at 373 nm acquired for the reaction in Figure 6-9 caption.. 147

Figure 6-12. Kinetic traces at 640 nm acquired in the diode array mode using stopped-flow techniques. Double mixing experiments : Fe^{III}(OOH) was generated by mixing 2 with H_2O_2 at -20 °C in acetonitrile and then variable amounts of 3-methoxybenzoic acid were added (1- 10 equiv of 3-methoxybenzoic acid w.r.t. iron; 2- 20 equiv; 3- 40 equiv). Single mixing experiments: 2 was mixed with 3-methoxybenzoic acid and H_2O_2 at -20 °C in acetonitrile (4- 20 equiv of 3-methoxybenzoic acid, 5- 30 equiv of 3-methoxybenzoic acid). Final concentration of 2 is 0.5 mM in both double and single mixing experiments, 10 equiv of hydrogen peroxide w.r.t. iron was used to generate Fe^{III}(OOH) species in double mixing experiments and 10 equiv of hydrogen peroxide was added to 2 together with 3-methoxybenzoic acid in a single mixing experiments. 149

Figure 6-13. Rate constants of the first process in double mixing experiments (Figure 6-11) versus amount of 3-methoxybenzoic acid added (constants determined using 650 nm kinetic traces and Kinetic Studio program). 150

Figure 6-14. Kinetic traces at 650 nm acquired in the diode array mode using stopped-flow techniques. Double mixing experiments: FeOOH was generated by mixing 2 (2 mM before mixing) with H_2O_2 (20 mM) at -20 °C in acetonitrile and then variable amounts of 3-methoxybenzoic acid were added (1- 10 equiv of 3-methoxybenzoic acid w.r.t. iron; 2- 20 equiv; 3- 40 equiv) or equal amount of 3-methoxybenzoic acid and acetic acid were added (4- 10 equiv of 3-methoxybenzoic acid and 10 equiv of acetic acid; 5- 20 equiv of 3-methoxybenzoic acid and 20 equiv of acetic acid). 151

Figure 6-15. Kinetic traces at 640 nm (for 3-methoxysalicylate) and 660 nm for (3,4,5-trimethoxysalicylate) acquired in the diode array mode using stopped-flow techniques. Double mixing experiments : Fe^{III}(OOH) was generated by mixing 2 (0.5 mM) with H_2O_2 (5 mM) at -20 °C in acetonitrile and then variable amounts of 3-methoxybenzoic acid were added (1- 10 equiv of 3-methoxybenzoic acid w.r.t. iron; 2- 20 equiv; 3- 40 equiv) or variable amounts of 3,4,5-trimethoxybenzoic acid were added (4- 10 equiv of 3,4,5-trimethoxybenzoic acid; 5- 20 equiv). 152

Figure 6-16. Kinetic traces at 660 nm acquired in the diode array mode using stopped-flow techniques. Double mixing experiments: Fe^{III}(OOH) was generated by mixing 2 (2 mM before mixing) with H_2O_2 (20 mM) at -20 °C in acetonitrile and then variable amounts of 3,4,5-trimethoxybenzoic acid were added (1- 10 equiv of 3,4,5-trimethoxybenzoic acid w.r.t. iron; 3- 20 equiv) or equal amount of 3,4,5-trimethoxybenzoic acid and acetic acid were added (2- 10 equiv of 3,4,5-trimethoxybenzoic acid and 10 equiv of acetic acid; 4- 20 equiv of 3,4,5-trimethoxybenzoic acid and 20 equiv of acetic acid). 154

LIST OF SCHEMES

Scheme 1-1. Complexes studied in this work: 5

Scheme 1-2: Conversion of benzoic acids to salicylates and phenolates by 1 or 2 12

Scheme 1-3. Mechanisms of *ortho*-hydroxylation and *ipso*-hydroxylation by **1** and **2**. .. 24

Scheme 2-1. (A) *ortho*- and /or *ipso*-hydroxylation of benzoic acids with H_2O_2 promoted by 1; (B) possible reactivity modes of $Fe^{III}(OOH)$ intermediate: $Fe^{III}(OOH)$ can either directly transfer oxygen to substrate, or decompose into a high-valent iron-oxo species that reacts with the substrate. 36

Scheme 2-2. The scope of hydroxylation reaction. 40

Scheme 2-3. Reaction of MPPH with iron center and products derived from MPPH. 55

Scheme 2-4. Mechanism of aromatic hydroxylation shown for 3-$^2H_1$-chlorobenzene. A- direct insertion; B- hydrogen abstraction; C- addition/rearrangement; D- formation of epoxide. 57

Scheme 2-5. Intermediates involved in aromatic hydroxylation catalyzed by 1. 63

Scheme 3-1. Structures of Fe^{II} complexes used in this work: 1- $[Fe^{II}BPMEN(CH_3CN)_2]^{2+}$; 75

Scheme 4-1. Schematic representation of oxygen activation on diiron center. 105

Scheme 4-2. Formation of acetamide from acetonitrile and hydrogen peroxide. 116

Scheme 4-3. Complexes with μ-carboxylato bridges do not activate hydrogen peroxide. 121

Scheme 5-1. Possible mechanism of *ipso*-hydroxylation. 126

Scheme 5-2. Possible pathways of acetylsalycilic acid hydroxylation. 127

Scheme 5-3. Decarboxylation, ipso-hydroxylation and radical coupling 130

Scheme 5-4. Possible products of *ipso*-hydroxylation reaction as determined by HMQC NMR. 131

Scheme 5-5 133

Scheme 5-6. Oxidative cyclization of diphenyl-2 carboxylic acid. 134

Scheme 6-1. Simultaneous formation of the two iron species that promote *ortho*-hydroxylation – branching in the hydroxylation pathway. 143

Scheme 6-2 148

LIST OF TABLES

Table 1-1: The amounts of *ortho*- and *ipso*-hydroxylation products relative to iron complex observed from the reactions of 1 and 2 with a FeL/benzoic acid/H_2O_2 ratio of 1/2/3 at room temperature based on UV-vis [a] (*ortho*) and GC (*ipso*) data. 10

Table 1-2. Raman vibrations of iron(III)-phenolate complexes 14

Table 3-1. Deterium retention in a competitive isotope effect experiment. 85

Table 3-2. Activation parameters for $Fe^{III}(OOH)$ formation from 1, SR-1, 3, and SR-3 and H_2O_2 88

Table 3-3. Reduction potentials vs. ferrocene/ferrocenium couple determined from CV experiments and second order rate constant of $Fe^{III}(OOH)$ formation at 20 ˚C. 92

Table 4-1. Rate constants 111

Table 4-2: The amounts of *ortho*- and *ipso*-hydroxylation products relative to iron observed from the reactions of $[Fe^{II}BPMEN(CH_3CN)_2](ClO_4)_2$ (monomer) and 5 (dimer) with a Fe/benzoic acid/H_2O_2 ratio of 1/2/3 at room temperature based on UV-vis [a] (*ortho*) and GC (*ipso*) data. 112

Table 6-1. Kinetic parameters obtained by fitting kinetic traces at 600 nm (Figure 6-5) to $A = A_{inf} + \Delta A_1 \exp(-k_1 t) + \Delta A_2 \exp(-k_2 t)$, ratio $\Delta A_2/\Delta A_1$ represents fraction of the second process in the overall kinetic trace. 140

Table 6-2. Kinetic parameters obtained by fitting kinetic traces at 600 nm (Figure 6-5) to A = Af – ((Af-An)/(1+k*t*C)) 141

Complexes, monomer:

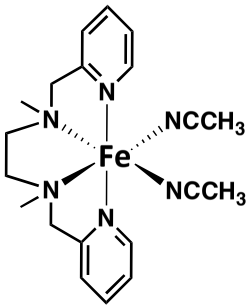

1

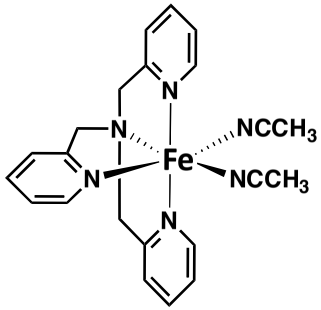

2

Intermediates supported by BPMEN ligand:

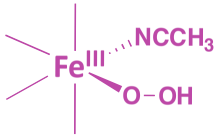

1a

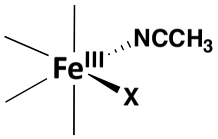

1b

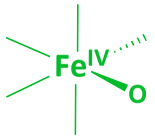

1c

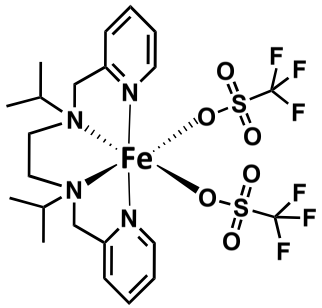

iPr-1

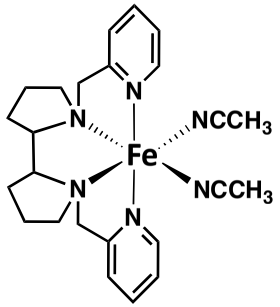

3

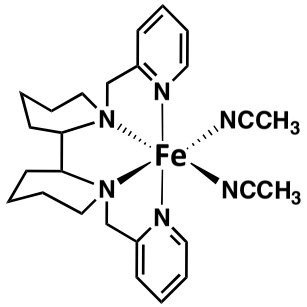

4

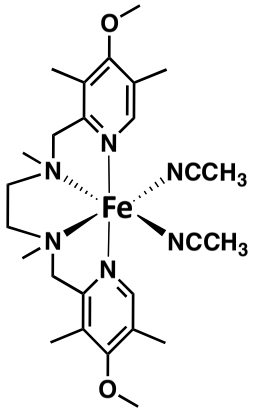

SR-1

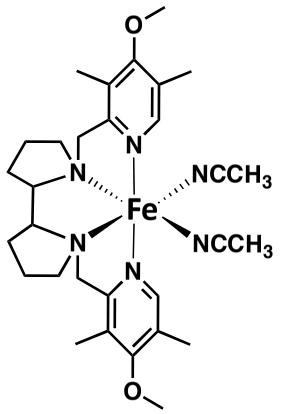

SR-3

Complexes, dimer:

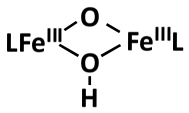

5

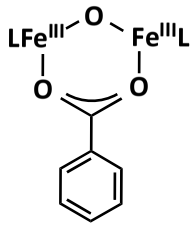

6

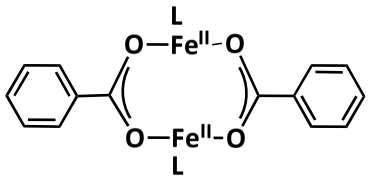

7

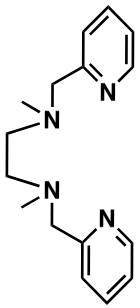

= L = BPMEN

Intermediates supported by SR-BPBP ligand:

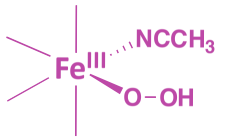

SR-3a

Aromatic hydroxylation at a non-heme iron center: insights into the nature of the metal-based oxidant

1 Iron-promoted ortho- and/or ipso-hydroxylation of benzoic acids with H_2O_2

1.1 Introduction

In nature, aromatic hydroxylations are catalyzed by mononuclear non-heme iron centers in pterin-dependent aromatic amino acid hydroxylases,[1-5] and non-heme diiron centers in bacterial multicomponent monooxygenases (BMMs) such as methane and toluene monooxygenases.[6-9] In both families of the enzymes, highly regioselective hydroxylations are accomplished by properly orienting the aromatic rings with respect to the metal active sites in the enzyme pockets. Strong evidence has been obtained for the involvement of high-valent iron-oxo species[10-12] that carry out electrophilic attack of the target aromatic rings.[13-15] Despite significant recent progress in understanding the mechanisms of enzymatic aromatic hydroxylations, a detailed mechanistic picture has yet to be developed for these reactions.

Synthetically, aromatic hydroxylations involving cheap, environment-friendly catalysts and oxidants (such as iron compounds and hydrogen peroxide) are very attractive for the late-stage oxidative derivatization and for metabolite preparation. Iron-catalyzed arene hydroxylations have been reported with Fenton's reagent (Fe salt/H_2O_2) [16-18] and related systems. Most of these reactions generate hydroxyl radicals,[19-21] but metal-based oxidants were also proposed in some cases.[22-27] While

these reactions are undoubtedly useful, they are often non-selective, yielding isomers of aromatic hydroxylation compounds as well as products of side chain oxidation.

Recently, efficient and selective intramolecular aromatic hydroxylations were reported with mononuclear[28, 29] or dinuclear[30-34] iron complexes where the aromatic ring is forced into close proximity of the iron center by a covalent linkage to the supporting polydentate ligand. The need to independently prepare the compounds containing both reactive iron center and the aromatic substrate, however, limits the applicability of these systems. Finding new selective intermolecular aromatic hydroxylation reactions remains an important challenge.

Orienting aromatic rings in close proximity to the metal center can be accomplished by coordinating aromatic substrates, via an anchoring group, to a vacant or labile site at the redox-active iron complex with a polydentate ligand. In one example of this strategy, phenols pre-bound to the iron center were hydroxylated selectively into the corresponding catecholato complexes.[35] We and others recently communicated additional examples of selective inner-sphere aromatic hydroxylation at non-heme iron centers: *ortho*-hydroxylation of benzoic acid with hydrogen peroxide promoted by $[Fe(BPMEN)]^{2+}$ (**1**)[36] and self-hydroxylation of perbenzoic acids promoted by $[Fe(TPA)]^{2+}$ (**2**)[37] (see Scheme 1 for ligand structures). Both complexes have aminopyridine ligands and are known to catalyze a number of oxidation reactions by activating H_2O_2,[38-41] including olefin epoxidation or *cis*-dihydroxylation[42-44] and alkane hydroxylation.[45, 46] A recent detailed comparative study of **1** and **2** in olefin epoxidation with H_2O_2 in the presence of acetic acid[44] provided important mechanistic information on the role of

various iron-oxygen intermediates, supporting carboxylic acid-assisted heterolytic O-O bond cleavage as the key step in generating a proposed Fe(V) oxidant. Although **1** and **2** share common reaction pathways in olefin epoxidation, **1** is the more active catalyst. However, only limited characterization is available for the rather short-lived intermediates derived from **1**,[47, 48] while the intermediates associated with **2** are longer lived and better characterized spectroscopically. These include $Fe^{III}(OOH)$,[49-51] $Fe^{III}(OOR)$,[29] [52, 53] and Fe^{IV}=O species.[54]

In the present work, the reactivities of non-heme iron complexes **1** and **2** are compared in the carboxylate-directed regioselective hydroxylation of various substituted benzoic acids. Both complexes promote efficient *ortho*-hydroxylation of substituted benzoic acids with H_2O_2 to generate salicylate products. Furthermore, a new reaction pathway has been found wherein the benzoic acid is hydroxylated at the *ipso* position with concomitant decarboxylation. A mechanistic scheme is proposed that invokes a common oxidant despite the divergent outcomes.

1.2 **Results and discussion**

1.2.1 Ortho-*hydroxylation*

We recently reported that addition of hydrogen peroxide to $[Fe^{II}(BPMEN)(CH_3CN)_2](ClO_4)_2$ (**1**) in the presence of benzoic acid resulted in rapid (ca. 5 min) formation of $[Fe^{III}(BPMEN)(salicylate)]^+$ at room temperature.[36, 55] The reaction was accompanied by the appearance of a deep blue color (λ_{max} = 590 nm). The final UV-vis spectrum was identical to that of the independently prepared salicylate complex

[Fe^{III}(BPMEN)(salicylate)](ClO_4), which was crystallographically characterized. A similar *ortho*-hydroxylation reaction was reported with a related iron(II) aminopyridine complex, [Fe^{II}(TPA)(CH_3CN)$_2$](OTf)$_2$ (**2**), but with *m*-chloroperbenzoic acid as oxidant.[37] In order to probe substituent effects on the *ortho*-hydroxylation reactions performed by these complexes, further studies have been carried out on both **1** and **2** and a variety of substituted benzoic acids with H_2O_2 as oxidant.

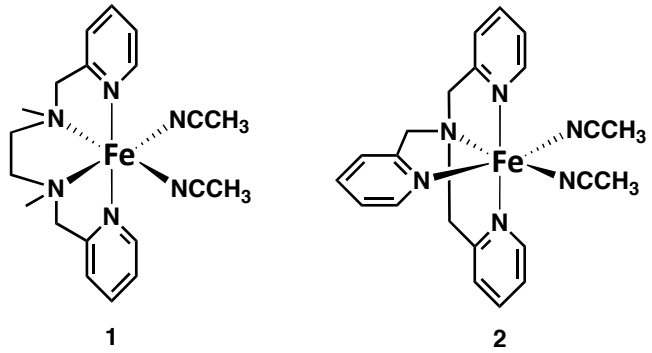

Scheme 1-1. Complexes studied in this work:
1, [Fe^{II}(BPMEN)(CH_3CN)$_2$](ClO_4)$_2$; **2**, [Fe^{II}(TPA)(CH_3CN)$_2$](OTf)$_2$

Both **1** and **2** were found to effect the *ortho*-hydroxylation of various benzoic acids with H_2O_2 as oxidant, but the amounts of salicylate formed depended upon the nature of ring substituents and the iron complex (Table 1). The outcomes of the hydroxylation reactions were conveniently monitored in solution by UV-vis spectroscopy following the appearance of the intense visible absorption bands of the iron(III)-salicylate products (Table A1). The maxima of these absorption bands depended on the electronic nature of the substituent, consistent with the assignment of this absorbance as a phenolate-to-iron(III) charge transfer band. As expected, electron-donating groups caused the λ_{max} of the salicylate complex to red-shift, whereas electron withdrawing groups had the

opposite effect (Table A1). For example, the λ_{max} of 590 nm for $[Fe^{III}(BPMEN)(salicylate)]^+$ was red-shifted to 695 nm in the corresponding 3- or 5-MeO-salicylate derivative (Figure 1-1, Table A1). The extinction coefficients were determined for representative salicylate complexes ($[Fe^{III}(BPMEN)(salicylate)]^+$, ε_{590} = 2300 $L*mol^{-1}*cm^{-1}$; $[Fe^{III}(TPA)(5\text{-Cl-salicylate})]^+$, ε_{560} = 2100 $L*mol^{-1}*cm^{-1}$; $[Fe^{III}(TPA)(5\text{-MeO-salicylate})]^+$, ε_{650} = 2100 $L*mol^{-1}*cm^{-1}$) and were assumed to be similar for all *ortho*-hydroxylation products. Crystal structures of $[Fe^{III}(TPA)(5\text{-MeO-salicylate})]^+$ (Figure 1-2) and $[Fe^{III}(TPA)(salicylate)]^+$ (Figure A1) were obtained from single crystals grown in the presence of air from a 1:1:1 reaction mixture of **2**, triethylamine and the appropriate salicylic acid. Details of the crystal data and structural refinement are provided in Appendix A (Table A2 and Table A3), and their structural parameters are compared with that of $[Fe^{III}(TPA)(5\text{-Cl-salicylate})]^+$ [37] in Table A4.

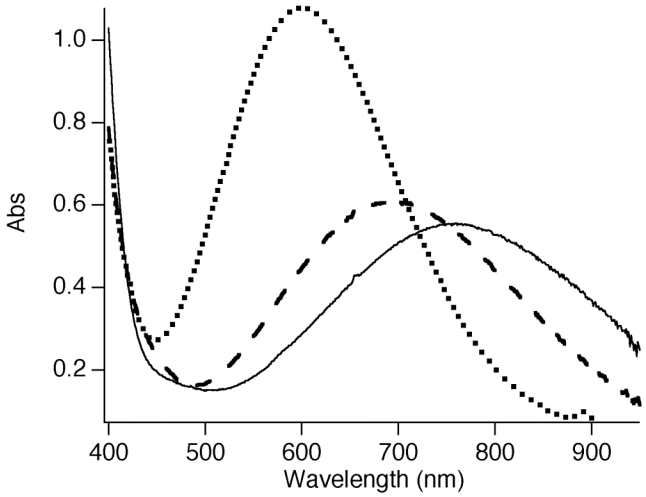

Figure 1-1. Visible spectra of oxidation products derived from benzoic (•••), 3-methoxybenzoic (– –) and 2-methoxybenzoic acids (—) in the reactions of **1** (0.5 mM), the appropriate acid (1 mM), and H_2O_2 (1.5 mM) in CH_3CN at 20 °C.

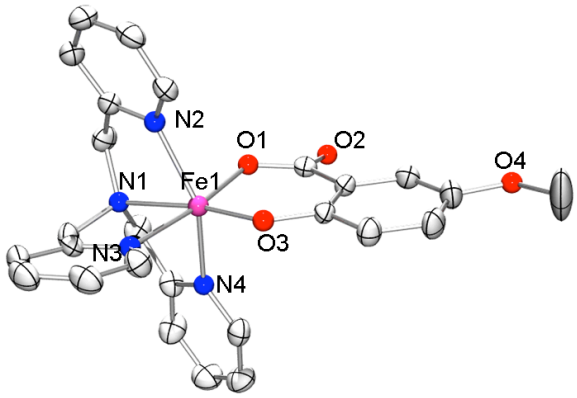

Figure 1-2. ORTEP representation of $[Fe^{III}(TPA)(5\text{-MeO-salicylate})]^+$. Hydrogen atoms have been omitted for clarity.

Salicylic acids were the main products of the reactions with benzoic acid and 3-substituted derivatives. For complex **1**, 90-95% yields of salicylate products were found for benzoic acid, 3-methylbenzoic acid and 3-chlorobenzoic acid with respect to the iron complex, while the yields were 50-60% for **2** (Table 1-1). In most cases, salicylic acid yields determined by NMR agreed reasonably well with the amounts of corresponding iron(III)-salicylates generated in solution (Table 1-1 and Table A1). The product yields were significantly lower for nitro-substituted substrates, presumably because of the lower reactivity of electron-poor nitrobenzoic acids and losses during the workup (which account for the yields determined by NMR). Another reason of obtaining lower yields of hydroxylated products is over-oxidation of the electron-rich salicylates by H_2O_2. This is the reason behind the lower yield of 3-OMe-benzoic compared to 3-Cl-benzoic acid in the *ortho*-hydroxylation. In fact, adding a smaller amount of H_2O_2 (2 equivalents relative to iron complex) led to the higher yield of salicylates (57% for 3-OMe and 62% for 3-Me for **2**).

For 3-substituted benzoic acids, there were two available positions for *ortho*-hydroxylation, which would generate 3- and/or 5-substituted salicylic acids. ^{1}H NMR analysis of the products of the reaction with **1** showed that the 5-substituted salicylic acid was the major product over 3-substituted isomer, 3:1 for 5-methylsalicylic acid and 4:1 for 5-chlorosalicylic acid (Figure A2). The preference for the 5-substituted isomer was not surprising on the basis of steric effects; the hydroxylation of the *para*-position with respect to substituent should be sterically less demanding than the incorporation of a hydroxyl group between two existing substituents. Similarly, a 3:1 selectivity in

favor of 5-methoxysalicylic acid was observed with complex **2** and 3-methoxybenzoic acid.

Our studies showed that **1**/H_2O_2 was more reactive than **2**/H_2O_2 (Table 1-1), effecting *ortho*-hydroxylation of a larger range of benzoic acids. In particular, **1**/H_2O_2 was able to convert electron-deficient nitrobenzoic acids to the corresponding salicylates. However, 3,5-dinitrobenzoic acid was completely unreactive. Unlike **1**/H_2O_2, **2**/H_2O_2 displayed a more limited scope of aromatic *ortho*-hydroxylation. The reactivity differences between **1** and **2** suggest that the oxidant produced by **1** is more powerful than that of **2**. This notion is consistent with the observed higher yield of oxidation products for **1** compared to **2** in the hydroxylation of cyclohexane.[45]

Table 1-1: The amounts of *ortho*- and *ipso*-hydroxylation products relative to iron complex observed from the reactions of **1** and **2** with a FeL/benzoic acid/H_2O_2 ratio of 1/2/3 at room temperature based on UV-vis [a] (*ortho*) and GC (*ipso*) data.

Substituent	Position	% yield of the hydroxylated products			
		1		**2**	
		ortho	*ipso*	*ortho*	*ipso*
OMe	2-	-	70	-	14
	3-	52	-	48	-
	4-	-	22	-	-
Me	2-	*	45	-	26
	3-	>95	-	58	-
	4-	*	21	-	30
H		94	-	51	21
Cl	2-	*	75	-	90
	3-	98	-	61	-
	4-	*	60	-	54
NO_2	2-	52	14	-	12
	3-	56	-	-	-
	4-	68	-	-	-

* *Ortho*- and *ipso*-hydroxylation products form concurrently, and their absorption bands partially overlap, so it is impossible to independently evaluate the yield of each product from UV-vis data.

'-' indicates no reaction

[a] UV-vis yields have been calculated using e = 2300 $L*mol^{-1}*cm^{-1}$ for all salicylate complexes.

1.2.2 Oxidative decarboxylation leading to ipso*-hydroxylation.*

The remarkable ability of mononuclear iron(II) complexes **1** and **2** to efficiently and selectively hydroxylate benzoic acids to their corresponding salicylic acids using H_2O_2 has some limitations. Surprisingly, some benzoic acids with electron donating substituents did not afford salicylate products, even in the reactions involving **1** (Scheme 1-2). For example, the reaction of **1**, the electron-rich 2-methoxybenzoic acid, and H_2O_2, in a 1/2/3 ratio did not afford the corresponding salicylate complex but instead generated a transient green species. At room temperature, this green intermediate formed upon mixing and decayed in 5 s, but its lifetime could be significantly extended at -40 ˚C. Its UV-vis spectrum showed a λ_{max} at 760 nm (Figure 1-1), distinctly different from the characteristic spectrum of independently synthesized $[Fe^{III}$(BPMEN)(6-MeO-salicylate)$]^+$ complex (λ_{max} = 608 nm). Moreover, a similar but not identical green species could also be observed after addition of H_2O_2 to a mixture of 2,6-dimethylbenzoic acid and **1** (Figure A3). Since both *ortho* positions of 2,6-dimethylbenzoic acid were occupied, the green complex could not result from an *ortho*-hydroxylation reaction. Quenching the reactions with 1-methylimidazole followed by acetylation and GC-MS analysis allowed us to identify the organic products as 2-methoxyphenol and 2,6-dimethylphenol, respectively, which were obtained in 70% and 20% yields from the reaction mixtures of **1**/benzoic acid/H_2O_2 in a 1/2/3 ratio. NMR analysis of these products corroborated the GC analysis. These phenol products resulted from oxidative decarboxylation of 2-methoxy- and 2,6-dimethylbenzoic acids followed by *ipso*-hydroxylation (Scheme 1-2). Coordination of the phenolate products to

[Fe(BPMEN)]$^{3+}$ then generated the observed green chromophores, the identities of which were confirmed by independent spectroscopic experiments described below. In the presence of excess H_2O_2, phenolates undergo further oxidation; this overoxidation is responsible for the transient nature of the observed green complexes under certain conditions.

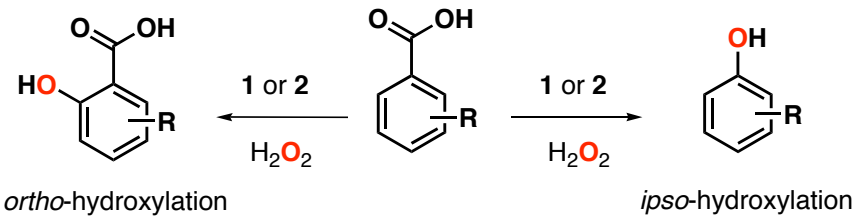

Scheme 1-2: Conversion of benzoic acids to salicylates and phenolates by **1** or **2**

Resonance Raman spectra of the green chromophores supported their formulation as $Fe^{III}(L)(OAr)$ species, showing vibrational features in the 500-1600 cm^{-1} region that are characteristic of Fe^{III}-phenolate complexes.[29, 56-58] For the 2-methoxybenzoic acid experiment, four modes were affected when $H_2{}^{18}O_2$ was used instead of $H_2{}^{16}O_2$ (Table 1-2). The 619 cm^{-1} band can be assigned to the Fe-OAr vibration by analogy to a band with the same frequency found in the Raman spectrum of the phenyl-hydroxylated product from Fe^{II}(6-Ph-TPA) and ^{t}BuOOH.[29] The other three vibrations were associated with phenolate C-O and ring deformation modes.[59, 60] Similar assignments can be made for the ^{18}O-isotope-sensitive vibrations observed for the green chromophore from the 2,6-dimethylbenzoic acid experiments (Table 1-2). These results also proved that the phenolate oxygen originated from H_2O_2.

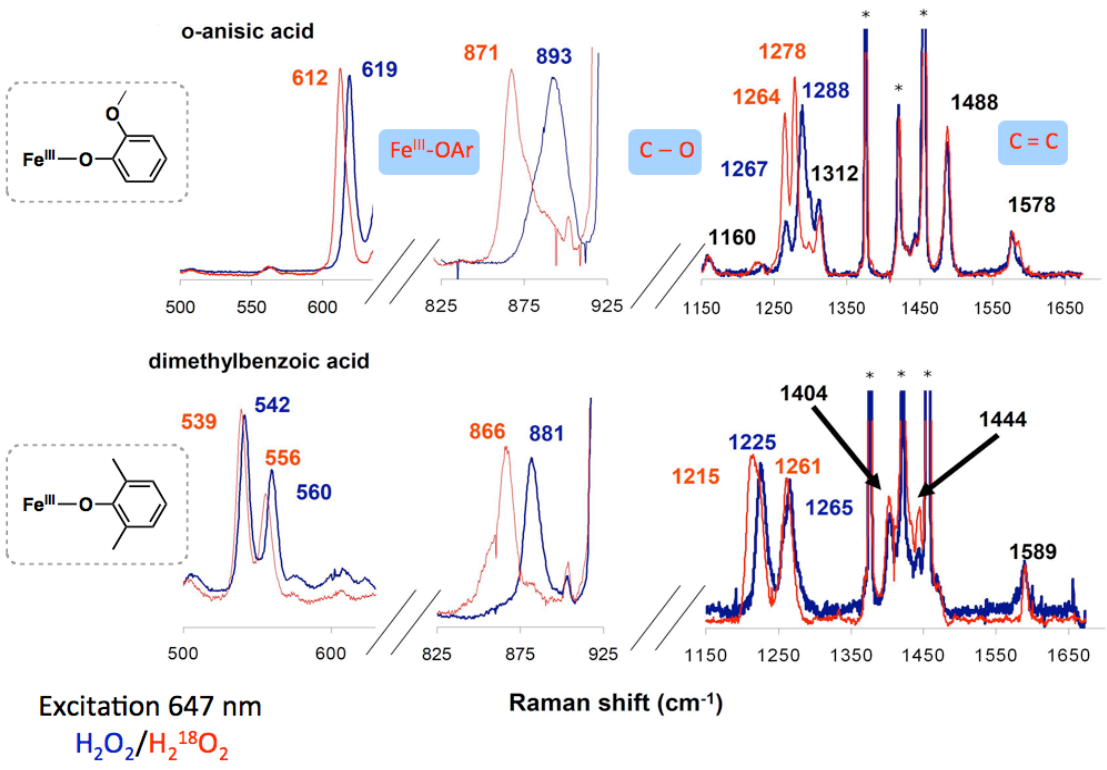

Figure 1-3**.** Resonance Raman spectra of the green complexes generated in acetonitrile at -40 °C by mixing **1,** 2-methoxybenzoic acid and hydrogen peroxide (above) and **1**, 2,6-dimethylbenzoic acid and hydrogen peroxide (below). Spectra in blue were obtained with $H_2{}^{16}O_2$, while spectra in red were obtained with $H_2{}^{18}O_2$. Spectra were acquired on frozen samples at 77 K with 647 nm excitation. Solvent peaks were denoted with *.

Table 1-2. Raman vibrations of iron(III)-phenolate complexes

Species / Complex	Raman Shift, cm^{-1} (D-^{18}O)					Ref
	n(Fe-O)		d(C-H)	n(C-O)	n(C=C)	
$[Fe^{III}$(BPMEN)(2-MeO-phenolate)$]^{2+}$	619 (-7)	893 (-22)	1160	1267 (-3), 1288 (-10), 1312	1488, 1578	This Work
$[Fe^{III}$(BPMEN)(2,6-Me_2-phenolate)$]^{2+}$	542 (-3), 560 (-4)	881 (-15)		1225 (-10) 1265 (-4)	1404, 1444, 1589	This Work
$[Fe^{III}Tp^{Ph2*}OBz]$	621 (-16)	861(-17), 961 (-19)		1254 (-9), 1273, 1298 (-4)	1451, 1480, 1559, 1598, 1606	[28]
ortho-hydroxylated Fe^{III}(6-PhTPA)	626, 642 662		1127, 1160	1249, 1279, 1297, 1314	1408, 1483, 1555, 1573, 1596	[29]
meso-$[Fe(EHPG)]^{-}$	614, 633	827, 893	1050, 1112, 1154	1270, 1366	1454, 1478, 1565, 1596	[57]
$[Fe^{III}$(salen)(4-Me-phenolate)$]^{2+}$	568 (-10)		1168	1272	1501, 1602	[56]

To provide further evidence for our description of the observed intermediates as Fe^{III}-phenolate species, the $[Fe^{III}$(BPMEN)(2-MeO-phenolate)$]^{2+}$ complex was independently prepared from reaction of **1,** 2-methoxyphenol and 1 equiv of Ce(IV) salt (Figure A4), and its Raman spectrum was recorded (Figure A5). The spectrum exhibited exactly the same features observed for the reaction of **1**, 2-methoxybenzoic acid and H_2O_2, confirming the identity of the observed hydroxylated complex (Figure 1-3). Thus the green chromophores in these reactions are Fe^{III}-phenolate complexes that formed *via* oxidative decarboxylation of benzoic acid substrates and subsequent *ipso*-hydroxylation.

Further experiments established that *ipso*-hydroxylation extended beyond the two examples described above. This transformation depended on the nature of the iron complex (**1** *vs.* **2**), the electronic properties of substituents on the benzoic acid, and their position with respect to -COOH group (Table 1-1). *Ipso*-hydroxylation could be observed for benzoic acids with either electron donating or electron withdrawing substituents in the 2- or 4-position, but not for 3-substituted benzoic acids where only *ortho*-hydroxylation was found. For some substrates, both *ortho*- and *ipso*-hydroxylation were observed (Table 1-1).

Despite their differences towards *ortho*-hydroxylation, both complexes **1** and **2** behaved similarly towards *ipso*-hydroxylation. Substituents that increase electron density in the *ipso* position with respect to carboxylate group promoted decarboxylation leading to *ipso*-hydroxylation. Blocking the sites for *ortho*-hydroxylation by placing substituents in 2- or and/or 6-positions with respect to carboxylate, also favored *ipso*-hydroxylation. *Meta*-substituted benzoic acids studied in this work did not afford *ipso*-hydroxylation products. Electron-withdrawing (NO_2, Cl) *meta* substituents drastically decreased electron density in the *ipso*-position and prevented the electrophilic attack by the metal-based oxidant, hampering the *ipso*-hydroxylation process. On the other hand, strong electron donating substituents (MeO) *meta* with respect to carboxylate preferentially underwent a competing electrophilic attack at the most electron-rich site of the aromatic ring, yielding *ortho*-hydroxylated products (salicylates).

1.2.3 Mechanistic insights

The similar reactivity profiles of complexes **1** and **2** suggest a common reaction mechanism (Scheme 1-3) for aromatic hydroxylations promoted by these two non-heme iron complexes. The regioselectivity of these reactions, which results in the incorporation of an –OH group either next to or in place of the carboxylate substituent, indicates a metal-based oxidant, rather than hydroxyl radical that would derive from metal promoted O-O bond homolysis of H_2O_2. Reactivity trends suggest that the oxidant is electrophilic. Coordination of aromatic carboxylic acids to **1** or **2** positions the aromatic ring in the immediate vicinity of the redox-active metal center. Isotope substitution studies provide additional insight into possible hydroxylation mechanisms. Experiments with the deuterated substrate, d_5-PhCOOH, exhibited no significant H/D kinetic isotope effect on the rates of *ortho*-hydroxylation with H_2O_2 in the presence of complex **1**. Competition experiments also showed no preference of **1** in reacting with either protio or deuterio isotopomers (Dr. Sonia Taktak, thesis), so C-H bond breaking on the phenyl ring cannot be a rate limiting step in this transformation.[36] Similarly small H/D KIE values (≤ 1) were also reported for other aromatic oxidations promoted by biological and synthetic iron centers,[8, 27, 29, 61-64] and interpreted in terms of either a rate-limiting formation of an iron-oxo intermediate[29] or a rate-limiting electrophilic attack of the aromatic ring by a metal-based oxidant (a process that is typically characterized by a small inverse isotope effect).[27, 61, 62, 65, 66]

^{18}O-labeling experiments with $H_2{}^{18}O_2$ unambiguously showed the incorporation of one oxygen atom into the phenolate or salicylate product derived from the oxidations of

benzoic acids, underscoring the fact that hydrogen peroxide is the sole source of the oxygen atom incorporated into the products. This conclusion applies to both *ortho*-hydroxylation and decarboxylation/*ipso*-hydroxylation, as determined by mass spectrometry (Figure A6 – Partha Das and Figure A7 - Dr. Sonia Taktak, thesis) and/or resonance Raman spectroscopy (Figure 1-3). Thus the metal-based oxidant must derive from the combination of the iron catalyst and H_2O_2.

An obvious starting point with respect to the identity of the metal-based oxidant is an Fe^{III}-OOH intermediate. Such species have been observed for both **1**[47, 48] and **2**.[50, 51] Although **1** afforded higher yields of aromatic hydroxylation than **2** (Table 1)**,** the Fe^{III}-OOH intermediate of **2** can be obtained in much higher yield and is thus better characterized. While the hydroperoxo intermediate of **1** was observed by low-temperature EPR,[48] its optical signature was not reported until our later work (see next chapter). We thus focused on experiments with **2** in our efforts to identify the active oxidant(s) in aromatic hydroxylation of benzoic acids with H_2O_2.

As previously reported, the reaction of **2** and excess H_2O_2 in CH_3CN at -40 °C gave the corresponding Fe^{III}-OOH intermediate (**2**a) with a λ_{max} at 540 nm (Figure 1-4, dashed-line spectra). Subsequent addition of 3-methoxybenzoic acid to this intermediate elicited a new band at 650 nm that is associated with the formation of the corresponding salicylate complex (Figure 1-4, solid-line spectra). Reversing the order of addition of the oxidant and the substrate also generated the same chromophore at 650 nm, but the 540-nm absorption feature of the Fe^{III}-OOH species was much less pronounced (Figure A8). Similar spectral changes were observed in parallel experiments for 2-

methoxybenzoic acid (Figure A9 and Figure A10). The Fe^{III}-OOH intermediate would thus appear to be involved in the aromatic hydroxylation.

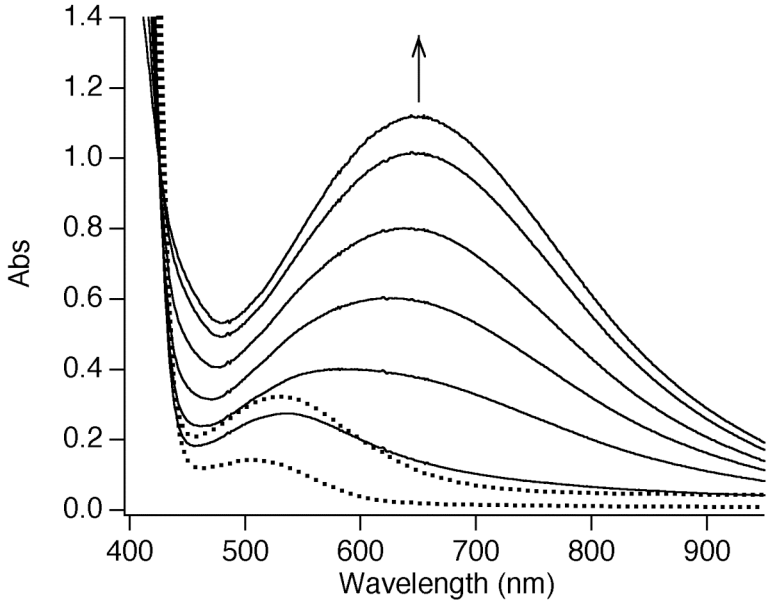

Figure 1-4. Spectral changes observed in the reaction of **2** (1 mM) with 3 equiv H_2O_2 and 12 equiv 3-methoxybenzoic acid at -40 °C. Dashed lines represent spectra obtained immediately after mixing **2** and H_2O_2 and after 9 min. Solid lines correspond to spectra obtained subsequent to the addition of 3-methoxybenzoic acid (taken at 10, 20, 50, 90, 150 and 210 min after addition of the acid).

Scheme 1-3 illustrates the various possible roles of the Fe^{III}-OOH intermediate (**1b** or **2b**) in this reaction, where it could either be the oxidant itself or the precursor thereof. A similar mechanistic landscape was discussed previously for olefin epoxidation and *cis*-dihydroxylation with H_2O_2/**1** or **2.**[43, 44] Three pathways were considered for the evolution of the Fe^{III}-OOH intermediate. The hydroperoxo ligand could attack the carboxylate of the bound benzoic acid to generate an acylperoxoiron(III) species (**1c** or

2c in Scheme 1-3). Formation of such an acetylperoxoiron(III) species has been detected[48] in a mixture of **1,** acetic acid, and H_2O_2, but the yield was very low. In addition, Nam and co-workers [37] reported the self-hydroxylation of peroxybenzoic acids in the presence of **2** to form salicylate products. This pathway however requires the formation of a doubly-labeled salicylate product from labeled H_2O_2 (Scheme 1-3). Since only singly labeled salicylate is observed in the ^{18}O-labeling experiments, this pathway can be excluded as the mechanistic option for the aromatic hydroxylations under our experimental conditions.

A second option for the evolution of the Fe^{III}-OOH intermediate is O-O bond homolysis, which would afford $[(TPA)Fe^{IV}(O)]^{2+}$ and hydroxyl radical (**1d** or **2d** in Scheme 1-3). The oxidative power of the Fe^{IV}=O species has been demonstrated in several iron-promoted oxidation reactions,[27, 54, 67-70] including aromatic hydroxylation of anthracene.[27] In fact, Fe^{IV}=O complexes were also detected in the reactions of **1** or **2** with hydrogen peroxide and acetic acid.[44, 48] However, a detailed study on **2**-catalyzed olefin epoxidation[44] clearly excluded $[(TPA)Fe^{IV}=O]^{2+}$ as the oxidant in this transformation. Similarly, even though we found that *meta*-chlorobenzoic acid was *ortho*-hydroxylated by **2** and H_2O_2 (Table 1), $[(TPA)Fe^{IV}=O]^{2+}$ did not effect the *ortho*-hydroxylation of *meta*-chlorobenzoic acid.[37] Even the more reactive electron-rich substrates (3-methoxybenzoic acid for *ortho*-hydroxylation, and 2-methoxybenzoic acid for *ipso*-hydroxylation) were not oxidized by independently generated $[(TPA)Fe^{IV}=O]^{2+}$ (Figure A11 and Figure A12, Partha Das, University of Minnesota). These observations conclusively eliminate Fe^{IV}=O as a probable oxidant in these aromatic hydroxylation

reactions. Furthermore, since hydroxyl radicals are known to attack benzoic acid, affording a statistical mixture of *o*-, *m*, and *p*-hydroxylated products,[71] the observed regioselectivity of aromatic hydroxylation with H_2O_2/**1** or **2** excludes the participation of OH-radicals.

With the arguments presented above, only two possible pathways remain for the Fe^{III}-OOH intermediate en route to the observed aromatic hydroxylation products (Scheme 1-3): either direct electrophilic attack of the organic substrate, or heterolytic cleavage of the O-O bond to generate a formally Fe^{V}=O species [43, 44, 72] that attacks the iron-bound benzoic acid. The limited existing data on the reactivity of Fe^{III}-OOH species[40] indicate that these appear to be sluggish oxidants.[73] In particular, the decay of $[(TPA)Fe^{III}(OOH)]^{2+}$ at -45 ˚C was shown not to depend on thioanisole or cyclohexene concentration,[73] although such substrates were oxidized by the combination of **2** and H_2O_2 at higher temperatures. We thus favor the carboxylic acid-assisted O-O bond heterolysis pathway leading to an unobserved Fe^{V}=O oxidant, which was postulated by Mas-Ballesté and Que in the efficient **2**-catalyzed epoxidation of olefins by H_2O_2 in the presence of acetic acid.[44] Although it may be argued that a direct electrophilic attack of the aromatic ring by **2b** is plausible, particularly for benzoic acids with electron donating substituents, the broad scope of both *ortho*- and *ipso*-hydroxylation reactions promoted by **1** and **2** suggests that a highly electrophilic intermediate is likely to be involved, which we propose is **1e** or **2e**. A similar oxidant has been proposed for the **2**-catalyzed self-hydroxylation of aryl peroxyacids,[37] for the intramolecular hydroxylation of the aromatic ring covalently appended to the analog of **1**,[33] and for the *ortho*-hydroxylation

of benzyl alcohol by another aminopyridine iron complex.[74] Although only one non-heme iron(V)-oxo complex has been directly observed at low temperature as a transient species and characterized by a variety of spectroscopic methods,[75] indirect evidence supporting participation of non-heme Fe(V)-oxo intermediates in oxidations of alcohols,[76] olefins,[43, 76, 77] and arenes[33, 74, 78] continues to accumulate. The coordination of the carboxylate *cis* to the oxo moiety in the putative oxoiron(V) oxidant **1e** or **2e** positions the aromatic ring well for the attack of the oxo group at the carbon atom *ortho* to the carboxylate function. Such an attack would form a six-membered ring in the transition state, facilitating formation of the product complex with a bidentate salicylate. Such directed reactivity was reported for an iron catalyst closely related to **1** by Chen and White.[79] The substrates that are consistently *ortho*-hydroxylated are those with substituents *meta* to the carboxylate functionality; in no case is *ipso*-hydroxylation observed. In addition, higher yields of salicylate products are obtained for substituents that enhance electron density at the carbon *ortho* or *para* to the substituent. The one exception is 3-methoxybenzoic acid, but the lower yield of salicylate is likely to result from over-oxidation.

In contrast, *ipso*-hydroxylation products are formed for benzoic acids with *ortho* or *para* substituents. The observation of *ipso*-hydroxylation products can most easily be rationalized by postulating formation of a coordinated arylcarboxyl radical (**1f** or **2f**) that undergoes spontaneous loss of CO_2,[44, 80] affording an aryl radical that immediately rebounds with the oxoiron(IV) center to form the phenolate product. The radical may derive from O-O bond homolysis of the precursor $Fe^{III}(OOH)(O_2CAr)$ intermediate (**1b** or

2b) or intramolecular electron transfer from the coordinated carboxylate to the oxoiron(V) center in **1e** or **2e**, in both cases generating the carboxyl radical and an oxoiron(IV) center. Oxidative decarboxylation is precedented in the reaction of phenylacetic acid with **2** and H_2O_2, where benzyl radical is formed and then trapped by O_2 to yield benzaldehyde as the observed product.[44] Unlike the resonance-stabilized benzyl radical, the phenyl radical would be expected to be short-lived and undergo rapid oxygen rebound. The fact that *ortho*-substituted benzoic acids are converted mainly to *ipso*-hydroxylation products suggests that steric factors may promote this reactivity mode, but the observation of low yields of phenols derived from electron-poor substrates (such as nitro-benzoic acids) indicate that electronic factors also contribute to the efficiency of *ipso*-hydroxylation. Since certain substrates can yield both *ortho*- and *ipso*-hydroxylation products, these reactions must proceed via competing pathways. The factors governing the outcome of this competition include relative electron density in the *ortho*- and *ipso*-positions, and steric accessibility of the *ortho* sites.

The reactivity data summarized in Table 1 show that **1** hydroxylates a broader range of substrates and often affords higher yields of hydroxylated products compared to **2**, strongly suggesting that a more powerful oxidant is generated in the case of the former. This notion is supported by the higher yields of cyclohexane oxidation products in the reactions of H_2O_2 with **1** or **2**.[45] Perhaps the three pyridine ligands in **2** (versus two in **1**) better stabilize the higher iron oxidation states required for the oxidation reactions. Indeed Fe^{III}-OOH and Fe^{IV}=O intermediates of **2** have been found to be stable enough to

accumulate at low temperature and be characterized by a number of spectroscopic methods.[50, 51, 54] In contrast, corresponding species of **1** are only fleetingly observed.[47, 48]

In summary, highly regioselective hydroxylation of a broad range of substituted aromatic acids with hydrogen peroxide in the presence of **1** or **2** proceeds readily at room temperature. The hydroxylation occurs exclusively in the vicinity of the anchoring carboxylate functional group: *ortho*-hydroxylation affords salicylates, and *ipso*-attack results in decarboxylation and *ipso*-hydroxylation, yielding phenolates. A similar proximity effect can be postulated for the highly selective hydroxylation of tertiary C-H bonds on carbons gamma to the carboxylate functionality in what Chen and White call the carboxylate-directed method to form 5-membered lactone rings.[79] An electrophilic, metal-based oxidant must be involved in carboxylic-acid directed aromatic hydroxylation. Fe^{IV}=O species are unreactive in aromatic hydroxylations described herein. Fe^{III}-OOH is definitely involved in the hydroxylation pathways, most likely via intramolecular acid-assisted O-O bond heterolysis, yielding transient, highly reactive Fe^{V}=O that has yet to be observed.

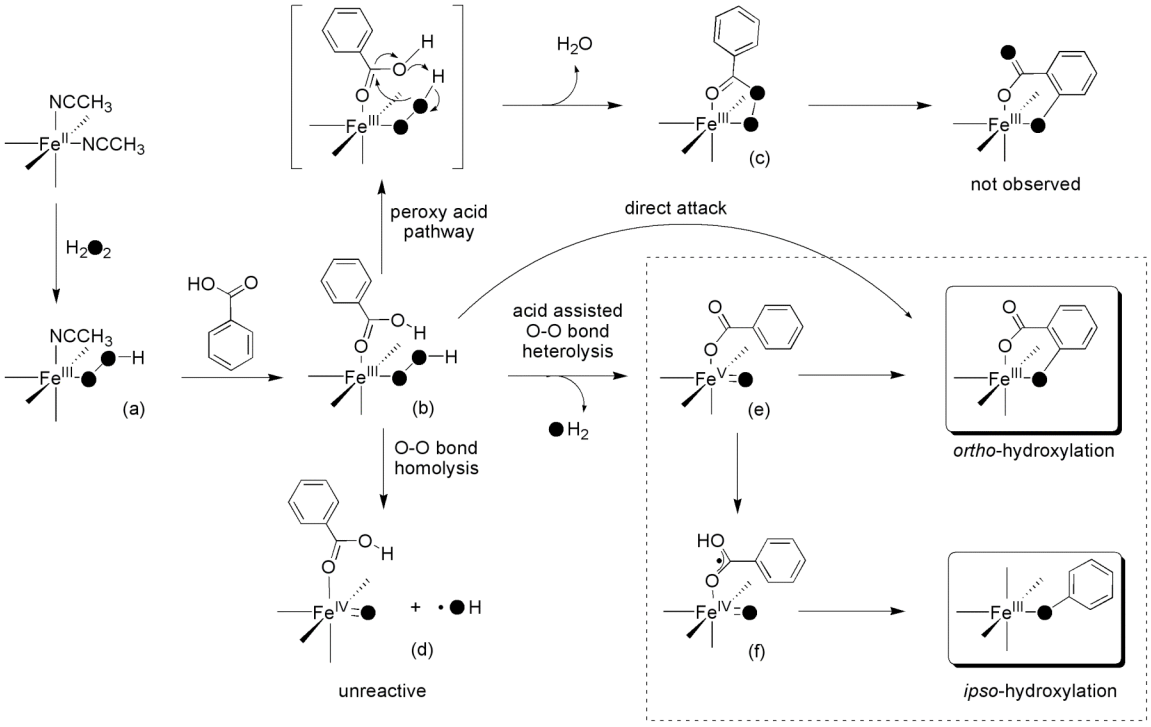

Scheme 1-3. Mechanisms of *ortho*-hydroxylation and *ipso*-hydroxylation by **1** and **2**.

1.3 **Experimental section**

1.3.1 Materials and methods

All chemicals and solvents were purchased from Aldrich, Acros Organics or Fisher Scientific and were used without additional purification unless otherwise noted. CH_3CN solvent was dried over CaH_2 before use. $H_2{}^{18}O_2$ (90% ^{18}O-enriched, 2% solutions in $H_2{}^{16}O$) was obtained from Cambridge Isotope Laboratories Inc. (Andover, MA). The complexes $[Fe^{II}(BPMEN)(CH_3CN)_2(ClO_4)_2]$ (**1**) and $[Fe^{II}(TPA)(CH_3CN)_2(OTf)_2]$ (**2**) were prepared in an anaerobic glove box according to the published procedures.[45, 54] UV-vis spectra were acquired on a JASCO V-570 spectrophotometer or a Hewlett-Packard (Agilent) 8452 diode array spectrophotometer over a 190-1100 nm range. In some

experiments quartz cuvettes were cooled to the desired temperature in a liquid nitrogen cryostat by Unisoku Co. Ltd. (Osaka, Japan). ESI-MS spectra were obtained on a Finnigan LTQ mass spectrometer or a Bruker Biotof-II mass spectrometer under conditions of a spray chamber voltage of 4000 Volt and a dry gas temperature of 200 °C. GCMS experiments were carried out using a Shimadzu GC-17A gas chromatograph (Rtx-xLB column) with a GCMS-QP 5050 mass detector or using an HP 6890 gas chromatograph (HP-5 column, 30m) with an Agilent 5973 mass detector. NMR spectra were recorded on a Bruker DPX-300 spectrometer or a Varian Unity 500 spectrometer at ambient temperature. Chemical shifts (ppm) were referenced to the residual protic solvent peaks. Resonance Raman spectra were collected on an Acton AM-506 spectrometer (1200 groove grating) using a Kaiser Optical holographic super-notch filters with a Princeton Instruments liquid-N_2-cooled (LN-1100PB) CCD detector with a 4 cm^{-1} spectral resolution. The 647 cm^{-1} laser excitation line was obtained with a Spectra Physics BeamLok 2060-KR-V krypton ion laser. The Raman frequencies were referenced to indene. Baseline corrections (polynomial fits) were carried out using Grams/32 Spectral Notebase Version 4.04 (Galactic). Time-resolved spectra of rapid hydroxylation reactions were acquired with TgK Scientific (formerly HiTech Schientific, Salisbury, Wiltshire, UK) SF-61DX2 cryogenic Stopped-flow system equipped with J&M Diode array (Spectralytics).

1.3.2 UV-vis studies of aromatic hydroxylation reactions

Ortho- and *ipso*-hydroxylation of various aromatic acids in the presence of **1** or **2** were performed by mixing the iron complex (0.5 mM – 1 mM) with 2 equiv acid in acetonitrile in a glove box and then adding 3 equiv of hydrogen peroxide at room temperature. Spectroscopic experiments with $[Fe^{II}(TPA)(CH_3CN)_2(OTf)_2]$ were performed on a 1 mM solution of **2** in CH_3CN in a 1 cm quartz cuvette precooled at -40 °C. A total of 87 mL of .07 M H_2O_2 (3 equiv) was added to a solution containing the iron complex and excess amount (12 equiv) of 3-methoxybenzoic acid. In other experiments meta stable $[(TPA)Fe^{III}(OOH)]^{2+}$ species was generated by adding 3 equiv of H_2O_2 to 1 mM solution of **2** at -40 °C. $[(TPA)Fe^{IV}(O)]^{2+}$ species was generated at -40 °C in acetonitrile by adding 0.03 mL of 0.07 M (1 equiv) CH_3CO_3H to the 1 mM solution of **2** according to the published procedure.[54]

1.3.3 Identification of ortho*-hydroxylation products by NMR*

For the identification of *ortho*-hydroxylated products, **1** (0.12 mmol, 72 mg) was dissolved in 20 mL of acetonitrile under argon atmosphere in a glove box and mixed with 1 equiv of substituted benzoic acid. A further 1.5 equiv of H_2O_2 solution was added to the prepared mixture. The solution was stirred for 20-30 min. In the next step, complex was decomposed by treating with aqueous Na_2EDTA solution (20 ml, 5% solution) followed by addition of concentrated HCl (final pH was about 0). Organic products were extracted with ethylacetate (3 x 20 mL) and the extract was dried over

$MgSO_4$. Evaporation of solvent resulted in brown residues (soluble in chloroform) that were analyzed by ^1H NMR.

1.3.4 Identification of ipso*-hydroxylation products by GCMS*

A mixture of complex **1** or **2** (1 mM) and 2 equiv of aromatic acid in acetonitrile was prepared under argon. H_2O_2 (3 equiv vs iron) was delivered into 1 mL of the mixture upon vigorous stirring. The reaction was quenched with 1-methylimidazole (0.1 mL) in 30 minutes followed by the addition of 1 mL acetic anhydride to esterify the products. Naphthalene or nitrobenzene was added as an internal standard. Organic products were extracted with chloroform or dichloromethane (1-2 mL) and subjected to the GC and GC-MS analysis. All experiments were run at least in duplicate, the reported data is the average of these reactions.

1.3.5 Resonance Raman studies and labeling experiments

To a solution of **1** (1 mM) in acetonitrile 1.5 equivalents of 2-methoxybenzoic or 2,6-dimethylbenzoic acid and 3 equivalents of H_2O_2 were added. The solution was analyzed by resonance Raman spectroscopy. Alternatively, $[Fe^{III}(BPMEN)(2\text{-}MeO\text{-}phenolate)]^{2+}$ complex was generated by injecting one equivalent of $(NH_4)_2Ce(NO_3)_6$ to the anaerobic solution of **1** (1 mM) and 2-methoxyphenol (2 mM) in acetonitrile, and also analyzed by Raman spectroscopy. Labeling experiments were carried out using solutions diluted in CH_3CN of $H_2{}^{18}O_2$ prepared from 2 % solution in $H_2{}^{16}O$ of 90 % ^{18}O-enriched hydrogen peroxide. The resulting green solutions were frozen 2-3 minutes after addition of the

oxidant (H_2O_2 or $(NH_4)_2Ce(NO_3)_6$) at 77 K using a gold-plated copper cold finger in thermal contact with a dewar containing liquid N_2. No photobleaching was observed upon repeated scans.

1.3.6 Crystallographic Studies (this work was done by Partha Das from University of Minnesota)

Each crystal was placed onto the tip of a 0.1 mm diameter glass capillary and mounted on a CCD area detector diffractometer for a data collection at 173(2) K.[81] A preliminary set of cell constants was calculated from reflections harvested from three sets of 20 frames. These initial sets of frames were oriented such that orthogonal wedges of reciprocal space were surveyed. This produced initial orientation matrices determined from 67 reflections for $[Fe^{III}(TPA)(5\text{-MeO-salicylate})]^+$ and 44 reflections for $[Fe^{III}(TPA)(salicylate)]^+$. The data collection was carried out using MoKa radiation (graphite monochromator) with a frame time of 60 seconds and a detector distance of 4.9 cm. A randomly oriented region of reciprocal space was surveyed to the extent of one sphere and to a resolution of 0.84 Å. Four major sections of frames were collected with 0.30º steps in w at four different f settings and a detector position of -28º in 2q. The intensity data were corrected for absorption and decay (SADABS).[82] Final cell constants were calculated from 2717 (for $[Fe^{III}(TPA)(5\text{-MeO-salicylate})]^+$) and 2950 (for $[Fe^{III}(TPA)(salicylate)]^+$) strong reflections from the actual data collection after integration (SAINT).[83] Please refer to Table S2-S3 for additional crystal and refinement information. The structure was solved and refined using Bruker SHELXTL.[84] The space

groups for $[Fe^{III}(TPA)(5\text{-MeO-salicylate})]^+$ and $[Fe^{III}(TPA)(salicylate)]^+$ were Fdd2 and P2(1)/n, respectively and were determined based on systematic absences and intensity statistics. A direct-methods solution was calculated which provided most non-hydrogen atoms from the E-map. Full-matrix least squares / difference Fourier cycles were performed which located the remaining non-hydrogen atoms. All non-hydrogen atoms were refined with anisotropic displacement parameters. All hydrogen atoms were placed in ideal positions and refined as riding atoms with relative isotropic displacement parameters. The final full matrix least squares refinement converged to $R1 = 0.0368$ and $wR2 = 0.0850$ for $[Fe^{III}(TPA)(5\text{-MeO-salicylate})]^+$ and $R1 = 0.0566$ and $wR2 = 0.1616$ for $[Fe^{III}(TPA)(salicylate)]^+$. CCDC-732099 & 732100 contain the supplementary crystallographic data for this paper. These data can be obtained free of charge from The Cambridge Crystallographic Data Centre via www.ccdc.cam.ac.uk/data_request/cif.

1.4 **References:**

[1] T. Flatmark, R. C. Stevens, *Chem. Rev.* **1999**, *99*, 2137.
[2] P. F. Fitzpatrick, *Biochemistry* **2003**, *42*, 14083.
[3] M. M. Abu-Omar, A. Loaiza, N. Hontzeas, *Chem. Rev.* **2005**, *105*, 2227.
[4] T. L. Foster, J. P. Caradonna, in *Comprehensive Coordination Chemistry II, Vol. 8* (Eds.: J. McCleverty, T. J. Meyer), Elsevier, Amsterdam, **2004**, pp. 343.
[5] P. C. A. Bruijnincx, G. van Koten, R. J. M. Klein Gebbink, *Chem. Soc. Rev.* **2008**, *37*, 2716.
[6] A. Fishman, Y. Tao, L. Rui, T. K. Wood, *J. Biol. Chem.* **2005**, *280*, 506.
[7] M. H. Sazinsky, J. Bard, A. D. Donato, S. J. Lippard, *J. Biol. Chem.* **2004**, *279*, 30600.
[8] K. H. Mitchell, C. E. Rogge, T. Gierahn, B. G. Fox, *Proc. Natl. Acad. Sci. U.S.A.* **2003**, *100*, 3784.
[9] L. J. Murray, S. J. Lippard, *Acc. Chem. Res.* **2007**, *40*, 466.
[10] B. E. Eser, E. W. Barr, P. A. Frantom, L. Saleh, J. M. Bollinger, C. Krebs, P. F. Fitzpatrick, *J. Am. Chem. Soc.* **2007**, *129*, 11334.
[11] C. Krebs, D. G. Fujimori, C. T. Walsh, J. M. Bollinger, *Acc. Chem. Res.* **2007**, *40*, 484.
[12] J. M. Bollinger Jr., C. Krebs, *J. Inorg. Biochem.* **2006**, *100*, 586.
[13] A. Liu, Y. Jin, J. Zhang, B. J. Brazeau, J. D. Lipscomb, *Biochem. Biophys. Res. Commun.* **2005**, *338*, 254.
[14] S.-K. Lee, J. C. Nesheim, J. D. Lipscomb, *J. Biol. Chem.* **1993**, *268*, 21569.
[15] S.-K. Lee, B. G. Fox, W. A. Froland, J. D. Lipscomb, E. Münck, *J. Am. Chem. Soc.* **1993**, *115*, 6450.
[16] C. Walling, R. A. Johnson, *J. Am. Chem. Soc.* **1975**, *97*, 363.
[17] T. Kurata, Y. Watanabe, M. Katoh, Y. Sawaki, *J. Am. Chem. Soc.* **1988**, *110*, 7472.
[18] D. T. Sawyer, A. Sobkowiak, T. Matsushita, *Acc. Chem. Res.* **1996**, *29*, 409.
[19] S. Udenfriend, C. T. Clark, J. Axelrod, B. B. Brodie, *J. Biol. Chem.* **1954**, *208*, 731.
[20] J. P. Hage, J. A. Powell, D. T. Sawyer, *J. Am. Chem. Soc.* **1995**, *117*, 12897.
[21] T. Tezuka, N. Narita, W. Ando, S. Oae, *J. Am. Chem. Soc.* **1981**, *103*, 3045.
[22] D. Mathieu, Y.-M. Frapart, J. F. Bartoli, J.-L. Boucher, P. Battioni, D. Mansuy, *Chem. Commun.* **2004**, 54.
[23] V. Balland, M.-F. Charlot, F. Banse, J.-J. Girerd, T. A. Mattioli, E. Bill, J.-F. Bartoli, P. Battioni, D. Mansuy, *Eur. J. Inorg. Chem.* **2004**, 301.
[24] J.-F. Bartoli, F. Lambert, I. Morgenstern-Badarau, P. Battioni, D. Mansuy, *C. R. Chim.* **2002**, *5*, 263.
[25] D. Bianchi, M. Bertoli, R. Tassinari, M. Ricci, R. Vignola, *J. Mol. Catal. A : Chem.* **2003**, *204*, 419.
[26] G. A. Hamilton, J. W. Hanifin, J. P. Friedman, *J. Am. Chem. Soc.* **1966**, *88*, 5269.
[27] S. P. de Visser, K. Oh, A.-R. Han, W. Nam, *Inorg. Chem.* **2007**, *46*, 4632.
[28] M. P. Mehn, K. Fujisawa, E. L. Hegg, L. Que Jr., *J. Am. Chem. Soc.* **2003**, *125*, 7828.

[29] M. P. Jensen, S. J. Lange, M. P. Mehn, E. L. Que, L. Que Jr., *J. Am. Chem. Soc.* **2003**, *125*, 2113.
[30] S. Ménage, J.-B. Galey, J. Dumats, G. Hussler, M. Seité, I. G. Luneau, G. Chottard, M. Fontecave, *J. Am. Chem. Soc.* **1998**, *120*, 13370.
[31] H. Furutachi, M. Murayama, A. Shiohara, S. Yamazaki, S. Fujinami, A. Uehara, M. Suzuki, S. Ogo, Y. Watanabe, Y. Maeda, *Chem. Commun.* **2003**, 1900.
[32] F. Avenier, L. Dubois, J.-M. Latour, *New J. Chem.* **2004**, *28*, 782.
[33] A. Nielsen, F. B. Larsen, A. D. Bond, C. J. McKenzie, *Angew. Chem. Int. Ed.* **2006**, *45*, 1602.
[34] M. Yamashita, H. Furutachi, T. Tosha, S. Fujinami, W. Saito, Y. Maeda, K. Takahashi, K. Tanaka, T. Kitagawa, M. Suzuki, *J. Am. Chem. Soc.* **2007**, *129*, 2.
[35] N. Kitajima, M. Ito, H. Fukui, Y. Morooka, *J. Am. Chem. Soc.* **1993**, *115*, 9335.
[36] S. Taktak, M. Flook, B. M. Foxman, L. Que Jr., E. V. Rybak-Akimova, *Chem. Commun.* **2005**, 5301.
[37] N. Y. Oh, M. S. Seo, M. H. Lim, M. B. Consugar, M. J. Park, J.-U. Rohde, J. Han, K. M. Kim, J. Kim, L. Que Jr., W. Nam, *Chem. Commun.* **2005**, 5644.
[38] S. Tanase, E. Bouwman, *Adv. Inorg. Chem.* **2006**, *58*, 29.
[39] M. Costas, M. P. Mehn, M. P. Jensen, L. Que Jr., *Chem. Rev.* **2004**, *104*, 939.
[40] S. V. Kryatov, E. V. Rybak-Akimova, S. Schindler, *Chem. Rev.* **2005**, *105*, 2175.
[41] L. Que Jr., W. B. Tolman, *Nature* **2008**, *455*, 333.
[42] M. C. White, A. G. Doyle, E. N. Jacobsen, *J. Am. Chem. Soc.* **2001**, *123*, 7194.
[43] K. Chen, M. Costas, J. Kim, A. K. Tipton, L. Que Jr., *J. Am. Chem. Soc.* **2002**, *124*, 3026.
[44] R. Mas-Ballesté, L. Que Jr., *J. Am. Chem. Soc.* **2007**, *129*, 15964.
[45] K. Chen, L. Que Jr., *Chem. Commun.* **1999**, 1375.
[46] K. Chen, L. Que Jr., *J. Am. Chem. Soc.* **2001**, *123*, 6327.
[47] E. A. Duban, K. P. Bryliakov, E. P. Talsi, *Mendeleev Commun.* **2005**, *15*, 12.
[48] E. A. Duban, K. P. Bryliakov, E. P. Talsi, *Eur. J. Inorg. Chem.* **2007**, 852.
[49] C. Kim, K. Chen, J. Kim, L. Que Jr., *J. Am. Chem. Soc.* **1997**, *119*, 5964.
[50] R. Y. N. Ho, G. Roelfes, B. L. Feringa, L. Que Jr., *J. Am. Chem. Soc.* **1999**, *121*, 264.
[51] A. Mairata i Payeras, R. Y. N. Ho, M. Fujita, L. Que Jr., *Chem. Eur. J.* **2004**, *10*, 4944
[52] Y. Zang, J. Kim, Y. Dong, E. C. Wilkinson, E. H. Appelman, L. Que Jr., *J. Am. Chem. Soc.* **1997**, *119*, 4197.
[53] N. Lehnert, R. Y. N. Ho, L. Que Jr., E. I. Solomon, *J. Am. Chem. Soc.* **2001**, *123*, 8271.
[54] M. H. Lim, J.-U. Rohde, A. Stubna, M. R. Bukowski, M. Costas, R. Y. N. Ho, E. Münck, W. Nam, L. Que Jr., *Proc. Natl. Acad. Sci. U.S.A* **2003**, *100*, 3665.
[55] I. V. Korendovych, S. V. Kryatov, E. V. Rybak-Akimova, *Acc. Chem. Res.* **2007**, *40*, 510.
[56] J. W. Pyrz, A. L. Roe, L. J. Stern, L. Que Jr., *J. Am. Chem. Soc.* **1985**, *107*, 614.
[57] C. J. Carrano, M. W. Carrano, K. Sharma, G. Backes, J. Sanders-Loehr, *Inorg. Chem.* **1990**, *29*, 1865.

[58] K. D. Sharma, L. A. Andersson, T. M. Loehr, J. Terner, H. M. Goff, *J. Biol. Chem.* **1989**, *264*, 12772.
[59] L. Que Jr., *Coord. Chem. Rev.* **1983**, *50*, 73.
[60] L. Que Jr., in *Biological Applications of Raman Spectroscopy, Vol. 3* (Ed.: T. G. Spiro), John Wiley & Sons, New York, **1988**, pp. 491.
[61] K. R. Korzekwa, D. C. Swinney, W. F. Trager, *Biochemistry* **1989**, *28*, 9019.
[62] M.-J. Kang, W. J. Song, A.-R. Han, Y. S. Choi, H. G. Jang, W. Nam, *J. Org. Chem.* **2007**, *72*, 6301.
[63] E. V. Kudrik, A. B. Sorokin, *Chem. Eur. J.* **2008**, *14*, 7123.
[64] J. A. Pavon, P. F. Fitzpatrick, *Biochemistry* **2006**, *45*, 11030.
[65] S. P. de Visser, S. Shaik, *J. Am. Chem. Soc.* **2003**, *125*, 7413.
[66] A. Sorokin, B. Meunier, *Eur. J. Inorg. Chem.* **1998**, 1269.
[67] J. Kaizer, E. J. Klinker, N. Y. Oh, J.-U. Rohde, W. J. Song, A. Stubna, J. Kim, E. Münck, W. Nam, L. Que Jr., *J. Am. Chem. Soc.* **2004**, *126*, 472.
[68] E. J. Klinker, S. Shaik, H. Hirao, L. Que Jr., *Angew. Chem. Int. Ed.* **2009**, *48*, 1291.
[69] W. Nam, *Acc. Chem. Res.* **2007**, *40*, 522.
[70] L. Que Jr., *Acc. Chem. Res.* **2007**, *40*, 493.
[71] G. W. Klein, K. Bhatia, V. Madhavan, R. H. Schuler, *J. Phys. Chem.* **1975**, *79*, 1767.
[72] A. Bassan, M. R. A. Blomberg, P. E. M. Siegbahn, L. Que Jr., *Chem. Eur. J.* **2005**, *11*, 692.
[73] M. J. Park, J. Lee, Y. Suh, J. Kim, W. Nam, *J. Am. Chem. Soc.* **2006**, *128*, 2630.
[74] J. Yoon, S. A. Wilson, Y. K. Jang, M. S. Seo, K. Nehru, B. Hedman, K. O. Hodgson, E. Bill, E. I. Solomon, W. Nam, *Angew. Chem. Int. Ed.* **2009**, *48*, 1257.
[75] F. T. de Oliveira, A. Chanda, D. Banerjee, X. Shan, S. Mondal, L. Que Jr., E. L. Bominaar, E. Münck, T. J. Collins, *Science* **2007**, *315*, 835.
[76] S. H. Lee, J. H. Han, H. Kwak, S. J. Lee, E. Y. Lee, H. J. Kim, J. H. Lee, C. Bae, S. N. Lee, Y. Kim, C. Kim, *Chem. Eur. J.* **2007**, *13*, 9393.
[77] A. Company, Y. Feng, M. Güell, X. Ribas, J. M. Luis, L. Que Jr., M. Costas, *Chem. Eur. J.* **2009**, *15*, 3359.
[78] Y. Feng, C. Ke, G. Xue, L. Que Jr., *Chem. Commun.* **2009**, 50.
[79] M. S. Chen, M. C. White, *Science* **2007**, *318*, 783.
[80] J. Wang, M. Tsuchia, K. Tokumaru, H. Sakuragi, *Tetrahedron* **1995**, *51*, 44.
[81] SMART V5.054, Bruker Analytical X-ray Systems, Madison, WI, **2001**.
[82] R. H. Blessing, *Acta Cryst. A* **1995**, *51*, 33.
[83] SAINT+ V6.45, Bruker Analytical X-Ray Systems, Madison, WI, **2003**.
[84] SHELXTL V6.14, Bruker Analytical X-Ray Systems, Madison, WI, **2000**.

2 Aromatic hydroxylation at a non-heme iron center: observed intermediates and insights into the nature of the active species

2.1 Abstract

Mechanism of substrate oxidations with hydrogen peroxide in the presence of highly reactive biomimetic aminopyridine iron compex, $[Fe^{II}BPMEN(CH_3CN)_2](ClO_4)_2$ (**1**), is elucidated. **1** has been shown to be an excellent catalyst for epoxidation and functional group- directed aromatic hydroxylation using H_2O_2, although its mechanism of action remains largely unknown.[1, 2] Efficient intermolecular hydroxylation of unfunctionalized benzene and substituted benzenes with H_2O_2 in the presence of **1** is found in the present work. Detailed mechanistic studies of the formation of iron(III) phenolate products are reported. We have identified, generated in high yield, and experimentally characterized the key $Fe^{III}(OOH)$ intermediate (λ_{max} = 560 nm, rhombic EPR signal with g = 2.21, 2.14, 1.96) formed by **1** and H_2O_2. Stopped-flow kinetic studies showed that $Fe^{III}(OOH)$ does not directly hydroxylate the aromatic rings, but undergoes rate-limiting self-decomposition producing transient reactive oxidant. The reactive species formation is facilitated by acid-assisted cleavage of the O-O bond in the iron-hydroperoxide intermediate. Acid-assisted benzene hydroxylation with **1** and a mechanistic probe, MPPH, correlates with O-O bond heterolysis. Independently generated Fe^{IV}=O species,

which may originate from O-O bond homolysis in $Fe^{III}(OOH)$, proved to be inactive toward aromatic substrates. The reactive oxidant derived from **1**, exchanges its oxygen atom with water, and electrophilically attacks the aromatic ring (giving rise to an inverse H/D kinetic isotope effect of 0.8). These results have revealed a detailed experimental mechanistic picture of the oxidation reactions catalyzed by **1,** based on direct characterization of the intermediates and products, and kinetic analysis of the individual reaction steps. Our detailed understanding of the mechanism of this reaction revealed both similarities and differences between synthetic and enzymatic aromatic hydroxylation reactions.

2.2 **Introduction**

Development of regio- and stereoselective catalytic oxidation of organic substrates is an important goal for organic synthesis. Biomimetic oxidations are particularly attractive, because they rely on cheap, non-toxic reactants (usually, O_2 or H_2O_2 as oxidants, and Fe, Cu, or Mn complexes as catalysts). Developing the chemistry of non-heme iron oxidations proved to be intellectually rewarding and productive, and impressive recent progress includes crystallization and characterizations of several high-valent iron intermediates, [3-5] as well as discovery of synthetically useful, regioselective epoxidations and hydroxylations catalyzed by biomimetic iron complexes.[6] One of the most successful olefin epoxidation catalysts is an iron(II) complex of a tetradentate aminopyridine ligand: $[Fe^{II}BPMEN(CH_3CN)_2](ClO_4)_2$ (**1**) that converts olefins into epoxides with high selectivity and efficiency using hydrogen peroxide as oxidant.[1] It has also been shown to be a selective catalyst for aliphatic C-H oxidation,[7] and regioselective

aromatic hydroxylation.[2, 8] Over the past decade the identity of the reactive intermediate in the catalytic oxidation promoted by **1** became a subject of interest. Although there is no general mechanism for a non-heme systems that activate oxygen,[9] several intermediates, including $Fe^{III}(OOH)$, $Fe^{IV}=O$, and $Fe^{V}=O$, have been proposed as active species in catalytic cycles of enzymes and enzyme models.[6, 10] Generally accepted scheme of the reaction of **1** and H_2O_2 included formation of the $Fe^{III}(OOH)$ intermediate that undergoes heterolytic O-O bond cleavage and yields active $Fe^{V}=O$ (Scheme 2-1 B). The recent progress in understanding of the mechanism of oxygen activation at **1** was based on indirect evidence and no reaction intermediates were reliably characterized, although Talsi *et al*. detected $Fe^{III}(OOH)$ by EPR at -60 ˚C in very low yield.[11] In this work we followed rapid reactions of **1** with H_2O_2 and found conditions to generate $Fe^{III}(OOH)$ in a high yield and characterized this intermediate by EPR. Furthermore, we have tested the reactivity of this novel intermediate.

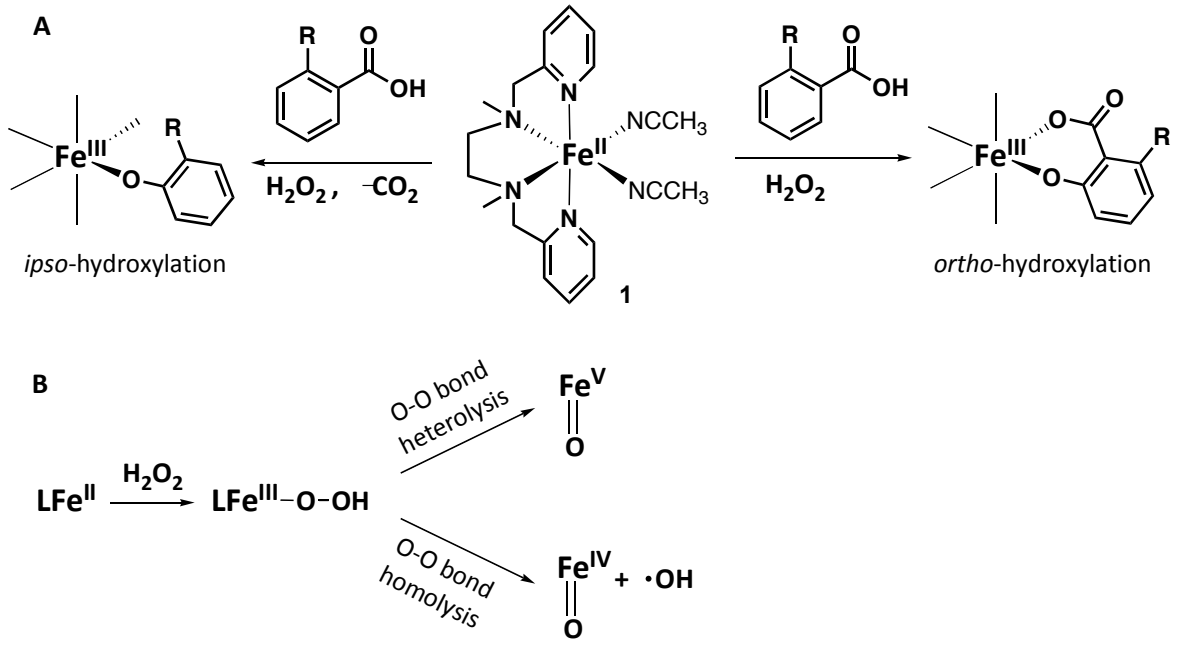

Scheme 2-1. (A) *ortho*- and /or *ipso*-hydroxylation of benzoic acids with H_2O_2 promoted by **1**; (B) possible reactivity modes of Fe^{III}(OOH) intermediate: Fe^{III}(OOH) can either directly transfer oxygen to substrate, or decompose into a high-valent iron-oxo species that reacts with the substrate.

Aromatic hydroxylation presents an excellent opportunity to gain detailed insights into the reactivity of complex **1**. We have recently reported that the hydroxylation of the aromatic ring of substituted benzoic acids occurs exclusively in the vicinity of the anchoring carboxylate functional group leading to *ortho*- or *ipso*-hydroxylated products (Scheme 2-1 A).[2] This carboxylic acid-directed regioselectivity implies involvement of a highly reactive, metal-based oxidant that attacks the aromatic ring next to the directing group. One specific question that needs to be addressed is the role of carboxylic acid

functionality in regioselective aromatic hydroxylations. In addition to being an anchoring, directing group that coordinates to the metal center of **1**, carboxylic acid can also serve as a source of protons. Other carboxylic acids, such as acetic acid, were used to improve performance of **1** as catalyst of olefin epoxidation and aliphatic C-H oxidation.[1, 7] Que and coworkers proposed that coordinated carboxylic acid promotes O–O bond heterolysis of the Fe^{III}(OOH) with formation of an Fe^{V}=O species.[12] In order to better understand the mechanism of oxidations with hydrogen peroxide promoted by **1**, we now report a detailed study of hydroxylation of non-coordinating aromatic hydrocarbons, and the effects of externally added carboxylic acids on the rates and mechanisms of aromatic hydroxylation. This approach, which places two critical components of aromatic hydroxylation in separate molecules, decouples the reactivity of the aromatic rings from the reactivity of carboxylic acids. Our kinetic studies and isotope labeling experiment show that Fe^{III}(OOH) is not the active oxidant in hydroxylation reaction but it produces the reactive high-valent species in the rate-limiting step. The reactive species formation is facilitated by protonation of the terminal oxygen in Fe^{III}(OOH), which leads to heterolytic cleavage of the O-O bond and formation of a putative Fe^{V}=O species.

2.3 **Results and Discussion**

*2.3.1 Hydroxylation of benzene by hydrogen peroxide in the presence of **1***

The reactivity of **1** in hydroxylation of aromatic hydrocarbons with hydrogen peroxide at room temperature was explored in the present work. Benzene reacts with

hydrogen peroxide in the presence of **1** to form a blue species (λ_{max} = 650 nm) that later decays (Figure 2-1). Quenching the reaction followed by a work up (see experimental part) and GCMS identified the oxidation product as phenol. Coordination of the deprotonated phenol to iron(III) in the oxidized form of **1** generates colored products, similarly to the formation of intensely colored salicylates upon hydroxylation of benzoic acids promoted by **1**.[2, 8] Screening and optimization of reaction conditions revealed that the best yields of hydroxylated products (phenolates) were obtained in acetonitrile at room temperature, with excess of H_2O_2 (10 equiv vs. **1**) and benzene (300 equiv vs. **1**). Strongly coordinating solvents, such as methanol and DMSO, suppress benzene hydroxylation promoted by **1**, presumably due to the substitution of labile acetonitrile in the coordination sphere of iron and blocking an access of the oxidant and the substrate to the iron center. Excess of hydrogen peroxide dramatically improves the conversion of benzene into phenol but also causes subsequent oxidation of phenol into dihydroxybenzenes (Figure B1). We utilized small excess of hydrogen peroxide (3 equiv) for kinetic and deuterium retention studies, for which formation of dihydroxybenzene would make interpretation of results more difficult, and larger quantities (10 equiv) to characterize metal-based intermediates using EPR and stopped-flow spectrophotometry. Time resolved UV-vis and GCMS data show that hydroxylation reaction is complete in 5 min; GC and spectrophotometric yields of phenol match closely (Figure B2, B3).[13]

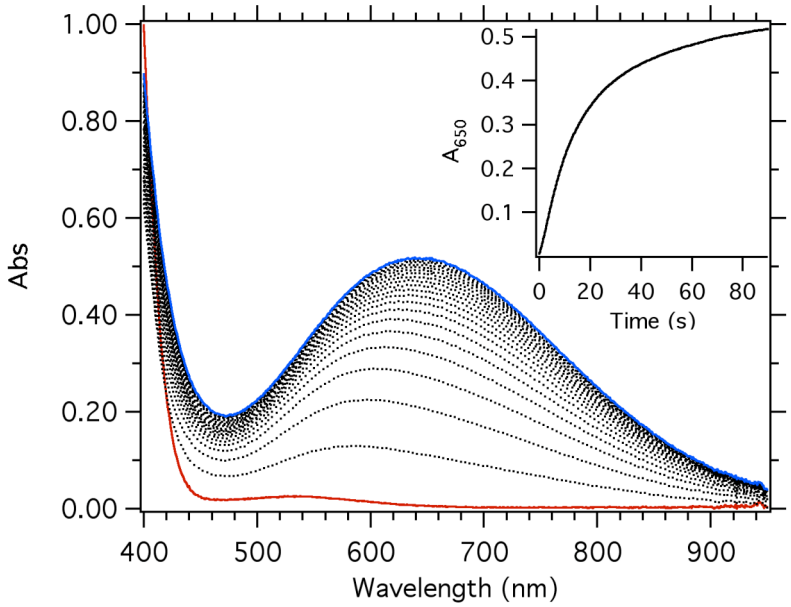

Figure 2-1. UV-vis spectral changes for the reaction of **1**, benzene and H_2O_2 in acetonitrile at 20 °C ([**1**] = 0.5 mM, [H_2O_2] = 5 mM, 200 equiv of benzene vs. **1**). Solid lines represent spectra of **1** (red, time 0 s) and a product $[(BPMEN)Fe^{III}\text{-}OPh]^{2+}$ (blue, run time 90 s). Inset: kinetic trace at 650 nm showing accumulation of $[(BPMEN)Fe^{III}\text{-}OPh]$.

2.3.2 The scope of the hydroxylation reaction

Although general, aromatic hydroxylation catalyzed by **1** is sensitive to the nature of substrate. Without an anchoring group it affords a mixture of o-, m- and p-substituted phenols (Scheme 2-2, Table B1). Sterically hindered substrates (e.g. 1-tert-butyl-3,5-dimethylbenzene) and substrates with strong electron-withdrawing groups (e.g. nitrobenzene) give very low yield of phenol (Table B1).

The **1**/H_2O_2 system favors aromatic hydroxylation over hydroxylation of methyl group (phenols: benzyl alcohol ~ 11:1 in toluene hydroxylation). However aliphatic chain is preferentially hydroxylated when a methylene group is available (Figure B4). Additions

of acetic acid can modulate both the activity and the selectivity of oxidation reactions mediated by **1** and related aminopyridine iron complexes. For example, olefin epoxidation is strongly favored in the presence of acetic acid, while dihydroxylation dominates in acid-free reactions.[1, 12] Similarly, we observed alteration of ethylbenzene hydroxylation in the presence of acetic acid: the yield of aromatic hydroxylation product increased, while the yield of methylene hydroxylation product decreased (Figure B4). Presumably, the nature of the reactive intermediates and/or their reactivity can be altered in presence of carboxylic acids.

Both steric and electronic effects in aromatic hydroxylation by **1**/H_2O_2 differ from non-selective reactivity of hydroxyl radicals (for example, nitrobenzene affords nitrophenols in reactions with HO• generated by photolysis of α-azohydroperoxide).[14] Moreover, hydroxylation of chlorobenzene with **1**/H_2O_2 in the presence of a radical trap (galvinoxyl radical, ~ 1 equiv vs. **1**) did not affect the yield of phenol. These observations suggest involvement of metal-based intermediates in non-radical aromatic hydroxylation with **1**/H_2O_2**.** Metal-based intermediate was also implicated in a related aromatic hydroxylation of benzoic acids with **1**/H_2O_2.[2]

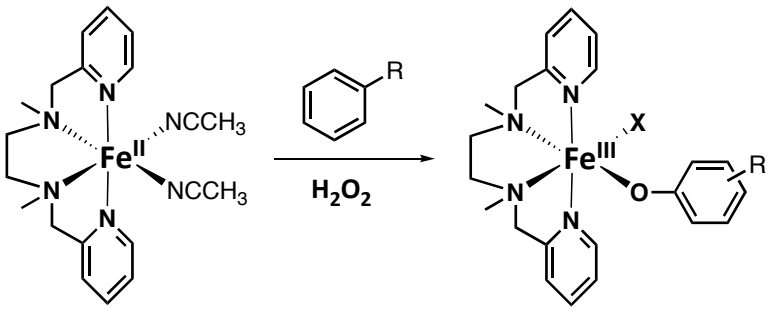

1 R = H, CH_3, Cl, F, Br, CN, Ac

Scheme 2-2. The scope of hydroxylation reaction.

2.3.3 Kinetic and mechanistic studies of benzene hydroxylation

The formation of a phenolate upon mixing of **1** with benzene/H_2O_2 appears as a two-exponential process (Figure B5). The effective pseudo-first order rate constants k_{1obs} and k_{2obs} do not depend on concentration of **1** indicating reaction's first-order in **1**. The first step of hydroxylation reaction was found to be first order in H_2O_2, while the second step is independent of [H_2O_2] (Figure B6). Neither k_{1obs} nor k_{2obs} depend on substrate concentration (Table B2), but the spectroscopic yield of phenol is proportional to the concentration of H_2O_2 (Figure B5) and benzene. Futhermore, the rate of hydroxylation is not affected by the nature of substrates (Table B3), but the spectroscopic yields of phenolate products under otherwise identical conditions generally increase for electron-rich substrates (Figure B7). These results suggest a mechanistic hypothesis: the first reaction step affords an intermediate that decomposes in a subsequent rate-limiting step producing an active oxidant. To test this assumption, we examined individual reaction steps and identified reactive intermediates.

*2.3.4 Reaction of complex **1** with H_2O_2: formation of the Fe^{III}(OOH) intermediate.*

Stopped-flow studies of the direct reaction between **1** and H_2O_2 under optimal hydroxylation conditions (room temperature, acetonitrile) identified a new purple intermediate with λ_{max} = 560 nm (species **1a**, Figure 2-2) that is short-lived at room temperature (half-life time 30 s). The optical spectrum of **1a** is similar to the spectra of known mononuclear Fe^{III}(OOH) complexes, that typically have an intense band at ~500-

550 nm ($\varepsilon \approx 1000\ M^{-1}cm^{-1}$).[15-22] $Fe^{III}(OOH)$ was proposed to be a plausible reaction intermediate in reactions of **1** with H_2O_2,[8, 12, 23] however due to the low yield of the intermediate (< 3 %) its absorption spectrum could not be recorded.[11] Our stopped-flow experiments confirmed that the addition of hydrogen peroxide to **1** at lower temperatures (− 80 to – 30 °C) affords only yellow species **1b,** and no purple species was detected (Figure B8). Unlike the majority of reactive intermediates, that are generated in higher yields at low temperature, the yield of **1a** at the time of its maximum accumulation increased as temperature increased from -20 °C to + 20 °C (Figure B9), although decomposition of **1a** also accelerated with temperature. The transient nature of this intermediate may have prevented its observation and trapping in the past.

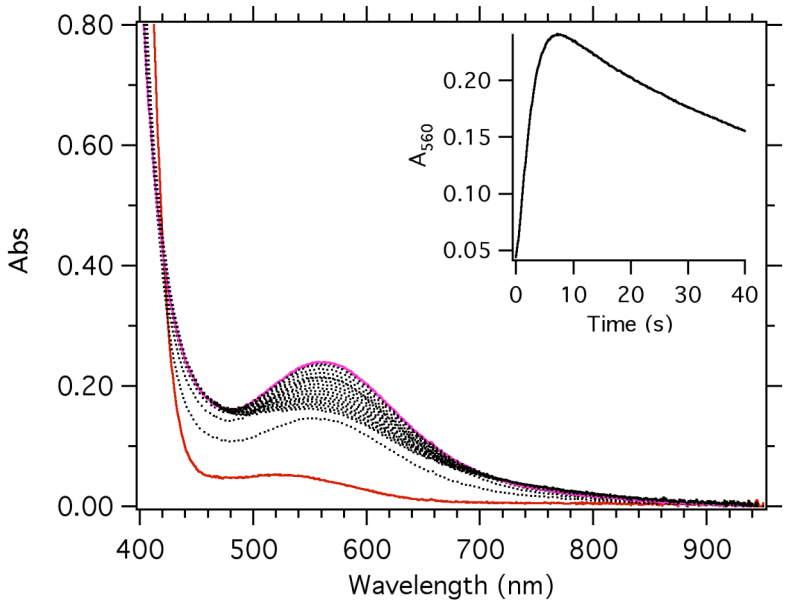

Figure 2-2. Time resolved UV-vis spectra of the $Fe^{III}(OOH)$ formation at 20 °C in acetonitrile ([**1**] **=** 1 mM, $[H_2O_2]$ = 10 mM). Inset: kinetic trace at 560 nm. Solid lines are spectra of **1** (red) and $Fe^{III}(OOH)$ (purple) at its maximum formation.

The plot of the observed rate constants versus hydrogen peroxide concentration under pseudo-first-order conditions (ca. 10-fold excess H_2O_2 with respect to **1**) is a straight line with a nearly zero intercept (Figure 2-5, B10), indicating first-order in H_2O_2 and the overall mixed second-order for the formation of $Fe^{III}(OOH)$:

$$V_{Fe(III)OOH\ formation} = k[\mathbf{1}][H_2O_2]$$

Relatively high activation enthalpy ($\Delta H^{\ddagger}$ = 55.0 kJ mol^{-1}, Figure B11) and large negative activation entropy ($\Delta S^{\ddagger}$ = - 29.3 J mol^{-1} K^{-1}, Figure B12) are consistent with a bimolecular rate-limiting step, although the activation parameters for a multi-step conversion of **1** into **1a** are likely to be composite values, and straightforward interpretation may be misguided.

Intermediates **1a** and **1b** were characterized by EPR and mass-spectrometry. The main product of the reaction between **1** and H_2O_2 at -30 ˚C was a low spin iron(III) species (**1b**) with g=2.41, 2.17 and 1.90 (Figure B13). Most likely, an oxidation of **1** without subsequent coordination of hydroperoxide, occurs under these conditions. Freezing the reaction solution at the maximum accumulation of **1a** (room temperature, Figure 2-2) gives a sample with two species: g values 2.21, 2.14, 1.96 and 2.41, 2.17 and 1.90 (Figure 2-3); the additional signal at 4.24 belongs to a small amount of a high-spin rhombic iron(III) product. The set of signals with g = 2.21, 2.14, 1.96 (ca. 30% of total iron) is typical of low-spin iron(III) hydroperoxo species (with characteristic range of g-values of 1.93-2.26)[24] and thus is assigned to **1a**. Simultaneous formation of two low-spin Fe(III) species has been previously observed when Fe^{II}(BLM) reacted with O_2,[25, 26] first signals of Fe^{III}(OOH)-BLM grew in (g=2.26, 2.17 and 1.94) and then the decay

product, Fe^{III}(BLM), accumulated (g=2.45, 2.18 and 1.89). Complexes with aminopyridyl ligands similar to BPMEN also react with hydrogen peroxide to produce a mixture of low-spin iron species (Table B4); one set of signals in EPR spectrum corresponds to Fe^{III}(OOH) and the other set was assigned to $[Fe^{III}LX]^{n+}$ (n=2 or 3, X=Cl, OH, H_2O, OMe, HOMe), [18, 19, 27] which presumably serves as a presursor to Fe^{III}(OOH). Taken together, the EPR and the stopped-flow UV-vis data indicate that **1a** is an Fe^{III}(OOH) species. This conclusion is supported by the observed ESI-MS of **1a,** which shows peaks at m/z = 425, 442, 456, and 481 consistent with ions $[Fe(BPMEN)](ClO_4)^+$, $[Fe(BPMEN)(OH)](ClO_4)^+$, $[Fe(BPMEN)(OMe)](ClO_4)^+$, $[Fe(BPMEN)(OOH)]Na(ClO_4)^+$ respectively (Figure B14).

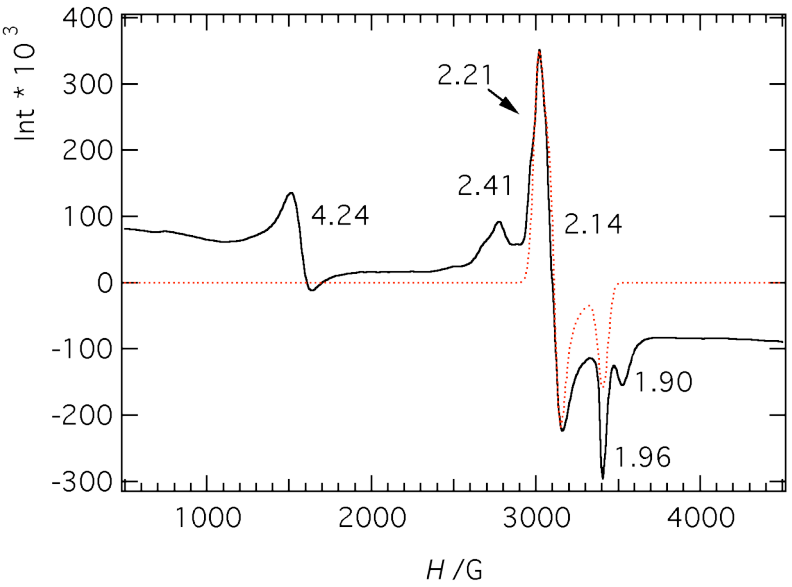

Figure 2-3. EPR spectrum (120 K) of Fe^{III}(OOH) in acetonitrile. 25 % yield of Fe^{III}(OOH) vs. initial concentration of iron was determined using $Cu(ClO_4)_2$ as an external standard. Signals at 2.41 and 1.90 correspond to **1b** that accompanies **1a** at all temperatures. Red dotted line is a simulation of EPR spectrum with g values 2.21, 2.14, 1.96 (calculated using SimFonia).

To directly probe whether $[Fe^{III}(OOH)(BPMEN)]^{2+}$ (**1a**) is involved in benzene hydroxylation, we added this substrate to a pre-generated **1a**, and observed the formation of a blue Fe^{III}-phenolate complex (Figure 2-4). However, this experiment does not prove that the intermediate **1a** itself attacks benzene; additional kinetic studies (detailed below) were performed in order to further probe the reactivity of **1a.**

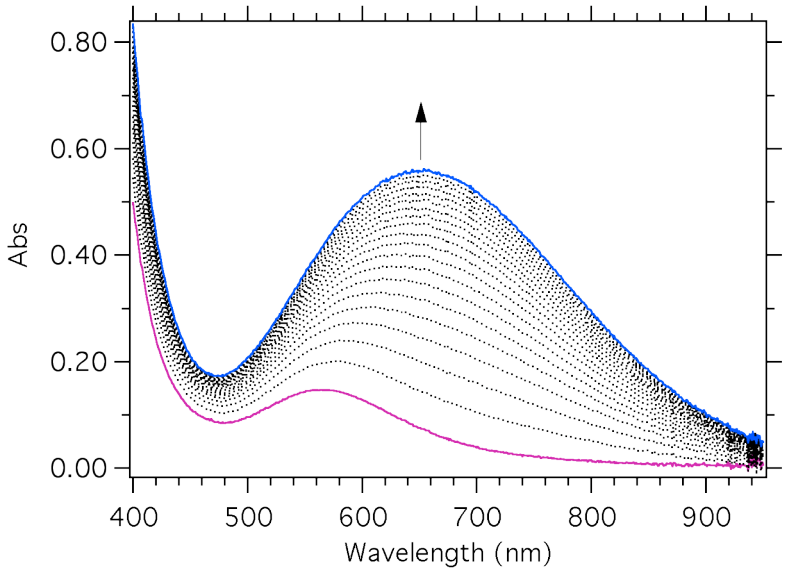

Figure 2-4. Time resolved UV-vis spectra of the reaction of $Fe^{III}(OOH)$ with benzene in acetonitrile at 20 °C ([**1**] = 0.5 mM, $[H_2O_2]$ = 5 mM, 200 equiv of benzene vs. **1**). Solid lines represent spectrum of **1a** (λ_{max} = 560 nm) at its maximum formation (age time 7 s) and a spectrum of a product [(BPMEN)Fe^{III}-OPh] (λ_{max} = 650 nm, run time 80 s).

2.3.5 $Fe^{III}(OOH)$ reactivity pathways and effect of acetic acid.

Iron hydroperoxide is often considered to be a reaction intermediate in non-heme iron systems[15, 16, 28, 29] that may either directly transfer an oxygen atom to the

substrate, or decompose into a high-valent iron-oxo species that reacts with the substrate.[12, 30, 31] However, the experimental data on the reactivity of $Fe^{III}(OOH)$ are limited, and hardly support a uniform view on their ability to directly oxidize substrates. For example, W. Nam *et al*. tested the ability of several synthetic iron hydroperoxo complexes to oxidize sulfides or olefins, and concluded that this intermediate is a sluggish oxidant.[32] On the other hand, Solomon *et al.* reported that $Fe^{III}(OOH)$ in activated bleomycin (ABLM) directly attacks DNA.[26]

Kinetic data for benzene hydroxylation compared with kinetics of the reaction of **1** with H_2O_2 (Figure B15) suggest that **1a** does not attack aromatic ring but decomposes into another, more active intermediate (Scheme 2-4). The rate constant of the formation of $Fe^{III}(OOH)$ from **1** and H_2O_2 is comparable to the observed rate constant of the first process in benzene hydroxylation studies (k_{1obs}, Figure B6). Both rate constants are directly proportional to $[H_2O_2]$. Since absorption bands of $Fe^{III}(OOH)$ and Fe^{III}-phenolates (λ_{max} = 560 nm and 650 nm respectively) partially overlap, we observe a two exponential process when **1** is mixed with benzene/H_2O_2, where k_{1obs} corresponds to the formation of $Fe^{III}(OOH)$ (Figure 2-5) and k_{2obs} is attributed to the hydroxylation of benzene. The rate constant of phenol formation (k_{2obs} in Figure 2-1, Figure 2-5) and the rate constant of $Fe^{III}(OOH)$ self-decay (Figure 2-2, Figure 2-5) are comparable and do not depend on $[H_2O_2]$. These observations indicate that self-decay of $Fe^{III}(OOH)$ yields reactive intermediate that rapidly attacks the aromatic ring. In order to test this hypothesis, the reactivity of pre-generated $Fe^{III}(OOH)$ was studied directly in a series of double-mixing experiments. The rate of phenolate accumulation did not depend on the

concentration of benzene added to a pre-generated Fe^{III}(OOH) (Table S5). Rate of hydroxylation also does not depend on the nature of substrate: when different substrates (benzene, chlorobenzene, toluene) were added to the pre-generated **1a**, the rate constants of Fe^{III}-phenolate formation were nearly identical (Table S3). Moreover, the rate of aromatic hydroxylation did not depend on the concentration of excess H_2O_2: Fe^{III}(OOH) was generated by mixing **1** and variable amounts of H_2O_2 (3, 10 and 20 equiv vs. **1**), followed by the addition of benzene at the maximum accumulation of Fe^{III}(OOH), and the rate constants of phenolate formation were equal in all of these experiments. All kinetic data suggest that Fe^{III}(OOH) does not directly attack the aromatic ring of the substrate, but this species decays into another species (presumably, Fe^{V}=O or Fe^{IV}=O) which rapidly hydroxylates the aromatic ring (Scheme 2-4).

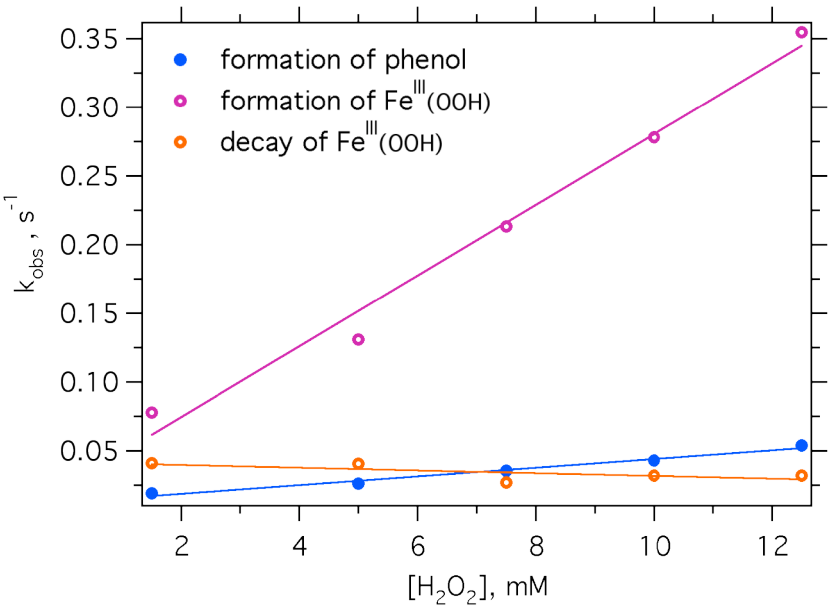

Figure 2-5**.** Rates of formation of phenol, Fe^{III}(OOH) and decay of Fe^{III}(OOH) in acetonitrile at 20 ˚C as a function of H_2O_2 concentration. Rate constant of hydroxylation was determined from a single mixing experiment, where **1** was mixed with benzene and H_2O_2 ([**1**]=0.5 mM, 300 equiv benzene vs. **1**). Kinetic traces at 650 nm were fitted in Kinetic Studio program using A→B→C model. Formation and decay of Fe^{III}(OOH) was monitored at 560 nm after **1** (0.5 mM) was mixed with H_2O_2; kinetic traces at 560 nm were fitted using A→B→C model, where the first process represents formation of Fe^{III}(OOH) and the second process is a decay of Fe^{III}(OOH).

Acetic acid facilitates Fe^{III}(OOH) decay in a concentration-dependent manner: larger amounts of acid lead to faster hydroperoxide decomposition (Figure B16). Additionally, acetic acid accelerates the rate of Fe^{III}-phenolate formation (Figure 2-6), and the rate constants of phenolate formation and those of self-decay of **1a** in the presence of 1

equivalent of acetic acid are comparable (Figure B17). These data indicate that acetic acid accelerates the decay of $Fe^{III}(OOH)$ into a reactive intermediate responsible for aromatic hydroxylation. Addition of acetic acid is known to increase catalytic activity of **1** in epoxidation and aliphatic C-H oxidation reactions.[1, 7] We have also observed a somewhat increased yield of aromatic hydroxylation products in reactions of benzenes with **1**/H_2O_2 in the presence of acetic acid (Figure B18).

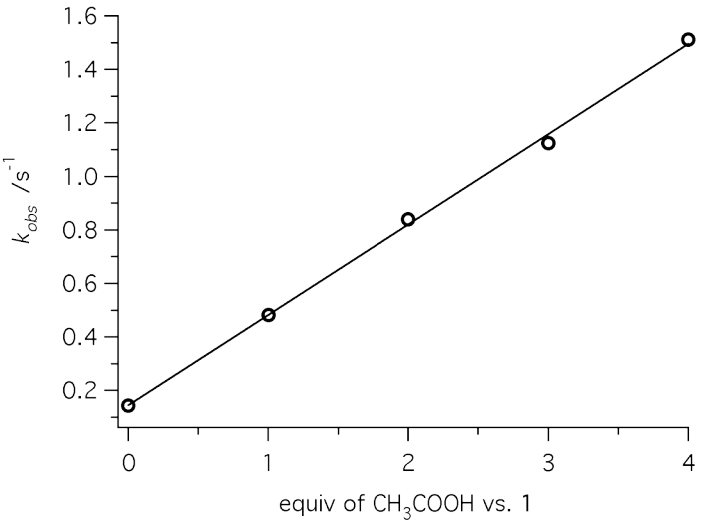

Figure 2-6. Rate constant of phenolate formation is directly proportional to [CH_3COOH] ([**1**] = 0.5 mM, [H_2O_2] = 5 mM, 560 equiv of benzene vs. **1,** 20 ˚C, acetonitrile).

2.3.6 Products of decomposition of $Fe^{III}(OOH)$ and their role in hydroxylation reaction.

Kinetic data suggest that decomposition of $Fe^{III}(OOH)$ yields an active oxidant and acetic acid accelerates this process. Therefore we trapped and characterized the decay product of $Fe^{III}(OOH)$ and probed its activity toward aromatic substrates.

We followed the decay of **1a** by UV-vis spectrophotometry and observed the formation of a green species **1c** with λ_{max} = 740 nm (Figure B19). This near-IR chromophore closely resembles low-spin (S=1) (L)Fe^{IV}=O complexes generated by O-O bond homolysis of (L)Fe^{III}(OOH) intermediates supported by several polyamine- or aminopyridine ligands analogous to BPMEN,[33] suggesting that **1c** can also be formulated as an Fe^{IV}=O intermediate. This formulation is consistent with the EPR-silent nature of the green intermediate **1c**: it was found that **1a** decayed over 70 s (k~0.01 s^{-1}, rt) at room temperature without formation of any new EPR-active species (Figure B20).

The chemical nature of **1c** suggested alternative methods of generating this intermediate. Similarly to literature precedents,[12] **1c** can be obtained faster and in higher yield from the reaction of **1a** with acetic acid (Figure 2-7), or by adding a mixture of H_2O_2 and acetic acid directly to **1** (Figure 2-8). Acetic acid, added directly into EPR tube to a pre-generated **1a**, accelerated decomposition of **1a** into an EPR-silent species **1c**, while **1b** (g values at 2.41, 2.17 and 1.90) remained intact (Figure 2-7, inset).

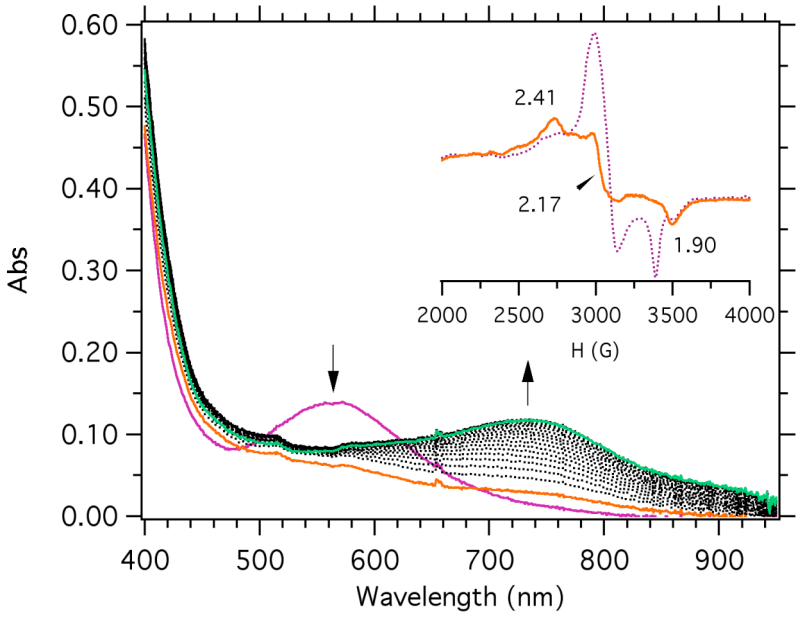

Figure 2-7. Stopped-flow time resolved UV-vis spectra of the reaction of Fe^{III}(OOH) with 1 equiv of acetic acid. Fe^{III}(OOH) was pre-generated by mixing **1** (0.5 mM) and H_2O_2 (5 mM) at 20 °C in acetonitrile over 10 s (solid line, λ_{max}=560 nm). Fe^{III}(OOH) decays quickly (2 s) upon addition of acetic acid (1 equiv vs. iron, dashed line) followed by slow (over 80 s) accumulation of Fe^{IV}=O (solid line, λ_{max} = 740 nm).[35] Inset shows EPR spectra of Fe^{III}(OOH) before (dotted line) and after (solid line) addition of acetic acid at room temperature.

ESI-MS spectrum of the mixture of **1**/H_2O_2 /CH_3COOH at room temperature shows peaks at m/z = 401, 425, 442 that correspond to $[Fe(BPMEN)(O)](OAc)^+$, $[Fe(BPMEN)](ClO_4)^+$, $[Fe(BPMEN)(OH)](ClO_4)^+$ respectively (Figure B21). Preliminary Mössbauer studies of the sample prepared by adding peracetic acid directly to **1** also confirms that the green species **1c** has an Fe^{IV}=O center.[34]

Additionally, we used an alternative, H_2O_2-free method to directly generate the green species **1c** from **1** and oxygen atom donors. Isopropyl ester of 2-iodoxybenzoic acid (IBX ester)[36] was recently developed as a stable, highly soluble source of oxygen atoms in organic oxidations. This reagent was also successfully used in metal-mediated oxidations catalyzed by phthalocyanin complexes.[37] We applied IBX ester as an oxygen atom transfer reagent in reactions that generate high-valent iron(IV)-oxo species. Upon mixing **1** and IBX ester (0.5-4 equiv vs. **1**) no purple species was observed but instead a green species **1c** formed, with an optical spectrum very similar to the spectra of the species generated from **1**, H_2O_2, and HOAc (Figure 2-8). The difference in spectra of the species **1c** derived from **1**/IBX-ester and **1**/H_2O_2/CH_3COOH can be attributed to the binding of HOAc or OAc to the Fe^{IV}=O center.[38]

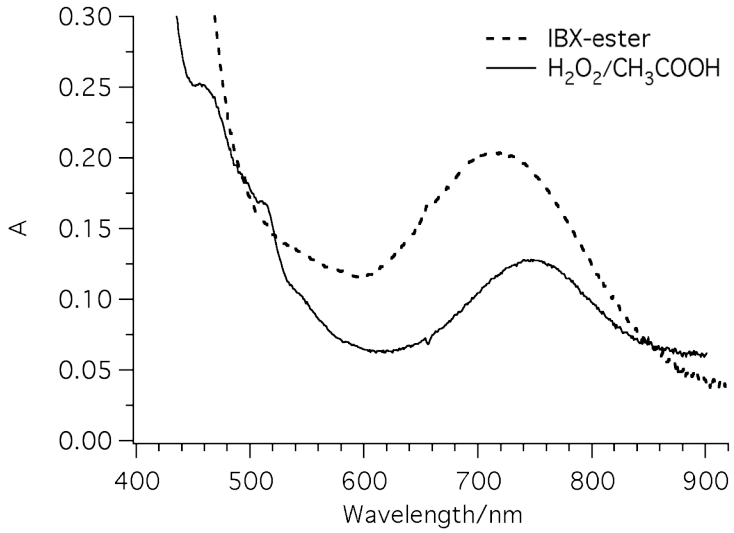

Figure 2-8. Spectra of green species **1c** obtained upon mixing of **1** with IBX ester ([**1**]=1 mM; [IBX-ester]=3.8 mM, acetonitrile, 10 °C) and **1** with H_2O_2/ CH_3COOH ([**1**] = 1 mM, [H_2O_2] = 10 mM, [CH_3COOH] = 0.5 mM, acetonitrile, 20 ˚ C).

To test the reactivity of iron-oxo center, we generated (BPMEN)Fe^{IV}=O by mixing **1**, H_2O_2 and acetic acid at 20 °C. After **1c** was formed in its maximum yield (60 s), benzene was added, however only self-decay of **1c** was observed. In a similar experiment, **1c** was prepared by mixing **1** and IBX ester at 10 ˚C, adding of benzene (280 equiv vs. iron) did not result in the formation of Fe^{III}-phenolate. It can be concluded that the Fe^{IV}=O intermediate (**1c**) is unable to hydroxylate the aromatic ring, and cannot act as kinetically competent intermediate in aromatic hydroxylation with H_2O_2 promoted by **1**. We also used the stopped-flow methodology to measure rates of Fe^{IV}=O decay in the presence of toluene and without toluene and found that they are comparable (Figure B22); therefore, (BPMEN)Fe^{IV}=O does not efficiently hydroxylate benzylic CH_3 groups.

2.3.7 Mechanistic insights into O-O bond cleavage in Fe(III) peroxides supported by BPMEN.

Isotope labeling experiments ($^{18}O/^{16}O$) are often useful in determining the mechanistic pathways of metal-assisted O-O bond cleavage. Incorporation of oxygen from water into oxidation product requires the formation of Fe^{IV}=O or Fe^{V}=O species and $^{16}O/^{18}O$ exchange with solvent water prior to reaction with substrates.[39, 40] In our system, hydroxylation experiments with labeled hydrogen peroxide ($H_2{}^{18}O_2$) in the presence of water ($H_2{}^{16}O$) show the incorporation of ^{16}O into phenol product: 19% of phenol contained ^{16}O and 81% of phenol contained ^{18}O. Hydroxylation of benzene with $H_2{}^{16}O_2$ in the presence of $H_2{}^{18}O$ led to 78% $H^{16}O$-C_6H_5 and 22% of $H^{18}O$-C_6H_5. The results of isotope-labeling studies are inconsistent with the mechanisms involving a direct

attack of $Fe^{III}(OOH)$ on the aromatic ring, because $Fe^{III}(OOH)$ cannot exchange with water. Similarly, ^{18}O-labeling studies showed some loss of the label when $H_2{}^{18}O_2$ was used as oxygen source for *cis*-dihydroxylation of naphthalene by Naphthalene 1,2-dioxygenase,[41] thus implicating oxygen exchange between the active intermediate and water, and suggesting a reaction pathway that invokes Fe(V)=O(OH) species. In another example,[31] a *cis*-dihydroxylation reaction of alkenes with hydrogen peroxide in the presence of $H_2{}^{18}O$ catalyzed by $[Fe^{II}(TPA)(CH_3CN)_2]^{2+}$ showed incorporation of ^{18}O into product, which was rationalized by water-assisted formation of Fe(V)=O(OH).

$^{18}O/^{16}O$ scrambling in aromatic hydroxylations with H_2O_2 promoted by **1** implies that the observed peroxo-intermediate, $Fe^{III}(OOH)$, is not the sole oxidant in this reaction and thus should undergo either a heterolytic O-O bond cleavage that affords $Fe^{V}=O$, or a homolytic O-O bond cleavage to produce $Fe^{IV}=O$. In similar reactions, organic peroxide MPPH (2-methyl-1-phenyl-2-propyl hydroperoxide) has been widely used as a mechanistic probe to distinguish homolytic versus heterolytic cleavage of the alkylhydroperoxide O-O bond.[42-45] Homolysis of RO-O bond would generate a $Fe^{IV}=O$ species and a transient RO• radical that decays into benzyl radical, eventually yielding benzyl alcohol under anaerobic conditions, or benzaldehyde in the presence of O_2 (Scheme 2-3). On the other hand, heterolytic cleavage of the O-O bond would generate $Fe^{V}=O$ and 2-methyl-1-phenyl-2-propyl alcohol (MPPol). Analysis of organic products provides the information on the mechanism of O-O bond cleavage in oxidations with MPPH.

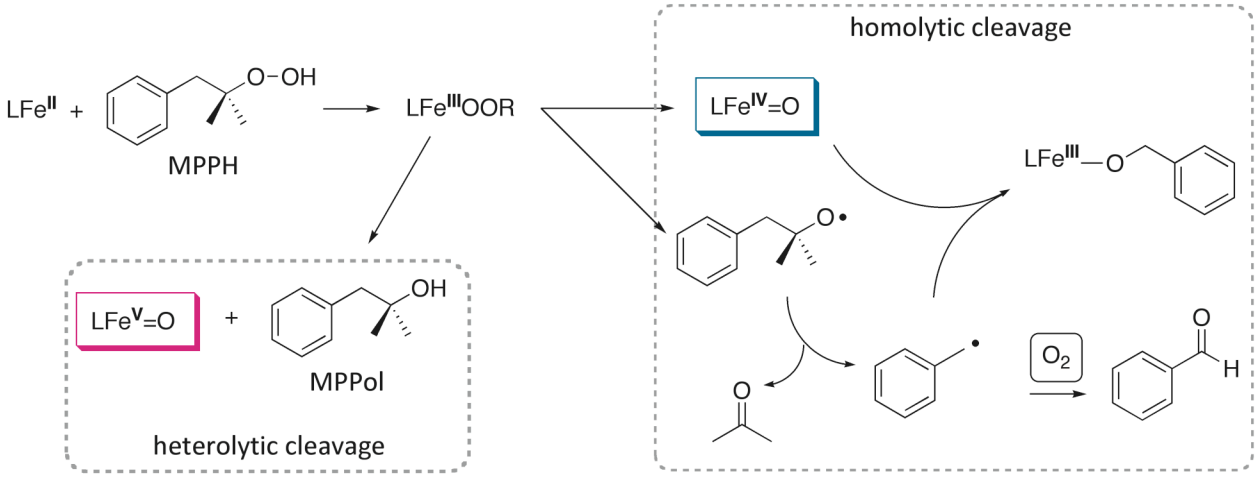

Scheme 2-3. Reaction of MPPH with iron center and products derived from MPPH.

Pure recrystalized MPPH reacted with **1**/benzene under aerobic conditions to yield mainly benzaldehyde, which indicated the O-O bond homolysis and the formation of Fe^{IV}=O (Scheme 2-3); the amount of MPPol, an indicator of O-O bond heterolysis, was small. Yield of phenol was low under these conditions (Figure 2-9a). In contrast, oxidation of benzene by MPPH in the presence of **1** and 0.5 equiv of acetic acid resulted in significant increase in the yields of both MPPol and phenol (Figure 2-9b). These results are consistent with O-O bond heterolysis as a major pathway that generates a competent oxidant for benzene, implying that Fe^{V}=O is the active species in the hydroxylation reaction. Acetic acid catalyzes heterolytic O-O bond cleavage and the formation of Fe^{V}=O, therefore acetic acid dramatically increased the yield of MPPol and the yield of aromatic hydroxylation product when MPPH is used as oxidant.

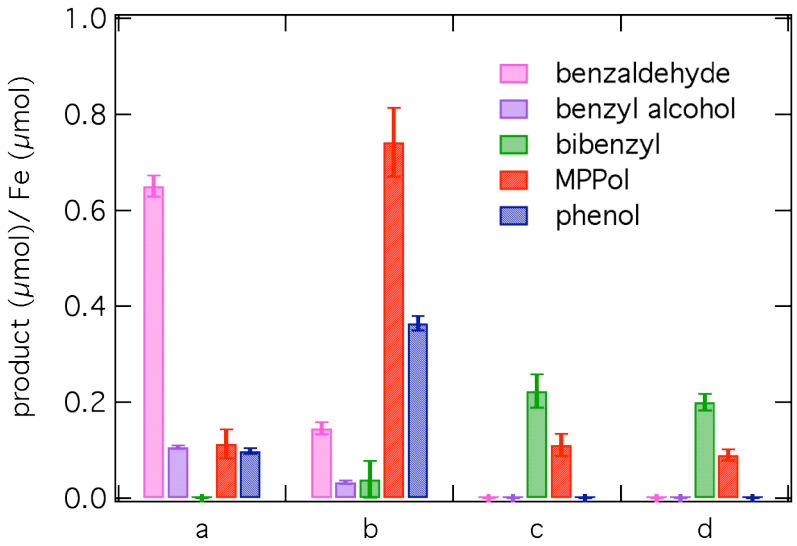

Figure 2-9. Product yields (in mol/1 mol Fe) and effects of acetic acid in aerobic reaction of benzene with **1**/MPPH (Scheme 2-3): **a**) [**1**] = 2 mM, 280 equiv of benzene vs. **1**, 1 equiv of MPPH; **b**) [**1**] = 2 mM, 280 equiv of benzene vs. **1**, 1 equiv of MPPH, 0.5 equiv of acetic acid; control experiments:[46] **c**) MPPH in acetonitrile (same amount as in **a** and **b**); **d**) MPPH and acetic acid (same amounts as in **b**). All samples were stirred for 30 min, then acetylated, products extracted with dichloromethane and analyzed by GCMS. Error bars show standard deviation.

*2.3.8 H/D Kinetic Isotope Effects in substrate oxidations with **1**/H_2O_2*

The mechanisms of interactions between the oxidant and the organic substrate can be evaluated by comparing the relative rates of hydroxylation of deuterated and unlabeled substrates. While detailed calculations are necessary for thorough interpretation of H/D kinetic isotope effects, some qualitative conclusions can be derived from the direct analysis of the experimental data. In particular, C-H bond

breakage (e.g. in a hydrogen atom abstraction or direct insertion, Scheme 2-4A,B) typically results in normal kinetic isotope effects (KIE > 1), but electrophilic attack on the aromatic ring accompanied by sp^2/sp^3 rehybridization often leads to small inverse kinetic isotope effects (Scheme 2-4C, D).[47]

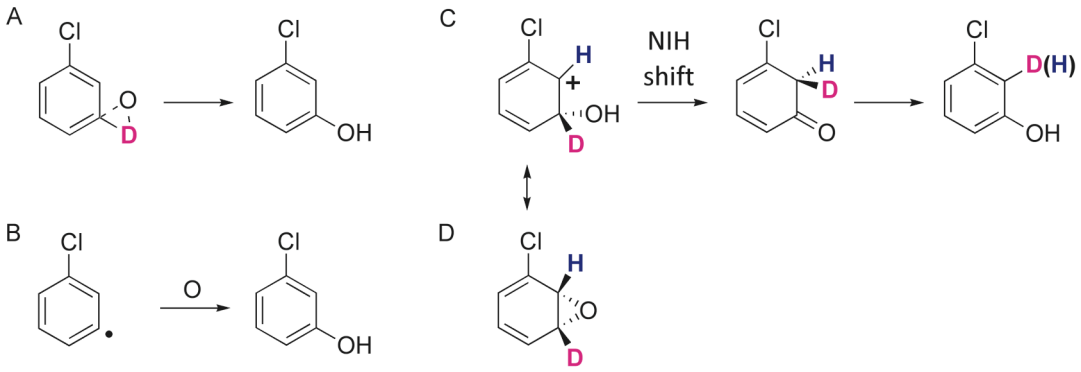

Scheme 2-4. Mechanism of aromatic hydroxylation shown for 3-$^2H_1$-chlorobenzene. A- direct insertion; B- hydrogen abstraction; C- addition/rearrangement; D- formation of epoxide.

Benzene hydroxylation in the presence of **1**/H_2O_2 resulted in inverse KIE kh/kd=0.8. The inverse kinetic isotope effect in benzene hydroxylation indicates a change in hybridization at a carbon bound to deuterium (sp2→sp3), which is consistent with an electrophilic addition to the aromatic ring or with an intermediate formation of epoxide.[48, 49] The inverse H/D kinetic isotope effect is inconsistent with an abstraction-recombination, which therefore can be excluded for aromatic hydroxylation with **1**/H_2O_2. Also toluene hydroxylation with H_2O_2 in the presence of **1** gave kinetic isotope effects of 0.7 for the aromatic ring hydroxylation and 1.3 for the methyl group

hydroxylation. These data indicate that a hydrogen atom abstraction is likely involved in benzylic hydroxylation of toluene, but not in the hydroxylation of the aromatic ring. The differences in isotope effects observed for hydroxylation of the aliphatic chain and the aromatic ring suggest that two different mechanisms are utilized to oxidize these molecular fragments, although both processes (aliphatic and aromatic hydroxylation) may share the same metal-based oxidant. Similarly, previously reported hydroxylation of p-xylene catalyzed by toluene 4-monooxygenase, a non-heme iron enzyme, gave normal isotope effect (2.22) for methyl hydroxylation and inverse isotope effect (0.735) for aromatic hydroxylation.[49] P450 was also shown to give normal isotope effect (7-10) for benzylic hydroxylation of xylene, in agreement with an oxygen rebound mechanism; in contrast, aromatic hydroxylation of xylenes was characterized by an inverse isotope effect (0.83-0.94).[50]

In addition to kinetic isotope effects, H/D migrations and rearrangements provide meaningful mechanistic information. In aromatic hydroxylations, a hydrogen atom shift (the so-called NIH shift) is common for reactions that proceed via an electrophilic attack of the oxidant on the aromatic ring with subsequent rearrangement of the cationic intermediate to a ketone intermediate (Scheme 2-4C).[51] We observed a non-zero NIH shift for hydroxylation of 3,5-$^{2}H_2$-chlorobenzene and 2,4,6-$^{2}H_3$-chlorobenzene with **1**/H_2O_2, these results corroborate electrophilic addition to the aromatic ring (Table B6).

The results obtained for aromatic hydroxylations with hydrogen peroxide in the presence of **1** are in line with a number of related oxidations at iron center that typically

show a small inverse kinetic isotope effect, and agree with an electrophilic attack on the aromatic ring.[48, 49, 52-54]

2.3.9 Discussion

High activity of complex **1** in oxidations of organic substrates with hydrogen peroxide[2, 7, 12] made this complex a promising candidate for exploring intermolecular aromatic hydroxylations of substrates lacking directing groups. Similarly to previously reported functional group-assisted hydroxylation of benzoic acids, we now found that **1** is equally efficient in promoting hydroxylation of benzenes. Although biological aromatic hydroxylations can be catalyzed by mononuclear non-heme iron centers in pterin-dependent aromatic amino acid hydroxylases,[55] and by non-heme diiron centers in bacterial multicomponent monooxygenases (BMMs) such as methane and toluene monooxygenases,[56] synthetic biomimetic systems capable of hydroxylating unfunctionalized aromatic rings are still limited.[57] Aside from variations of classical Fenton reaction, which are usually non-selective and often low-yielding, iron phthalocyanines[58] and iron complexes with aminopyridine ligands[59] are among a handful of recent examples of non-porphyrin complexes reactive in intermolecular aromatic hydroxylations. Complex **1** promotes nearly quantitative conversion of aromatic hydrocarbons to phenolates at room temperature within several minutes, with H_2O_2 as the oxidant. Importantly, a range of substituted benzenes, including electron-poor substrates (such as chlorobenzene) readily undergoes hydroxylation with **1**/H_2O_2. However, strongly electron-withdrawing substituents (e.g. nitro-groups) significantly

decrease yield of hydroxylated product. Despite high reaction rates in aromatic hydroxylation with **1**/H_2O_2, efficient catalysis is precluded by strong coordination of the phenolate products to the iron(III) center. This coordination, however, has two beneficial effects: it prevents overoxidation of phenols, thus greatly improving product selectivity, and it gives rise to intensely colored iron(III) – phenolate products, thus enabling spectrophotometric monitoring of the reaction progress. The latter feature was particularly useful for the present study, which was focused on identifying metal-based intermediates that are competent hydroxylating agents.

Plausible intermediates that were proposed for non-heme iron systems include $Fe^{III}(OOH)$, $Fe^{IV}=O$, and some kind of a fleeting Fe(V) species; all of these species were previously implicated in various iron-promoted oxidations, and most of them were spectroscopically observed for some non-heme iron complexes.[6] For intermolecular hydroxylations of non-functionalized aromatic compounds, a number of active non-heme iron reagents or catalysts is limited, and the active species in these systems were not identified.[60, 61] Although $Fe^{III}(OOH)$ was proposed to participate in aromatic hydroxylation,[61] the reactivity of this species was not studied in direct experiments. For example, anisol is hydroxylated with H_2O_2 in the presence of Fe^{II}(TPEN) analogs, and hydroperoxo intermediates were proposed to be responsible for catalytic activity, but no specific experiments that support this hypothesis were described.[61] Pre-generated $Fe^{III}OOH$ species supported by several aminopyridine ligands (including tris-picolylamine, TPA) were shown to be sluggish oxidants that did not react with olefins, sulfide, or phosphines[32] at low temperatures. However, very little information is available about

Fe(BPMEN)-derived intermediates, therefore we developed methods to generate BPMEN supported $Fe^{III}(OOH)$ in reasonable yield, and probed its reactivity under ambient conditions where high-yielding hydroxylation takes place.

Formation of the $[Fe^{III}(OOH)(BPMEN)]^{2+}$ intermediate, involved in hydroxylation, was observed by stopped-flow kinetic measurements with spectrophotometric registration, by EPR, and by mass-spectrometry. The yield of the $Fe^{III}(OOH)$ intermediate significantly depends on temperature; counterintuitively, it can be generated in relatively high yield only at or near room temperature. Using stopped-flow techniques we established that $[Fe^{III}(OOH)(BPMEN)]^{2+}$ does not directly attack aromatic substrates: reaction rates were independent on the concentration of benzenes, and on the nature of substituent on the aromatic ring. Also, ^{18}O labeling experiments demonstrated that active intermediate responsible for aromatic hydroxylation exchanges with water and thus $Fe^{III}(OOH)$ can not be the sole oxidant. These results are in line with generally low oxidizing reactivity of $Fe^{III}(OOH)$ intermediates.[62] A somewhat different situation was found for iron bleomycin, a natural antibiotic that causes oxidative DNA cleavage in the presence of iron and dioxygen.[63] Although earlier studies indicated nearly identical decay rates of ABLM with and without substrate present,[64] the more recent study by Solomon and coworkers,[26] which took advantage of a distinct signature of ABLM in MCD spectra, provides evidence in favor of direct interaction between this $Fe^{III}(OOH)$ intermediate and the substrate. Differences in reactivity of synthetic $Fe^{III}(OOH)$ complexes (which are sluggish oxidants) compared to a natural system, ABLM, can be

attributed, at least in part, to differences in spin states of iron(III), and to enzyme-like proximity effects due to bleomycin intercalation between the DNA base pairs.

Results presented herein, suggest that self-decomposition of Fe^{III}(OOH) generates an active species capable of oxidizing an aromatic substrate. Fe^{III}(OOH) can udergo heterolytic or homolytic O-O bond cleavage to produce Fe^{V}=O or Fe^{IV}=O respectively (Scheme 5). It is believed that mononuclear non-heme iron enzymes that hydroxylate aromatic substrates, pterin-dependent oxygenases (PheH, TyrH, TrpH), function by means of high-spin Fe^{IV}=O,[65] recently this intermediate was trapped in the reaction catalyzed by Tyrosine hydroxylase (TyrH) and characterized by rapid freeze-quench Mössbauer spectroscopy.[66] By now many synthetic Fe^{IV}=O complexes have been generated and characterized spectroscopically and, in several cases, crystallographically,[3-5] and in some cases, this species was able to carry out an oxidation of organic substrates (cyclooctene,[67, 68] cyclohexane,[43] thioanisole,[67] triphenylmethane,[60, 69] alcohol,[60, 70] anthracene[53]). Intramolecular, regioselective hydroxylation of the appended aromatic ring in reaction of $[Fe^{II}(6\text{-Ph-TPA})(CH_3CN)_2)^{2+}$ with tBuOOH also reportedly proceeds via a homolytic pathway that generates an Fe^{IV}=O species as a competent oxidant.[42] However, we recently showed that (TPA)Fe^{IV}=O intermediate does not hydroxylate benzoic acids.[2] In addition, an Fe^{IV}=O intermediate supported by a substituted TPEN did not oxidize anisole (although efficient anisole hydroxylation with H_2O_2 was promoted by this iron complex).[61] In the present work, we were able to generate, in high yield, an Fe^{IV}=O intermediate supported by BPMEN, and confirmed that (BPMEN)Fe^{IV}=O does not hydroxylate aromatic rings.

Similarly to Fe^{III}-hydroperoxo intermediates, the differences in reactivity of ferryl(IV) species in enzymes and in synthetic complexes can be attributed to different spin states of iron(IV)[63, 71] (high-spin in mononuclear non-heme iron enzymes,[72] and low-spin in synthetic intermediates supported by aminopyridine ligands[73]), and by proximity effects in enzymes (and also in intramolecular ligand hydroxylations by iron(IV) species in synthetic systems).[42, 63]

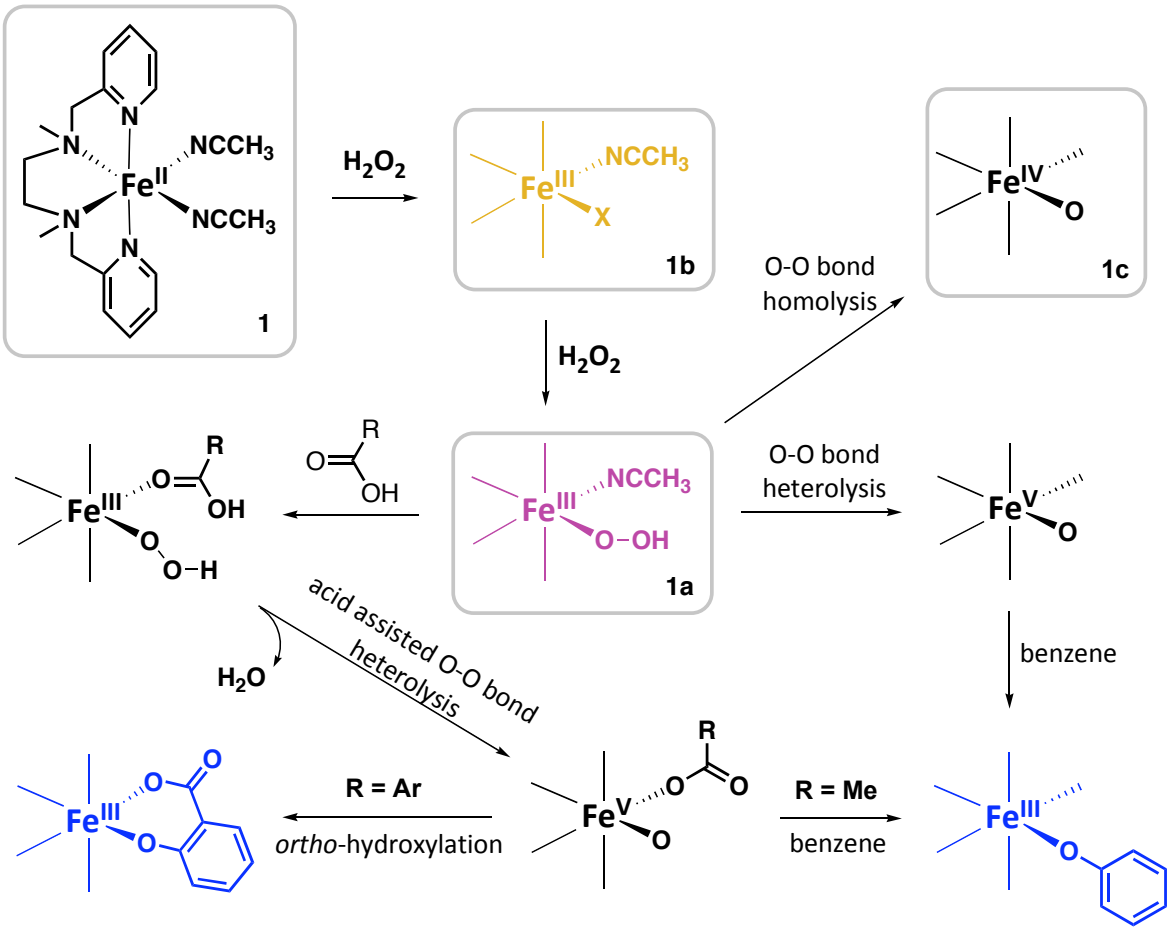

Scheme 2-5. Intermediates involved in aromatic hydroxylation catalyzed by **1**.

We have shown that acetic acid facilitates decay of $Fe^{III}(OOH)$ and leads to faster Fe^{III}-phenolate formation, thus acetic acid promotes formation of reactive species responsible for aromatic hydroxylation. Moreover, acetic acid-assisted O-O bond heterolysis of a mechanistic probe MPPH in the presence of **1** and benzene was accompanied by a significant growth in yields of hyroxylated products (phenolates), these results suggest that hydroxylation is performed by Fe^{V}=O species. Carboxylic acid-assisted O-O bond heterolysis pathway leading to an as-of-yet unobserved Fe^{V}=O oxidant has been proposed[12] by Mas-Ballesté and Que in the efficient epoxidation of olefins by H_2O_2 in the presence of acetic acid and $[Fe^{II}(TPA)(CH^3CN)_2]^{2+}$, and it also appears to be a likely mechanism of regioselective benzoic acid hydroxylations.[2] Recently, another example of aromatic hydroxylation involving a proposed Fe^{V}=O intermediate was reported. Upon addition of CH_3CO_3H to a solution containing $[Fe^{II}(bqen)]^{2+}$ and benzyl alcohol, aromatic ring was hydroxylated at the *ortho*-position.[60] Interestingly, corresponding Fe^{IV}=O species did not hydroxylate aromatic ring but produced benzaldehyde. Intermediate responsible for aromatic hydroxylation was found to rapidly exchange with $H_2{}^{18}O$ and was formulated as an Fe^{V}=O species. A similar oxidant has been proposed for the iron-catalyzed self-hydroxylation of aryl peroxyacids,[74] and for the intramolecular hydroxylation of the aromatic ring covalently appended to the analog of **1**.[75] Although only one non-heme iron(V)-oxo complex has been directly observed at low temperature as a transient species and characterized by a variety of spectroscopic methods,[76] and recent (albeit preliminary)[77] EPR results suggested transient, low-yield generation of Fe(V) from $Fe(BPMEN)^{2+}$ and H_2O_2,[78]

indirect evidence supporting participation of non-heme Fe(V)-oxo intermediates in oxidations of alcohols,[79] olefins,[79-81] and arenes[60, 75, 82] continues to accumulate.

2.4 **Conclusions**

In summary, $Fe(BPMEN)^{2+}$ (complex **1**) is efficient in promoting hydroxylation of aromatic hydrocarbons with hydrogen peroxide, and the reaction is greatly accelerated by additions of carboxylic acids. The system reported herein is a rare example of an efficient aromatic hydroxylation with non-heme iron complex and hydrogen peroxide that allows for an unambiguous interpretation of the role of the Fe^{III}-hydroperoxo intermediates. A new $(BPMEN)Fe^{III}(OOH)$ intermediate is definitely involved in the reaction pathway, but it does not attack the aromatic rings directly, generating a different, metal-based active oxidant instead. Another new intermediate, $(BPMEN)Fe^{IV}=O$, was generated and shown to be unreactive with aromatic substrates. An acid-assisted O-O bond heterolysis of coordinated peroxides is likely involved in the reaction pathway (Scheme 2-4). Inverse H/D kinetic isotope effects and the NIH shift in hydroxylations of selectively deuterated substituted benzenes imply an electrophilic attack of the aromatic ring by the oxidant and exclude a hydrogen atom abstraction as the key step in the hydroxylation pathways.

2.5 **Experimental section.**

2.5.1 General

All chemicals and solvents were purchased from Aldrich, Acros Organics or Fisher Scientific and were used without additional purification unless otherwise noted. $H_2{}^{18}O_2$ (90 % isotopic purity, 2 % solution in water) was obtained from ICON Isotopes, $H_2{}^{18}O$ (98 %) was purchased from Cambridge Isotope Laboratories. Use of anhydrous HPLC grade acetonitrile is imperative in order to obtain $Fe^{III}(OOH)$ intermediate. GCMS experiments were carried out using a Shimadzu GC-17A gas chromatograph (Rtx-xLB column) with a GCMS-QP 5050 mass detector. Time-resolved spectra of rapid hydroxylation reactions were acquired with TgK Scientific (formerly HiTech Schientific, Salisbury, Wiltshire, UK) SF-61DX2 cryogenic Stopped-flow system equipped with J&M Diode array (Spectralytics).

2.5.2 Materials

Isopropyl ester of 2-iodoxybenzoic acid (IBX-ester),[36] N,N'-dimethyl-N,N'-bis(2-pyridylmethyl)ethane-1,2-diamine (BPMEN)[83] and $[Fe(BPMEN)(CH_3CN)_2](ClO_4)_2$ (**1**)[84] were prepared using published procedures. 2-methyl-1-phenyl-2-propyl hydroperoxide (MPPH), generously provided by Prof. John Caradonna, was recrystallized from pentane (20 °C) prior to use until iodometric titration proved > 98 % activity.[44] For iodometric titration solid KI (210 mg) was added to recrystallized MPPH (30 mg) dissolved in aqueous acetic acid (20 mL, 25% v/v). The reaction was allowed to proceed for 10 hr in a

sealed flask followed by quick titration of the resulting brown solution with $Na_2S_2O_3$ (0.1 M aqueous solution). mCPBA was washed with phosphate buffer (pH = 7.4), solid was filtered and left to dry on the filter and then recrystallized from DCM. Note: dry solution using $MgSO_4$ if needed, warm up DCM solution (~35 ˚C) to dissolve mCPBA.

2.5.3 Determination of phenol yield using GCMS

Mixture of **1** with benzene in CH_3CN was prepared in a glove box. Hydrogen peroxide was prepared aerobically and delivered at room temperature; the resulting solution was stirred for 30 min for reaction to complete. Reaction mixtures were acetylated (0.1 mL of 1-methylimidazole and 1 mL of acetic anhydride) for 30 min followed by addition of 1 M HCl (2 mL) and extraction with dichloromethane (1 mL). The organic layer was washed with saturated aqueous $NaHCO_3$ (2 mL), water (2 mL) and finally dried over $MgSO_4$. Internal standard (nitrobenzene or naphthalene) was added prior to the extraction. Yields of hydroxylated products were established by GCMS relative to the internal standard and converted to absolute yields using a calibration curve with phenyl acetate and the corresponding standard, determined prior to each run.

All experiments were run at least in triplicate, reported yields are average of these trials.

2.5.4 Stopped-flow experiments

Kinetic measurements were performed in the diode array mode using stopped-flow instrument. Reactivity of **1** with hydrogen peroxide in the presence of benzene was

studied in acetonitrile at 20 °C. In a single mixing experiment, solution of **1** with benzene was prepared in a glove box and mixed with H_2O_2 in the stopped-flow. In a double mixing experiment **1** was mixed with H_2O_2, the reaction mixture was incubated to reach the highest yield of Fe^{III}(OOH) (age time), followed by addition of benzene. Effect of acetic acid on hydroxylation rate was studied in a double mixing experiment, where Fe^{III}(OOH) was pre-generated by mixing **1** and H_2O_2 at 20 ˚C followed by addition of benzene with variable amounts of acetic acid (1-4 equiv vs. **1**). Concentrations of all reagents are reported in the figure captions for the onset of the reaction (after mixing). Kinetic parameters were determined in SPECFIT (global fitting), Kinetic Studio or IgorPro using single-exponential (A→B) or double exponential (A→B→C) models. Single-exponential fit was calculated to $A = A_{inf} + \Delta A \exp(-kt)$, where A_{inf} is absorbance of the reaction mixture after reaction is complete, $\Delta A = A_0 - A_{inf}$, A_0 is initial absorbance. Similarly, double-exponential fit was calculated using $A = A_{inf} + \Delta A_1 \exp(-k_1 t) + \Delta A_2 \exp(-k_2 t)$. All experiments were run in at least triplicate and averaged rate constants are reported.

The activation enthalpy and entropy for Fe^{III}(OOH) formation were calculated from linear Arrhenius and Eyring plots.

2.5.5 Isotope-Labeling Studies

Mixture of **1** (2 mM) and of benzene (280 equiv vs. **1**) was prepared in a glove box. In experiments with labeled hydrogen peroxide, 11 μL of $H_2{}^{18}O_2$ (0.53 M, 3 equiv vs. **1**) was added to **1**/benzene mixture (1 mL) at room temperature. In experiment with labeled

water, 11 μL of $H_2{}^{18}O$ (98 %) was added to solution of the **1**/benzene (1 mL) prior to the addition of H_2O_2 (60 μL of 0.1 M H_2O_2 diluted by CH_3CN from 70 % stock solution). After 30 min the reaction mixture was subjected to GCMS analysis as described above.

2.5.6 EPR studies

Purple species **1a** was generated directly in the EPR tube by mixing **1** (3 mM, 0.15 mL) with H_2O_2 (30 mM, 0.15 mL) in acetonitrile at room temperature. The tube was frozen immediately after all hydrogen peroxide was injected (5 s). **1a** decays fast when treated with acetic acid: **1a** was pre-generated in the EPR tube as described above and then acetic acid (1.5 mM, 0.11 mL, <0.5 equiv vs. iron) was injected into the tube and reaction quenched in liquid nitrogen (reaction time 5 s). All EPR spectra were acquired at 120 K. EPR spectra simulation were done using SimFonia (Bruker).

2.5.7 MPPH cleavage

O_2 was bubbled through 1 mL of anaerobically prepared solution of **1** (2mM) and benzene (280 equiv vs. iron) in acetonitrile for 20 s followed by injection of MPPH (60 μL, 2 μmol, 1 equiv vs. iron) at room temperature. After addition of MPPH, solutions were stirred for ~30 min and prepared for GCMS analysis as described above. When looking at the effects of H^+ on the reactivity, acetic acid (10 μL, 1 μmol, 0.5 equiv vs. iron) was added to **1**/benzene mixture before purging it with O_2.

Blank solutions containing only 1 mL of pure acetonitrile were treated same way as **1**/benzene solutions. Control samples with pure bibenzyl, benzyl alcohol acetate,

benzaldehyde, 2-methyl-1-phenyl-2-propyl alcohol acetate (MPPol), phenyl acetate and nitrobenzene were run to find detector response for each product against nitrobenzene.

2.6 **References:**

[1] M. C. White, A. G. Doyle, E. N. Jacobsen, *J. Am. Chem. Soc.* **2001**, *123*, 7194.

[2] O. V. Makhlynets, P. Das, S. Taktak, M. Flook, R. Mas-Balleste, E. V. Rybak-Akimova, L. Que, Jr., *Chem. Eur. J.* **2009**, *15*, 13171.

[3] J.-U. Rohde, J.-H. In, M. H. Lim, W. W. Brennessel, M. R. Bukowski, A. Stubna, E. Münck, W. Nam, L. Que, Jr., *Science* **2003**, *299*, 1037.

[4] J. England, Y. Guo, E. R. Farquhar, V. G. Young, Jr., E. Münck, L. Que, Jr., *J. Am. Chem. Soc.* **2010**, *132*, 8635.

[5] E. J. Klinker, J. Kaizer, W. W. Brennessel, N. L. Woodrum, C. J. Cramer, L. Que, Jr., *Angew. Chem. Int. Ed.* **2005**, *44*, 3690.

[6] L. Que, Jr., W. B. Tolman, *Nature* **2008**, *455*, 333.

[7] M. S. Chen, C. White, *Science* **2007**, *318*, 783.

[8] S. Taktak, M. Flook, B. M. Foxman, L. Que, Jr., E. V. Rybak-Akimova, *Chem. Commun.* 2005, *42*, 5301.

[9] L. Que, Jr., *J. Biol. Inorg. Chem.* **2004**, *9*, 684.

[10] I. V. Korendovych, S. V. Kryatov, E. V. Rybak-Akimova, *Acc. Chem. Res.* **2007**, 40, 510.

[11] E. A. Duban, K. P. Bryliakov, E. P. Talsi, *Eur. J. Inorg. Chem.* **2007**, 852.

[12] R. Mas-Ballesté, L. Que, Jr., *J. Am. Chem. Soc.* **2007**, *129*, 15964.

[13] Although blue species decays over time this process is not due to overoxidation reaction, GCMS analysis showed that the blue solution (maximum accumulation of phenolate) and the yellow solution (1 h after the onset of the reaction) contain the same amount of phenol (Figure S2).

[14] H. Marusawa, K. Ichikawa, N. Narita, H. Murakami, K. Ito, T. Tezuka, *Bioorg. Med. Chem.* **2002**, *10*, 2283.

[15] C. Kim, K. Chen, J. Kim, L. Que, Jr., *J. Am. Chem. Soc.* **1997**, *119*, 5964.

[16] M. Lubben, A. Meetsma, E. C. Wilkinson, B. Ferinda, L. Que, Jr., *Angew. Chem. Int. Ed.* **199**5, *34*, 1512.

[17] P. Mialane, A. Nivorojkine, G. Pratviel, L. Azema, M. Slany, F. Godde, A. Simaan, F. Banse, T. Kargar-Grisel, G. Bouchoux, J. Sainton, O. Horner, J. Guilhem, L. Tchertanova, B. Meunier, J.-J. Girerd, *Inorg. Chem.* **1999**, *38*, 1085.

[18] B. Bernal, I. M. Jensen, K. B. Jensen, C. J. McKenzie, H. Toftlund, J.-P. Tuchagues, *J. Chem. Soc., Dalton Trans.* **1995**, 3667.

[19] K. B. Jensen, C. J. McKenzie, N. P. Nielsen, J. Z. Pedersen, H. M. Svendsen, *Chem. Commun.* **1999**, 1313.
[20] T. J. Mizoguchi, S. J. Lippard, *J. Am. Chem. Soc.* **1998**, *120*, 11022.
[21] V. Balland, F. Banse, E. Anxolabehere-Mallart, M. Ghiladi, T. A. Mattioli, C. Philouze, G. Blondin, J.-J. Girerd, *Inorg. Chem.* **2003**, *42*, 2470.
[22] A. J. Simaan, S. Dopner, F. Banse, S. Bourcier, G. Bouchoux, A. Boussac, P. Hildebrandt, J.-J. Girerd, *Eur. J. Inorg. Chem.* **2000**, *7*, 1627.
[23] D. Quiñonero, K. Morokuma, D. G. Musaev, R. Mas-Ballesté, L. Que, Jr., *J. Am. Chem. Soc.* **2005**, *127*, 6548.
[24] J.-J. Girerd, F. Banse, A. J. Simaan, *Structure and Bonding* **2000**, *97*, 145.
[25] R. M. Burger, S. B. Horwitz, J. Peisach, J. B. Wittenberg, *J. Biol. Chem.* **1979**, *254*, 12999.
[26] M. S. Chow, L. V. Liu, E. I. Solomon, *Proc. Natl. Acad. Sci. U.S.A.* **2008**, *105*, 13241.
[27] I. Lippai, R. S. Magliozzo, J. Peisach, *J. Am. Chem. Soc.* **1999**, *121*, 780.
[28] C. Nguyen, R. J. Guajardo, P. K. Mascharak, *Inorg. Chem.* **1996**, *35*, 6273.
[29] W. Nam, R. Ho, J. S. Valentine, *J. Am. Chem. Soc.* **1991**, *113*, 7052.
[30] X. Shan, L. Que, Jr., *J. Inorg. Biochem.* **2006**, *100*, 421.
[31] K. Chen, M. Costas, L. Que, Jr., *J. Chem. Soc., Dalton Trans.* **2002**, *5*, 672.
[32] M. J. Park, J. Lee, Y. Suh, J. Kim, W. Nam, *J. Am. Chem. Soc.* **2006**, *128*, 2630.
[33] Y. Zhou, X. Shan, R. Mas-Balleste, M. R. Bukowski, A. Stubna, M. Chakrabarti, L. Slominski, J. A. Halfen, E. Münck, L. Que, Jr., *Angew. Chem. Int. Ed.* **2008**, *47*, 1896.
[34] R. Mas-Ballesté, E. Münck, L. Que, Jr., *manuscript in preparation*.
[35] Acetic acid facilitates O-O bond cleavage of Fe^{III}(OOH) (purple) and formation of very unstable active species that quickly converts into iron(III) complex (yellow), the later reacts with hydrogen peroxide (in excess) to produce Fe^{IV}=O. To test this hypothesis we generated Fe^{III}(OOH) by mixing **1** and 1.5 equiv of H_2O_2 (stoichiometric amount) and then added acetic acid to the preformed **2**, as expected we saw a decay of Fe^{III}(OOH) and very low yield of Fe^{IV}=O (Figure S23).
[36] V. V. Zhdankin, D. N. Litvinov, A. Y. Koposov, T. Luu, M. J. Ferguson, R. McDonald, R. R. Tykwinski, *Chem. Commun.* **2004**, 106.
[37] I. M. Geraskin, O. Pavlova, H. M. Neu, M. S. Yusubov, V. N. Nemykin, V. V. Zhdankin, *Adv. Synth. Catal.* **2009**, *351*, 733.
[38] J.-U. Rohde, A. Stubna, E. Bominaar, E. Münck, W. Nam, L. Que, Jr., *Inorg. Chem.* **2006**, *45*, 6435.
[39] M. S. Seo, J.-H. In, S. O. Kim, N. Y. Oh, J. Hong, J. Kim, L. Que Jr., W. Nam, *Angew. Chem. Int. Ed.* **2004**, *43*, 2417.
[40] B. Meunier, J. Bernadou, *Structure and bonding* **2000**, *97*, 1.
[41] M. D. Wolfe, J. D. Lipscomb, *J. Biol. Chem.* **2003**, *278*, 829.
[42] I. M. Jensen, S. J. Lange, M. P. Mehn, E. L. Que, L. Que, Jr., *J. Am. Chem. Soc.* **2003**, *125*, 2113.
[43] T. L. Foster, J. Caradonna, *J. Am. Chem. Soc.* **2003**, *125*, 3678.
[44] G. T. Rowe, E. V. Rybak-Akimova, J. P. Caradonna, *Chem. Eur. J.* **2008**, *14*, 8303.

[45] P. A. MacFaul, K. U. Ignold, D. D. M. Wayner, L. Que, Jr., *J. Am. Chem. Soc.* **1997**, *119*, 10594.
[46] To check stability of MPPH during the work up and GCMS experiments we set up two control experiments containing a) MPPH and b) MPPH with equimolar amount of acetic acid. In both cases the main product was bibenzyl (product of benzyl radical coupling) with small amount of MPPol. For hydroxylation experiments we used 1 equiv of MPPH to minmize any contribution of MPPH self-decomposition.
[47] R. P. Hanzlik, G. O. Shearer, *Biochem. Pharm.* **1978**, *27*, 1441.
[48] K. R. Korzekwa, D. C. Swinney, W. F. Trager, *Biochemistry* **1989**, *28*, 9019.
[49] K. H. Mitchell, C. E. Rogge, T. Gierahn, B. G. Fox, *Proc. Natl. Acad. Sci. U.S.A.* **2003**, *100*, 3784.
[50] R. P. Hanzlik, K.-H. J. Ling, *J. Am. Chem. Soc.* **1993**, *115*, 9363.
[51] D. R. Boyd, J. W. Daly, D. M. Jerina, *Biochemistry* **1972**, *11*, 1961.
[52] M.-J. Kang, W. J. Song, A.-R. Han, Y. S. Choi, H. G. Jang, W. Nam, *J. Org. Chem.* **2007**, *72*, 6301.
[53] S. P. de Visser, K. Oh, A.-R. Han, W. Nam, *Inorg. Chem.* **2007**, *46*, 4632.
[54] G. R. Moran, A. Derecskei-Kovacs, P. J. Hillas, P. F. Fitzpatrick, *J. Am. Chem. Soc.* **2000**, *122*, 4535.
[55] P. C. A. Bruijnincx, G. van Koten, R. J. M. Klein Gebbink, *Chem. Soc. Rev.* **2008**, *37*, 2716.
[56] L. J. Murray, S. J. Lippard, *Acc. Chem. Res.* **2007**, *40*, 466.
[57] D. A. Alonso, C. Nájera, I. M. Pastor, M. Yus, *Chem. Eur. J.* **2010**, *16*, 5274.
[58] E. V. Kudrik, A. B. Sorokin, *Chem. Eur. J.* **2008**, *14*, 7123.
[59] A. Thibon, J.-F. Bartoli, R. Guillot, J. Sainton, M. Martinho, D. Mansuy, F. Banse, *J. Mol. Catal. A* **2008**, *287*, 115.
[60] J. Yoon, S. A. Wilson, Y. K. Jang, M. S. Seo, K. Nehru, B. Hedman, K. O. Hodgson, E. Bill, E. Solomon, W. Nam, *Angew. Chem. Int. Ed.* **2009**, *48*, 1.
[61] A. Thibon, J.-F. Bartoli, S. Bourcier, F. Banse, *Dalton. Trans.* **2009**, 9587.
[62] E. V. Rybak-Akimova, in *Physical inorganic chemistry* (Ed.: A. Bakac), Wiley, Hoboken, **2010**, pp. 109.
[63] E. I. Solomon, S. D. Wong, L. V. Liu, A. Decker, M. S. Chow, *Curr. Opin. Chem. Biol.* **2009**, *13*, 99.
[64] R. M. Burger, J. Peisach, S. B. Horwitz, *J. Biol. Chem.* **1981**, *256*, 11636.
[65] E. G. Kovaleva, J. Lipscomb, *Nat. Chem. Biol.* **2008**, *4*, 186.
[66] B. E. Eser, E. W. Barr, P. A. Frantom, L. Saleh, J. M. Bollinger, C. Krebs, P. F. Fitzpatrick, *J. Am. Chem. Soc.* **2007**, *129*, 11334.
[67] M. H. Lim, J.-U. Rohde, A. Stubna, M. R. Bukowski, M. Costas, R. Y. N. Ho, E. Münck, W. Nam, L. Que, Jr., *Proc. Natl. Acad. Sci. U.S.A.* **2003**, *100*, 3665.
[68] M. Martinho, F. Banse, J.-F. Bartoli, T. Mattioli, P. Battioni, O. Horner, S. Bourcier, J.-J. Girerd, *Inorg. Chem.* **2005**, *44*, 9592.
[69] J. Kaizer, E. J. Klinker, N. Y. Oh, J.-U. Rohde, W. J. Song, A. Stubna, J. Kim, E. Münck, W. Nam, L. Que, Jr., *J. Am. Chem. Soc.* **2004**, *126*, 472.

[70] N. Y. Oh, Y. Suh, M. J. Park, M. S. Seo, J. Kim, W. Nam, *Angew. Chem. Int. Ed.* **2005**, *44*, 4235.
[71] G. Xue, R. De Hont, E. Münck, L. Que Jr., *Nat. Chem.* **2010**, *2*, 400.
[72] J. M. Bollinger, Jr., C. Krebs, *J. Inorg. Biochem.* **2006**, *100*, 586.
[73] W. Nam, *Acc. Chem. Res.* **2007**, *40*, 522.
[74] N. Y. Oh, M. S. Seo, M. H. Lim, M. B. Consugar, M. J. Park, J.-U. Rohde, J. Han, K. M. Kim, J. Kim, L. Que, Jr., W. Nam, *Chem. Commun.* **2005**, 5644.
[75] A. Nielsen, F. B. Larsen, A. D. Bond, C. J. McKenzie, *Angew. Chem. Int. Ed.* **2006**, *45*, 1602.
[76] F. T. de Oliveira, A. Chanda, D. Banerjee, X. Shan, S. Mondal, L. Que, Jr., E. Bominaar, E. Münck, T. J. Collins, *Science* **2007**, *315*, 835.
[77] We have not been able to trap the intermediate described in the paper.
[78] O. Y. Lyakin, K. P. Bryliakov, G. J. P. Britovsek, E. P. Talsi, *J. Am. Chem. Soc.* **2009**, *131*, 10798.
[79] S. H. Lee, J. H. Han, H. Kwak, E. Y. Lee, H. J. Kim, J. H. Lee, C. Bae, S. N. Lee, Y. Kim, C. Kim, *Chem. Eur. J.* **2007**, *13*, 9393.
[80] K. Chen, M. Costas, J. Kim, A. K. Tipton, L. Que, Jr., *J. Am. Chem. Soc.* **2002**, *124*, 3026.
[81] A. Company, Y. Feng, M. Güell, X. Ribas, J. M. Luis, L. Que, Jr., M. Costas, *Chem. Eur. J.* **2009**, *15*, 3359.
[82] Y. Feng, C. Ke, G. Xue, L. Que, Jr., *Chem. Commun.* **2009**, 50.
[83] S. Poussereau, G. Blondin, M. Cesario, J. Guilhem, G. Chottard, F. Gonnet, J.-J. Girerd, *Inorg. Chem.* **1998**, *37*, 3127.
[84] K. Chen, L. Que, Jr., *Chem. Commun.* **1999**, 1375.
[85] W. A. E. McBryde, *Can. J. Chem.* **1968**, *46*, 2385.
[86] T. Kurata, Y. Watanabe, M. Katoh, Y. Sawaki, *J. Am. Chem. Soc.* **1988**, *110*, 7472.
[87] G. C. Swain, J. E. Sheats, D. G. Gorenstein, K. G. Harbison, *J. Am. Chem. Soc.* **1975**, *97*, 791.
[88] S. H. Korzeniowski, L. Blum, G. W. Gokel, *J. Org. Chem.* **1977**, *42*, 1469.

3 Studies of the modified complexes with ligands structurally similar to BPMEN

3.1 Introduction

Regioselective hydroxylation of aromatic acids with hydrogen peroxide proceeds readily in the presence of an iron(II) complex utilizing a tetradentate aminopyridine ligand: $[Fe^{II}BPMEN(CH_3CN)_2](ClO_4)_2$ (**1**). In previous work we have identified, generated in high yield, and experimentally characterized the key $Fe^{III}(OOH)$ intermediate (λ_{max} = 560 nm, rhombic EPR signal with g = 2.21, 2.14, 1.96) formed by **1** and H_2O_2 (chapter 2). Stopped-flow kinetic studies showed that $Fe^{III}(OOH)$ does not directly hydroxylate the aromatic rings, but undergoes rate-limiting self-decomposition producing transient reactive oxidant. The reactive species formation is facilitated by acid-assisted cleavage of the O-O bond in the iron-hydroperoxide intermediate. Acid-assisted benzene hydroxylation with **1** and a mechanistic probe, MPPH, correlates with O-O bond heterolysis. Independently generated Fe^{IV}=O species, which may originate from O-O bond homolysis in $Fe^{III}(OOH)$, proved to be inactive toward aromatic substrates. Direct characterization of the intermediates and products, and kinetic analysis of the individual reaction steps suggests that Fe^{V}=O is the active oxidant responsible for aromatic hydroxylation in **1**/H_2O_2 system. Unfortunately, this reactive intermediate could not be trapped and characterized by available to us methods (stopped-flow, EPR, resonance Raman). In attempt to observe the reactive intermediate, we have modified BPMEN

ligand and crystallized a series of Fe(II) complexes that all share cis-α topology and are reactive toward aromatic substrates (Scheme 3-1). We expected that more electron-donating ligands would stabilize high oxidation state of iron and thus we would have better chances to observe the putative Fe^{V}=O.

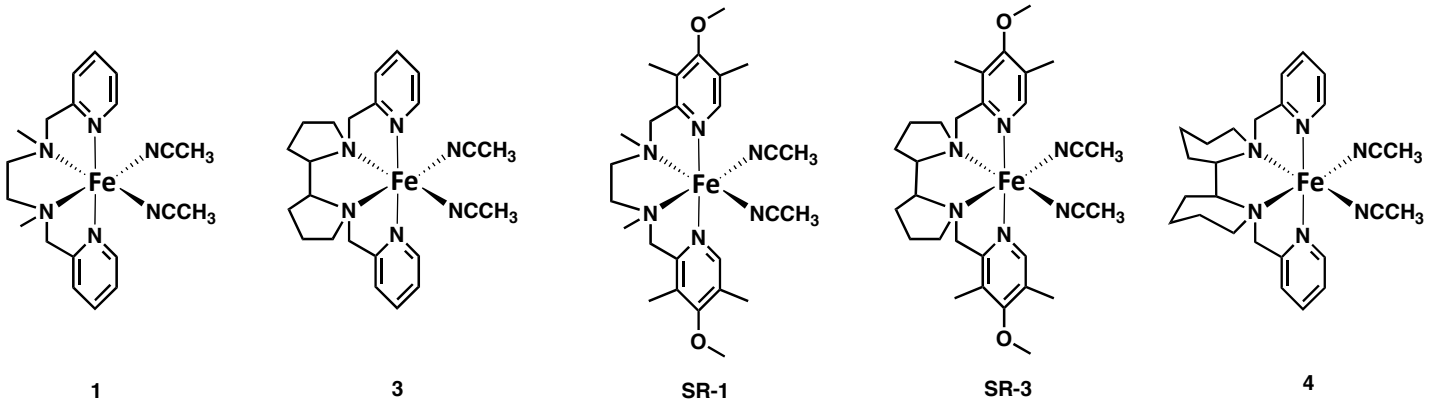

Scheme 3-1. Structures of Fe^{II} complexes used in this work: **1**- $[Fe^{II}BPMEN(CH_3CN)_2]^{2+}$; **3**-$[Fe^{II}(BPBP)(CH_3CN)_2]^{2+}$; **SR-1** - $[Fe^{II}(SR\text{-}BPMEN)(CH_3CN)_2]^{2+}$; **SR**-**3**- $[Fe^{II}(SR\text{-}BPBP)(CH_3CN)_2]^{2+}$, where SR-BPBP means super rich BPBP; **4**-$[Fe^{II}PYBP(CH_3CN)_2](ClO_4)_2$

3.2 **Experimental part**

3.2.1 General

All chemicals and solvents were purchased from Aldrich, Acros Organics or Fisher Scientific and were used without additional purification unless otherwise noted. Use of anhydrous HPLC grade acetonitrile is imperative in order to obtain $Fe^{III}(OOH)$ intermediate. (S,S)-2,2'-bipyrrolidine was purchased from OBITER Research. $H_2{}^{18}O_2$ (90

% isotopic purity, 2 % solution in water) was obtained from ICON Isotopes. ^{57}Fe metal (94 %) was purchased from CIL. GCMS experiments were carried out using a Shimadzu GC-17A gas chromatograph (Rtx-xLB column) with a GCMS-QP 5050 mass detector. Time-resolved spectra were acquired with TgK Scientific (formerly HiTech Schientific, Salisbury, Wiltshire, UK) SF-61DX2 cryogenic Stopped-flow system equipped with J&M Diode array (Spectralytics) or Hi-Tech tungsten lamp. Resonance Raman spectra were collected on an Acton AM-506 spectrometer (1200 groove grating) using a Kaiser Optical holographic super-notch filters with a Princeton Instruments liquid-N_2-cooled (LN-1100PB) CCD detector with a 4 cm^{-1} spectral resolution. The Raman frequencies were referenced to indene. Baseline corrections (polynomial fits) were carried out using Grams/32 Spectral Notebase Version 4.04 (Galactic). EPR spectra were acquired on Bruker EMX EPR spectrometer at 120 K (unless noted otherwise). Cyclic voltammetry experiments were performed on a EG&G PAR 273 potentiostat using a three electrod cell with a glassy carbon working electrode and platinum wire counter- and reference electrodes.

3.2.2 Synthesis

Isopropyl ester of 2-iodoxybenzoic acid (IBX-ester),[1] N,N'-dimethyl-N,N'-bis(2-pyridylmethyl)ethane-1,2-diamine (BPMEN) [2] and $[Fe(BPMEN)(CH_3CN)_2](ClO_4)_2$ (**1**) [3] were prepared using published procedures. *(S,S)-BPBP* ligand and $[Fe(BPBP)(CH_3CN)_2](SbF_6)_2$ (**3**) were synthesized using a slightly modified published procedure. [4]

BPBP: Reaction flask was charged with (S,S)-2,2'-bipyrrolidine (300 mg, 2.14 mmol), dichloromethane (5 mL) and water (5 mL). Solid 2-picolyl chloride hydrochloride (0.7 g, 4.28 mmol, 2 equiv) was added to the mixture. Sodium hydroxide (560 mg, 14 mmol, 6.4 equiv) was dissolved in water (5 mL) and ¼ of the resulting solution was added to the biphasic mixture upon vigorous stirring. The rest of sodium hydroxide solution was added dropwise over 4 hr. Aqueous layer was extracted with dichloromethane (3x7 mL), organic layers combined and washed once with water (10 mL) and then dried over $MgSO_4$. Ligand was used without further purification. NMR spectrum is in the SI (Figure C1).

$[Fe^{II}(BPBP)(CH_3CN)_2](SbF_6)_2$ (**3**): Complex was synthesized and stored in the glove box under argon atmosphere. (S,S)-BPBP (543 mg, 1.68 mmol) was dissolved in acetonitrile (5 mL) and $FeCl_2*4H_2O$ was added as a solid (334 mg, 1.68 mmol, 1 equiv) to a stirring solution. Bright orange precipitate formed immediately and mixture was left to react. In 24 h solid was washed with ether and dried in the glove box. Fe(S,S-BPBP)Cl_2 (750 mg, 1.55 mmol) was suspended in acetonitrile (5 mL) and $AgSbF_6$ (1.07 g, 3.11 mmol, 2 equiv) was added upon stirring and resulting reaction mixture was stirred for 24 h. Red-purple solution was filtered through 0.45µm GHP Acrodisc® membrane twice, concentrated in vacuo and solid redisolved in acetonitrile (2 mL). Needle crystals were obtained by ether diffusion in ~ 2 weeks.

SR-BPMEN: (N,N'-dimethyl-N,N'-bis(2-(3,5-dimethyl-4-methoxy-pyridylmethyl)ethane-1,2-diamine) was synthesized following protocol similar to synthesis of (S,S)-BPBP. N,N'-Dimethylethylenediamine (194 mg, 2.2 mmol) was dissolved in water (5 mL) and then 2-

chloromethyl-4-methoxy-3,5-dimethylpyridine hydrochloride (977 mg, 4.4 mmol, 2 equiv) and CH_2Cl_2 (5 mL) were added to the flask. Sodium hydroxide (528 mg, 13.2 mmol, 6 equiv) was dissolved in water (5 mL) and 1/3 of the resulting solution was added to the biphasic mixture upon vigorous stirring. The rest of sodium hydroxide solution was added dropwise over 4 hr. In 17-20 h aqueous layer was extracted with dichloromethane (3x7 mL), organic layers combined and washed once with water (10 mL) and then dried over $MgSO_4$. Ligand was purified by silica gel chromatography (5% MeOH, 2 % NH_4OH in dichloromethane). [4] 1H NMR ($CDCl_3$): δ (ppm) 2.18 (s, 3H, -CH3), 2.23 (s, 3H -CH3), 2.28 (s, 3H, -CH3), 2.60 (s, 2H, N-CH2-CH2-N), 3.58 (s, 2H, py-CH2-N), 3.74 (s, 3H, -OMe), 8.16 (s, 1H) – Figure C2.

$[Fe^{II}$(SR-BPMEN)$(CH_3CN)_2](ClO_4)_2$ (**SR-1**): SR-BPMEN in acetonitrile (280 mg,72 mmol, 2 mL acetonitrile) was added dropwise to the solution of $Fe(ClO_4)_2*6H_2O$ in acetonitrile (263 mg, 0.72 mmol, 1 equiv in 2 mL of acetonitrile). Crystals of **SR-1** suitable for X-ray were obtained by ether diffusion. Elemental analysis: calculated for $[Fe^{II}$SR-BPMEN$(CH_3CN)_2](ClO_4)_2$ ($C_{26}H_{40}Cl_2FeN_6O_{10}$): C, 43.17; H, 5.57; Fe, 7.72; N, 11.62; found C, 42.42; H, 5.61; Fe, 7.61; N, 11.25.

SR-BPBP ligand was synthesized using procedure described above for SR-BPMEN ligand and purified by recrystallization from acetonitrile. For NMR spectrum of recrystallized ligand see SI (Figure C3).

$[Fe^{II}$SR-BPBP$(CH_3CN)_2](ClO_4)_2$ (**SR-3**): Purple crystals of **SR-3** were obtained by mixing equal amounts of $Fe(ClO_4)_2*6H_2O$ (dissolved in acetonitrile) and SR-BPBP ligand (add as a solid), stir resulting dark purple solution (ligand dissolves in the presence of iron salt)

for 1 hour and filter dark brown precipitate using 0.45µm GHP Acrodisc® membrane and set up ether diffusion. Dark block-shaped purple crystals crystallize along with bright orange needle crystals. To get purple crystals only, stop crystallization early before orange needles start to form. For identity of orange material see results and discussion section.

[^{57}Fe^{II}SR-BPBP(CH$_3$CN)$_2$](ClO$_4$)$_2$ (**^{57}SR-3**): $^{57}FeCl_2$ was prepared by dissolving ^{57}Fe metal in concentrated HCl under nitrogen, after removing water under flow of nitrogen $^{57}FeCl_2$ was kept in the glove box with argon atmosphere. $^{57}FeCl_2$,dissolved in acetonitrile, was mixed with SR-BPBP ligand (1:1), mixture turned yellow (note: no precipitate). $AgClO_4$ (2 equiv) was added to the bright yellow solution, as a result white ppt appeared and color of solution slowly changed to dark purple. In 30 min, solution was filtered using 0.45 µm GHP Acrodisc and crystallized by ether diffusion.

iPr-BPMEN: ligand was synthesized from picolyl chloride (2 equiv) and N,N'-diisopropylethylenediamine (1 equiv) in DCM/H_2O mixture by slowly adding ~6 equiv of NaOH (over 6 hours). In 2 days extract organic products using chloroform and purify the ligand by high vacuum distillation. For NMR spectrun see SI (Figure C4).

Fe^{II}(iPr-BPMEN)(OTf)$_2$: $Fe(OTf)_2$ was dissolved in EtCN and ligand was dissolved in about the same volume of DCM, solution of ligand was slowly added to solution of triflate. Pale green complex was crystallized using ether diffusion technique after about a week.

3.2.3 EPR studies

It is very important to use HPLC grade anhydrous acetonitrile! To prepare $Fe^{III}(OOH)$ from **3** and **1-SR**, acetonitrile solution of complex (2 mM, 0.2 mL) was placed in an EPR tube and hydrogen peroxide (20 mM, 0.2 mL) was injected at 0 ˚C and -20 ˚C correspondingly, mixtures were incubated at 0 ˚C for 30 s (**3**) and at -20 ˚C for 200 s (**SR-1**). For experiments with acetic acid, **3** or **1-SR** was mixed with H_2O_2 at 0 ˚C and incubated in acetone/dry ice bath for 30 s and then acetic acid was added and sample frozen immediately in liquid nitrogen ([**3**] = [**1-SR**] = 0.75 mM, [H_2O_2] = 75 mM, [CH_3COOH] = 0.25 mM after mixing). $Fe^{III}(OOH)$ intermediate supported by SR-BPBP was generated in acetonitrile by adding H_2O_2 (0.2 mL, 20 mM) directly into EPR tube that contains solution of **SR-3** (0.2 mM, 2 mM) at 10 ˚C and freezing the sample immediately in liquid nitrogen. EPR sample of SR-3X intermediate was prepared by mixing acetonitrile solutions of **SR-3** (0.2 mL, 2 mM) and H_2O_2/HOAc (0.2 mL, [H_2O_2] = 10 mM, [HOAc] = 2 mM) directly in the EPR tube at -30 ˚C, and incubating the sample at -30 ˚C for 50 s.

3.2.4 Resonance Raman samples

Samples of $Fe^{III}(OOH)$ (5 mM) were prepared by running reaction between **SR-3** (0.2 mL, 10 mM) and H_2O_2 (0.1 mL, 0.1 M, 5 equiv vs. Fe) directly in the EPR tube at 0 ˚C and quenching it in liquid nitrogen immediately after mixing reagents. ^{18}O labeled $Fe^{III}(OOH)$ was generated using same protocol, however 0.1 M solution of $H_2{}^{18}O_2$ in acetonitrile must be thoroughly dried with $MgSO_4$. Sample of **SR-3X** (5 mM) was prepared from **SR-3**

(0.2 mL, 10 mM) and HOAc/H_2O_2 (0.1 mL, [H_2O_2] = 50 mM, [HOAc] = 10 mM) directly in the EPR tube at -40 ˚C, reaction was quenched in liquid nitrogen immediately after mixing reagents.

3.2.5 Mössbauer samples

$^{57}Fe^{III}$(OOH) was generated directly in Mössbauer cup by mixing ^{57}Fe(SR-BPBP) (0.2 mL, 2 mM) and H_2O_2 (0.2 mL, 20 mM) at room temperature and freezing the mixture in liquid nitrogen immediately (orange-pink). Sample of ^{57}Fe labeled **SR-3X** intermediate (2 mM) was generated from ^{57}Fe(SR-BPBP) (0.4 mL, 4 mM) and HOAc/H_2O_2 (0.4 mL, [H_2O_2] = 20 mM, [HOAc] = 4 mM) after both solutions were precooled to -30 ˚C (aceton/dry ice bath). After incubating the sample at -30 ˚C for 25 s transfer ~ 0.2 mL of the mixture into Mössbauer cup and freeze it (pale red).

3.2.6 Electrochemical experiments

Cyclic voltammetry experiment (CV) were done under argon atmosphere in dry acetonitrile, acetone or methanol with $TBAPF_6$ as electrolyte. In all experiments concentration of complex was 1 mM, concentration of electrolyte – 0.1 M, scan rate – 0.1 V/s.

3.3 **Results and discussion**

3.3.1 New complexes

Topology of the complex and presence of labile ligands are important for catalysis, as acetonitrile molecules can be easily displaced by oxygen and substrate, therefore positioning oxidant and substrate adjacent to each other. [5,6] Complexes **1-4, SR-1** and **SR-3** contain six-coordinate ferrous center coordinated with two acetonitrile molecules and tetradentate ligand in cis-α topology (Scheme 3-1, Figure 3-1). Crystal structures of **1,**[3] **3,**[4] and **4** (manuscript in preparation) have been published before. Ether diffusion into acetonitrile solution containing SR-BPBP (or SR-BPMEN) ligand and $Fe(ClO_4)_2$ gives two types of crystals: dark purple (Figure 3-1) and orange needle-shaped crystals. Purple complex crystallizes first, so removing crystals before crystallization is complete is efficient method to separate purple and orange material. X-ray analysis of orange complex identified it as differic (μ-O) (μ-OH) species (Figure C5).

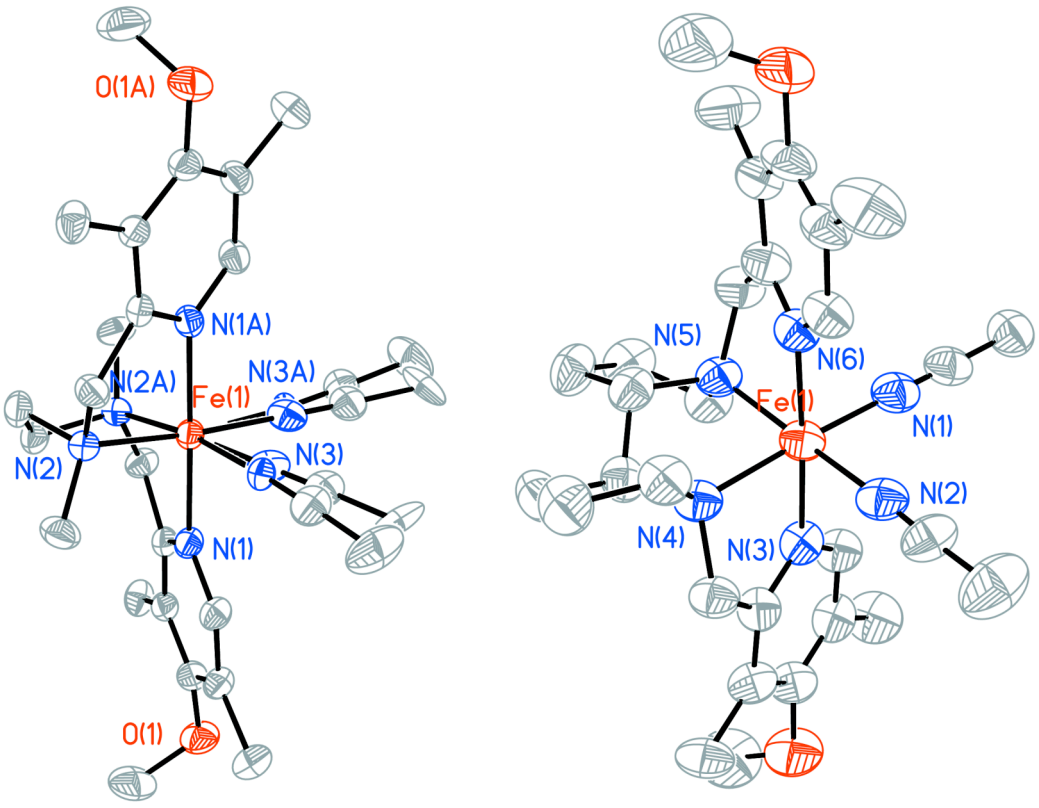

Figure 3-1. X-Ray structure of the complex: left- $[Fe^{II}SR\text{-}BPMEN(CH_3CN)_2]^{2+}$ (**SR-1**) and right- $[Fe^{II}SR\text{-}BPBP(CH_3CN)_2]^{2+}$ (**SR-3**) with 50% probability thermal ellipsoids (hydrogen atoms omitted for clarity). Structure of **SR-3** was acquired at room temperature (Albany, Dr. Alexander Filatov).

3.3.2 Hydroxylation of benzene

We have previously reported that **1** promotes efficient aromatic hydroxylation of benzenes (chapter 2), [7] here we show that **3**, **4**, **SR-1** and **SR-3** can also hydroxylate benzene (Figure 3-2). GCMS analysis shows about the same yield of phenol with **1**, **3**, **SR-1** and **SR-3** in the range of 0.6-0.7 TON. When we followed formation of phenolate in

2/H_2O_2/benzene system we did not observe 650 nm band of phenolate but only the formation of (TPA)Fe^{III}(OOH) (λ_{max} = 540 nm). However, GCMS yield of phenolate with **2** is 0.5 TON (0.6 TON for **1**). Presumably (TPA)Fe(III)-phenolate is unstable and does not accumulate. Orange complex that cocrystallizes with **SR-1** and was formulated as (μ-O)(μ-OH) species (see 3.3.1) did not hydroxylate benzoic acid and, when mixed with H_2O_2, did not produce any intermediates that we could identify from UV-vis spectrum (Figure C6).

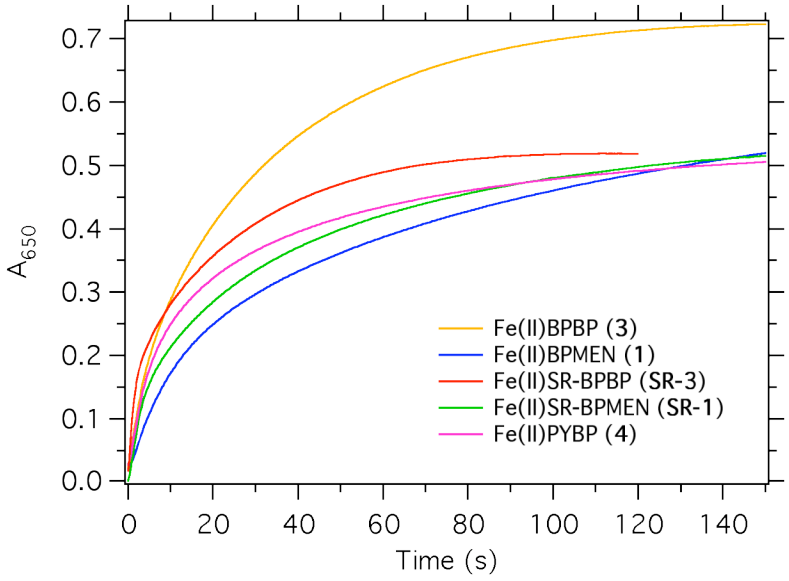

Figure 3-2. Kinetic traces at 650 nm represent formation of Fe(III)-phenolate product, complexes **1**, **3**, **4**, **SR-1**, and **SR-3** are capable of hydroxylating benzene. Experiment was performed in a single mixing mode: [Fe^{II}L] = 0.5 mM, [H_2O_2] = 5 mM, 300 equiv of benzene vs. iron.

H/D migrations and rearrangements provide meaningful mechanistic information. In aromatic hydroxylations, a hydrogen atom shift (the so-called NIH shift) is common for

reactions that proceed via an electrophilic attack of the oxidant on the aromatic ring with subsequent rearrangement of the cationic intermediate to a ketone intermediate. [8] We observed a non-zero NIH shift for hydroxylation of 3,5-$^2H_2$-chlorobenzene and 2,4,6-$^2H_3$-chlorobenzene with **1**/H_2O_2, these results corroborate electrophilic addition to the aromatic ring (Table 3-1). More rigid complex **3** showed higher deuterium retention (NIH shift) presumably due to lesser side reactions (hydroxylation by OH radicals would give zero NIH shift).

Table 3-1. Deterium retention in a competitive isotope effect experiment.

complex	Chlorobenzene substrate	Deuterium retention in chlorophenol products, % *			reference
		ortho	*meta*	*para*	
1[a]	$^2H_0$/3,5-$^2H_2$	97.0 (0.5)	11.9 (2.4)	93.6 (0.9)	[7]
1[a]	$^2H_0$/2,4,6-$^2H_3$	17.1 (1.1)	93.1 (1.5)	32.7 (1.6)	[7]
3[b]	$^2H_0$/2,4,6-$^2H_3$	32.5 (0.6)	91.8 (1.4)	55.5 (0.8)	This work

*Average and standard deviation of at least five independent experiments, each sample was analyzed twice. Substrate composition: $^2H_0$/^2H_x=1; reaction conditions: [a] [**1**] = 2 mM, 280 equiv of chlorobenzenes, 3 equiv of H_2O_2 vs. **1**, 0 ° C, [b] [**3**] = 1 mM, 300 equiv of chlorobenzenes, 3 equiv of H_2O_2 vs. **3,** rt.

3.3.3 Formation of the Fe^{III}(OOH) intermediate, spectroscopic characterization

In previous work we have shown that **1** reacts with H_2O_2 under optimal conditions to give high yields of Fe^{III}(OOH). In this work we report that all new complexes (**SR-3, 3, SR-1, 4**) also afford Fe^{III}(OOH) (λ_{max} = 560 nm) upon reaction with H_2O_2 (Figure 3-4, C7, C8, C9 correspondingly). The plot of the observed rate constants versus hydrogen peroxide concentration under pseudo-first-order conditions (ca. 10-fold excess H_2O_2 with respect to Fe^{II}L) is a straight line with a nearly zero intercept (Figure C10), indicating first-order in H_2O_2 and the overall mixed second-order for the formation of Fe^{III}(OOH). Unlike the majority of reactive intermediates, that are generated in higher yields at low temperature, no Fe^{III}(OOH) can be observed when **1** and H_2O_2 are mixed at -30 ˚C but the yield of Fe^{III}(OOH) increased as temperature increased from -30 °C to + 20 °C (Figure C11). Similar behavior was observed for complexes **3, SR-1** and **SR-3** (Figure C12), however when new complexes are used we can generate significant amount of intermediate even at -30 ˚C. Rate constant of Fe^{III}(OOH) formation and its decay are comparable at low temperatures, therefore the intermediate does not accumulate at low temperatures; rate constant of Fe^{III}(OOH) formation increases significantly with temperature while rate constant of its decay does not depend on temperature (Figure C13), as a result yield of Fe^{III}(OOH) increases with temperature.

It has been proposed that water promotes O-O bond cleavage in Fe^{III}(OOH), this hypothesis is best supported by the observation that one oxygen of the *cis*-diol product is derived from H_2O_2 and the other from added isotope labeled water.[9] Stopped-flow

studies of Fe^{III}(OOH) decay in the presence of variable amounts of water corroborates previously proposed mechanism of water assisted O-O bond cleavage (Figure 3-3).

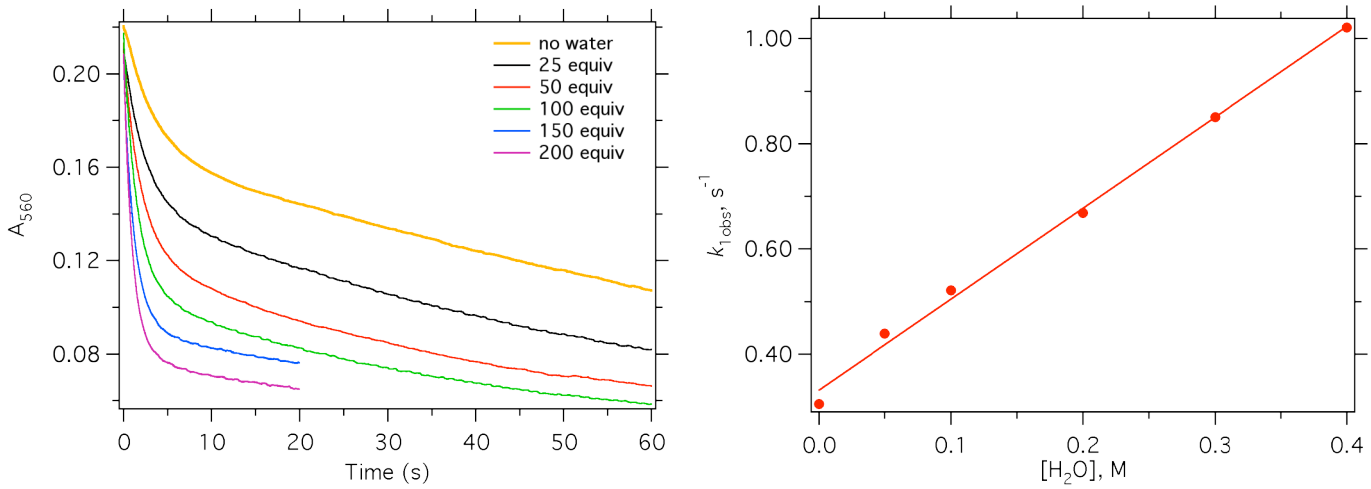

Figure 3-3. Kinetic traces at 560 nm show decomposition of Fe^{III}(OOH) in the presence of variable amounts of water (left). Experiment was performed using stopped-flow in double mixing mode, Fe^{III}(OOH) was pregenerated by reacting **3** and H_2O_2 in acetonitrile at 20 ˚C, at the maximum accumulation of this intermediate (5 s) water was added (0-200 equiv vs. **3**); [**3**] = 0.5 mM, [H_2O_2] = 5 mM. Kinetic traces were fitted to two-exponential rate law and first observed rate constant was plotted against concentration of water (right).

Activation parameters provide additional insight into the mechanism of Fe^{III}(OOH) formation. All complexes showed similar activation enthalpy for the formation of Fe^{III}(OOH). Eyring plots for the Fe^{III}(OOH) formation and decay in a reaction between **SR-3, 3, SR-1** and H_2O_2 are in SI (Figure C14, C15, C16).

Table 3-2. Activation parameters for Fe^{III}(OOH) formation from **1**, **SR-1**, **3**, and **SR-3** and H_2O_2.

	$\Delta H^{‡}$, kJ/mol formation of Fe^{III}(OOH)	$\Delta S^{‡}$, kJ/(mol K) formation of Fe^{III}(OOH)	k 283 K, s^{-1} M^{-1} formation of Fe^{III}(OOH)	$\Delta H^{‡}$, kJ/mol decay of Fe^{III}(OOH)	$\Delta S^{‡}$, kJ/(mol K) decay of Fe^{III}(OOH)
Fe^{II}BPMEN (**1**)	55.0	-29.3	11.9		
Fe^{II}BPBP (**3**)	55.6	-18.3	36.1	44.4	-92.9
Fe^{II}SR-BPMEN (**SR-1**)	59.2	-2.5	51.9	56.3	-39.3
Fe^{II}SR-BPBP (**SR-3**)	51.5	-23.4	108.4		

The least favorable entropy was expected for the bulkiest complex (**SR-3**), however experimental results showed a different trend (Table 3-2). Activation parameters for a multi-step conversion of Fe^{II}L into Fe^{III}(OOH) are likely to be composite values, and straightforward interpretation may be misguided. Formation of Fe^{III}(OOH) from Fe^{II}L and H_2O_2 is at least two step process – first ferrous iron is oxidized into ferric iron and then Fe^{III}L reacts with H_2O_2 to afford Fe^{III}(OOH). These two steps can be observed in stopped-flow using double mixing mode: mixing Fe^{II}L and 0.5 equiv of H_2O_2 shows only Fe^{II}→Fe^{III} oxidation (slight growth at 460 nm, Figure C17), subsequent addition of hydrogen peroxide gives Fe^{III}(OOH). Unfortunately, it is very difficult to determine the age time looking at Fe^{II}/Fe^{III} oxidation (λ = 460 nm) because absorbance does not change much; therefore we failed to obtain linear Eyring plots for the Fe^{III}→ Fe^{III}(OOH) step.

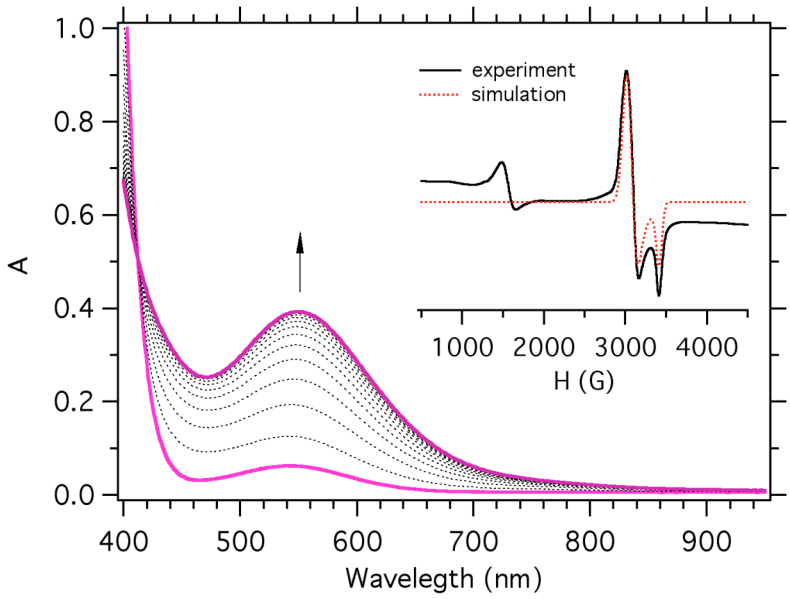

Figure 3-4. Time resolved UV-vis spectra of the Fe^{III}(OOH) formation at 20 °C in acetonitrile ([**SR-3**] **=** 1 mM, [H_2O_2] = 10 mM). Maximum accumulation of Fe^{III}(OOH) was seen in 2 s after mixing reagents (shown in the graph). Inset: EPR spectrum (120 K) of the Fe^{III}(OOH), generated by mixing **SR-3** and H_2O_2 in acetonitrile at 0 ˚C and frozen in 30 s after reagents were mixed ([**SR-3**] = 1 mM, [H_2O_2] = 10 mM after mixing). G values 2.18, 1.99 and 1.95.

EPR spectrum of a purple intermediate generated from **3** has signals at g = 2.175, 2.000 and 1.955 (Figure C18) which are associated with Fe^{III}(OOH) species. Electron-rich analog of **3** – complex **SR-3** – produced Fe^{III}OOH with g values very similar to those of (BPBP)Fe^{III}(OOH) (Figure 3-4, Figure 3-10). Similarly to **1**, complex **SR-1** produced two species with H_2O_2 at room temperature: one of them features g values at 2.40, 2.16 and 1.90 and another at 2.18, 1.99 and 1.95 (Figure C19). EPR and UV-vis spectra give

evidence that $Fe^{III}(OOH)$ is formed when Fe(II) complexes with BPMEN-like ligands react with H_2O_2. **4** gives low yield of $Fe^{III}(OOH)$ or this intermediate does not accumulate and we see only traces, g values are similar to those of $Fe^{III}(OOH)$ described in this paragraph (Figure C9). All EPR spectra were acquired at 120 K; increasing the temperature of data acquisition decreased intensity of the signals but the shape of the spectrum remained the same in the range of temperatures between 120 K and 200 K (Figure C20), therefore composition of the sample does not change (we were looking for a spin crossover [10]).

rRaman spectra of the hydroperoxoiron(III) complex **SR-3a** were collected at 676.4, 568.1, 514.5, 457.9, and 406.7 nm (Figure 3-5 left). None of these spectra exhibited isotope sensitive features and as the laser excitation wavelength neared the UV-region, ligand vibrations were resolved, as confirmed by comparison of the rRaman spectrum of the parent complex at λ_{ex} = 406.7 nm (Figure 3-5 right). Color of $Fe^{III}(OOH)$ species changes upon freezing from purple to orange-pink. Similar behavior was observed with $(TPA)Fe^{III}(OOH)$ complex in acetonitrile.[11] The problem was solved by preparing purple $(TPA)Fe^{III}(OOH)$ species in DCM/ACN mixture (1:1) as color did not change upon freezing. However changing solvent in **SR-3**/H_2O_2 system did not give the same positive result, on contrary attempts to generate $Fe^{III}(OOH)$ in solvents other than acetonitrile gave very low to zero yields of this species (Figure C21). Mixing **1** and H_2O_2 in PrCN gave species with g values different from those assigned to $(BPMEN)Fe^{III}(OOH)$ (**1a**), however small signal at g = 1.96 indicates that some of **1a** has been formed (Figure C22). EPR spectra of $(TPA)Fe^{III}(OOH)$ in acetonitrile (orange/pink when frozen) and DCM/acetonitrile are

identical (Figure C23), so both samples contain Fe^{III}(OOH), however change in color may be effecting rRaman results.

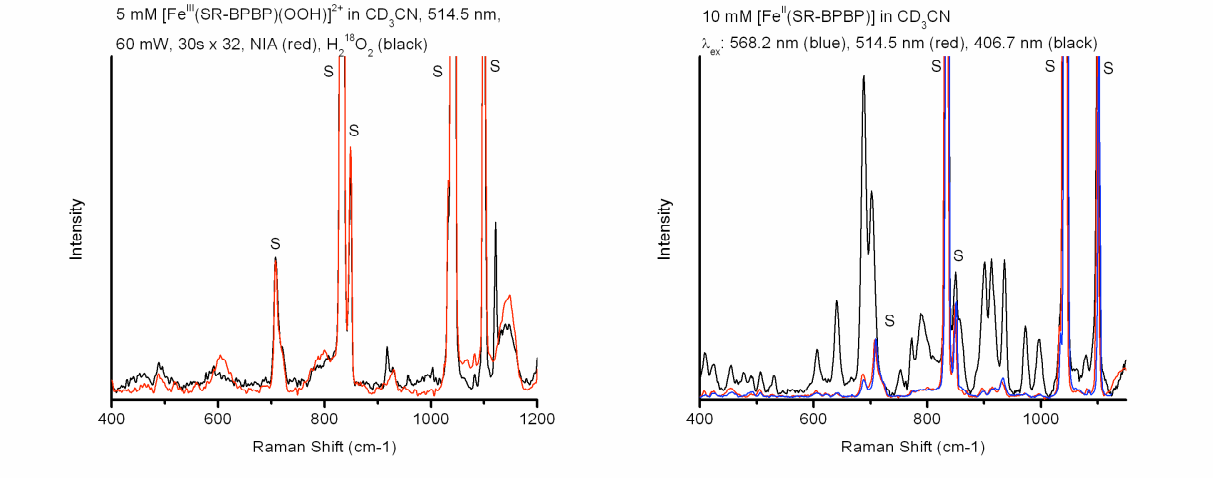

Figure 3-5. Resonance Raman spectra of Fe^{III}(OOH) (**SR-3a**) and **SR-3** in CD_3CN. Left: rRaman spectra acquired using 514.5 nm laser on samples containing ~ 5 mM Fe^{III}(OOH) (red) and ^{18}O labeled Fe^{III}(OOH) (black); right: rRaman spectra of Fe^{II}SR-BPBP using 568.2 (blue), 514.5 (red) and 406.7 (black) excitation wavelength.

3.3.4 Cyclic voltammetry studies

To evaluate what complex would be the easiest to oxidize and thus to support a high valent iron, we determined redox-potentials of **1, 3, SR-1, SR-3,** and **4** (Figure C24, C25, C26, C27, and C28). As expected, complexes with electron-donating ligands have lower reduction potentials and higher rates of Fe^{III}(OOH) formation (Table 3-3).

Table 3-3. Reduction potentials vs. ferrocene/ferrocenium couple determined from CV experiments and second order rate constant of $Fe^{III}(OOH)$ formation at 20 ˚C.

complex	ligand	E (Fe^{2+}/Fe^{3+}), V	k 293 K, s^{-1} M^{-1}
1	BPMEN	0.728	35
3	BPBP	0.660	82
SR-1	SR-BPMEN	0.600	130
SR-3	SR-BPBP	0.529	225
4	PYBP	0.656	

3.3.5 CH_3COOH promotes decomposition of $Fe^{III}(OOH)$ into reactive oxidant

We have shown previously that acetic acid facilitates decay of $Fe^{III}(OOH)$ and leads to faster Fe^{III}-phenolate formation, thus acetic acid promotes formation of reactive species responsible for aromatic hydroxylation. Moreover, acid-assisted O-O bond heterolysis of a mechanistic probe MPPH in the presence of **1** and benzene was accompanied by a significant growth in yields of hydroxylated product (phenolate), these results suggest that hydroxylation is performed by Fe^{V}=O species (chapter 2).[7] Carboxylic acid-assisted O-O bond heterolysis pathway leading to a yet to be observed Fe^{V}=O oxidant has been proposed by Mas-Ballesté and Que in the efficient epoxidation of olefins by H_2O_2 in the presence of acetic acid and $[Fe^{II}(TPA)(CH_3CN)_2]^{2+}$, and it also appears to be a likely mechanism of regioselective benzoic acid hydroxylations. Therefore we postulated that Fe^{V}=O is generated in reaction between $Fe^{III}(OOH)$ with acetic acid. When acetic acid is added at the maximum formation of (SR-BPBP)$Fe^{III}(OOH)$ (**SR-3a**), another intermediate (**SR-3X**) accumulates quickly (1 s at 20 ˚C, λ_{max} = 465 nm,

Figure 3-6). **SR-3X** is unstable and decays into species that looks like low spin Fe^{IV}=O (this conclusion is based on UV-vis spectrum only, see Figure C29). Species with λ_{max} = 750 nm (Fe^{IV}=O) did not form when reaction between (SR-BPBP)Fe^{III}(OOH) and H_2O_2/HOAc was carried out at -10 ˚C (compare Figure C29 left and right). Fe^{III}(OOH) intermediate generated from **3** and H_2O_2 also decays quickly when acetic acid is added with subsequent accumulation of Fe^{IV}=O (based on UV-vis spectrum only: λ_{max} = 750 nm, Figure C30). Both **1** and **3** afford Fe^{III}(OOH) that decomposes in the presence of acetic acid into featureless intermediate which later gives Fe^{IV}=O. On the other hand, Fe^{III}(OOH) supported by electron rich ligands (generated from **SR-1** and **SR-3**) reacts with acetic acid to form intermediate that absorbs in visible region (Figure 3-6).

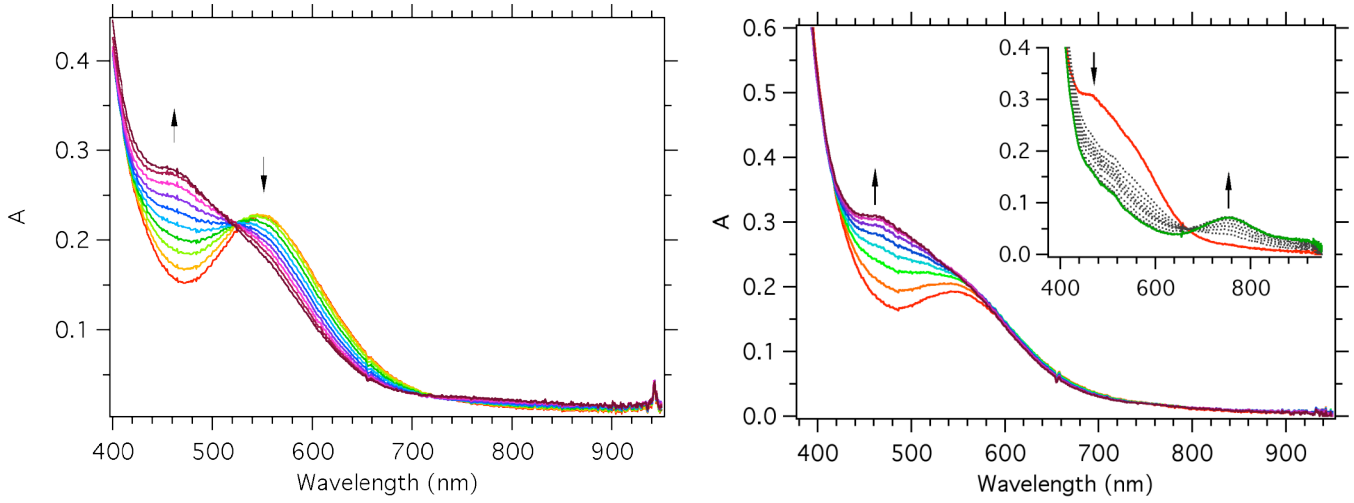

Figure 3-6. Spectral changes upon addition of acetic acid to Fe^{III}(OOH) in acetonitrile at 20 ˚C. Left: Fe^{III}(OOH) was pregenerated from **SR-3** and H_2O_2 and then acetic acid was added, time scale shown is 1 s. Right: Fe^{III}(OOH) was pre-generated by mixing **SR-1** and H_2O_2 at 20 °C in acetonitrile over 5 s. Fe^{III}(OOH) decays quickly (~3 s) upon addition of acetic acid followed by slow (over 80 s) accumulation of Fe^{IV}=O (λ_{max} = 760 nm, see inset); ([$\mathbf{Fe^{II}L}$] = 0.5 mM, [H_2O_2] = 5 mM, [CH_3COOH] = 0.5 mM after double mixing).

$Fe^{III}(OOH)$ generated from **4** and H_2O_2 does not quickly decay in the presence of acetic acid which is different behavior from we have seen for other complexes (Figure C31).

To get a spectroscopic signature of **SR-3X** we followed the reaction between **SR-3a** and acetic acid by EPR (Figure 3-7). EPR signals at g = 2.18, 1.99 and 1.95 were assigned to (SR-BPBP)$Fe^{III}(OOH)$. When acetic acid is added (<1 equiv), (SR-BPBP)$Fe^{III}(OOH)$ decays fast (7 s at 0 ˚C) into a EPR-silent species. Signals at g = 2.4, 2.16 and 1.90 presumably belong to a low spin $Fe^{III}L$. Same experiment but with **SR-1** and **3** resulted in very similar EPR spectrum (Figure C32).

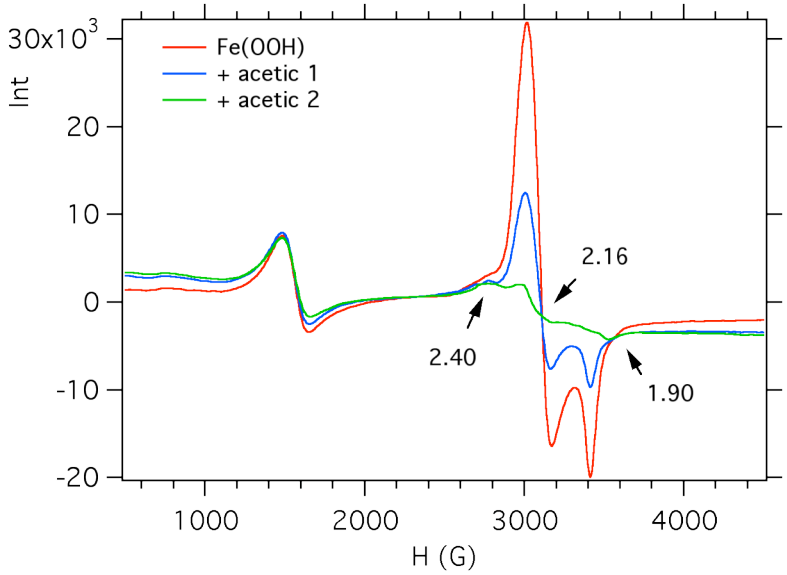

Figure 3-7. EPR spectra (120 K) of (SR-BPBP)$Fe^{III}(OOH)$ and a product of its decay. Acetonitrile solutions of **SR-3** and H_2O_2 were mixed in the EPR tube at 0 ˚C and incubated at 0 ˚C for 30 s, then acetic acid was added and reaction quenched in ~5 s (acetic 1) and ~7 s (acetic 2), ([**SR-3**] = 0.8 mM, [H_2O_2] = 8 mM, [CH_3COOH] = 0.4 mM).

To summarize, $Fe^{III}(OOH)$ obtained from complexes **3, SR-1, SR-3** decomposes in the presence of acetic acid to form a new intermediate, which has a prominent absorption band in visible region when supported by electron-donating ligand. This new intermediate is EPR silent at 120 K.

3.3.6 Reactivity of the new intermediate

SR-3 has the lowest reduction potential among ferrous complexes with BPMEN-like ligands (Table 3-3); therefore it could be most efficient in stabilizing high valent iron. Since acetic acid accelerates hydroxylation of benzene in **1**/H_2O_2 system, it has been postulated that acetic acid promotes conversion of $Fe^{III}(OOH)$ into reactive oxidant. As shown in Figure 3-6, addition of acetic acid to pregenerated $Fe^{III}(OOH)$ yields a new intermediate with λ_{max} = 465 nm (**SR-3X**) which is presumably an active oxidant in hydroxylation reaction. **SR-3X** can be generated in one step by mixing **SR-3**, H_2O_2 and acetic acid (Figure 3-8). Same spectrophotometric yield of **SR-3X** was observed with 2, 5 and 10 equiv of H_2O_2.

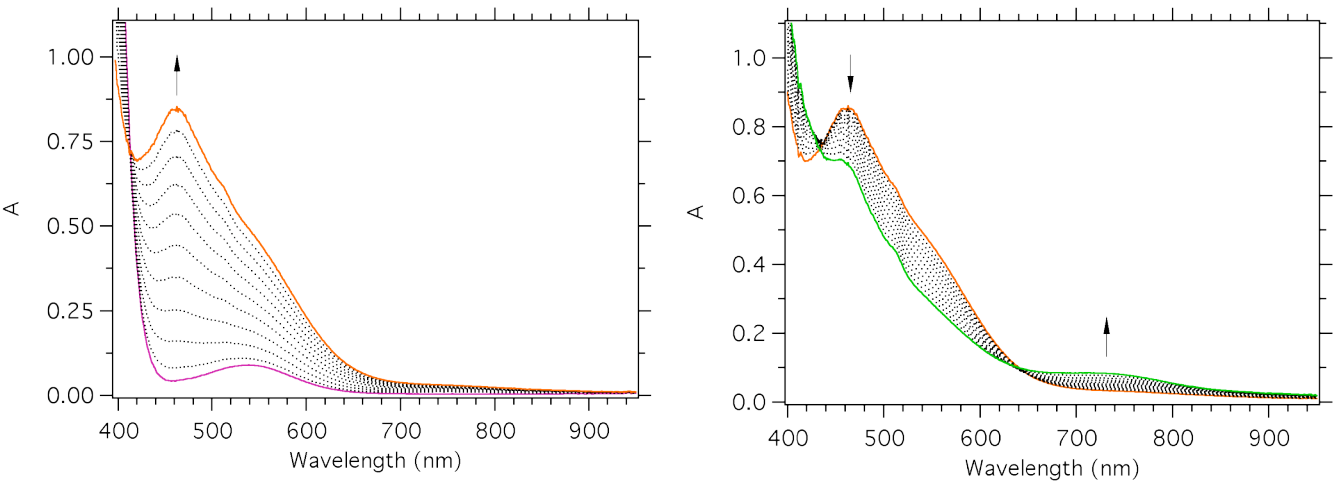

Figure 3-8. Spectral changes after mixing **SR-3**, H_2O_2 and acetic acid in acetonitrile at -30 ˚C ([**SR-3**] = 1 mM, [H_2O_2] = 5 mM, [CH_3COOH] = 1 mM). Formation of **SR-3X** is shown on the left (0-62 s) and its decay (62-120 s) is on the right.

Stopped-flow studies of the reaction between **SR-3X** and benzene showed accumulation of hydroxylated product (Fe^{III}-phenolate) only when excess of H_2O_2 was present (5 equiv and above). **SR-3X**, generated using 1 equiv of H_2O_2, does not hydroxylate benzene (Figure C33), however if benzene/H_2O_2 mixture is added to pregenerated **SR-3X** hydroxylation takes place (Figure C34). When reaction between **SR-3**, benzene and H_2O_2 is performed in one step phenolate product accumulates; upon mixing **SR-3** and H_2O_2 Fe^{III}(OOH) is formed, so it would be expected that this species decomposes with formation of an active Fe-based oxidant. However Fe^{III}(OOH) self decay does not yield **SR-3X** (Figure C35). A mixture of H_2O_2 with acetic acid can oxidize **SR-3** into **SR-3X**, thus peroxy acid could serve as an oxidant in this reaction. Interestingly, when mCPBA is used as an oxidant **SR-3X** can be observed but formation

of the intermediate is obscured by the absorption of Fe(III)-salycilate which is the hydroxylation product (Figure 3-9). This observation means that peroxy acids can generate **SR-3X** and this species can promote self-hydroxylation of mCPBA. **2** reacts with mCPBA as well to form low-spin Fe^{IV}=O (λ_{max} = 720 nm) and then self-hydroxylation product accumulates.[12] Differences in the reactivity will be discussed in the next section.

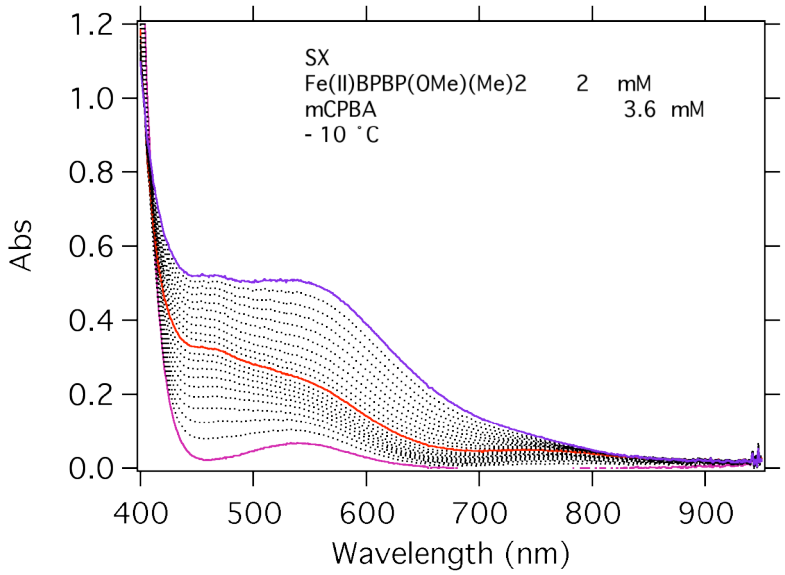

Figure 3-9. Spectral changes during the reaction between **SR-3** and recrystallized mCPBA in acetonitrile at -10 ˚C. First, change in absorbance at 460 nm is observed (red) and then product accumulates (blue). [**SR-3**] = 1 mM, [mCPBA] = 1.8 mM, time scale shown 10 s.

*3.3.7 Identity of the new intermediate **SR-3X***

Acetic acid promotes O-O bond heterolysis of Fe^{III}(OOH) and thus formation of Fe^{V}=O. However, **SR-3X** species was found to be EPR silent (Figure 3-7) which is

inconsistent with **SR-3X** being Fe^{V}=O. EPR spectrum of **SR-3X** at 2.4 K (Figure 3-10) is very similar to the one acquired at 120 K (Figure 3-7).

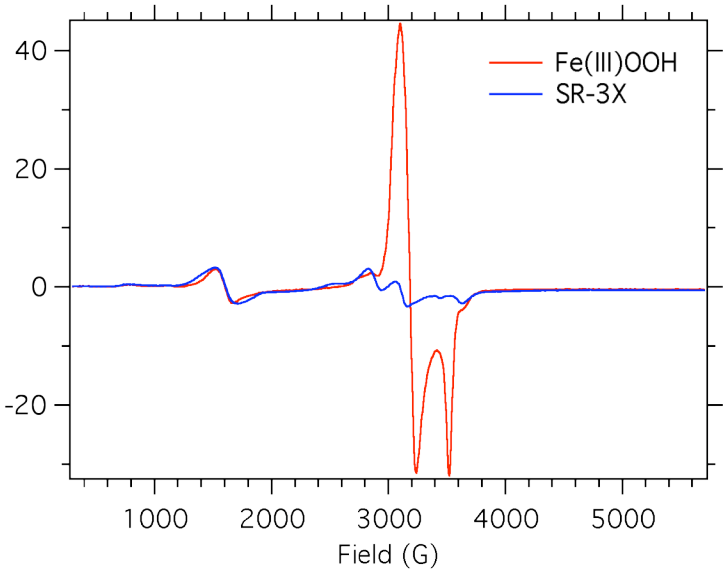

Figure 3-10. EPR spectra of (SR-BPBP)Fe^{III}(OOH) (**SR-3a**) and **SR-3X** intermediate acquired at 2.4 K. Fe^{III}(OOH): **SR-3** (0.2 mM, 2 mM) + H_2O_2 (0.2 mL, 20 mM); **SR-3X** : **SR-3** (0.2 mL, 2 mM) and H_2O_2/HOAc (0.2 mL, [H_2O_2] = 10 mM, [HOAc] = 2 mM).

Increasing concentration of complex five fold and running reaction between **SR-3** and H_2O_2/HOAc led to the same EPR signals as at lower concentration of complex (Figure 3-11). Signals denoted with * may belong to a low-spin Fe^{III}L (Fe^{II}→Fe^{III} oxidation) that accompanies Fe^{III}(OOH) and is stable in the presence of acetic acid. It appears that the main species in the sample (**SR-3X**) is EPR silent and therefore has iron with integer spin (S = 1, S = 2). Low-spin Fe^{IV}=O (S = 1) has a maximum in near IR region (720-760 nm), [13-16] so its electronic spectrum is not consistent with **SR-3X** (λ_{max} = 465 nm).

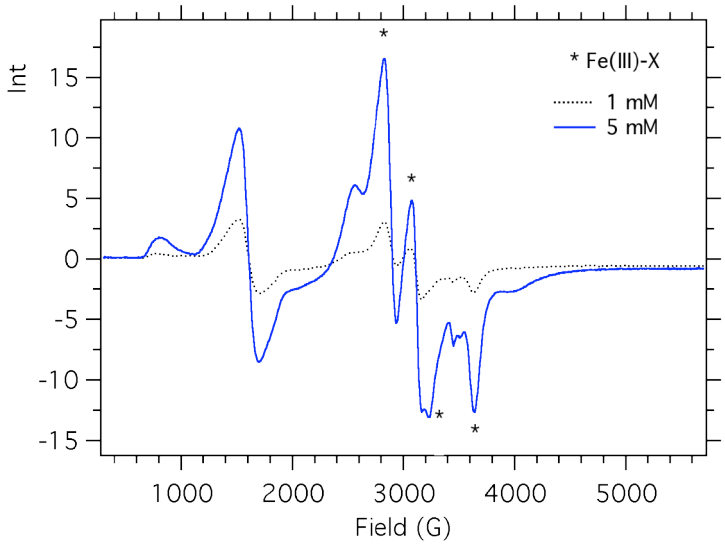

Figure 3-11. EPR spectra of **SR-3X** intermediate acquired at 2.4 K. 5 mM: **SR-3** (0.2 mL, 10 mM) + HOAc/H_2O_2 (0.1 mL, [H_2O_2] = 50 mM, [HOAc] = 10 mM); 1 mM: **SR-3** (0.2 mL, 2 mM) and H_2O_2/HOAc (0.2 mL, [H_2O_2] = 10 mM, [HOAc] = 2 mM).

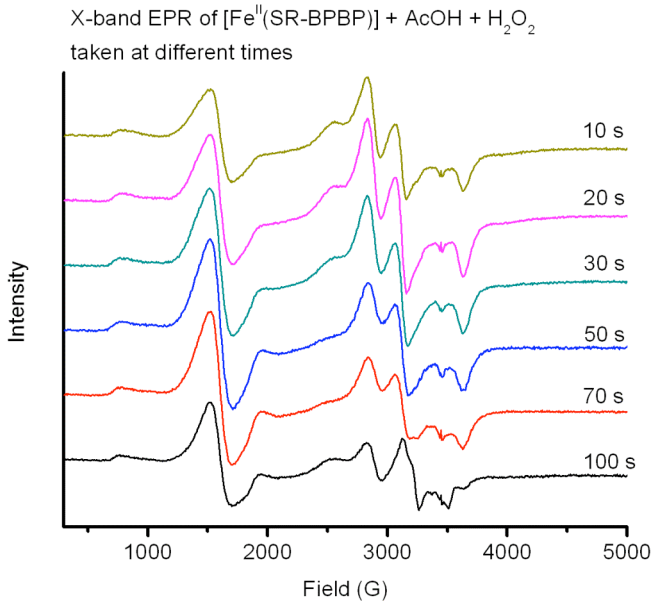

Figure 3-12. EPR spectra of samples prepared by reacting **SR-3** with H_2O_2/HOAc and incubating reaction mixture at -35 ˚C for 10, 20, 30, 50, 70 and 100 s; [**SR-3**] = 1 mM, [HOAc] = 1 mM, [H_2O_2] = 5 mM.

Low-spin Fe^{IV}=O species can be formed upon reaction of Fe^{II}L with the following reagents: H_2O_2/HOAc, peroxyacetic acid, IBX-ester, iodosobenzene. Interesting to note, that mixing **SR-3** with IBX-ester would only give low-spin Fe^{IV}=O (Figure C36), on the other hand reaction of **SR-3** with mCPBA or H_2O_2/HOAc results in formation of **SR-3X**. Recently, a synthetic high-spin oxoiron(IV) complex was synthesized and spectroscopically characterized.[17] High-spin Fe^{IV}=O has been proposed as an active oxidant in a variety of oxygen-activating enzymes and in some cases this species was trapped in characterized.[18] Electronic spectrum of high-spin Fe^{IV}=O is significantly different from that of low-spin Fe^{IV}=O (λ_{max} = 750 nm) - synthetic high-spin Fe^{IV}=O has a maximum at 400 nm [17] and high-spin Fe^{IV}=O from TauD has a maximum at 320 nm. [19] Since intermediate **SR-3X** is EPR silent and has a maximum at 465 nm it could be high-spin Fe^{IV}=O.

To monitor the formation of **SR-3X** we mixed **SR-3** and H_2O_2/HOAc and quenched reaction in liquid nitrogen at different times. EPR spectra of these samples show that composition does not change much in the time range 10-70 s, although the relative yield of low-spin species appears to be higher in samples with short reaction time (Figure 3-12).

It is known that acetic acid can serve as a bridge and promote formation of $[Fe_2(\mu\text{-}O)(\mu\text{-}OOCCH_3)(BPMEN)_2]^{3+}$.[20] Taking into account that **SR-3X** is EPR silent and that ferric centers can antiferromagnetically couple in a dimer, **SR-3X** could be a dimeric species with a bridging carboxylate, therefore acetic acid could play two roles - bridging motif

and a source of protons. Non-coordinating triflic acid appears to be less efficient in generating **SR-3X** (Figure C37). We also tried to generate **SR-3X** using different carboxylic acids (acetic, cycloxehylcarbonic, trimethylacetic) and observed no changes in λ_{max}, so if acid is coordinated to iron in **SR-3X** the difference is not sufficient to change electronic properties of the intermediate.

rRaman analysis of **SR-3X** did not help to identify the intermediate as no resonance enhanced signals were observed (Figure 3-13). It is known from published literature that high-spin Fe^{IV}=O showed vibration at 843 cm^{-1} that shifted to 810 cm^{-1} upon ^{18}O labeling.[17]

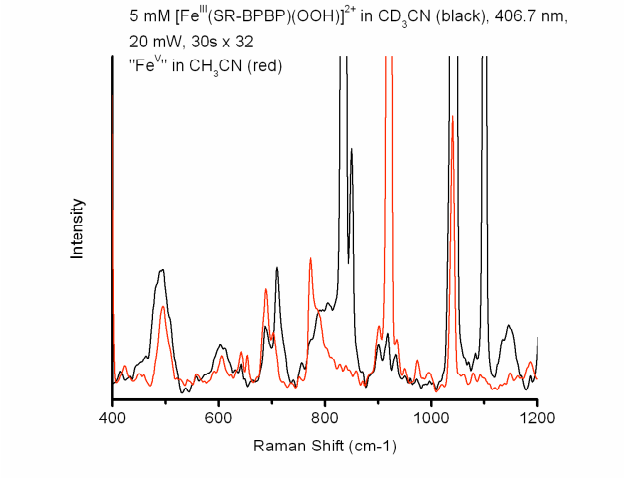

Figure 3-13. Resonance Raman spectra of $[(SR\text{-}BPBP)Fe^{III}(OOH]^{2+}$ in CD_3CN (black) and SR-3X in CH_3CN (red) acquired using 406.7 nm laser.

Unlike **SR-3a**, intermediate **SR-3X** can be generated in EtCN, however the yield is lower than in acetonitrile (Figure C38). Generating **SR-3X** in EtCN or PrCN may be

beneficial when formation of a glass upon freezing of the sample is crucial for spectroscopic analysis.

*3.3.8 Studies with Fe^{II}(iPr-BPMEN)$(OTf)_2$ (**1-iPr**)*

1-iPr (Figure 3-14) is a pale green complex that does not change color when dissolved in acetonitrile. Mixing **1-iPr**, benzoic acid and H_2O_2 did not result in formation of salicylate; complex can epoxidize cyclooctene, however yield of epoxide with **1-iPr** was about 1/3 of that with **1**. Cyclic voltammogram of **1-iPr** in acetonitrile shows several waves in the reduction segment (Figure C39).

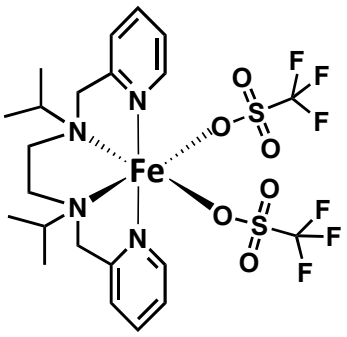

iPr-1

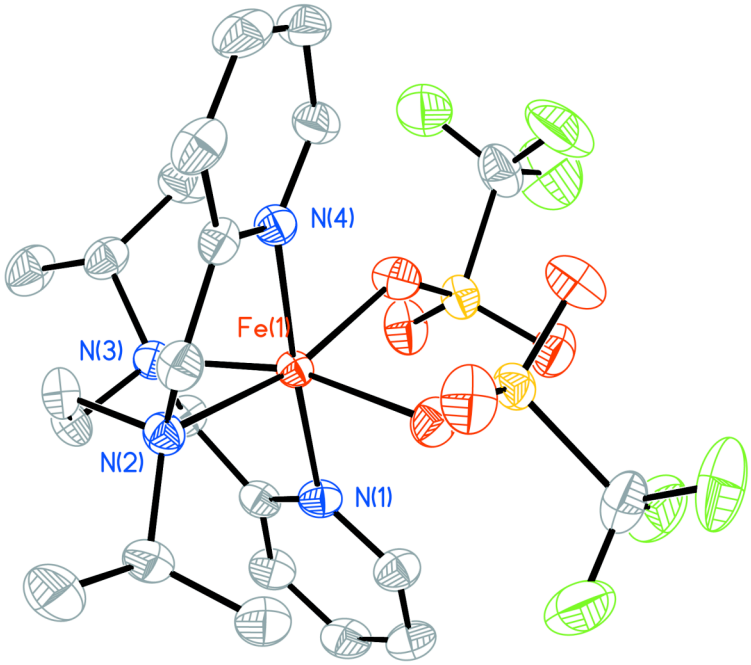

Figure 3-14. X-Ray structure of the complex Fe^{II}(iPr-BPMEN)$(OTf)_2$ with 50% probability thermal ellipsoids (hydrogen atoms omitted for clarity).

3.4 **Conclusions**

In order to improve hydroxylation catalyst **1**, we have modified BPMEN ligand and synthesized a series of new ferrous complexes. Complexes **3**, **4**, **SR-1** and **SR-3** share features important for catalysis – cis-α topology and two labile acetonitrile ligands; all complexes promote aromatic hydroxylation of benzenes and benzoic acids. Mechanistic studies revealed that $Fe^{III}(OOH)$ is formed upon mixing of $Fe^{II}L$ and H_2O_2. In the presence of acetic acid $Fe^{III}(OOH)$ decomposes into new intermediate **SR-3X**, the same intermediate can be formed in one step by mixing **SR-3** and $HOAc/H_2O_2$ (or peroxyacid). **SR-3X** can hydroxylate aromatics when excess of hydrogen peroxide is present; therefore **SR-3X** is a precursor to the active oxidant. Identity of **SR-3X** is under current investigation.

3.5 **References:**

[1] V. V. Zhdankin, D. N. Litvinov, A. Y. Koposov, T. Luu, M. J. Ferguson, R. McDonald, R. R. Tykwinski, *Chem. Commun.* **2004**, 106.

[2] S. Poussereau, G. Blondin, M. Cesario, J. Guilhem, G. Chottard, F. Gonnet, J.-J. Girerd, *Inorg. Chem.* **1998**, *37*, 3127.

[3] K. Chen, L. Que, Jr., *Chem. Commun.* **1999**, 1375.

[4] M. S. Chen, C. White, *Science* **2007**, *318*, 783.

[5] P. D. Oldenburg, L. Que, Jr., *Catalysis Today* **2006**, *117*, 15.

[6] L. Que, Jr., W. B. Tolman, *Nature* **2008**, *455*, 333.

[7] O. V. Makhlynets, E. V. Rybak-Akimova, *Chem. Eur. J.* **2010**, *16*, 13995.

[8] D. R. Boyd, J. W. Daly, D. M. Jerina, *Biochemistry* **1972**, *11*, 1961.

[9] K. Chen, M. Costas, J. Kim, A. K. Tipton, L. Que Jr., *J. Am. Chem. Soc.* **2002**, *124*, 3026.

[10] K. P. Bryliakov, E. A. Duban, E. P. Talsi, *Eur. J. Inorg. Chem.* **2005**, 72.

[11] A. Mairata i Payeras, R. Y. N. Ho, M. Fujita, L. Que, Jr., *Chem. Eur. J.* **2004**, *10*, 4944

[12] N. Y. Oh, M. S. Seo, M. H. Lim, M. B. Consugar, M. J. Park, J.-U. Rohde, J. Han, K. M. Kim, J. Kim, L. Que, Jr., W. Nam, *Chem. Commun.* **2005**, 5644.

[13] M. P. Jensen, M. Costas, R. Y. N. Ho, J. Kaizer, A. Mairata i Payeras, E. Münck, L. Que Jr., J.-U. Rohde, A. Stubna, *J. Am. Chem. Soc.* **2005**, *127*, 10512.
[14] J. Kaizer, E. J. Klinker, N. Y. Oh, J.-U. Rohde, W. J. Song, A. Stubna, J. Kim, E. Münck, W. Nam, L. Que Jr., *J. Am. Chem. Soc.* **2004**, *126*, 472.
[15] M. H. Lim, J.-U. Rohde, A. Stubna, M. R. Bukowski, M. Costas, R. Y. N. Ho, E. Münck, W. Nam, L. Que Jr., *PNAS* **2003**, *100*, 3665.
[16] J.-U. Rohde, J.-H. In, M. H. Lim, W. W. Brennessel, M. R. Bukowski, A. Stubna, E. Münck, W. Nam, L. Que Jr., *Science* **2003**, *299*, 1037.
[17] J. England, M. Martinho, E. R. Farquhar, J. R. Frisch, E. L. Bominaar, E. Münck, L. Que Jr., *Angew. Chem. Int. Ed.* **2009**, *48*, 3622.
[18] C. Krebs, D. G. Fujimori, C. T. Walsh, J. M. Bollinger, Jr., *Acc. Chem. Res.* **2007**, *40*, 484.
[19] J. C. Price, E. W. Barr, B. Tirupati, J. M. Bollinger, Jr., C. Krebs, *Biochemistry* **2003**, *42*, 7497.
[20] R. Hazell, K. B. Jensen, C. J. McKenzie, H. Toflund, *J. Chem. Soc. Dalton Trans.* **1995**, 707.

4 Reactivity of $[Fe^{III}_2(\mu\text{-}O)(\mu\text{-}OH)(BPMEN)_2](ClO_4)_3$ in aromatic hydroxylation: dimer vs. monomer

4.1 Introduction

Non-heme diiron (III) complexes are of great interest as chemical models for a series of enzymes involved in oxygen activation chemistry and aromatic hydroxylation: MMOH, toluene hydroxylase, phenol hydroxylase.[1] Methane monooxygenase (MMO) catalyzes oxidation of methane to methanol at room temperature and at atmospheric pressure.[2, 3] A great variety of alkanes, including aromatic compounds, are also substrates for MMO.[4] Structurally similar ToMOH (toluene monoxydroxylase) also promotes regiospecific hydroxylation of aromatics.[3] General mechanism for oxygen activation on diiron enzymes includes formation of peroxodiiron species that later decays into high-valent iron-oxo intermediate (Scheme 4-1), in MMO this intermediate is named Q and is responsible for methane oxidation.[5]

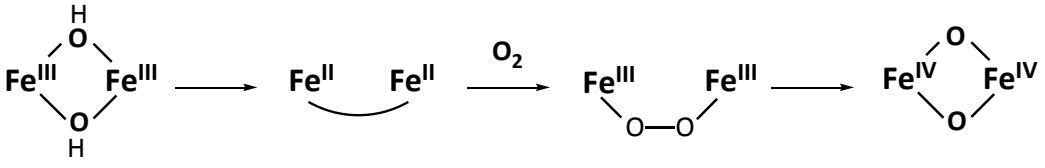

$MMOH_{ox}$ resting state | $MMOH_{red}$ | H_{peroxo} | Q

Scheme 4-1. Schematic representation of oxygen activation on diiron center.

Synthetic diiron models that hydroxylate phenyl group of the supporting ligand have been reported.[6-10] In our previous work we have shown that synthetic mononuclear

iron(II) complex supported by a tetradentate aminopyridine ligand: $[Fe^{II}BPMEN(CH_3CN)_2](ClO_4)_2$ (**1**) is efficient in aromatic hydroxylation of benzoic acids and benzenes.[11-13] Since mononuclear ferrous complexes with BPMEN-like ligands hydroxylate a wide variety of aromatic substrates[11, 12, 14-16] and direffic iron complexes are known to promote aromatic hydroxylation as well [6-10], we explored the ability of diiron complexes supported by BPMEN to hydroxylate benzoic acids. The potential advantage of the diiron(III) complex over its iron(II) mononuclear counterpart in developing synthetically useful reactions is the stability of ferric complexes in air: synthetic protocols that do not require anaerobic conditions would be simple and convenient.

4.2 **Experimental section**

4.2.1 General

All chemicals were purchased from Aldrich, Acros Organics or Fisher Scientific and were used without additional purification unless otherwise noted. Anhydrous HPLC grade acetonitrile was used in all experiments. GCMS experiments were carried out using a Shimadzu GC-17A gas chromatograph (Rxi-XLB nonpolar column) with a GCMS-QP 5050 mass detector. Time-resolved spectra were acquired with TgK Scientific (formerly HiTech Schientific, Salisbury, Wiltshire, UK) SF-61DX2 cryogenic Stopped-flow system equipped with J&M Diode array (Spectralytics). Spectrophotometric yield of Fe^{III}-salicylate were determined using JASCO spectrophotometer. N,N'-dimethyl-N,N'-bis(2-pyridylmethyl)ethane-1,2-diamine (BPMEN),[17] $[Fe^{III}_2(\mu\text{-}O)(\mu\text{-}OH)(BPMEN)_2](ClO_4)_3$ (**5**)[17]

and $[Fe(BPMEN)(CH_3CN)_2](ClO_4)_2$ (**1**)[18] were prepared using published procedures. $[Fe^{II}_2(\mu\text{-}OOCPh)_2(BPMEN)_2](ClO_4)_3$ (**7**) was prepared by dissolving **1** and $(NEt_4)OOCPh$ (1:1) in acetonitrile followed by ether diffusion. To make $(NEt_4)OOCPh$ salt, acid was added (as a solid) to aqueous solution of tetraethylammonium hydroxide in 1:2 ratio, mixture was stirred for about 2 hours, water removed by rotary evaporation and residue was washed with acetone and dried by multiple additions of toluene and evaporating the resulting azeotrope. $[Fe^{III}_2(\mu\text{-}O)(\mu\text{-}OOCPh)(BPMEN)_2](ClO_4)_3$ (**6**) was synthesized from BPMEN, $Fe(ClO_4)_3*6H_2O$, benzoic acid and triethylamine (1:1:1:1) in acetonitrile, crystals were obtained after vapor diffusion of diethyl ether.

4.2.2 Determination of phenol (ipso-hydroxylation product) yield using GCMS

Mixture of **1** (1 mM) with benzoic acids (2 mM) in CH_3CN was prepared in a glove box. Hydrogen peroxide (3 equiv, 30 µL of 0.1 M) was prepared aerobically and delivered at room temperature; the resulting solution was stirred for 30 min for reaction to complete. Solution of **5** in acetonitrile (1 mM vs. iron, 0.5 mM vs. **5**, 1 mL in each sample) was prepared aerobically fresh before the experiment. Premixed benzoic acid (2 equiv vs. iron, 100 µL of 20 mM solution) and H_2O_2 (3 equiv, 30 µL of 0.1 M solution) were delivered quickly at room temperature and reaction mixture was stirred for 30 min. All reaction mixtures were acetylated (0.1 mL of 1-methylimidazole and 1 mL of acetic anhydride) for 30 min followed by addition of 1 M HCl (2 mL) and extraction with dichloromethane (1 mL). The organic layer was washed with saturated aqueous $NaHCO_3$

(2 mL), water (2 mL) and finally dried over $MgSO_4$. Internal standard (nitrobenzene) was added prior to the extraction. Yields of hydroxylated products were established by GCMS relative to the internal standard and converted to absolute yields using a calibration curve with phenyl acetate and the corresponding standard, determined prior to each run. All experiments were run at least in triplicate, reported yields are average of these trials. Yield calculated as amount of phenolate formed per iron.

4.2.3 Determination of Fe(III)-salicylate (ortho-hydroxylation product) yield using UV-vis

Ortho-hydroxylation of various aromatic acids in the presence of **1** was performed by mixing **1** (0.5 mM) with 2 equiv of acid in acetonitrile in a glove box and then adding 3 equiv of hydrogen peroxide at room temperature. Solution of **5** (0.25 mM vs. dimer or 0.5 mM vs. iron, 2.2 mL) was placed in quartz cell and then premixed benzoic acid (2 equiv vs. iron, 110 µL of 20 mM solution) with H_2O_2 (3 equiv vs. iron, 165 µL of 20 mM) were delivered at once and optical absorption of resulting solution was followed over 10 min at λ_{max} of corresponding salicylate (see SI in [12]). UV-vis yields have been calculated using ε = 2300 $L*mol^{-1}*cm^{-1}$ for all salicylate complexes.[12]

Solution of **7** was prepared under argon atmosphere by mixing equal amounts of $[Fe^{II}BPMEN(CH_3CN)_2](ClO_4)_2$ (0.5 mM) and NEt_4OOCPh (0.5 mM). H_2O_2 (3 equiv, 100 µL) was injected through septum and change of absorbance was monitored at 600 nm over 5 min. Maximal absorbance for each experiment is reported in the graph. Variable

amount of triflic acid (0-50 µL) was added to solution of **7** in the glove box prior injecting H_2O_2; one equiv of triflic acid converts all benzoate into benzoic acid.

4.3 **Results**

4.3.1 ortho- and ipso- Hydroxylation promoted by diferric complex: one iron is better than two

Oxo-, hydroxo-bridged diiron (III) complex $[Fe^{III}_2(\mu\text{-}O)(\mu\text{-}OH)(BPMEN)_2](ClO_4)_3$ (**5**) was found to be reactive and quantitatively converted to mononuclear Fe(III)-salicylate when added to premixed benzoic acid and hydrogen peroxide solution (Figure 4-1).

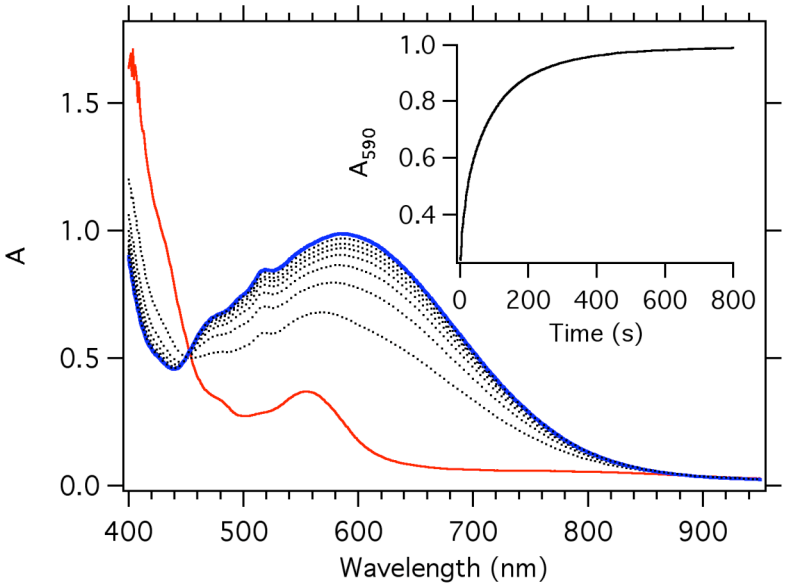

Figure 4-1**.** Spectral changes upon reaction of **5** (red), H_2O_2 and 3,5-dichlorobenzoic acid in acetonitrile at 20°C; [**5**] = 0.5 mM, [3,5-dichlorobenzoic acid] = 2 mM, [H_2O_2] = 10 mM after mixing) indicate formation of Fe(III)-salicylate complex (blue). Inset shows kinetic trace at 590 nm, hydroxylation reaction is complete in 800 s.

We observed a higher spectrophotometric yield of salicylate (60 % instead of 42 %, Figure D1) when reaction between **5** and a mixture of 3,5-dichlorobenzoic with hydrogen peroxide was carried out in the presence of water (0.7 M in acetonitrile, Figure D2). Rate constants of hydroxylation reaction in the presence of water and without water are similar (Table 4-1). Hydroxylation of benzoic acid using **5** is much slower process than the same reaction promoted by monomeric complex **1** (27.211 M^{-1} s^{-1}); in addition, yields of salicylate (*ortho*-hydroxylation) and phenolate (*ipso*-hydroxylation) products are lower in the presence of dimer (Table 4-2). These observations suggest that the reaction pathway of aromatic hydroxylation promoted by dinuclear iron(III) complex likely involves initial formation of a monomer and then follows the mechanism proposed for **1** (see chapter 2). In solution, **5** is sensitive towards carbon dioxide, reacting to give $[Fe^{III}_2(\mu\text{-}O)(\mu\text{-}CO_3)(BPMEN)_2]^{3+}$,[19] therefore solutions of **5** should be prepared fresh before experiment or kept under CO_2- free atmosphere.

Table 4-1. Rate constants

[**5**], mM	[ArCOOH], mM	[H_2O_2], mM	[H_2O], mM	k	fit model	equation
0.5	2	10	-	0.0462 s^{-1} M^{-1}	second order	f(x) = Af-(ΔA/(1+k*C*x))
0.5	2	10	700	0.0437 s^{-1} M^{-1}	second order	f(x) = Af-(ΔA/(1+k*C*x))
0.5	2	-	-	0.0094 s^{-1}	one exponential	f(x) = Af + ΔA exp(-kt)
0.5	-	10	-	k_{1obs} = 0.022 s^{-1} k_{2obs} = 0.002 s^{-1}	two exponential	$A = A_{inf} + \Delta A_1 \exp(-k_1 t) + \Delta A_2 \exp(-k_2 t)$
0.063	-	-	450	0.925 s^{-1}	one exponential	f(x) = Af + ΔA exp(-kt)

ΔA = A0-Af, A0 is the initial absorbance Af – final absorbance.

Table 4-2: The amounts of *ortho*- and *ipso*-hydroxylation products relative to iron observed from the reactions of $[Fe^{II}BPMEN(CH_3CN)_2](ClO_4)_2$ (monomer) and **5** (dimer) with a Fe/benzoic acid/H_2O_2 ratio of 1/2/3 at room temperature based on UV-vis [a] (*ortho*) and GC (*ipso*) data.

Substituent	Position	% yield of the hydroxylated products			
		monomer		dimer	
		ortho	*ipso*	*ortho*	*ipso*
OMe	*ortho*	-	70		12
	meta	52	-	23	-
	para	-	22		4
Me	*ortho*	*	45		20
	meta	>95	-	31	
	para	*	21		10
H		94	-	33	
Cl	*ortho*	*	75		28
	meta	98	-	35	
	para	*	60		30
NO_2	*ortho*	52	14		-
	meta	56	-	28	
	para	68	-		

* *Ortho*- and *ipso*-hydroxylation products form concurrently, and their absorption bands partially overlap, so it is impossible to independently evaluate the yield of each product from UV-vis data; '-' indicates no reaction

[a] UV-vis yields have been calculated using e = 2300 $mol^{-1}cm^{-1}L$ for all salicylate complexes.

4.3.2 *Formation of $[Fe^{III}_2(\mu\text{-}O)(\mu\text{-}OOCPh)(BPMEN)_2]^{3+}$*

Complex **5** is known to react with additional ligands in the protonated form, HA (HOAc, HCO_3^-, $CO(NH_2)_2$) to yield $[Fe^{III}_2(\mu\text{-}O)(\mu\text{-}A)(BPMEN)_2]^{3+}$ species.[19, 20] Indeed, in the absence of hydrogen peroxide, **5** reacts with benzoic acid to form diiron(III) complex **6** in 96 % yield (Figure 4-2, Figure 4-3). Crystal structure of **6** is provided in the SI (Figure D3).

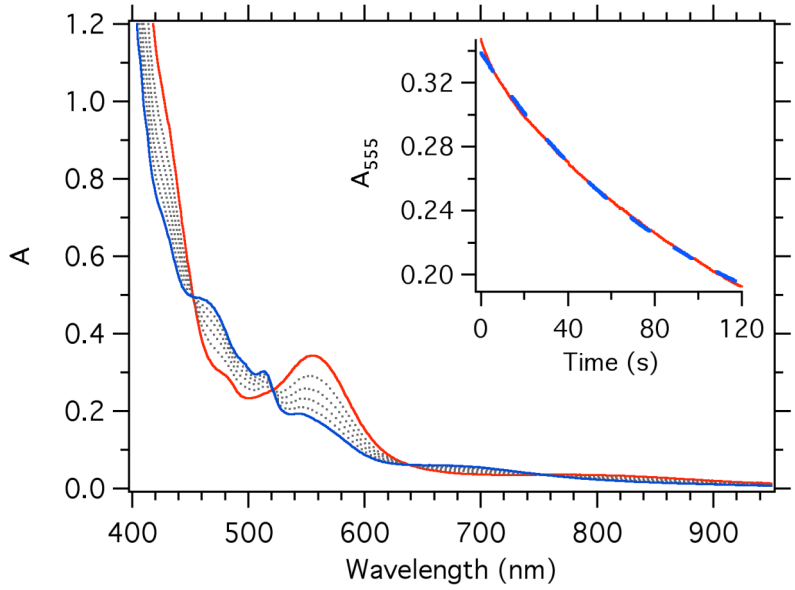

Figure 4-2. Spectral changes upon reaction of **5** (red) with benzoic acid (BA) in acetonitrile at 20 ˚C; [**5**] = 0.5 mM, [BA] = 2 mM. Blue spectrum corresponds to the $[Fe^{III}_2(\mu\text{-}O)(\mu\text{-}OOCPh)(BPMEN)_2]^{3+}$. Inset: kinetic trace at 555 nm (red) was fitted to one exponential equation (fit in blue) , k_{obs} = 0.01 s^{-1} (average of three).

Electronic spectra of complexes with doubly bridged Fe^{III}_2 and less acute Fe-O-Fe angles than in the $Fe^{III}(\mu\text{-}O)(\mu\text{-}OH)Fe^{III}$ diamond core are characterized by two distinctive bands in the 400-550 nm region. As previously described for $[Fe^{III}_2(\mu\text{-}O)(\mu\text{-}$

OAc)(BPMEN)$_2$]$^{3+}$ and other carboxylate complexes[21, 22], the band at 490 nm is independent of the Fe-O-Fe angle, while the remaining features at 520 nm blue-shift or lose intensity when the Fe-O-Fe angle increases.[23, 24]

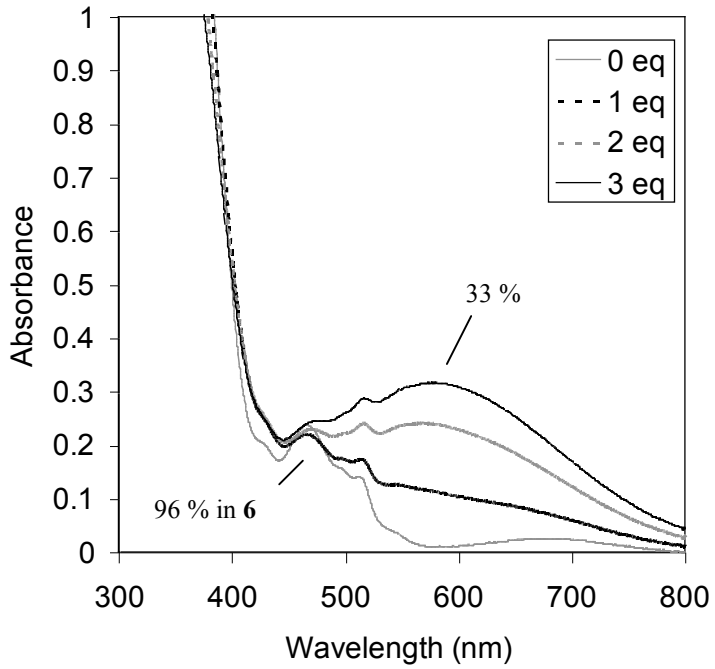

Figure 4-3. Spectral change upon addition of different amounts of hydrogen peroxide premixed with benzoic acid to **5** in acetonitrile (0 to 3 molar equivalents of H_2O_2 versus **5**, with 0.2 mM of **5** and 0.2 mM of benzoic acid). Yield of major products are indicated on the graph.

[Fe^{III}_2(μ-O)(μ-OAc)(BPMEN)$_2$]$^{3+}$ does not react with H_2O_2[25] because carboxylate bridge prevents facile coordination of added H_2O_2 to the metal centers. In this work we observed no salicylate formed when H_2O_2 was added to **6**, therefore benzoic acid and H_2O_2 have to be premixed and then added to dimer **5**. In the presence of hydrogen

peroxide (1 to 3 equiv vs. **5**) premixed with benzoic acid, two competing processes are observed, yielding Fe^{III}-salicylate and **6** (Figure 4-3, Scheme 4-3). Higher concentrations of H_2O_2 increase the yield of salicylate and reduce the amount of **6**.

4.3.3 Reaction of $[Fe^{III}_2(\mu\text{-}O)(\mu\text{-}OH)(BPMEN)_2]^{3+}$ with H_2O_2

The ultimate questions that need to be addressed is the nature of the metal –based oxidant that originates from **5** and H_2O_2 and whether or not it is beneficial to have two irons in the complex instead of one. Complexes with $Fe^{III}_2(\mu\text{-}O)(\mu\text{-}OH)$ core supported by TPA ligands are known to give spectroscopically distinct intermediates upon reaction with H_2O_2,[26, 27] such as diferric Fe-O-Fe-OOH and $Fe^{III}(\mu\text{-}O)_2Fe^{IV}$. Unfortunately, upon mixing of dimer **5** and hydrogen peroxide we have not observed any intermediates characteristic for monomeric complex **1** or diferric complexes. Instead, bands typical for μ-X bridge formation (X = OAc, urea, acetamide) appear when **5** reacts with H_2O_2 (Figure 4-4). It has been reported that **5** promotes acetonitrile hydrolysis[19], however electronic spectrum of $Fe^{III}(\mu\text{-}O)(\mu\text{-}OH)Fe^{III}$ dissolved in acetonile did not change over a period of ~10 hours. Hydroperoxide ion is a very reactive nucleophile – reaction of HO_2^- with nitriles generates peroxyimidate and then acetamide[28, 29] that can bridge two ferric centers and cause observed change in the spectrum (Scheme 4-2).

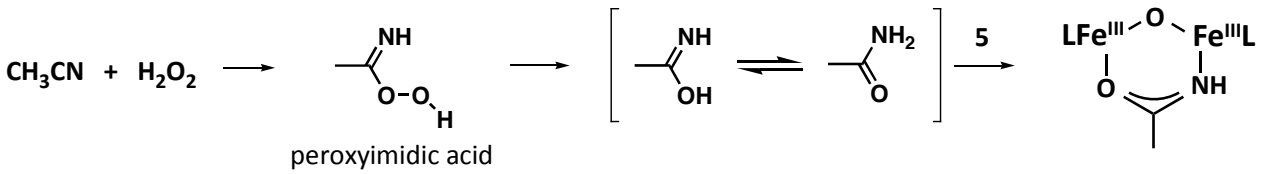

Scheme 4-2. Formation of acetamide from acetonitrile and hydrogen peroxide.

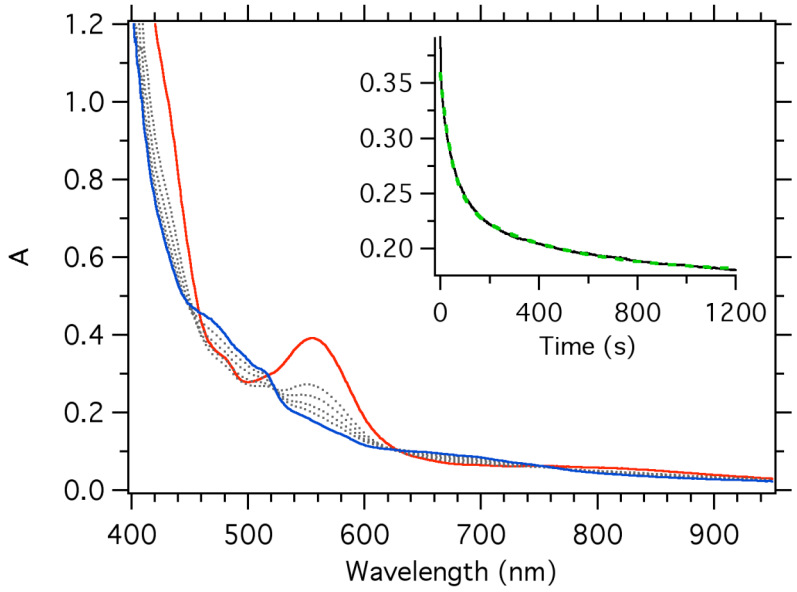

Figure 4-4. Spectral change upon reaction of **5** with H_2O_2 in acetonitrile at 20 ˚C; [**5**] = 0.5 mM, [H_2O_2] = 10 mM. Inset shows kinetic trace at 555 nm (black) and its double exponential fit (light green, dashed line); k_{1obs} = 0.022 s^{-1}, k_{2obs} = 0.002 s^{-1}

Hydration of the (μ-O)(μ-OH) complex **5** results in opening of the dimond core and formation of (μ-O) hydroxyl-aqua species (Scheme 4-3).[17, 20] Water can stabilize $[Fe^{III}_2(\mu\text{-}O)(\mu\text{-}OH)TPA_2]^{3+}$ and increase the yield of observed intermediates (unpublished observation) as open core complex doesn't promote acetonitrile hydrolysis as fast as

$[Fe^{III}_2(\mu\text{-}O)(\mu\text{-}OH)TPA_2]^{3+}$ does. When **5**, premixed with water (900 equiv vs. **5**), reacted with H_2O_2 we observed spectral changes (Figure D4) similar to those for the reaction in the absence of water.

4.3.4 Protonation state of substrate is important

$[Fe^{II}(BPMEN)(CH_3CN)_2]^{2+}$ **1** is efficient in promoting hydroxylation of aromatic carboxylic acids with hydrogen peroxide. However, mixing NEt_4OOCPh and **1** resulted in the formation of bright yellow bis-carboxylato-bridged diiron(II) species $[Fe^{II}_2(\mu\text{-}OOCPh)_2(BPMEN)_2](ClO_4)_3$ (**7**) which proved to be inactive in hydroxylation reaction. Similar complex $[Fe^{II}_2(\mu\text{-}OOCCH_3)_2(BPMEN)_2](ClO_4)_3$ was previously synthesized and fully characterized.[19]

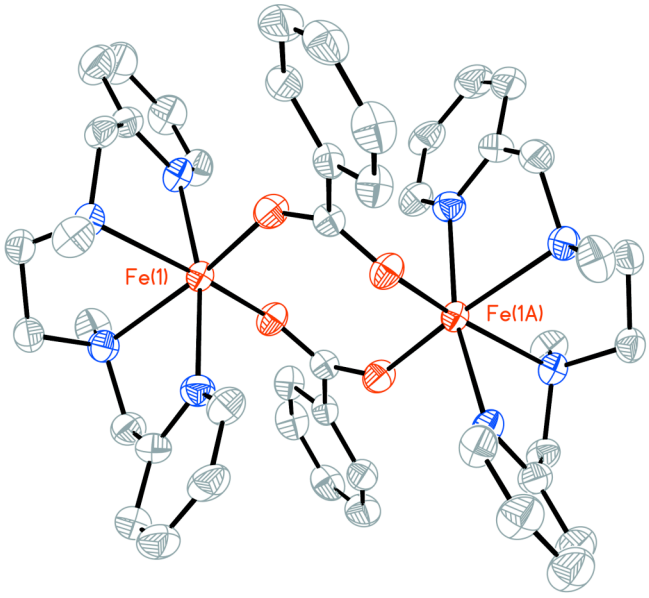

Figure 4-5. X-Ray structure of the complex $[Fe^{II}_2(\mu\text{-}OOCPh)_2(BPMEN)_2](ClO_4)_3$ (**7**) with 50% probability thermal ellipsoids (hydrogen atoms omitted for clarity).

Triflic acid protonates benzoate and therefore dimeric species **7** is converted into monomer **1**, change is color was observed upon addition of triflic acid to the solution of **7**. High yield of salicylate (70 % vs. **1**) was measured with 1 equiv of triflic acid vs. benzoate (Figure 4-6).

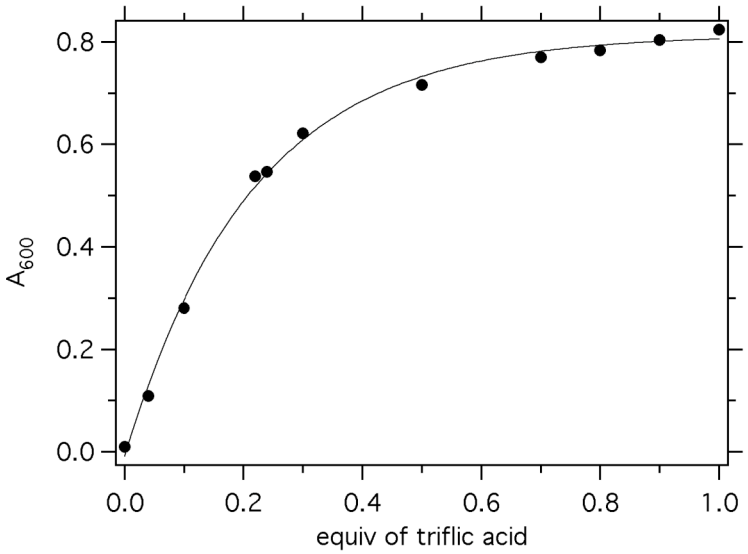

Figure 4-6. Hydroxylation of benzoate by **1**/H_2O_2 can occur only in the presence of triflic acid (equiv vs. iron content). A_{600} represent spectrophotometric yield of Fe^{III}-salicylate.

4.4 **Discussion**

Dinuclear oxo, hydroxo-bridged iron(III) complex **5** is able to promote aromatic hydroxylation reaction. We tested the scope of hydroxylation reaction promoted by this dimer and found that the Fe(III) dimer is less efficient compared to the Fe(II) monomeric complex **1**. The outcome of hydroxylation reaction depends on the electronic nature of the substituent and its position on the ring: 2- and to a lesser extend 4- substituted

benzoic acids yield *ipso*- hydroxylated product as well as *ortho*-hydroxylated products, however 3-substituted acids give only *ortho*-hydroxylated product. Dimeric complex gave the same products distribution as the monomer, suggesting the same metal-based oxidant is formed upon reaction of the complex (monomer or dimer) with hydrogen peroxide. Yields of salicylate are higher if hydroxylation reaction is carried out in the presence of water (1350 equiv vs. 5) because side reactions are slower when water is added and less acetamide-bridged side product is formed. This hypothesis is consistent with UV-vis spectral changes as bands of acetamide-bridged complex (490 nm, 530 nm) are less pronounced if water is added (compare Figure 4-1 and D2).

Isolated (μ-O)diiron(III) complex with additional benzoate bridge (**6**) did not react with H_2O_2 and thus no hydroxylation was observed. Similarly, analogous complex $[Fe^{III}_2(\mu\text{-}O)(\mu\text{-}OAc)(BPMEN)_2]^{3+}$ did not activate H_2O_2.[30] The ability of $[Fe^{III}_2(\mu\text{-}O)(\mu\text{-}OH)(BPMEN)_2](ClO_4)_3$ (**5**) to undergo ring opening reaction in the presence of water (Scheme 4-3)[17] explains the difference in reactivity between **5** and **6**, as labile sites (water) in open core can be displaced by H_2O_2 and then reactive metal-based oxidant could be formed from **5**.[30, 31] Diferrous dimer with two carboxylato bridging ligands (**7**) was also shown to be inactive in aromatic hydroxylation with H_2O_2, presumably because H_2O_2 is unable to displace carboxylato ligands and therefore get activated. However, addition of triflic acid to **7** followed by H_2O_2 leads to high yields of hydroxylated product. The role of acid is to protonate benzoate and to open the bridge between irons, converting dicarboxylato-bridged complex into monomeric species **1**. Similar rearrangement of carboxylate ligands (carboxylate shift) in observed in diiron enzymes

during catalytic cycle, this process is important in controlling the number of open coordination sites and in changing Fe-Fe distances.[32, 33] Protonation promotes dissociation of carboxylate ligand from its bridging position and as a result facilitates substrate access to the diiron center.[34, 35]

In summary, dinuclear oxo, hydroxo-bridged iron(III) complex supported by BPMEN ligand can promote both *ipso*- and *ortho*-hydroxylation of benzoic acids, however diferric complex is less efficient than ferrous monomer. Similar selectivity towards substrates and lower yields of hydroxylated products with dimer suggest that dimer breaks into monomeric species that carry out hydroxylation. Diferric dimers with carboxylato bridge(s) do not activate H_2O_2 and no salicylate product was detected in these systems. However, protonation of benzoate bridges in diferrous complex **7** causes dissociation of carboxylate ligands and restores activity of the complex in hydroxylation reaction.

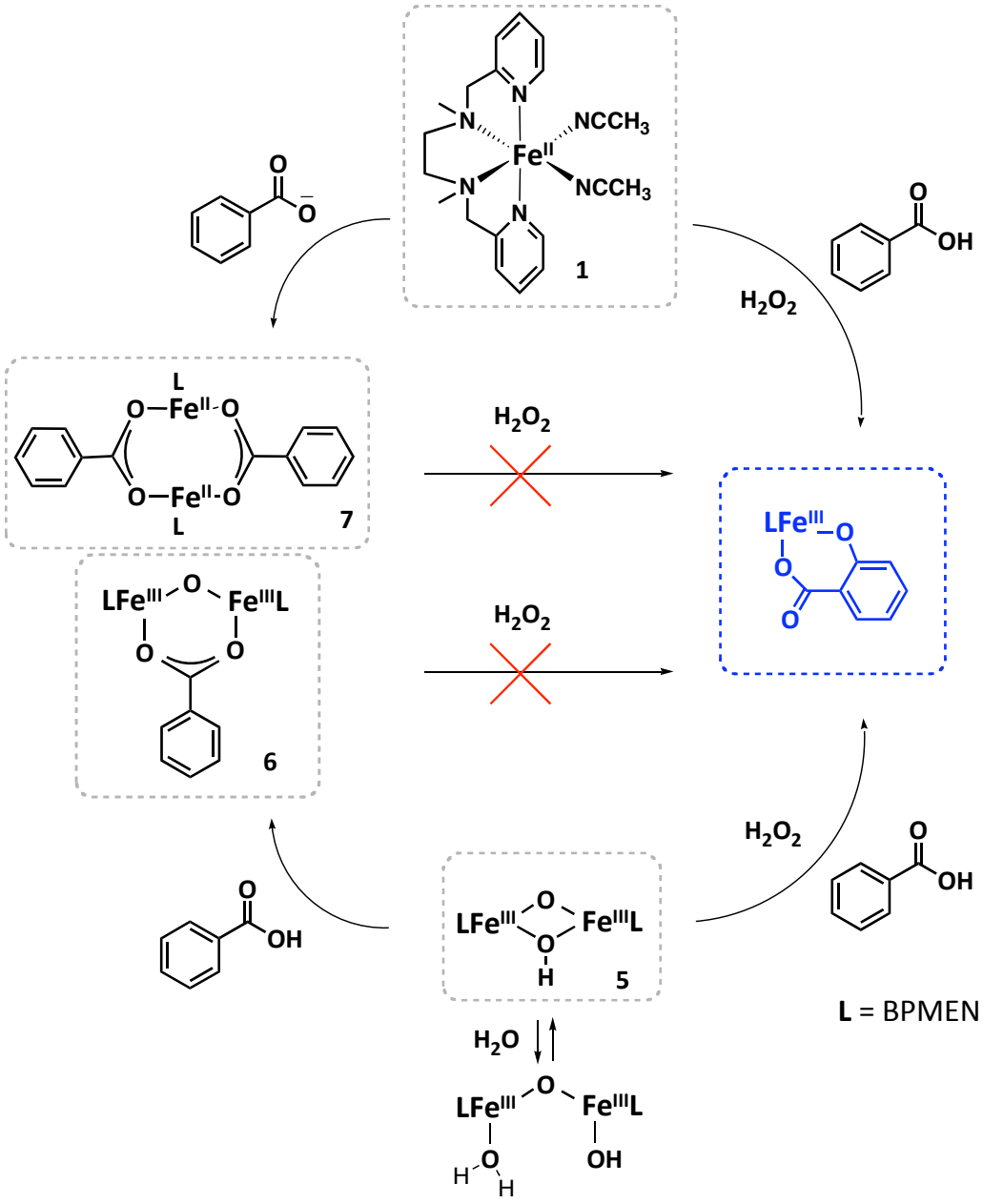

Scheme 4-3. Complexes with μ-carboxylato bridges do not activate hydrogen peroxide.

4.5 **References**

[1] L. J. Murray, S. J. Lippard, *Acc. Chem. Res.* **2007**, *40*, 466.
[2] M.-H. Baik, M. Newcomb, R. A. Friesner, S. J. Lippard, *Chem. Rev.* **2003**, *103*, 2385.
[3] M. H. Sazinsky, S. J. Lippard, *Acc. Chem. Res.* **2006**, *39*, 558.
[4] J. Green, H. Dalton, *J. Biol. Chem.* **1989**, *264*, 17698.
[5] M. Merkx, D. A. Kopp, M. H. Sazinsky, J. L. Blazyk, J. Müller, S. J. Lippard, *Angew. Chem. Int. Ed.*, *40*, 2782.
[6] H. Furutachi, M. Murayama, A. Shiohara, S. Yamazaki, S. Fujinami, A. Uehara, M. Suzuki, S. Ogo, Y. Watanabe, Y. Maeda, *Chem. Commun.* **2003**, 1900.
[7] F. Avenier, L. Dubois, J.-M. Latour, *New. J. Chem.* **2004**, *28*, 782.
[8] S. Menage, J.-B. Galey, J. Dumats, G. Hussler, M. Seite, I. G. Luneau, G. Chottard, M. Fontecave, *J. Am. Chem. Soc.* **1998**, *120*, 13370.
[9] E. C. Carson, S. J. Lippard, *Inorg. Chem.* **2006**, *45*, 828.
[10] M. Yamashita, H. Furutachi, T. Tosha, S. Fujinami, W. Saito, Y. Maeda, K. Takahashi, K. Tanaka, T. Kitagawa, M. Suzuki, *J. Am. Chem. Soc.* **2006**, *129*, 2.
[11] O. Makhlynets, E. V. Rybak-Akimova, *Chem. Eur. J.* **2010**, *16*, 13995.
[12] O. Makhlynets, P. Das, S. Taktak, M. Flook, R. Mas-Balleste, L. Que, Jr., E. V. Rybak-Akimova, *Chem. Eur. J.* **2009**, *15*, 13171.
[13] S. Taktak, M. Flook, B. M. Foxman, L. Que, Jr., E. V. Rybak-Akimova, *Chem. Commun.* **2005**, *42*, 5301.
[14] R. Mas-Ballesté, L. Que, Jr., *J. Am. Chem. Soc.* **2007**, *129*, 15964.
[15] J. Yoon, S. A. Wilson, Y. K. Jang, M. S. Seo, K. Nehru, B. Hedman, K. O. Hodgson, E. Bill, E. Solomon, W. Nam, *Angew. Chem. Int. Ed.* **2009**, *48*, 1.
[16] M. S. Chen, C. White, *Science* **2007**, *318*, 783.
[17] S. Poussereau, G. Blondin, M. Cesario, H. Guilhem, G. Chottard, F. Gonnet, J.-J. Girerd, *Inorg. Chem.* **1998**, *37*, 3127.
[18] K. Chen, L. Que, Jr., *Chem. Commun.* **1999**, 1375.
[19] R. Hazell, K. B. Jensen, C. J. McKenzie, H. Toflund, *Dalton Transaction* **1995**, 707.
[20] S. Taktak, S. V. Kryatov, E. V. Rybak-Akimova, *Inorg. Chem.* **2004**, *43*, 7196.
[21] S. Yan, D. D. Cox, L. L. Pearce, C. Juarez-Garcia, L. Que, Jr., J. H. Zhang, C. J. O'Connor, *Inorg. Chem.* **1989**, *28*, 2507.
[22] R. C. Holz, T. E. Elgren, L. L. Pearce, J. H. Zhang, C. J. O'Connor, L. Que, Jr., *Inorg. Chem.* **1993**, *32*, 5844.
[23] R. E. Norman, R. C. Holz, S. Menage, C. J. O'Connor, J. H. Zhang, L. Que, Jr., *Inorg. Chem.* **1990**, *29*, 4629.

[24] R. C. Reem, J. M. McCormick, D. E. Richardson, F. J. Devlin, P. J. Stephens, R. L. Musselman, E. I. Solomon, *J. Am. Chem. Soc.* **1989**, *111*, 4688.
[25] S. Taktak, S. V. Kryatov, T. E. Haas, E. V. Rybak-Akimova, *J. Mol. Cat. A* **2006**, *259*, 24.
[26] Y. Dong, H. Fujii, M. P. Hendrich, R. A. Leising, G. Pan, C. R. Randall, E. C. Wilkinson, Y. Zang, L. Que, Jr., B. G. Fox, K. Kauffmann, E. Münck, *J. Am. Chem. Soc.* **1995**, *117*, 2778.
[27] S. V. Kryatov, E. V. Rybak-Akimova, *J. Chem. Soc., Dalton. Trans.* **1999**, 3335.
[28] N. D. Gillitt, J. Domingos, C. A. Bunton, *J. Phys. Org. Chem.* **2003**, *16*, 603.
[29] L. Shu, Y. Shi, *Tetrahedron* **2001**, *57*, 5213.
[30] J. Y. Ryu, J. Kim, M. Costas, K. Chen, W. Nam, L. Que, Jr., *Chem. Commun.* **2002**, 1288.
[31] K. Chen, M. Costas, J. Kim, A. Tipton, L. Que, Jr., *J. Am. Chem. Soc.* **2002**, *124*, 3026.
[32] D. A. Whittington, S. J. Lippard, *J. Am. Chem. Soc.* **2001**, *123*, 827.
[33] R. L. Rardin, W. B. Tolman, S. J. Lippard, *New. J. Chem.* **1991**, *15*, 417.
[34] L. H. Do, T. Hayashi, P. Moënne-Loccoz, S. J. Lippard, *J. Am. Chem. Soc.* **2010**, *132*, 1273.
[35] C. E. Tinberg, S. J. Lippard, *Biochemistry* **2009**, *48*, 12145.

5 *Ipso*-Hydroxylation: evidence of a radical reaction?

5.1 Introduction

Ipso-hydroxylation was introduced in chapter 1, however there are more results on *ipso*-hydroxylation that provide detailed NMR characterization of the products and argue for the formation of a radical as an important mechanistic step in *ipso*-hydroxylation pathway. This chapter contains unpublished data that may help to understand prerequisites of *ipso*-hydroxylation and mechanism of this reaction.

5.2 Experimental section

5.2.1 General

All chemicals and solvents were purchased from Aldrich, Acros Organics or Fisher Scientific and were used without additional purification unless otherwise noted. Anhydrous 99.9 % acetonitrile from Sigma-Aldrich was used in all experiments. UV-vis spectra were acquired on a JASCO V-570 spectrophotometer or a Hewlett-Packard (Agilent) 8452 diode array spectrophotometer over a 190-1100 nm range. GCMS experiments were carried out using a Shimadzu GC-17A gas chromatograph (Rtx-xLB column) with a GCMS-QP 5050 mass detector. NMR spectra were recorded on a Bruker DPX-300 spectrometer and chemical shifts (ppm) were referenced to the residual protic solvent peaks.

5.2.2 Identification of ortho-hydroxylation products by NMR

For the identification of *ortho*-hydroxylated products, **1** (0.12 mmol, 72 mg) was dissolved in 20 mL of acetonitrile under argon atmosphere in a glove box and mixed with 1 equiv of substituted benzoic acid. A further 1.5 equiv of H_2O_2 solution was added to the prepared mixture. The solution was stirred for 20-30 min. In the next step, complex was decomposed by treating with aqueous Na_2EDTA solution (20 ml, 5% solution) followed by addition of concentrated HCl (final pH was about 0). Organic products were extracted with ethylacetate (3 x 20 mL) and the extract was dried over $MgSO_4$. Evaporation of solvent resulted in brown residues (soluble in chloroform) that were analyzed by ^1H NMR.

5.2.3 Identification of hydroxylation products by GCMS

A mixture of complex **1** (1 mM) and 2 equiv of aromatic acid in acetonitrile was prepared under argon. H_2O_2 (3 equiv vs iron) was delivered into 1 mL of the mixture upon vigorous stirring. The reaction was quenched with 1-methylimidazole (0.1 mL) in 30 minutes followed by the addition of 1 mL acetic anhydride to esterify the products. Nitrobenzene was added as an internal standard. Organic products were extracted with dichloromethane (1 mL) and subjected to the GC-MS analysis. All experiments were run at least in triplicate, the reported data is the average of these reactions. To identify carboxylic acids by GCMS we derivatized products using silylating agent BSA (bistrimethylsilylacetamide) and performed GCMS analysis on stabilwax column (BSA is

not compatible with carbowax). Silylation procedure: add BSA (0.1 mL) to 0.5 mL of acetonitrile solution containing products; heat the mixture for 20 min at 60-80 ˚C.

5.3 **Results**

5.3.1 Branching in hydroxylation reaction

Detailed studies of hydroxylation of aromatic acids with hydrogen peroxide in the presence of non-heme iron complexes identified two major reaction pathways: *ortho* hydroxylation, and decarboxylation/*ipso*-hydroxylation.[1] The later process can most easily be rationalized by postulating formation of a coordinated arylcarboxyl radical that undergoes spontaneous loss of CO_2, affording an aryl radical that immediately rebounds with the oxoiron(IV) center to form the phenolate product (Scheme 5-1).

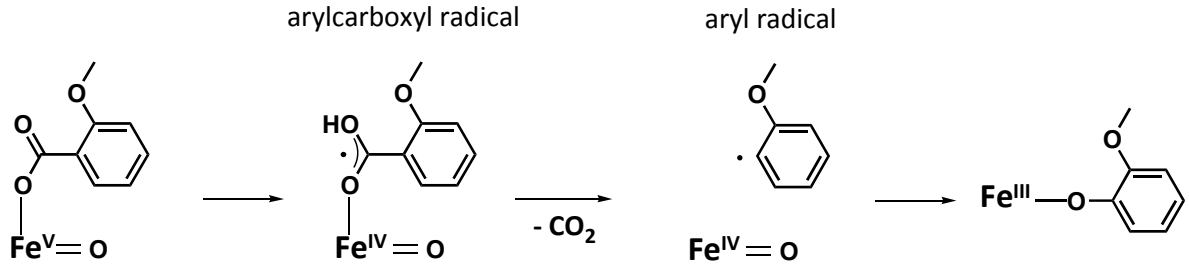

Scheme 5-1. Possible mechanism of *ipso*-hydroxylation.

These pathways are not mutually exclusive (see Table 1-1) as hydroxylation of a range of substrates bifurcates into two parallel reaction pathways. For example, 2-chlorobenzoic acid yielded 6-chloro-salicylic acid and 2-chlorophenol. Two major peaks

with m/z values 470 and 496 were observed in ESI-MS (positive mode) immediately after an injection of hydrogen peroxide (Figure E1), identified as $[Fe^{III}(BPMEN)(C_6H_4Cl\text{-}O^-)(^-OH)]^+$ and $[Fe^{III}(BPMEN)^-OOC\text{-}C_6H_3Cl\text{-}O^-]^+$ respectively. When hydrogen peroxide reacted with 2,6-dichlorobenzoic acid in the presence of **1** blue color appeared in several seconds followed by a slow decay of the blue species (Figure E2). Since both *ortho* positions are blocked, blue color can not be assigned to the formation of Fe(III)-salycilate complex. A similar behavior was found for another substrate, acetylsalicylic acid, which also instantly generated blue product(s) (λ_{max} = 650 nm) upon treatment with H_2O_2 and **1**. Careful analysis of reaction products was necessary for this substrate, because hydrolysis may have been responsible for the formation of colored complexes (Scheme 5-2, pathway C).

Scheme 5-2. Possible pathways of acetylsalycilic acid hydroxylation.

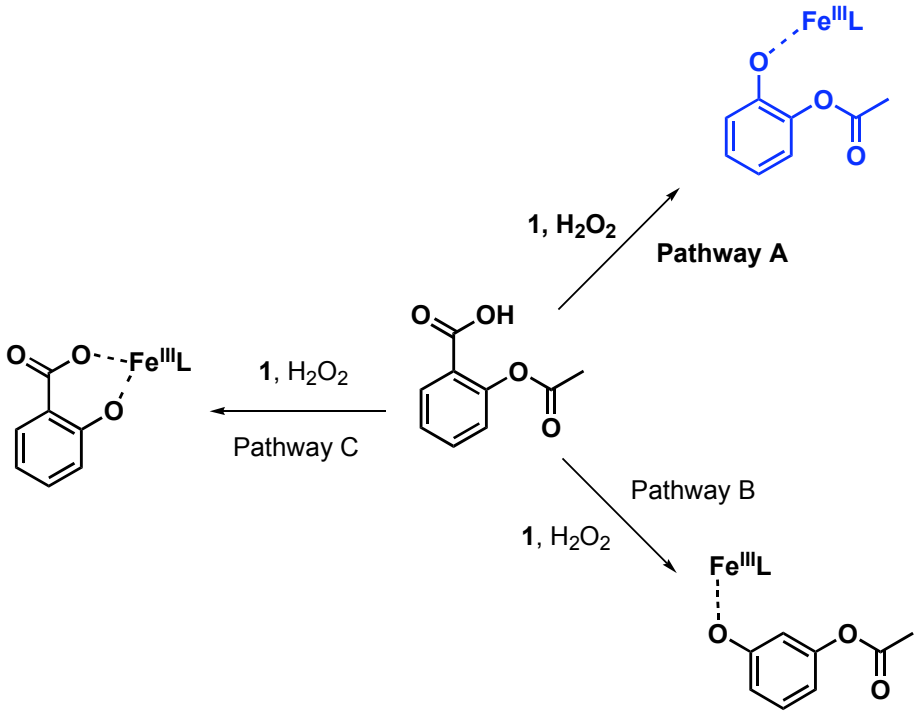

An evidence of *ortho*-hydroxylation was provided by ESI-MS – a peak with m/z 520^{+} corresponds to $[Fe^{III}(BPMEN)^{-}OOC\text{-}C_6H_3OOCCH_3\text{-}O^{-}]^{+}$ (Figure E3). Another large peak in electrospray mass spectrum appeared concurrently, m/z = 494^{+}, and could be attributed to $[Fe^{III}(BPMEN)^{-}O\text{-}C_6H_4OOCCH_3(OH^{-})]^{+}$, a mono-acetylated dihydroxybenzene. Two structural isomers were feasible for this oxidation product (Scheme 5-2): catehol monoacetate (which could result from *ipso*-hydroxylation – pathway A) or resorcinol monoacetate (potentially resulting from decarboxylation of *ortho*-hydroxylated acetylsalicylic acid – pathway B). Separation of the products of acetylsalicylic acid and H_2O_2 in the presence of **1** using chromatography column followed by ^{1}NMR analysis allowed us to recover and characterize one of the major products as cetechol monoacetate (Figure E4). NMR analysis of the reaction mixture (acetylsalicylic acid, H_2O_2 and **1**) quenched in 5 minutes demonstrated that 6-hydroxy-acetylsalicylic acid and catehol monoacetate are present in about equal amounts (Figure E5). Longer reaction times lead to partial bleaching of the blue color of *ortho*- and *ipso*-hydroxylation products and accumulation of diiron(III) carboxylate-bridged complex in the resulting yellow-gray solution (Figure E6). NMR analysis of the reaction mixture quenched after 3 min (blue) and ~12 hours (yellow) showed almost same composition (Figure E7), probably bleaching of the blue color is due to the protonation of organic products and decomposition of Fe(III)-salicylate and Fe(III)-phenolate. No blue species was observed when hydrogen peroxide reacted with $Fe(ClO_4)_2$ and acetylsalicylic acid that means formation of the blue product is not a result of hydrolysis (Pathway C).

5.3.2 Subsequent oxidation of ipso-hydroxylated products

Phenolate complexes generated in the reactions between substituted benzoic acids, hydrogen peroxide, and **1** underwent further oxidation with excess of hydrogen peroxide. These phenol oxidation processes may be responsible for the transient nature of iron(III)-phenolates detected by time-resolved UV-Vis spectrophotometry: formation of intensely colored phenolate complexes was immediately followed by their decay under most reaction conditions. Chemical nature of the final oxidation products with **1** and H_2O_2 for three benzoic acids with *o*-, *p*-electron-donating substituents was determined by NMR analysis (Scheme 5-3). This structural information provided additional evidence for regioselectivity of benzoic acid hydroxylation. The reactions between these substrates, H_2O_2 and complex **1** were quenched after the green color of initially formed phenolates disappeared, the products of subsequent oxidation were isolated and separated using preparative TLC, and analyzed by mass-spectrometry and NMR. For 2-methoxybenzoic acid, NMR analysis (Figure E8-E9) and mass spectrum (m/z 163 after acetylation) of the product are consistent with hydroxy-methoxy-phenylacetonitrile (Scheme 5-3A). The positions of substituents were established by detailed NMR analysis.

Scheme 5-3. Decarboxylation, ipso-hydroxylation and radical coupling

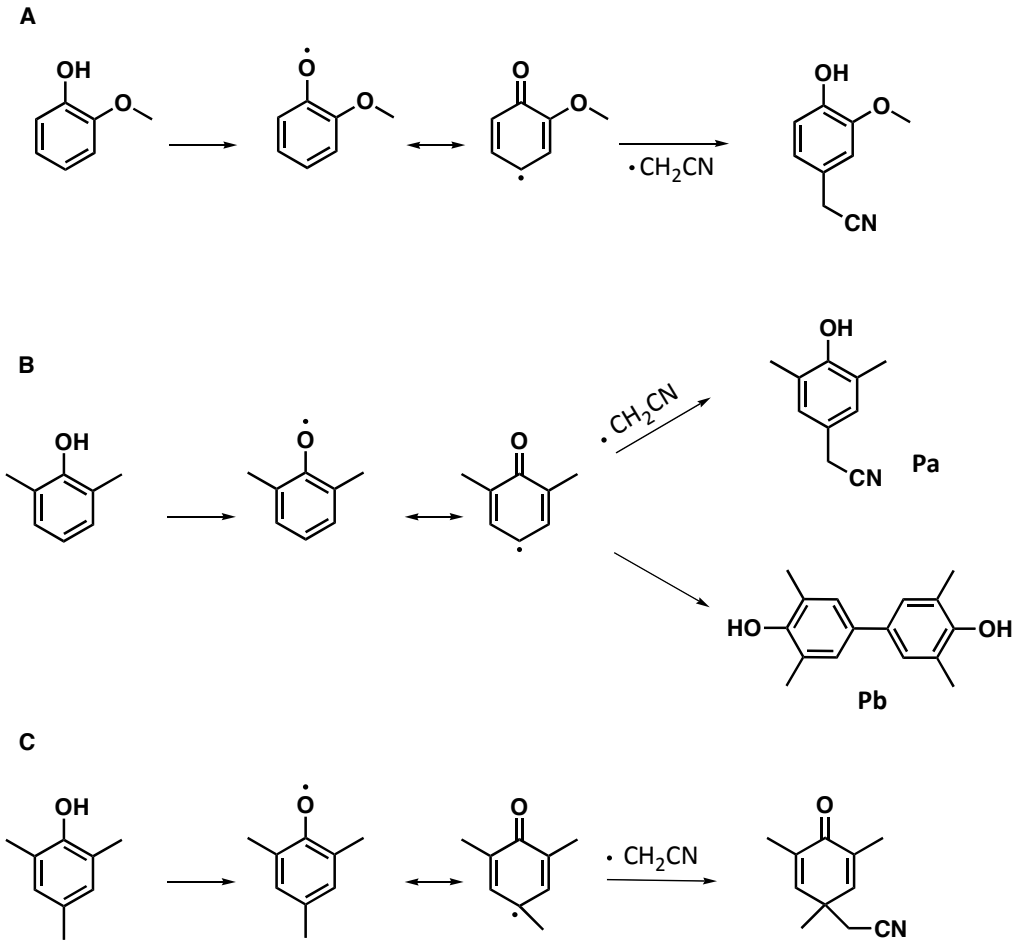

An HMQC spectrum (Figure E10) of a purified oxidation product reveals the doublet of doublets and a singlet in the aromatic region, consistent only with a 1,2,4-substitution pattern. 2D NOESY experiment helped us to choose among three possible structural isomers (Scheme 5-4). The experimental spectrum depicted in Figure E11 shows cross-peak between Ha aromatic ring proton and methoxy group protons and two cross-peaks between the aromatic protons and the $–CH_2$-CN protons, in agreement with the structure b - 4-hydroxy-3-methoxyphenylacetonitrile (Scheme 5-4, Scheme 5-3 A).

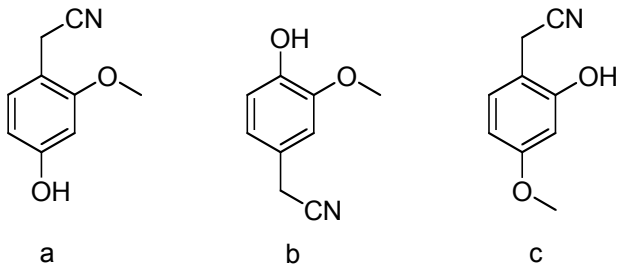

Scheme 5-4. Possible products of *ipso*-hydroxylation reaction as determined by HMQC NMR.

The conversion of 4-hydroxy-3-methoxyphenylacetonitrile determined by NMR is 28%. GCMS studies of reaction products of **1**/2-methoxybenzoic acid/H_2O_2 (1 equiv/2 equiv/3 equiv) gave a TON 0.65 (32 %). Increasing the amount of 2-methoxybenzoic acid up to 100 equiv and hydrogen peroxide up to 10 equiv we found a higher TON of 3.33. If reaction is carried out at excess conditions (1:2-methoxybenzoic acid:H_2O_2 = 1:100:10) the major product is 2-methoxyphenol, but 4-hydroxy-3-methoxyphenylacetonitrile is also present. It is interesting to note that the yield of phenol depends on the concentration of complex (Figure E12): 1 mM concentration of complex was more favorable for the phenol formation compared to 2 mM when 100 fold excess of substrate was used (**1**: 2-methoxybenzoic acid: H_2O_2 = 1:100:10). Presumably higher concentrations of all components of the reaction facilitate overoxidation of phenolate product.

2-methylbenzoic acid produced blue product when mixed with **1**/H_2O_2 (λ_{max} ~ 600 nm), while two products were observed in GCMS after silylation: 4-hydroxy-3-methylphenylacetonitrile and 6-methylsalicylic acid. Similar reaction pathway with

radical coupling operates in oxidation of 2,6-dimethylbenzoic acid by hydrogen peroxide in the presence of **1** (Scheme 5-3B). In addition to 4-hydroxy-3,5-dimethylphenylacetonitrile (14% isolated yield, Pa), a biphenyl product was also obtained with 4% conversion (Pb, Figure E13-E14) and identified as 3,5,3',5'-tetramethyl-biphenyl-4,4'-diol by NMR (Table E1). Selective oxidative C-C coupling of 2,6- dimethylphenol with formation of a 3,5,3',5'-tetramethyl- biphenyl-4,4'-diol was previously reported by J.Reedijk and coworkers.[2] Increase in the initial concentrations of **1**, 2,6-dimethylbenzoic acid and hydrogen peroxide results in a higher yield of biphenyl product and a smaller yield of 4-hydroxy-3,5-dimethylphenylacetonitrile (yields were determined by NMR, Figure E15).

Interestingly, 2,4,6-trimethylbenzoic acid (*para* position is blocked) also interacts with hydrogen peroxide and **1** through *ipso*-hydroxylation (as evidenced by the formation of a green intermediate, λ_{max} ~750 nm) followed by a radical oxidation pathway with addition of a solvent molecule (Scheme 5-3C). The main product of the reaction, isolated in 17% yield, was identified as 2,5-cyclohexadien-1-one, 2,4,6-trimethyl-4-acetonitrile (Scheme 5-3C) by EI-GSMS (m/z = 175), ESI-MS (176+), and NMR. Proton NMR (Figure E16) of the product shows only one singlet in aromatic region (δ = 6.6 ppm). Relatively low chemical shift of a signal of aromatic protons and a signal with a high chemical shift (186 ppm) in carbon NMR (Figure E17) suggest that this product is a quinone. DEPT 135 (Figure E18) unambiguously indicates the presence of a CH_2 unit in the structure.

The substitution patterns of the oxidation products, obtained from decarboxylated benzoic acids, confirm regioselectivity of the initial hydroxylation step: the OH group is replacing the carboxylate. Therefore, regioselective *ipso*-hydroxylation is taking place with 2-substituted benzoic acids, especially when electron-donating *ortho*-substituents are present. These results suggest the participation of a metal-based oxidant in the inner-sphere oxidation process. The alternative mechanism involving free arylcarboxyl radicals (which are known to readily undergo decarboxylation would lead to mixtures of hydroxylated products (Scheme 5-5; aryl radicals would easily rearrange, leading to statistical mixtures of substituted phenols). Rate of decarboxylation depends on the position of the substituent on the aromatic ring [3] and the nature of the substituent.[4-6] *Ortho*-substituted benzoic acids give the highest yield of *ipso*-hydroxylated product (Table 1-1), these results can be attributed to a nonplanar geometry of the arylcarboxyl radical and twisting of the carbonyloxyl group due to steric effects of the substituents.[4]

Scheme 5-5

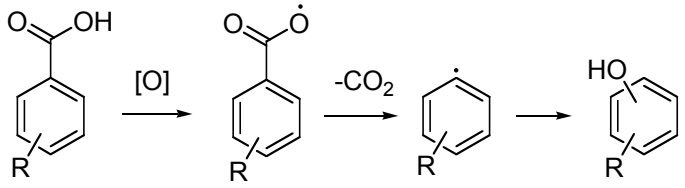

Another evidence of formation of arylcarboxyl radicals is an oxidative cyclization of diphenyl-2-carboxylic acid (Scheme 5-6). The dehydrogenation of diphenyl-2 carboxylic acid to the lactone has been performed by oxidation with chromic acid or hydrogen peroxide. [7] According to the proposed mechanism of decarboxylation and *ipso*-

hydroxylation (charter 1), arylcarboxyl radicals are formed in the system **1**, carboxylic acid and hydrogen peroxide, then arylcarboxyl radical can attack aromatic ring to yield 3,4-benzocoumarin or it undergoes decarboxylation to produce 2-phenylphenol (Scheme 5-6). Mixture of **1**, diphenyl-2 carboxylic acid turned green upon addition of hydrogen peroxide, which is another evidence that 2-phenylphenol is formed in this reaction. NMR analysis of the reaction between **1**, diphenyl-2 carboxylic acid and H_2O_2 represents a mixture of products with major species being starting material diphenyl-2-carboxylic acid (Figure E19) and 3,4-benzocoumarin; signals of 3,4-benzocoumarin were assigned based on literature data.[8] GSMS yield of 3,4-benzocoumarin is 20 %.

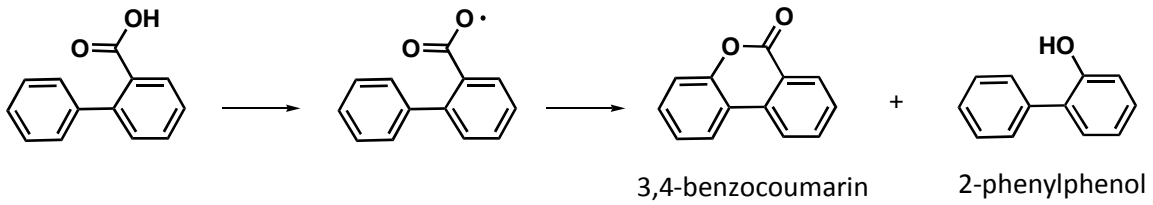

Scheme 5-6. Oxidative cyclization of diphenyl-2 carboxylic acid.

It is interesting to note that an analog of **1** promotes lactonisation of tetrahydrogibberelic acid in the presence of hydrogen peroxide, in this case hydroxylation occurs selectively at the 2˚ C-H bond closest to the carboxylate moiety. [9] Presumably this aliphatic C-H oxidation reaction involves formation of carboxyl radical and its attack on a nearby aliphatic chain.

5.4 **Summary**

Electron-donating substituents that increase electron density in the *ipso* position with respect to carboxylate promote decarboxylation, *ipso*-hydroxylation and radical coupling. Placing substituents in 2- or 2,6-positions with respect to carboxylate, thus blocking *ortho*-hydroxylation and introducing steric hindrance in the immediate vicinity of carboxylate group, also favors *ipso*-hydroxylation. Phenols that resulted from *ipso*-hydroxylation are susceptible to further oxidations via radical reactions; these radical processes are especially pronounced for electron-rich substrates. The final product is a result of oxidation of phenol into phenoxyl radical, followed by a radical coupling with a solvent molecule (which is being introduced into the *para* position to *ipso*-hydroxyl group).

5.5 **References:**

[1] O. V. Makhlynets, P. Das, S. Taktak, M. Flook, R. Mas-Balleste, E. V. Rybak-Akimova, L. Que, Jr., *Chem. Eur. J.* **2009**, *15*, 13171.

[2] C. Boldron, G. Aromi, G. Challa, P. Gamez, J. Reedijk, *Chem. Commun.* **2005**, 5808.

[3] J. Li, T. B. Brill, *J. Phys. Chem. A* **2003**, *107*, 2667.

[4] J. Wang, H. Itoh, M. Tsuchiya, K. Tokumaru, H. Sakuragi, *Tetrahedron* **1995**, *51*, 11967.

[5] J. Wang, T. Tateno, H. Sakuragi, K. Tokumaru, *J. Photochem. Photobiol. A: Chemistry* **1995**, *92*, 53.

[6] J. Chateauneuf, J. Lusztyk, K. U. Ignold, *J. Am. Chem. Soc.* **1988**, *110*, 2886.

[7] G. W. Kenner, M. A. Murray, C. M. B. Tylor, *Tetrahedron* **1957**, *1*, 259.

[8] Q. J. Zhou, K. Worm, R. E. Dolle, *J. Org. Chem.* **2004**, *69*, 5147.

[9] M. Chen, M. C. White, *Science* **2007**, *318*, 783.

6 Hydroxylation of benzoic acids with H_2O_2 in the presence of 1

6.1 Reaction between 1, benzoic acid and H_2O_2

6.1.1 Kinetic studies with variable [H_2O_2]

Hydroxylation of benzoic acid with hydrogen peroxide on **1** is accompanied by a drop in absorbance in the near UV region with the disappearance of the band at λ = 373 nm (ε = 4350 L mol^{-1} cm^{-1}) characteristic of complex **1** (Figure 6-1) and increase in absorbance in the visible region with the appearance of a band at λ = 600 nm (ε = 2300 L mol^{-1} cm^{-1}) characteristic of the Fe(III)-salicylate complex.

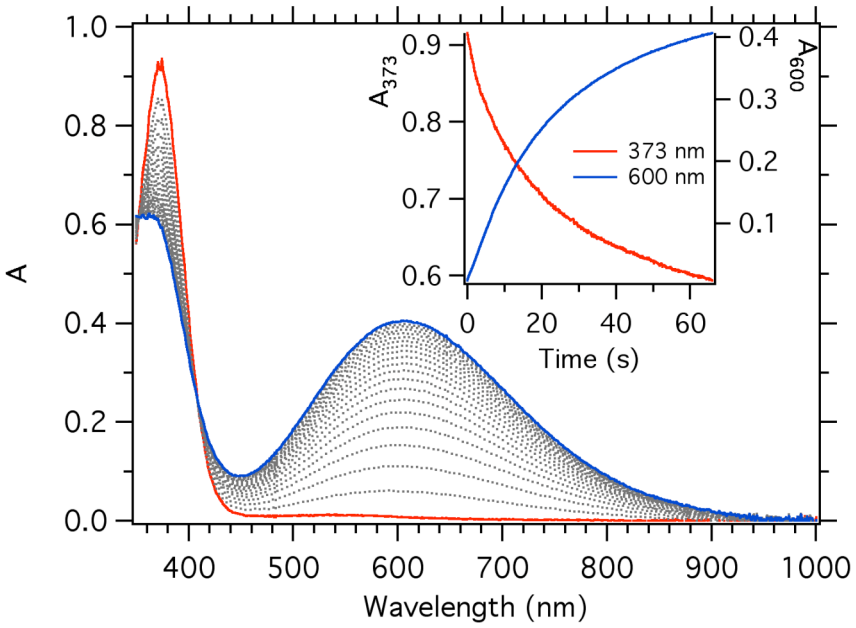

Figure 6-1. Spectral changes upon reaction of **1**, H_2O_2 and benzoic acid (BA) at 25 ˚C in acetonitrile; [**1**] = 0.25 mM, [H_2O_2] = 1 mM, [BA] = 1 mM.

Kinetic traces at 600 nm can be best fitted to a double exponential rate law $A = A_{inf} + \Delta A_1 \exp(-k_1 t) + \Delta A_2 \exp(-k_2 t)$: both k1 and k2 increase with [H_2O_2]. Isosbestic point at 410

nm (Figure 6-1) indicates that species with λ_{max} = 373 nm decomposes with the same rate as Fe(III)-salicylate formed, in other words species with λ_{max} = 373 nm is directly converted into Fe(III)-salicylate; however when higher concentrations of H_2O_2 used, a band at 373 nm disappears faster than salicylate formed (Figure F1, Figure 6-2 left). Please note that traces at 373 nm and 400 nm represent the same process (Fe^{II} → Fe^{III}).

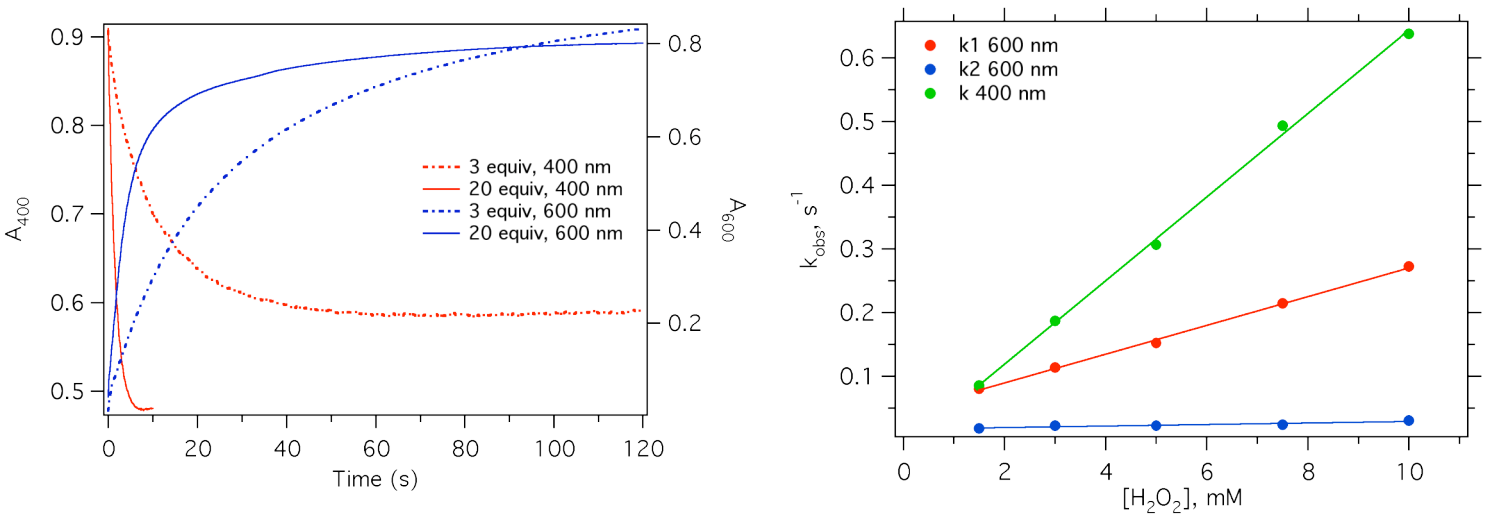

Figure 6-2. Left: kinetic traces at 400 nm and 600 nm for reaction of **1** (0.5 mM), H_2O_2 and benzoic acid (1 mM) at 20 ˚C in acetonitrile. Right: observed rate constants as a function of [H_2O_2]. Kinetic traces at 600 nm were fitted to a double exponential equation (k1 600 nm and k2 600 nm); kinetic traces at 400 nm were fitted to a single exponential equation (k 400 nm).

The plots of the observed rate constant at 400 nm versus hydrogen peroxide concentration under pseudo-first-order conditions are straight lines with almost zero intercept indicating a first-order in hydrogen peroxide (Figure 6-3 and Figure 6-2).

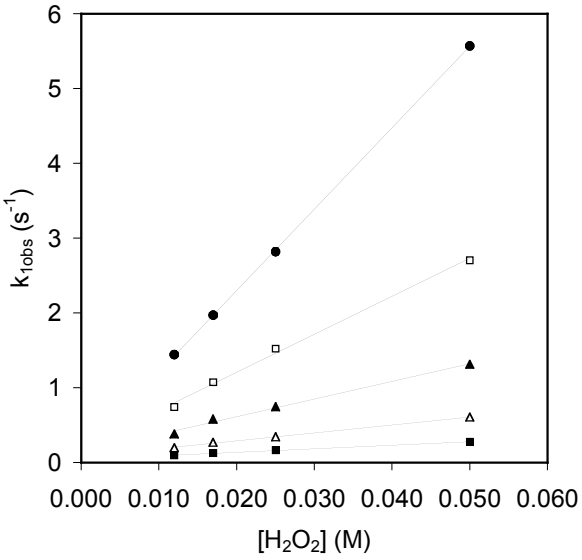

Figure 6-3. Plot of the observed rate constant at 410 nm versus hydrogen peroxide concentration after mixing with **1** and benzoic acid acquired by stopped-flow technique at different temperatures (0.50 mM of **1** premixed with 1.5 equivalent of benzoic acid and 12-50 mM of hydrogen peroxide after mixing): T = -15 °C (■), -5 °C (Δ), 5 °C (▲), 15 °C (□), 25 °C (●).

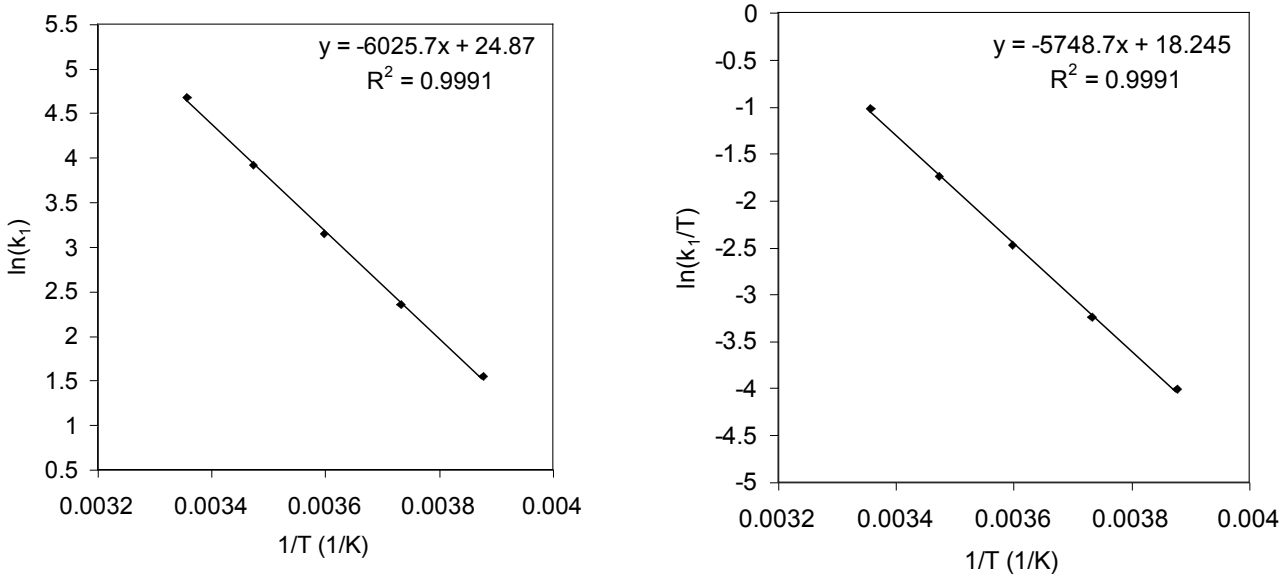

A B

Figure 6-4. Arrhenius plot (A) and Eyring plot (B) for the first step of the reaction between **1**, benzoic acid and hydrogen peroxide.

The observed rate constants were found to be independent of complex **1** concentration and benzoic acid concentration indicating a first order in complex **1** and zero order in benzoic acid. The activation enthalpy ($\Delta H^{\ddagger}$ = 47.8 ± 0.8 kJ mol^{-1}) and entropy ($\Delta S^{\ddagger}$ = -45.9 ± 0.7 J mol^{-1} K^{-1}) for this step were calculated from linear Arrhenius and Eyring plots (Figure 6-4). The negative activation entropy observed is indicative of an associative process, most probably binding of hydrogen peroxide with oxidation of the iron center.

*6.1.2 Kinetic studies with variable [**1**]*

The second, slower step was accompanied by an increase in absorbance in the visible region with the appearance of a band at λ = 600 nm (ε = 2300 L mol^{-1} cm^{-1}) characteristic of the Fe(III)-salicylate complex (Figure 6-1). Unlike the first step, which was found to be first-order in **1**, the kinetics of salicylate formation are more complex and were found to depend, under some conditions, on the concentration of **1**, indicating a possible higher order in **1**. Higher concentrations in **1** significantly increased the rate of the salicylate degradation process. When decomposition interfered, the apparent rate of salicylate formation increased substantially, and continued to increase with an increase in concentration of **1**. At low temperature and low concentrations of hydrogen peroxide, salicylate formation was first-order in **1**, and salicylate decomposition was negligible (Figure 6-5). For comparison, rate of benzene hydroxylation also does not depend on concentration of **1 (**first-order in **1**) when [**1**] < 1 mM (Figure F3).

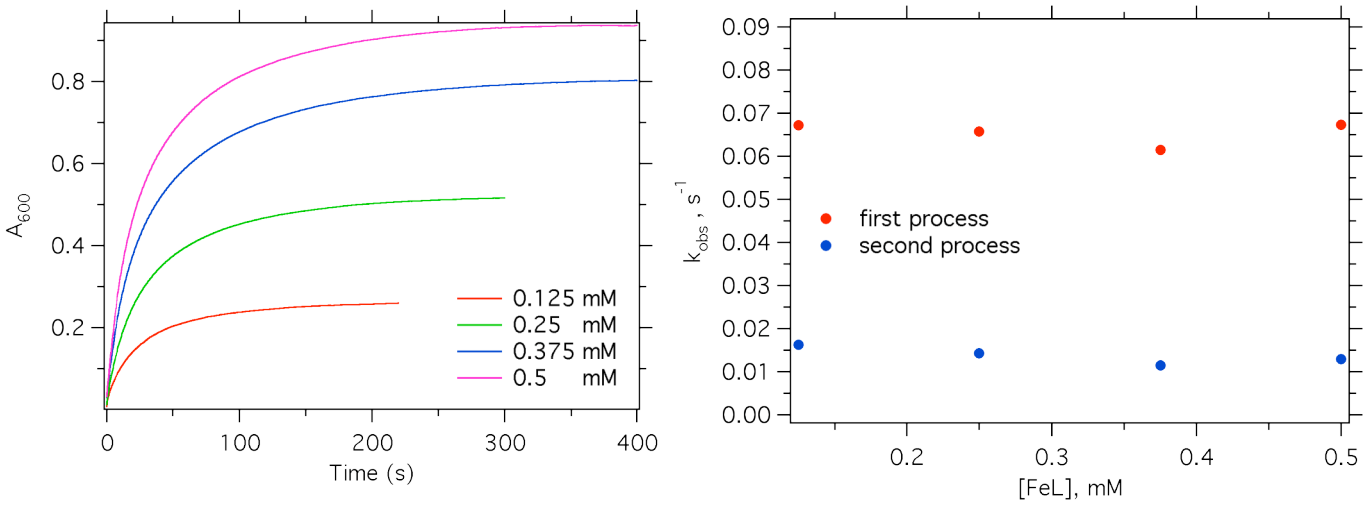

Figure 6-5. Left: kinetic traces at 600 nm for the reaction between **1,** benzoic acid and H_2O_2 ; [**1**] = 0.125 mM, 0.25 mM, 0.375 mM and 0.5 mM, [BA] = 1 mM, [H_2O_2] = 1.5 mM. Right: kinetic traces at 600 nm (left) were fitted to a double exponential rate law and corresponding observed rate constants plotted against [**1**].

Table 6-1. Kinetic parameters obtained by fitting kinetic traces at 600 nm (Figure 6-5) to $A = A_{inf} + \Delta A_1 \exp(-k_1 t) + \Delta A_2 \exp(-k_2 t)$, ratio $\Delta A_2/\Delta A_1$ represents fraction of the second process in the overall kinetic trace.

[**1**], mM	ΔA_1	ΔA_2	$\Delta A_2/\Delta A_1$	k_1, s^{-1}	k_2, s^{-1}
0.125	0.12	0.13	1.08	0.068	0.016
0.25	0.23	0.27	1.2	0.063	0.013
0.375	0.36	0.41	1.14	0.061	0.011
0.5	0.43	0.47	1.10	0.067	0.013

In addition, kinetic traces at 600 nm can be fitted to a second order equation A = Af – ((Af-An)/(1+k*t*C)), where Af is a final absorbance and An- initial absorbance (Figure F2); corresponding rate constants do not depend on [**1**] (Table 6-2).

Table 6-2. Kinetic parameters obtained by fitting kinetic traces at 600 nm (Figure 6-5) to A = Af – ((Af-An)/(1+k*t*C))

[**1**], mM	k
0.125	0.067
0.25	0.062
0.375	0.059
0.5	0.063

Kinetic traces at 600 nm give good fits to second order rate law when high concentration of hydrogen peroxide used (20 equiv vs. iron). Rate constant obtained from fit to f(x) = Af-((Af-An)/(1+k*C*x)) equation increases with [H_2O_2] (Figure F5).

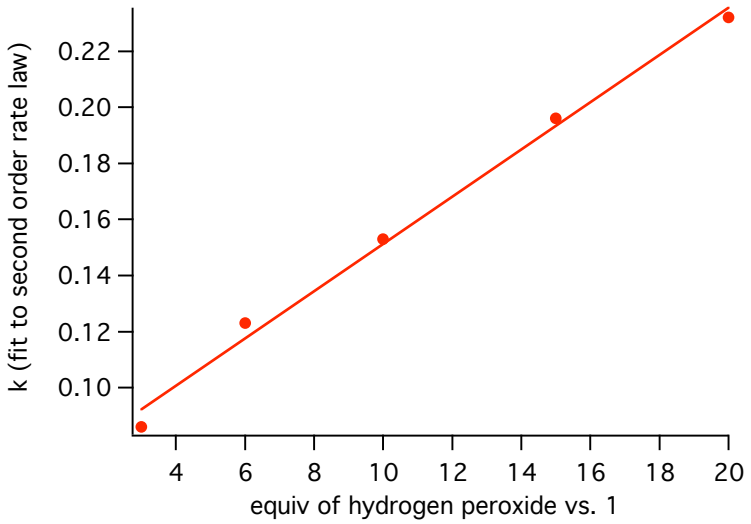

Figure 6-6. Kinetic traces at 600 nm were acquired for the reaction of **1**, benzoic acid and variable amounts of H_2O_2 and fitted to a second order rate law f(x) = Af-((Af-An)/(1+k*C*x)). Corresponding rate constant linearly increase with [H_2O_2].

6.1.3 Discussion

Kinetic traces at 600 nm (salicylate formation) fit well to a double exponential rate law. Reaction of **1** with H_2O_2/benzene also gives two exponential kinetic traces at 600 nm (chapter 2, Figure 2-1): the first process was assigned to formation of $Fe^{III}(OOH)$ (λ_{max} = 560 nm) and the second process is formation of hydroxylated product Fe(III)-phenolate (λ_{max} = 650 nm). However, we have not observed formation of $Fe^{III}(OOH)$ when **1** was mixed with H_2O_2/HOAc, therefore we can not attribute the first process in benzoic acid hydroxylation to the formation of $Fe^{III}(OOH)$. Two exponential behavior can be explained by the formation of two iron-based oxidants that compete for the substrate. For example branching can happen at the initial stages of the reaction after Fe(II)→Fe(III) oxidation: Fe(III) reacts with H_2O_2 to give $Fe^{III}(OOH)$ or it can form a μ-O diferric dimer (Scheme 6-1) that was also shown to promote aromatic hydroxylation (chapter 4). However, both observed rate constants of hydroxylation do not depend on [**1**] (Figure 6-5), this experiment argues against dimer being involved in hydroxylation pathway. In case dimer would be responsible for the second step in hydroxylation reaction, fraction of ΔA_2 would increase with concentration of [**1**] (Table 6-1) but experimental data show the same ratio $\Delta A_2/\Delta A_1$ when [**1**] = 0.125-0.5 mM. Therefore we conclude that Fe-based species other than dimer promotes second slower step of the hydroxylation reaction.

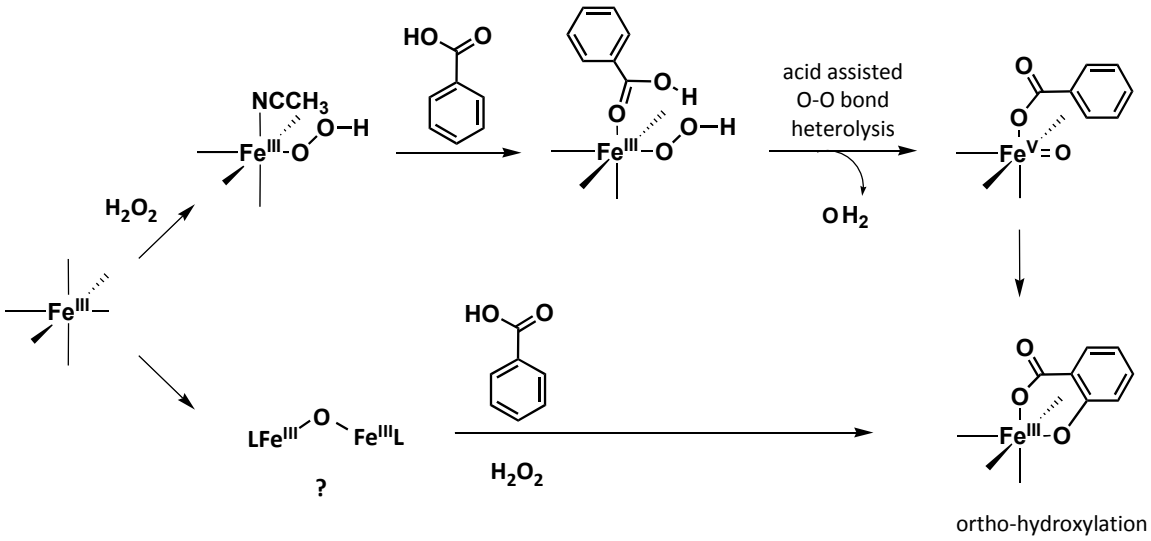

Scheme 6-1. Simultaneous formation of the two iron species that promote *ortho*-hydroxylation – branching in the hydroxylation pathway.

6.2 **Effect of acids on hydroxylation rate**

The rate of salicylate formation (2nd step in the overall reaction) was independent of the concentration of benzoic acid. On the other hand, rate of hydroxylation increased with [HOAc]. To suppress side reactions - formation of μ-O μ-carboxylato (see chapter 4) – we pregenerated Fe^{III}(OOH) and then added a mixture of benzoic and acetic acids (Figure 6-7).

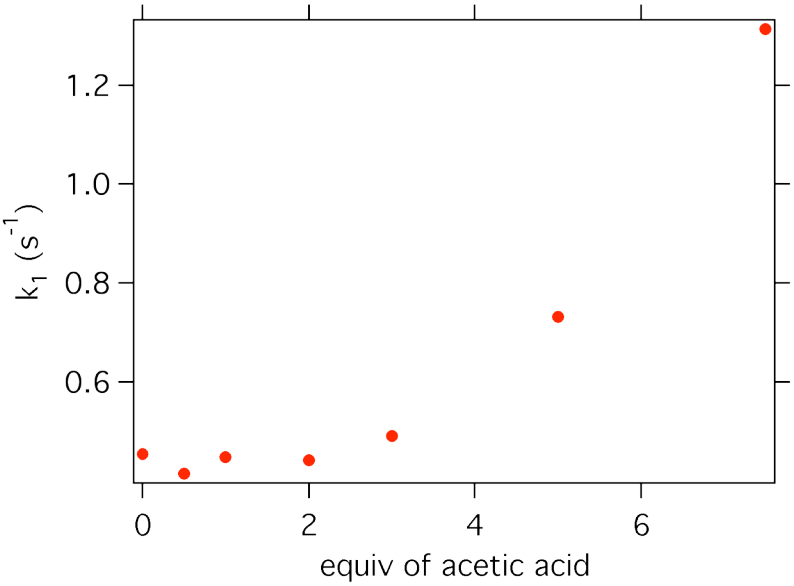

Figure 6-7. Rate constant of Fe(III)-salicylate formation increases with concentration of acetic acid. $Fe^{III}(OOH)$ was pregenerated by mixing **1** (0.5 mM after DX) and H_2O_2 (10 equiv vs. iron) followed by addition of benzoic acid (2 equiv vs. iron) with variable amounts of acetic acid (0-7.5 equiv vs. iron) at 20 °C (V-14). Each kinetic trace at 700 nm was fitted using A→B→C model, first rate constants (k_{1obs}) were plotted against acetic acid concentration. Second rate constant (k_{2obs}) was much smaller compared to k_{1obs}.

Similar experiment with pregenerated $Fe^{III}(OOH)$ was done using triflic acid and benzene as a substrate instead of benzoic acid. First observed rate constant was independent of triflic acid up to 1 equiv, then reaction became two exponential with very fast first process and very slow second process (Figure 6-8). It is plausible that large amounts of triflic acid help generate radicals from **1** and H_2O_2 (Fenton chemistry).

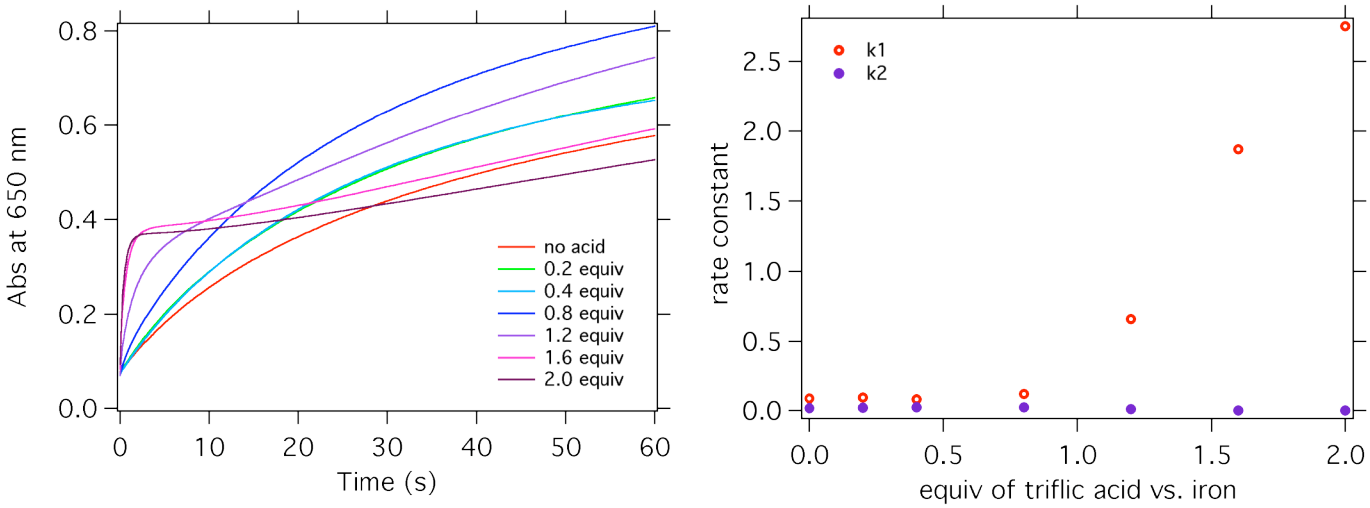

Figure 6-8. Effect of triflic acid on the rate of hydrohylation. Left: kinetic traces at 650 nm acquired in the diode array mode using stopped-flow technique. Double mixing experiments: Fe^{III}(OOH) was generated by mixing **1** (0.5 mM) with H_2O_2 (5 mM) at 20 °C in acetonitrile and then benzene (560 equiv) and variable amounts of triflic acid (0-2 equiv vs. iron) were added. Age time: 8 s, run time 60 s. Right: all kinetic traces were fitted using A→B→C model and both k_{1obs} and k_{2obs} plotted against equiv of triflic acid.

6.3 **Self-hydroxylation of mCPBA**

Peroxo acids, which may form from carboxylic acids and hydrogen peroxide, are plausible oxidants. Nam *et al.* reported self-hydroxylation of peroxobenzoic acid in the presence of **2.**[1] In our studies we tested peroxobenzoic acid as a potential oxidant in benzoic acid/ hydrogen peroxide system with **1** and **2**. Parallel experiments with **1** and m-CPBA or 3-chlorobenzoic acid and hydrogen peroxide as oxidant showed that both oxidants lead to the salicylate (Figure 6-10), however when mCPBA is used as an oxidant, hydroxylation reaction is clearly two exponential (Figure 6-10). Rate of

hydroxylation does not depend on the nature of substrate – same rate was calculated for 3-chlorobenzoic acid and benzoic acid (Figure F4), therefore hydroxylation is not a rate-limiting step.

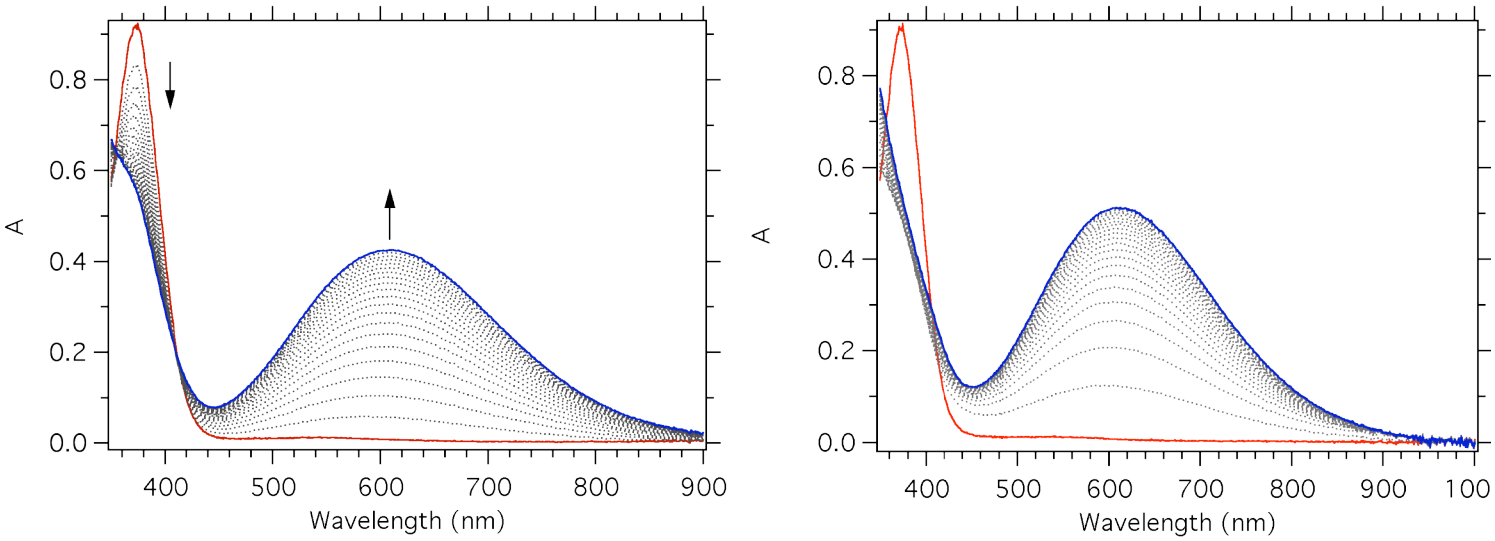

Figure 6-9. Left: spectral changes upon reaction of **1**, 3-chlorobenzoic (mClBA) acid and H_2O_2 in acetonitrile at 25 ˚C; [**1**] = 0.25 mM, [mClBA] = 1 mM, [H_2O_2] = 1 mM. Right: spectral changes upon reaction of **1** and mCPBA in acetonitrile at 25 ˚C; [**1**] = 0.25 mM, [mCPBA] = 1 mM.

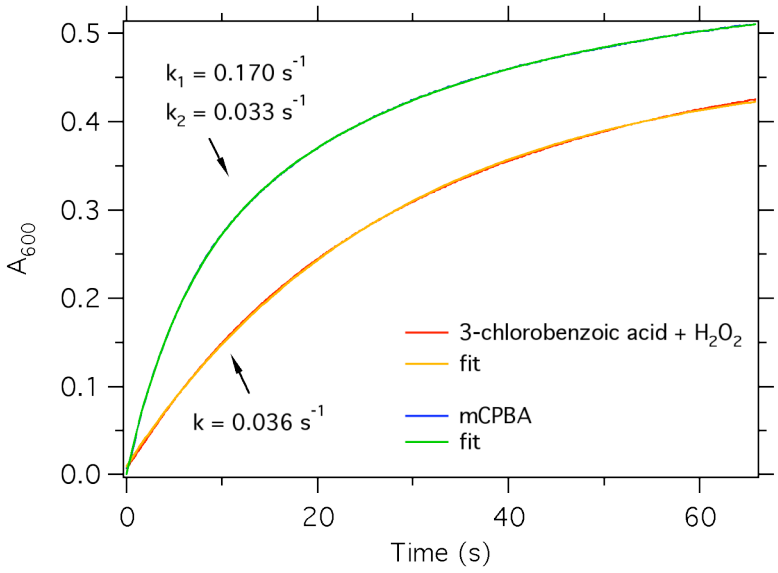

Figure 6-10. Kinetic traces at 600 nm acquired for the reaction between **1** (0.25 mM), 3-chlorobenzoic acid (1 mM) and H_2O_2 (1 mM) and for the reaction between **1** (0.25 mM) and mCPBA (1 mM). Kinetic traces were fitted to one exponential (3-chlorobenzoic acid + H_2O_2) or double exponential (mCPBA) equation, corresponding observed rate constants are shown on the graph.

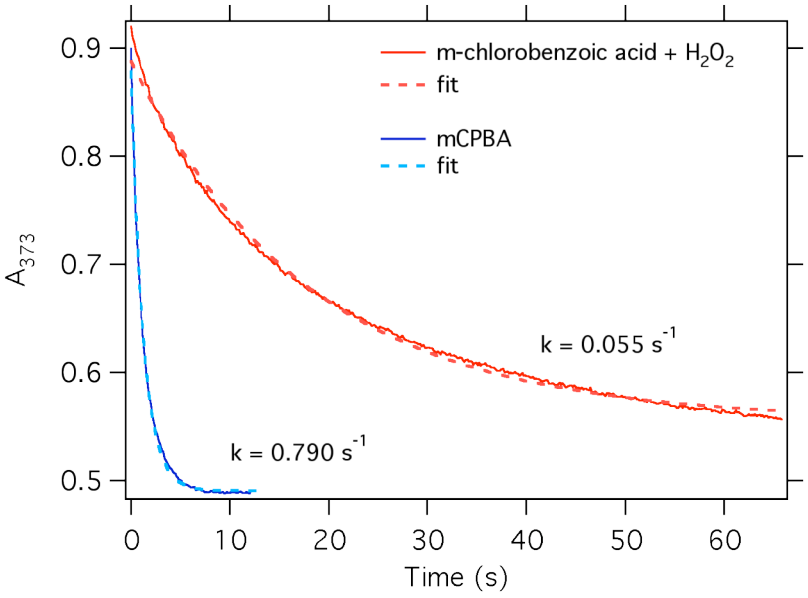

Figure 6-11. Kinetic traces at 373 nm acquired for the reaction in Figure 6-9 caption.

^{18}O-labeling experiments with $H_2{}^{18}O_2$ and **1**/benzoic acid[2] or **2** / 3-methoxybenzoic acid[3] unambiguously showed the incorporation of one oxygen atom in the salicylate product. These results underscore the importance of hydrogen peroxide as a sole source of the oxygen atom incorporated in *ortho*-hydroxylated products. However, oxygen-labeling incorporation is inconsistent with peroxo acid pathway, which would result in doubly-labeled products (Scheme 6-2).

Scheme 6-2

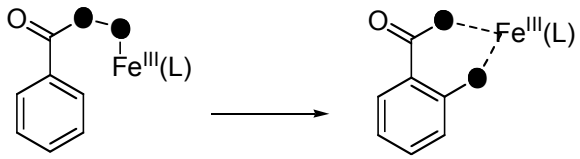

6.4 **Kinetics with FeTPA**

In double-mixing stopped-flow experiments, (TPA)Fe^{III}(OOH) was generated in reaction between **2** and excess H_2O_2, and then the substrate (such as 3-methoxybenzoic acid) was added in the second mixing. The overall spectral changes in these experiments were similar to those observed with a regular spectrophotometer. Formation of salicylate from 3-methoxybenzoic acid and (TPA)Fe^{III}(OOH) (in the presence of excess H_2O_2) was clearly biphasic (Figure 6-12). In contrast, only one, slower process was observed upon addition of H_2O_2 to the mixture of **2** and 3-methoxybenzoic acid in single-mixing experiments (Figure 6-12). Therefore, the first, rapid process seen in double-mixing experiments can be attributed to the direct interaction between (TPA)Fe^{III}(OOH) and the substrate. This process is sensitive to the concentration of 3-methoxybenzoic acid: the observed rate constant (Figure 6-13) and the amount of

salicylate product formed via this process increases at higher concentrations of the substrate.

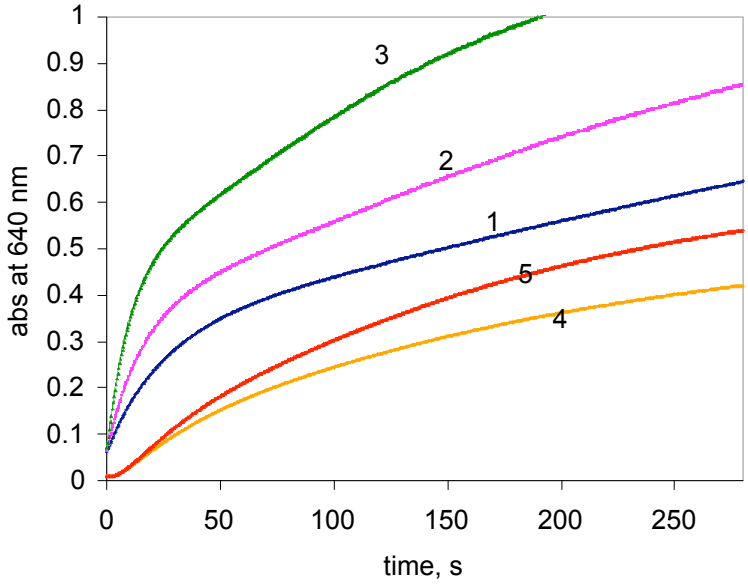

Figure 6-12**.** Kinetic traces at 640 nm acquired in the diode array mode using stopped-flow techniques. Double mixing experiments : $Fe^{III}(OOH)$ was generated by mixing **2** with H_2O_2 at -20 °C in acetonitrile and then variable amounts of 3-methoxybenzoic acid were added (1- 10 equiv of 3-methoxybenzoic acid w.r.t. iron; 2- 20 equiv; 3- 40 equiv). Single mixing experiments: **2** was mixed with 3-methoxybenzoic acid and H_2O_2 at -20 °C in acetonitrile (4- 20 equiv of 3-methoxybenzoic acid, 5- 30 equiv of 3-methoxybenzoic acid). Final concentration of **2** is 0.5 mM in both double and single mixing experiments, 10 equiv of hydrogen peroxide w.r.t. iron was used to generate $Fe^{III}(OOH)$ species in double mixing experiments and 10 equiv of hydrogen peroxide was added to **2** together with 3-methoxybenzoic acid in a single mixing experiments.

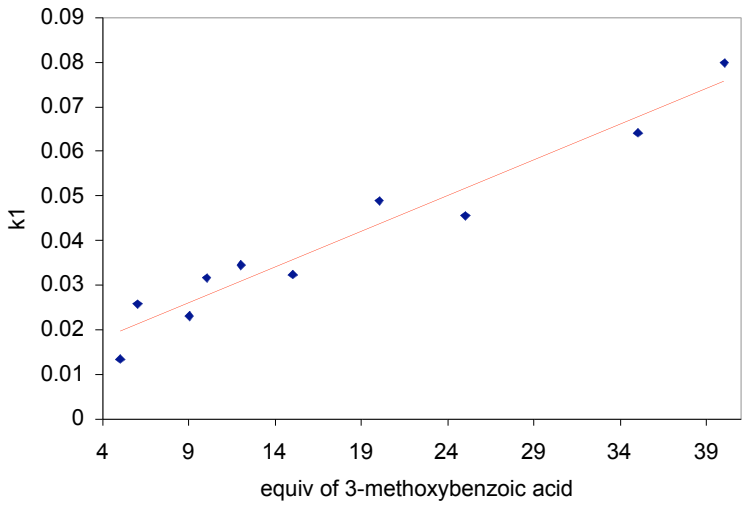

Figure 6-13. Rate constants of the first process in double mixing experiments (Figure 6-12) versus amount of 3-methoxybenzoic acid added (constants determined using 650 nm kinetic traces and Kinetic Studio program).

The second, slower process of 3-methoxysalicylate formation did not depend on the substrate concentration in a well-defined manner. The addition of acetic acid converted the reaction between (TPA)Fe^{III}(OOH) and 3-methoxybenzoic acid into a single-exponential process (Figure 6-14); however the initial rates of salicylate formation are essentially independent on the concentration of acetic acid. This suggests that acetic acid suppresses competing non-productive decomposition of iron(III)-hydroperoxo intermediate, which generates less reactive iron species responsible for slower substrate hydroxylation in the second reaction step. The first, substrate-dependent but acid-independent process in hydroxylation of 3-methoxybenzoic acid with (TPA)Fe^{III}(OOH), may involve a direct attack of the coordinated hydroperoxide on the electron-rich aromatic ring. Alternatively, carboxylic acid of the substrate may facilitate

heterolytic O-O bond cleavage in (TPA)Fe^{III}(OOH) intermediate. In the former case, the hydroxylation rate would depend on substituents on the aromatic ring: electron-donating substituents would make the ring more susceptible to oxidation.

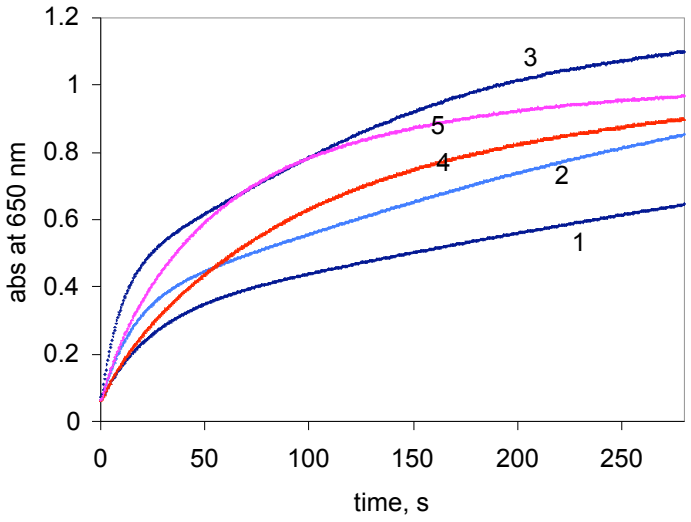

Figure 6-14. Kinetic traces at 650 nm acquired in the diode array mode using stopped-flow techniques. Double mixing experiments: FeOOH was generated by mixing **2** (2 mM before mixing) with H_2O_2 (20 mM) at -20 °C in acetonitrile and then variable amounts of 3-methoxybenzoic acid were added (1- 10 equiv of 3-methoxybenzoic acid w.r.t. iron; 2- 20 equiv; 3- 40 equiv) or equal amount of 3-methoxybenzoic acid and acetic acid were added (4- 10 equiv of 3-methoxybenzoic acid and 10 equiv of acetic acid; 5- 20 equiv of 3-methoxybenzoic acid and 20 equiv of acetic acid).

Experimental studies of the reaction between (TPA)Fe^{III}(OOH) and an electron-rich substrate, 3,4,5-trimethoxybenzoic acid, revealed relatively slow hydroxylation and low yields of salicylate product (Figure 6-15). A more careful examination of the kinetic

traces clearly showed a biphasic reaction qualitatively similar to hydroxylation of a less electron-rich 3-methoxybenzoic acid (Figure 6-14, traces 1-3). The first, rapid process has nearly equal initial rates for both substrates under the same conditions (Figure 6-15).

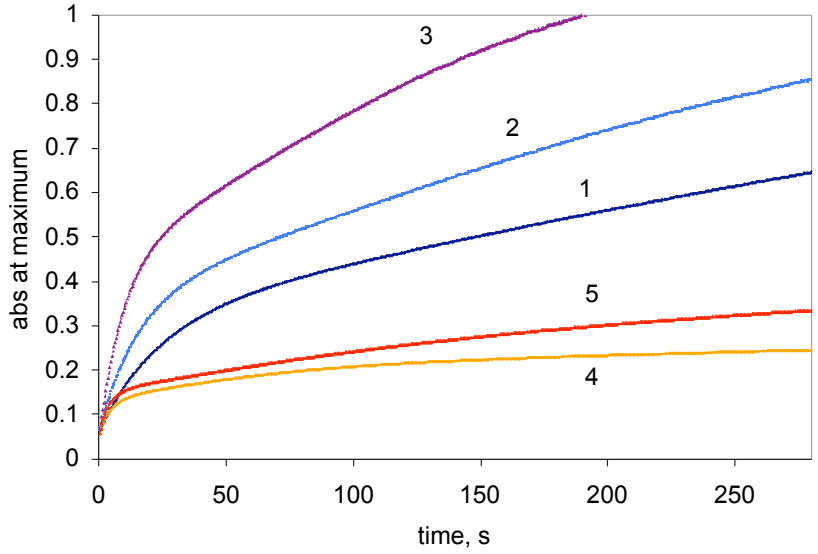

Figure 6-15. Kinetic traces at 640 nm (for 3-methoxysalicylate) and 660 nm for (3,4,5-trimethoxysalicylate) acquired in the diode array mode using stopped-flow techniques. Double mixing experiments : $Fe^{III}(OOH)$ was generated by mixing **2** (0.5 mM) with H_2O_2 (5 mM) at -20 °C in acetonitrile and then variable amounts of 3-methoxybenzoic acid were added (1- 10 equiv of 3-methoxybenzoic acid w.r.t. iron; 2- 20 equiv; 3- 40 equiv) or variable amounts of 3,4,5-trimethoxybenzoic acid were added (4- 10 equiv of 3,4,5-trimethoxybenzoic acid; 5- 20 equiv).

This observation argues in favor of a rate-limiting O-O bond cleavage in hydroxylation of both substrates. Additions of acetic acid slightly accelerate the initial

hydroxylation rate of 3,4,5-trimethoxybenzoic acid, supporting the proposal of acid-assisted O-O bond cleavage at the rate-limiting step. 3,4,5-trimethoxybenzoic acid (pK_a = 4.23) is a weaker acid than 3-methoxybenzoic acid and its hydroxylation is more sensitive to additional amounts of externally added CH_3COOH (Figure 6-16). It should be noted, however, that side reactions (such as the formation of quinone-type structures) are much more pronounced for 3,4,5-trimethoxybenzoic acid. Therefore, the rates of accumulation of salicylate have to be interpreted with caution. Also of note is the inhibiting effect of acetic acid on the second process in the hydroxylation of 3,4,5-trimethoxybenzoic acid, which can be attributed to the formation of redox-inactive oxo, carboxylato-bridged diiron(III) complex (easily identified by its characteristic optical absorbance at 450 and 510 nm (see 4.3.2). This behavior differs from the hydroxylation of 3-methoxybenzoic acid, and is consistent with much higher concentrations of iron(III) side products in the reaction with easily oxidizable 3,4,5-trimethoxybenzoic acid. Acetic acid accelerates hydroxylation but formation of the inactive μ-O, μ-carboxylato complex also becomes faster.

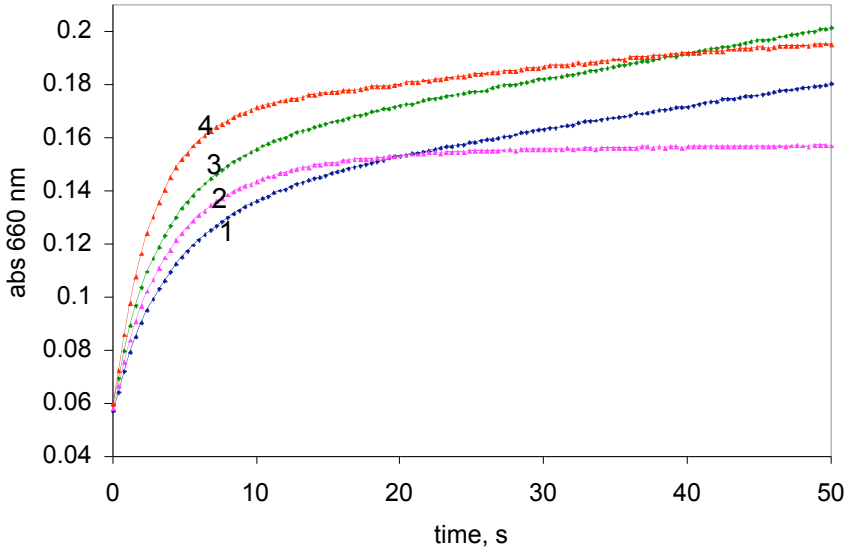

Figure 6-16. Kinetic traces at 660 nm acquired in the diode array mode using stopped-flow techniques. Double mixing experiments: $Fe^{III}(OOH)$ was generated by mixing **2** (2 mM before mixing) with H_2O_2 (20 mM) at -20 °C in acetonitrile and then variable amounts of 3,4,5-trimethoxybenzoic acid were added (1- 10 equiv of 3,4,5-trimethoxybenzoic acid w.r.t. iron; 3- 20 equiv) or equal amount of 3,4,5-trimethoxybenzoic acid and acetic acid were added (2- 10 equiv of 3,4,5-trimethoxybenzoic acid and 10 equiv of acetic acid; 4- 20 equiv of 3,4,5-trimethoxybenzoic acid and 20 equiv of acetic acid).

6.5 **Conclusions**

Hydroxylation of benzoic acid with hydrogen peroxide on **1** is at least two-step process. The first, rapid step was accompanied by a drop in absorbance in the near UV region with the disappearance of the band at λ = 375 nm characteristic of complex **1**. The observed rate constants were found to be independent of complex **1** concentration and benzoic acid concentration indicating a first order in complex **1** and zero order in benzoic acid. Enthalpy and entropy of activation were calculated for the first step (decay at 373 nm in the presence of large excess of hydrogen peroxide). The activation enthalpy ($\Delta H^{\ddagger}$ = 47.8 ± 0.8 kJ mol^{-1}) and entropy ($\Delta S^{\ddagger}$ = -45.9 ± 0.7 J mol^{-1} K^{-1}) for this step are consistent with a bimolecular rate-limiting step.

Hydroxylation was accompanied by an increase in absorbance in the visible region with the appearance of a band at λ = 600 nm (ε = 2300 L mol^{-1} cm^{-1}) characteristic of the Fe(III)-salicylate complex. Kinetic traces at 600 nm cannot be fitted to a one exponential equation but double exponential, therefore two species promote hydroxylation of benzoic acid . Hydroxylation of electron-rich benzoic acids with H_2O_2 using pregenerated $TPAFe^{III}(OOH)$ is also a two-exponential process.

Rate of salicylate formation does not depend on concentration of BA and triflic acid (< 1 equiv vs. **1**), but its rate increases as acetic acid is added. Larger concentrations of triflic acid accelerate hydroxylation reaction, presumably radical (Fenton0 chemistry takes place when [HOTf] > [**1**].

6.6 **References**

[1] N. Y. Oh, M. S. Seo, M. H. Lim, M. B. Consugar, M. J. Park, J.-U. Rohde, J. Han, K. M. Kim, J. Kim, L. Que Jr., W. Nam, *Chem. Commun.* **2005**, 5644.

[2] S. Taktak, M. Flook, B. M. Foxman, L. Que Jr., E. V. Rybak-Akimova, *Chem. Commun.* **2005**, 5301.

[3] O. V. Makhlynets, P. Das, S. Taktak, M. Flook, R. Mas-Balleste, E. V. Rybak-Akimova, L. Que, Jr., *Chem. Eur. J.* **2009**, *15*, 13171.

7 Appendix A (Chapter 1)

Table A1. Reactivity of substituted benzoic acids in *ortho*-hydroxylation reaction with hydrogen peroxide in the presence of **1** and **2**, λ_{max} of the salicylates and the salicylate product yields (%) obtained by ^{1}H NMR after reaction.

Substituent		**1**	**2**
H		590 nm, 80%	560 nm
OCH_3	*2*-	-	-
	3-	695 nm	650 nm
	4-	-	-
CH_3	*2*-	594 nm	-
	3-	634 nm, 85%	595 nm
	4-	591 nm, 70%	-
Cl	*2*-	580 nm	-
	3-	605 nm, 85%	568 nm
	4-	561 nm, 47%	-
NO_2	*2*-	538 nm, 42%	-
	3-	540 nm	-
	4-	540 nm, 37%	-

'-' indicates that *ortho*-hydroxylation is not observed

Table A2. Crystal data and structure refinement for $[Fe^{III}(TPA)(5\text{-MeO-salicylate})]^{+}$

Empirical formula	$C_{27}\ H_{24}\ F_3\ Fe\ N_4\ O_7\ S$	
Formula weight	661.41	
Temperature	173(2) K	
Wavelength	0.71073 Å	
Crystal system	Orthorhombic	
Space group	Fdd2	
Unit cell dimensions	*a* = 26.279(2) Å	a = 90°
	b = 52.814(5) Å	b = 90°
	c = 8.3068(8) Å	g = 90°
Volume	11529.0(18) $Å^3$	
Z	16	
Density (calculated)	1.524 Mg/m^3	
Absorption coefficient	0.667 mm^{-1}	
F(000)	5424	
Crystal color, morphology	Blue, Needle	
Crystal size	0.50 x 0.07 x 0.06 mm^3	
Theta range for data collection	1.54 to 25.04°	
Index ranges	0 £ *h* £ 31, 0 £ *k* £ 62, -9 £ *l* £ 9	
Reflections collected	22656	
Independent reflections	5092 [*R*(int) = 0.0496]	
Observed reflections	4182	
Completeness to theta = 25.04°	100.0%	
Absorption correction	Multi-scan	
Max. and min. transmission	0.9611 and 0.7314	
Refinement method	Full-matrix least-squares on F^2	
Data / restraints / parameters	5092 / 9 / 399	
Goodness-of-fit on F^2	1.055	
Final *R* indices [*I*>2sigma(*I*)]	*R*1 = 0.0368, *wR*2 = 0.0790	
R indices (all data)	*R*1 = 0.0516, *wR*2 = 0.0850	
Absolute structure parameter	0.024(16)	
Largest diff. peak and hole	0.279 and -0.265 e.$Å^{-3}$	

Table A3**.** Crystal data and structure refinement for $[Fe^{III}(TPA)(salicylate)]^{+}$

Empirical formula	C26 H22 F3 Fe N4 O6 S	
Formula weight	631.39	
Temperature	173(2) K	
Wavelength	0.71073 Å	
Crystal system	Monoclinic	
Space group	P2(1)/n	
Unit cell dimensions	*a* = 8.014(2) Å	a = 90°
	b = 13.079(3) Å	b = 94.309(4)°
	c = 25.250(7) Å	g = 90°
Volume	2639.1(12) $Å^3$	
Z	4	
Density (calculated)	1.589 Mg/m^3	
Absorption coefficient	0.722 mm^{-1}	
F(000)	1292	
Crystal color, morphology	purple, needles	
Crystal size	0.38 x 0.20 x 0.03 mm^3	
Theta range for data collection	1.62 to 25.14°	
Index ranges	-9 £ *h* £ 9, -15 £ *k* £ 15, -29 £ *l* £ 29	
Reflections collected	17334	
Independent reflections	4696 [*R*(int) = 0.0608]	
Observed reflections	3241	
Completeness to theta = 25.14°	99.4%	
Absorption correction	Multi-scan	
Max. and min. transmission	0.9787 and 0.7710	
Refinement method	Full-matrix least-squares on F^2	
Data / restraints / parameters	4696 / 48 / 395	
Goodness-of-fit on F^2	1.058	
Final *R* indices [*I*>2sigma(*I*)]	*R*1 = 0.0566, *wR*2 = 0.1404	
R indices (all data)	*R*1 = 0.0905, *wR*2 = 0.1616	
Largest diff. peak and hole	0.640 and -0.824 e.$Å^{-3}$	

Table A4: Comparison of the crystallographic data of $[Fe^{III}(TPA)(5\text{-MeO-salicylate})]^+$ with $[Fe^{III}(TPA)(5\text{-Cl-salicylate})]^+$ and $[Fe^{III}(TPA)(salicylate)]^+$. Atoms have been numbered as per the $[Fe^{III}(TPA)(5\text{-MeO-salicylate})]^+$ structure published in this report. The bonds and bond angels in the same row represent the $[Fe^{III}(TPA)(5\text{-MeO-salicylate})]^+$ counterparts in the other two structures.

Bonds/Bond Angles	***[Fe(TPA)(5-OMe-sal)]$^+$***	***[Fe(TPA)(5-Cl-sal)]$^+$***	***[Fe(TPA)(sal)]$^+$***
Fe1-O3	1.851(2)	1.845(7)	1.859(3)
Fe1-O1	1.928(2)	1.914(7)	1.919(3)
Fe1-N2	2.142(3)	2.156(10)	2.140(4)
Fe1-N4	2.125(3)	2.137(8)	2.142(4)
Fe1-N3	2.137(3)	2.216(9)	2.131(3)
Fe1-N1	2.201(3)	2.129(9)	2.191(3)
C20-O3	1.344(4)	1.342(11)	1.352(5)
C25-O1	1.299(4)	1.316(11)	1.323(5)
C25-O2	1.215(4)	1.200(12)	1.219(5)
O3-Fe1-N2	106.62(10)	106.3(3)	99.97(13)
O3-Fe1-N4	99.55(10)	100.8(4)	106.23(13)
O3-Fe1-N3	92.69(10)	88.5(3)	91.82(12)
O3-Fe1-N1	171.21(11)	168.4(3)	170.80(13)
O3-Fe1-O1	93.83(10)	93.8(3)	93.88(12)

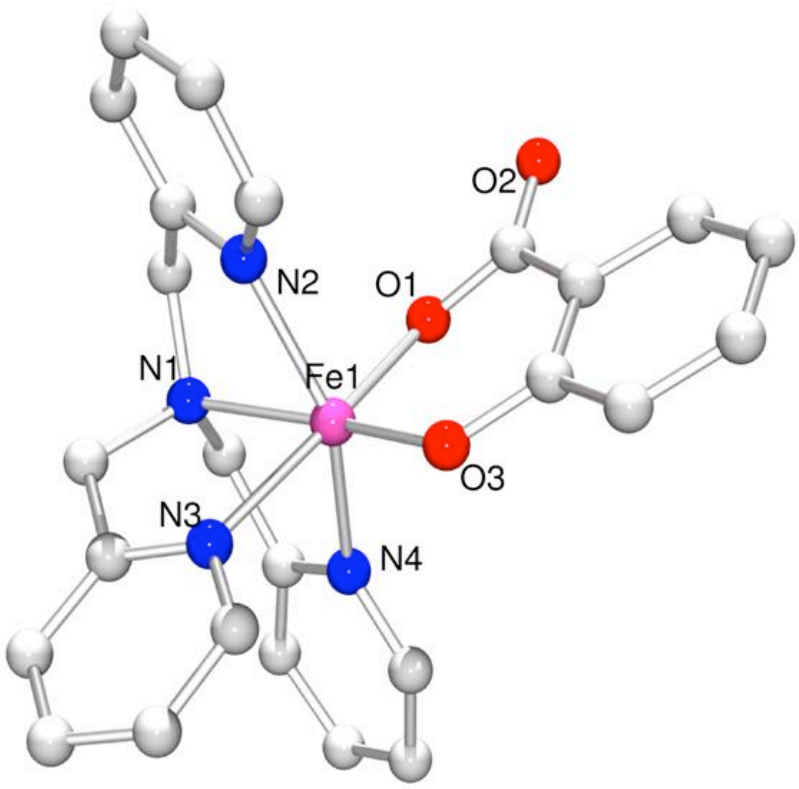

Figure A1. ORTEP representation of $[Fe^{III}(TPA)(salicylate)]^{+}$. Hydrogen atoms have been omitted for clarity.

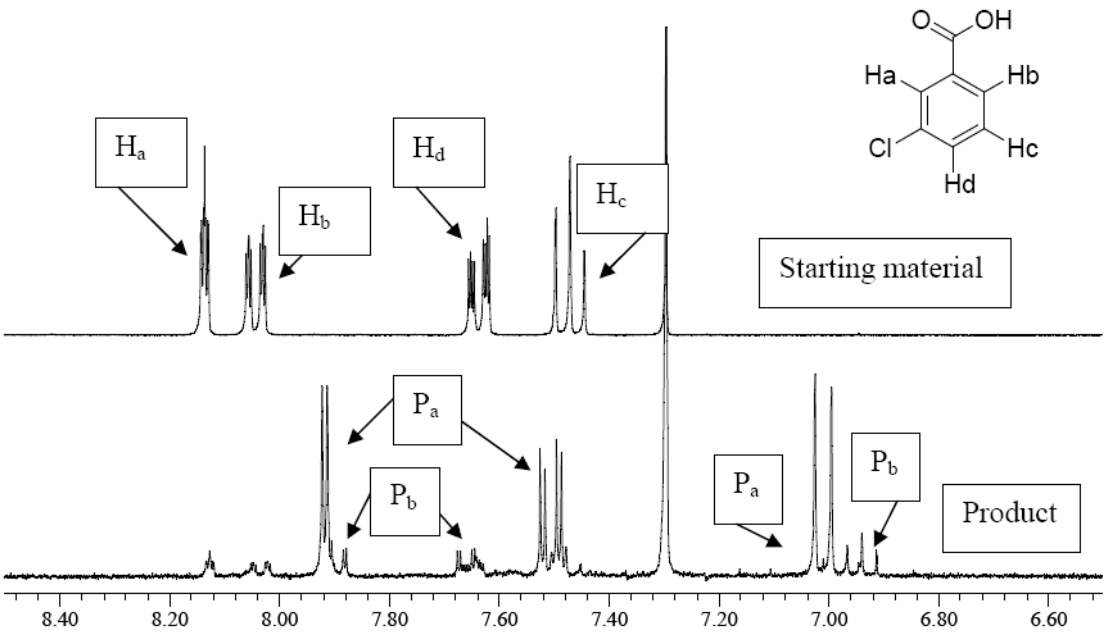

Figure A2. ^{1}H NMR spectra of 3-chlorobenzoic acid (starting material) and products extracted after hydroxylation reaction. Reaction conditions: solution of **1** with 1 equiv of 3-chlorobenzoic acid was prepared under argon, 1.5 equiv of hydrogen peroxide were added to the mixture. 85% conversion of 3-chlorobenzoic acid was calculated based on 3 runs.

Pa = OH group on the opposite side of the chloro substituent (3-chlorosalicylic acid)

Pb = OH group on same side as the chloro substituent (5-chlorosalicylic acid)

80% selectivity for Pa

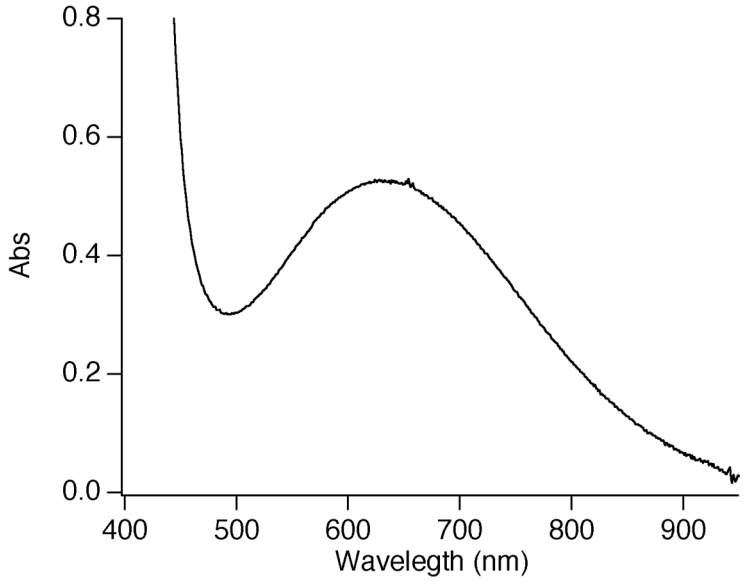

Figure A3. UV-Vis spectrum of *ipso*-hydroxylation products derived from 2,6-dimethylbenzoic acid. Reaction condition: solution of **1** (3 mM) and 2,6-dimethylbenzoic acid (6 mM) was mixed with 9 mM hydrogen peroxide in a 1:1 ratio at 20 °C.

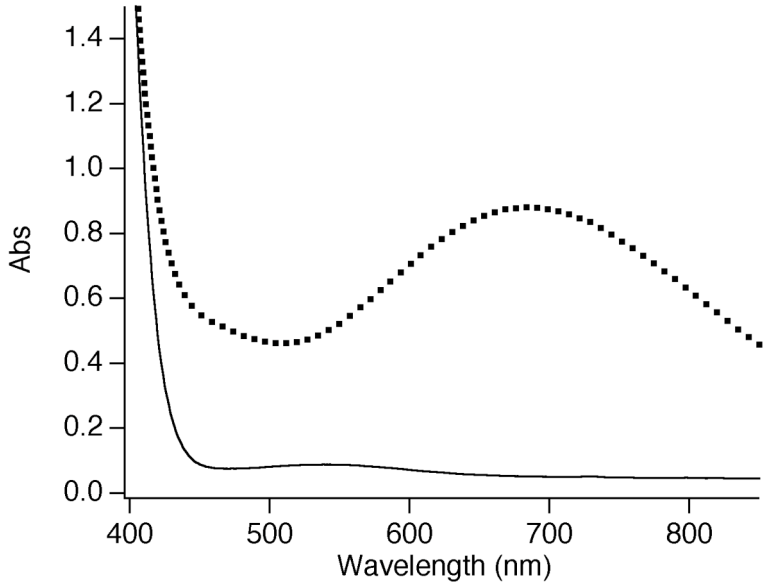

Figure A4. UV-Vis spectra of complex **1** (1 mM) with 2-methoxyphenol (2 mM) under argon (—); complex **1** (1 mM), 2-methoxyphenol (2 mM) and 1 equiv of $(NH_4)_2Ce(NO_3)_6$ (•••).

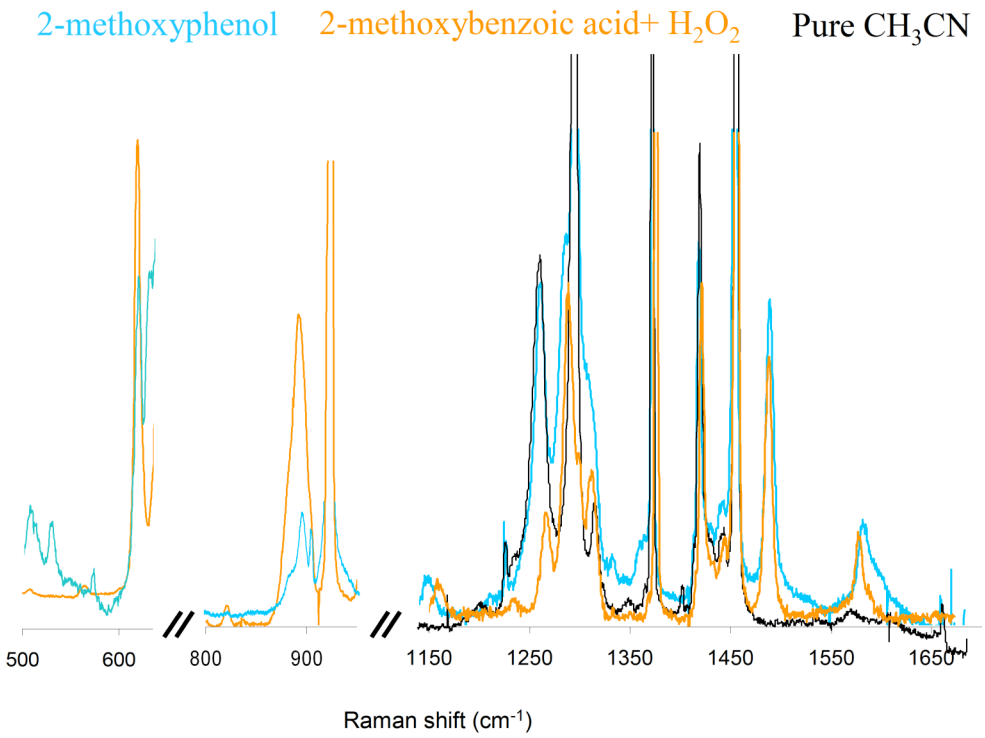

Figure A5**.** Comparison of the Resonance Raman spectrum of the independently generated $[Fe^{III}(BPMEN)(2\text{-MeO-phenolate})]^{2+}$ complex (1 mM) to that of the species generated from the reaction of **1** (1 mM), 2-methoxybenzoic acid (1.5 mM) and H_2O_2 (3 mM). Spectra were obtained on frozen samples at 77 K with 647 nm excitation.

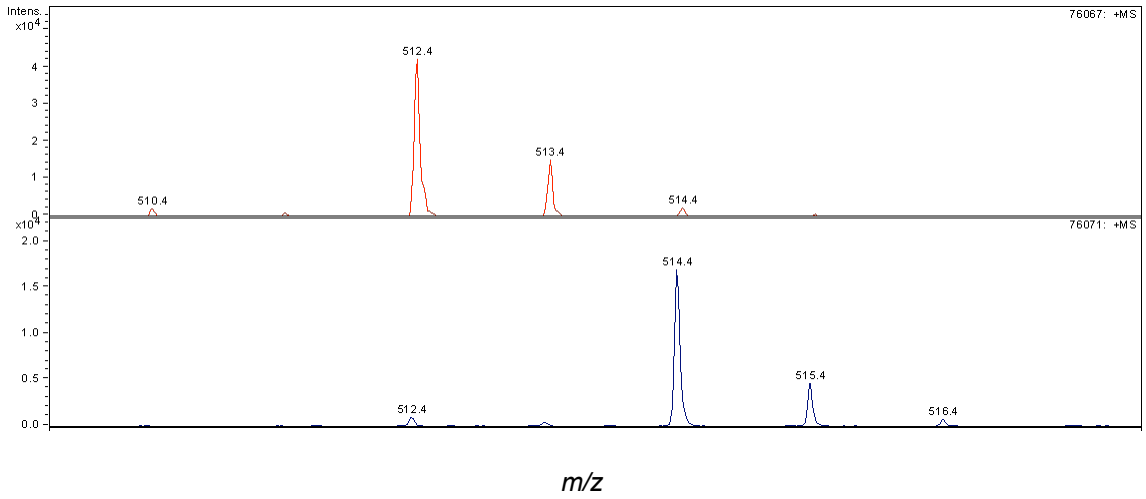

Figure A6. ESI-MS analysis of end product of the aromatic hydroxylation reaction performed by **2**, 3-methoxybenzoic acid and normal or ^{18}O-labeled H_2O_2. The labeling study with $H_2{}^{18}O_2$ suggested the incorporation of one oxygen atom from H_2O_2 in the hydroxylated aromatic product.

A

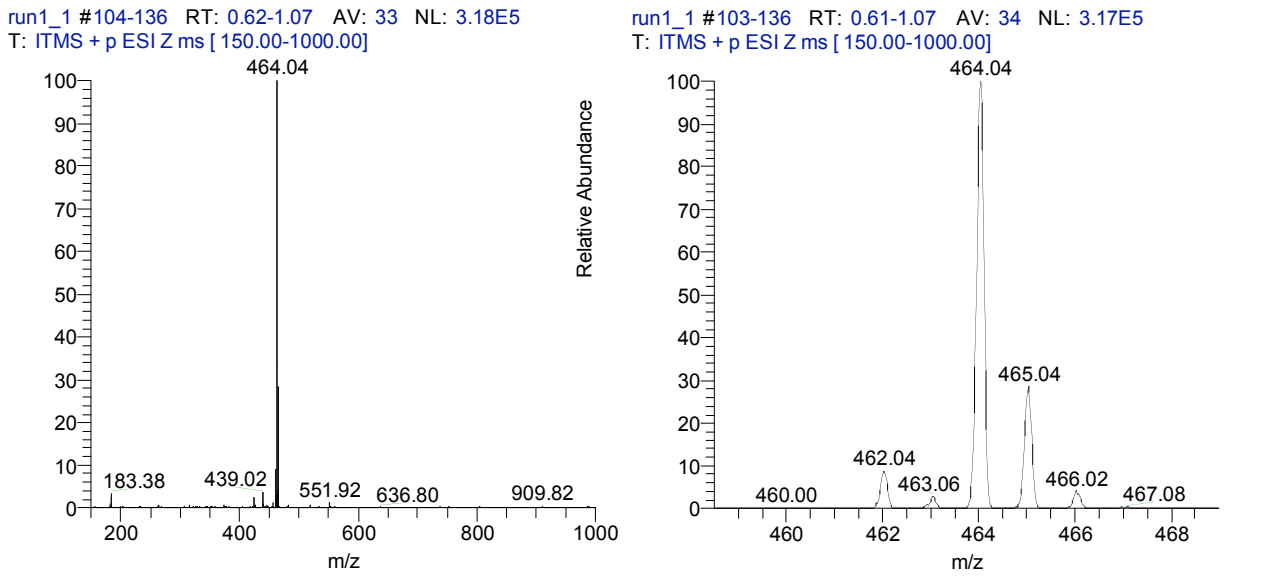

B

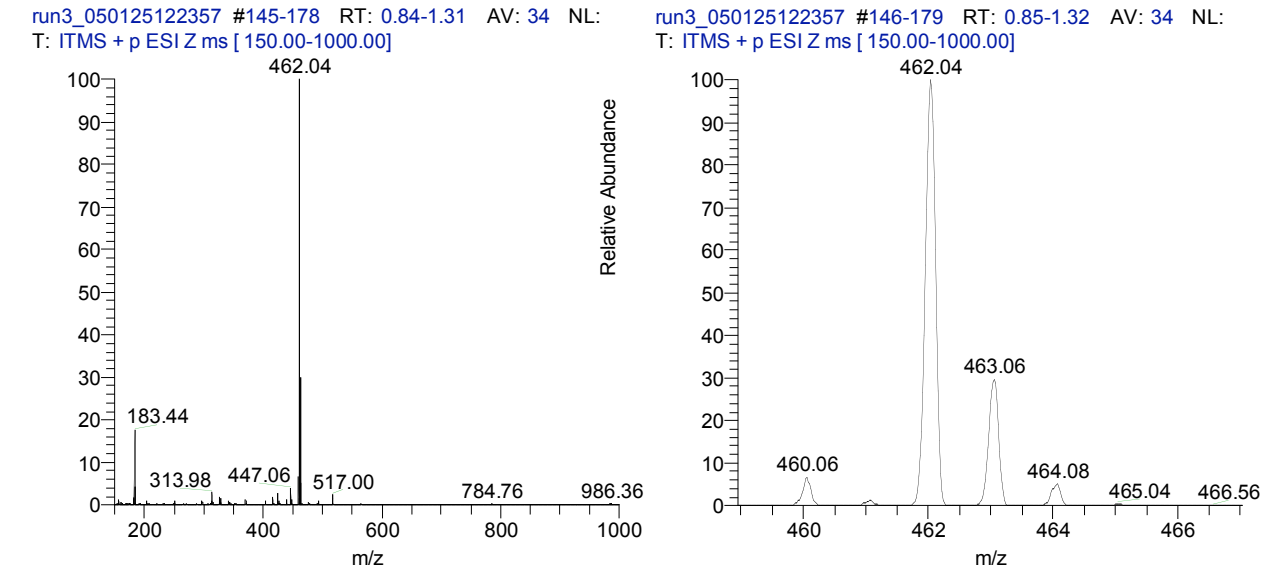

Figure A7. ESI-MS after mixing **1**/benzoic acid and 3 molar equivalents of ^{18}O hydrogen peroxide (90% atom) in the presence of non-enriched (predominantly ^{16}O) water. Full ^{18}O incorporation observed (A); ESI-MS after mixing **1**/benzoic acid and 3 molar equivalents of non-enriched (predominantly^{16}O) hydrogen peroxide in the presence of 300 equivalents of non-enriched (predominantly^{16}O) water (B).

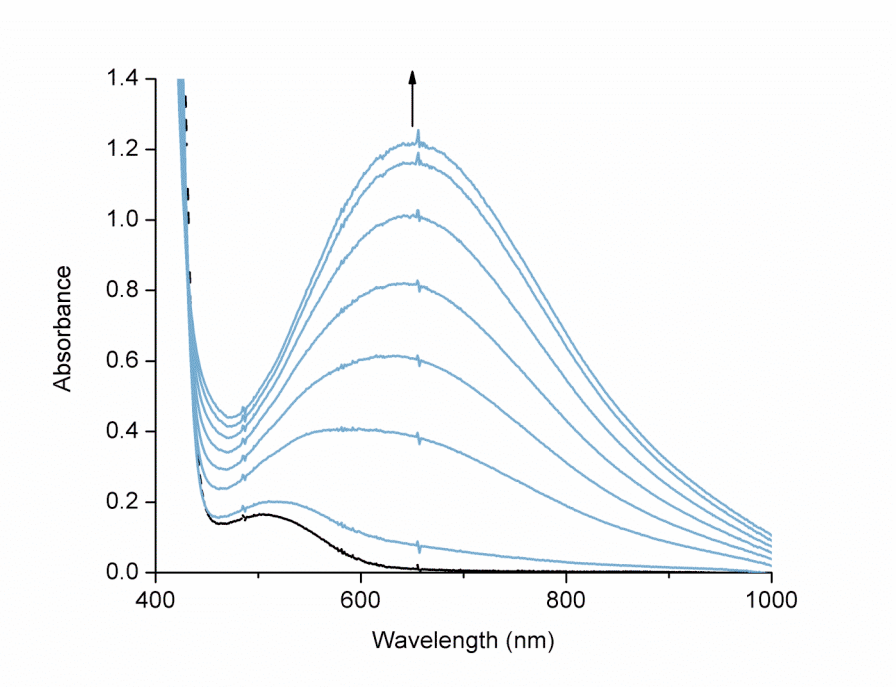

Figure A8. Spectral changes upon addition of 3 equivalents of H_2O_2 to the mixture of **2** (1 mM) and 3-methoxybenzoic acid (12 equiv) at -40 °C. The first spectrum was taken immediately after mixing. Subsequent spectra (shown in turquoise; absorbance increases over time) were taken at 5, 24, 36, 47, 59 and 73 minutes.

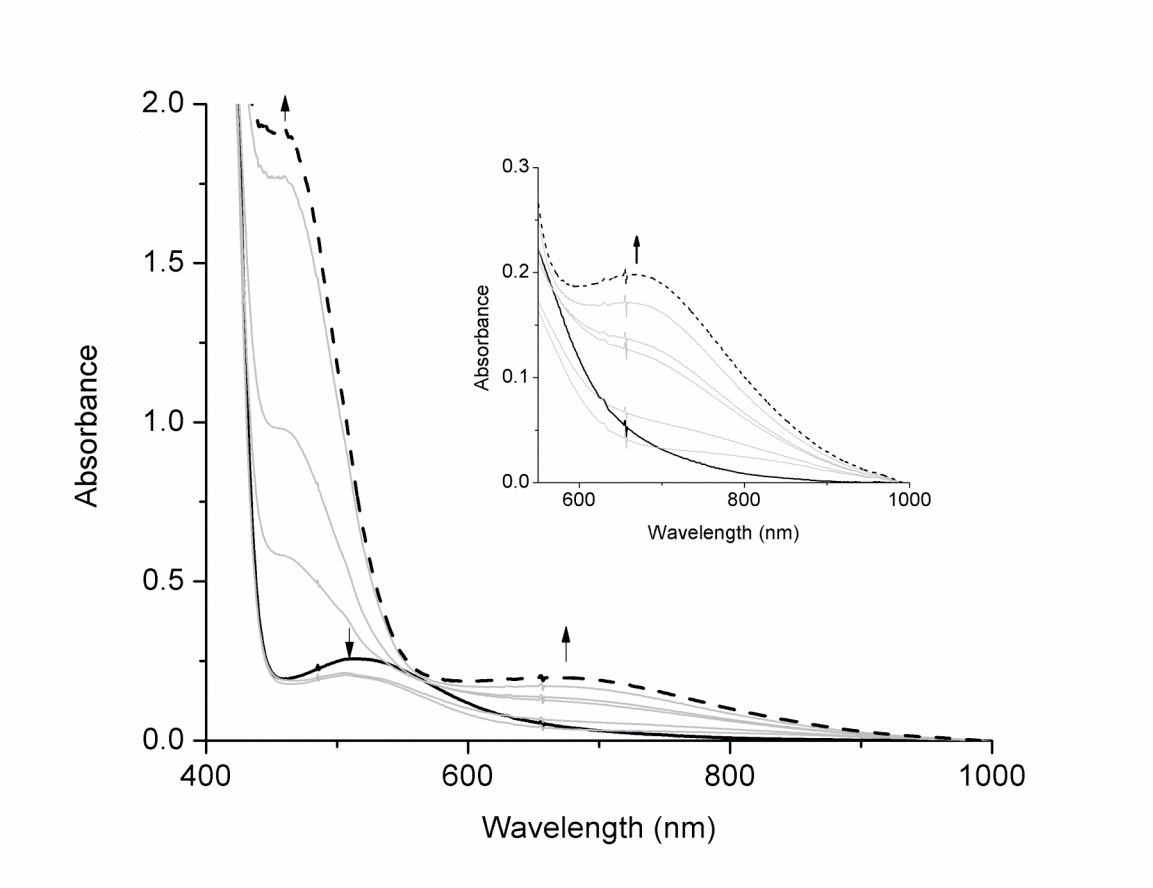

Figure A9. UV-vis spectral change upon addition of 2-methoxybenzoic acid (12 equiv) to a solution of preformed Fe^{III}-OOH (prepared by reacting 3 eq H_2O_2 with 1 mM **2**) at -40 °C. Addition of 2-methoxybenzoic acid led to the formation of a band around 460 nm and 650 nm. Inset is the blow up of 650 nm region of the spectra. The black spectrum was collected immediately after mixing. The gray spectra, in ascending order, were taken at 8, 9, 19, 25, and 33 minutes. The final dashed black spectrum was taken at 45 minutes.

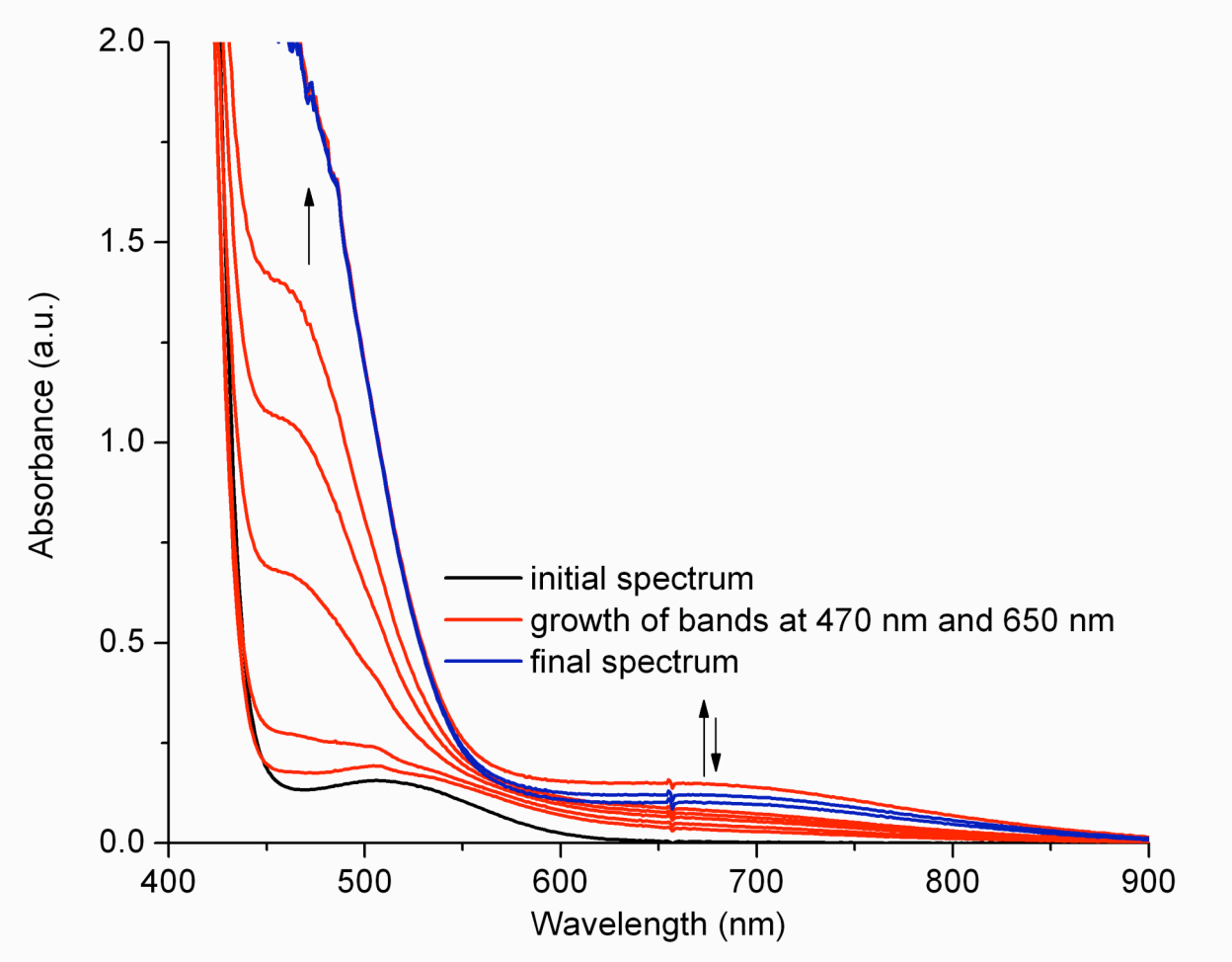

Figure A10. UV-Vis spectral change upon addition of H_2O_2 (3 equiv) to **2**/2-methoxybenzoic acid solution (1 mM in **2**, 12 equiv 2-methoxybenzoic acid vs **2**) at -40 °C. Addition of hydrogen peroxide led to the formation of a band around 470 nm and 650 nm. Inset is the blow up of 650 nm region of the spectra. The black spectrum was recorded immediately after mixing. The red spectra in ascending order were taken at 6, 11, 18, 24, 29, 54 minutes. The final two blue spectra were taken at 65 and 72 minutes.

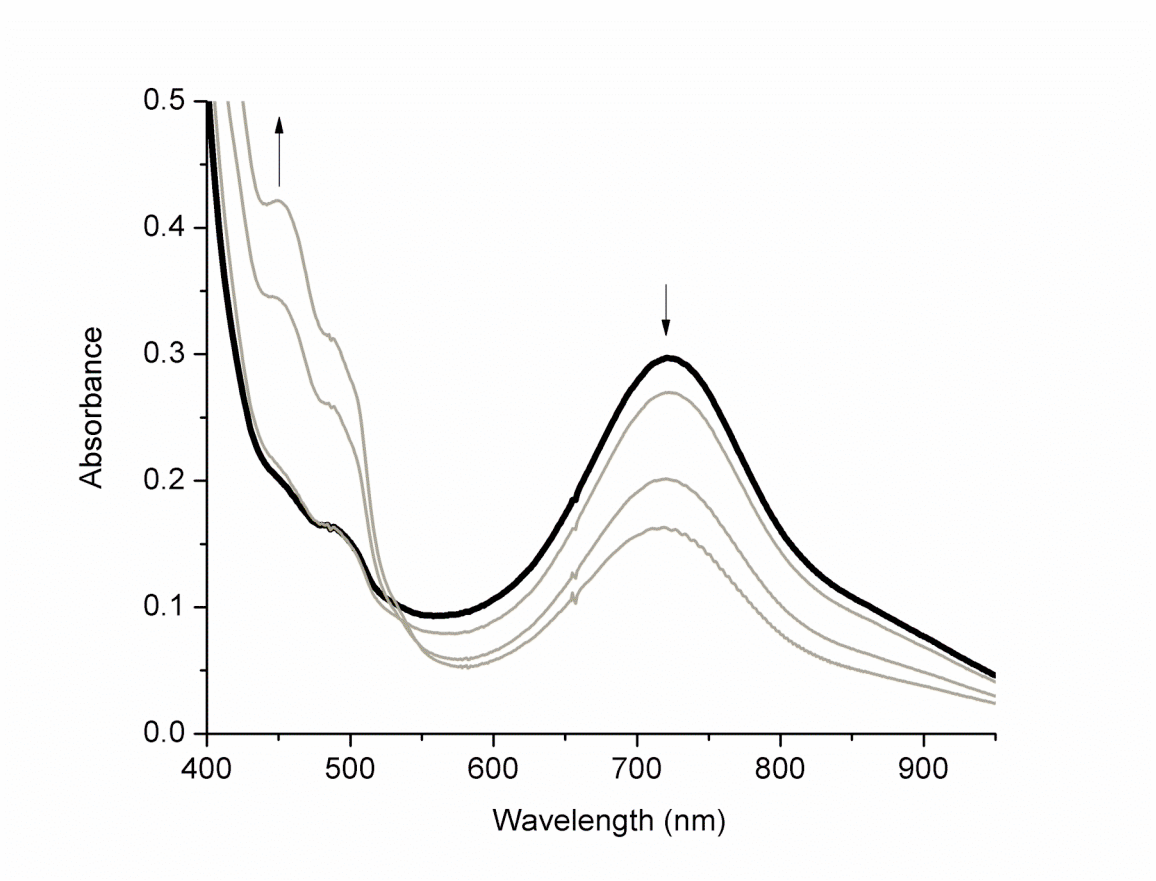

Figure A11. UV-vis spectral changes indicating the decay of Fe^{IV}=O (bold solid line) upon addition of 3-methoxybenzoic acid to pre-formed (TPA)Fe^{IV}=O (1 mM in CH_3CN), which was generated at 0 °C after addition of 1 eq of CH_3CO_3H to **2** (**2**:CH_3CO_3H:3-methoxybenzoic acid = 1:1:12). The other three spectra (from top to bottom) were taken after 2, 40 and 99 minutes of reaction, respectively.

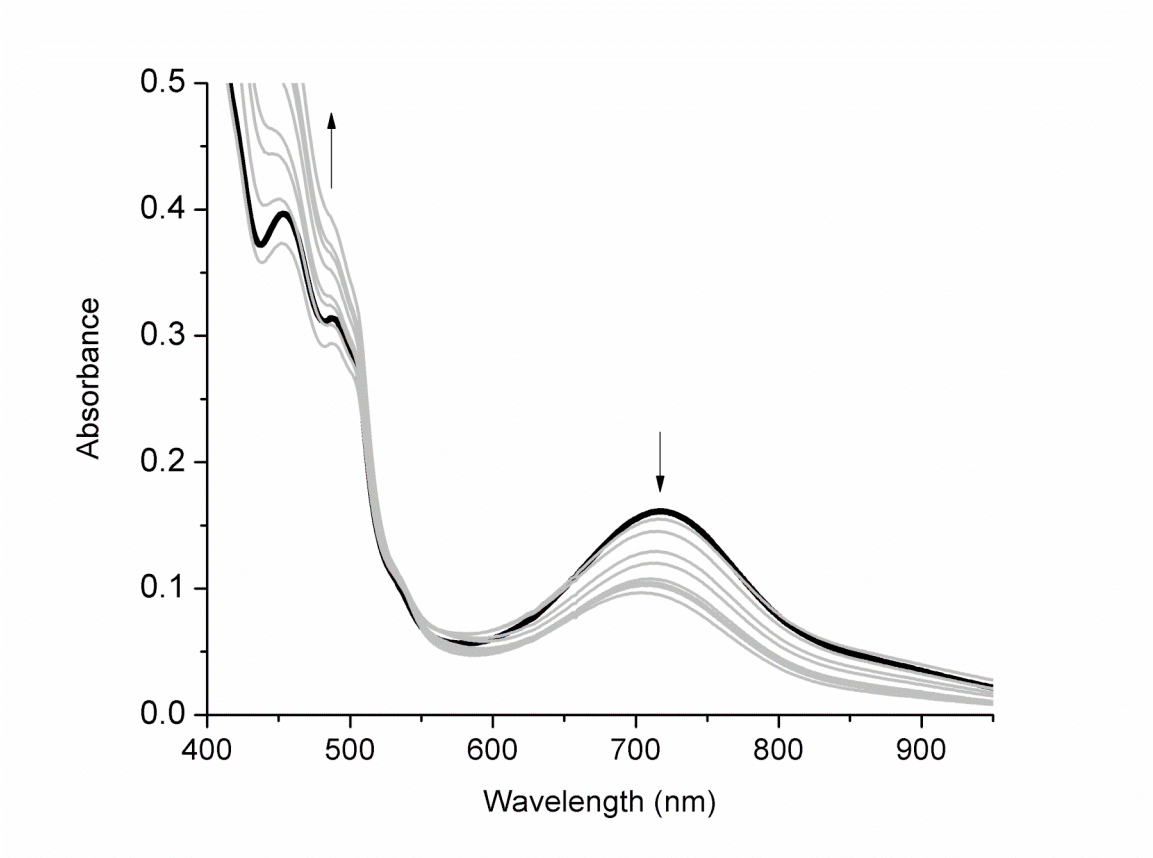

Figure A12. UV-vis spectral changes indicating the decay of Fe^{IV}=O (bold solid line) upon addition of 2-methoxybenzoic acid to pre-formed (TPA)Fe^{IV}=O (1 mM in CH_3CN), which was generated at 0 °C after addition of 1 eq of CH_3CO_3H to **2** (**2**:CH_3CO_3H:2-methoxybenzoic acid = 1:1:12). (TPA)Fe^{IV}=O (black spectrum) is almost instantly recorded after addition of CH_3CO_3H to the solution of **2**. The other spectra (from top to bottom) are taken at 1.2, 1.3, 1.5, 1.7, 3.1, 4.7, 6, and 13 minutes, respectively.

8 Appendix B (Chapter 2)

Yield of hydroxylated products as a function of H_2O_2 added. Mixture of **1** with benzene in CH_3CN was prepared in a glove box ([**1**] = 1 mM, 300 equiv of benzene, 0.5 mL of **1**/benzene in each sample). Variable amounts of hydrogen peroxide (1.5, 3, 10, 20, 40 equiv vs. **1** in 0.5 mL) were delivered all at once at room temperature and the resulting solution was stirred for 30 min for reaction to complete. Reaction mixtures were subjected to acetylation followed by extraction with dichloromethane; yield of hydroxylated product was determined using GCMS.

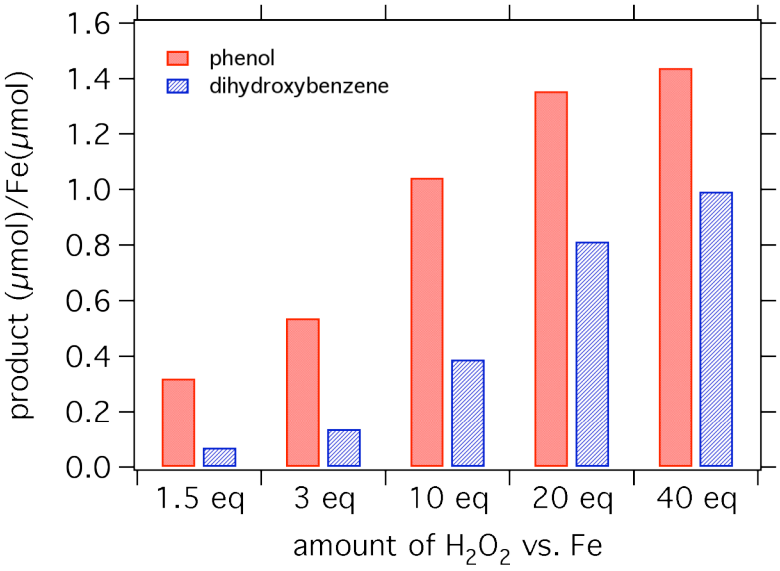

Figure B1. Yield of benzene hydroxylation products (TON versus iron) as a function of H_2O_2 added.

Optimal reaction time. H_2O_2 (10 mM, 2.5 mL) was delivered all at once at room temperature to a solution (2.5 mL in a vial with septum) of **1** with benzene in CH_3CN prepared in a glove box ([**1**] = 1 mM, 300 equiv of benzene). Hydroxylation reaction was quenched at different reaction times by adding 1-methylimidazole and acetic anhydride to aliquots (0.5 mL) of the reaction mixture. In 30 min after last aliquot was taken, organic products were extracted with CH_2Cl_2 and yields were determined by GCMS (see experimental section).

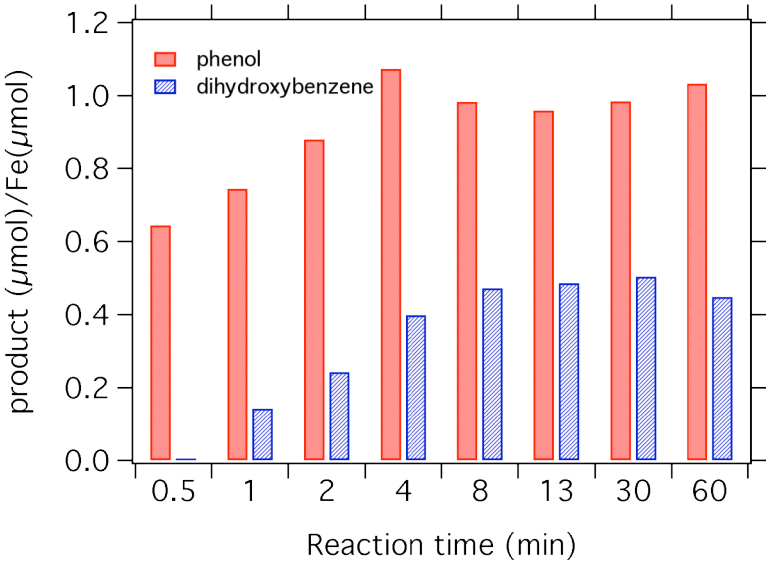

Figure B2. Yield of phenol and dihydroxybenzene as a function of the reaction time.

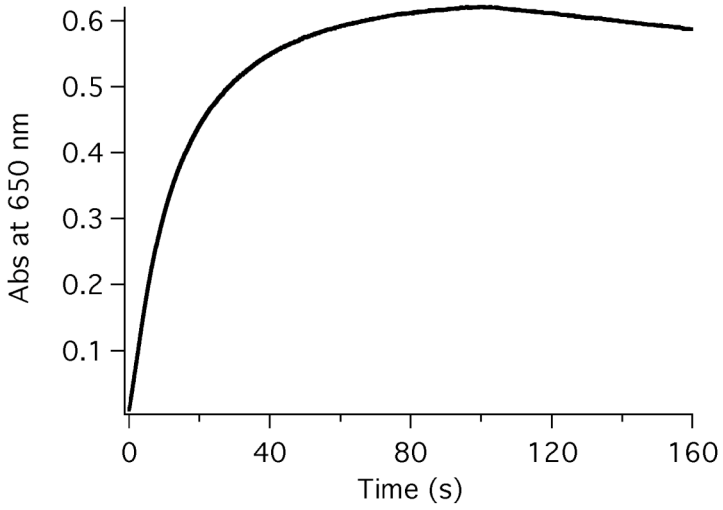

Figure B3. Kinetic trace acquired in the stopped-flow diode array mode for benzene hydroxylation reaction with H_2O_2 in the presence of **1** ([**1**] = 0.5 mM, [H_2O_2] = 5 mM 300 equiv benzene vs. **1**, reaction run in acetonitrile at 20 ˚C). A_{max}=0.62 which corresponds to 88 % yield of phenol (amount of phenol*100%/amount of iron). Amount of phenol calculated using ε = 1400 M^{-1} cm^{-1}, ε was taken from ref. [1]. The referenced work was done in water, therefore extinction coefficient may be different.

Table B1. Hydroxylation yields for substituted benzenes.[a]

Substituted benzene	TON	phenols		
		ortho	*meta*	*para*
m-xylene	0.93			
toluene	2.8 (*o,m,p*); 1.7*(*o,m,p*)	35	-	18
ethylbenzene	0.62; **2.46**	42	24	34
	0.58[d]	50	18	32
benzene	1.0*[b]	-	-	-
fluorobenzene	1.4	50	14	36
chlorobenzene	1.66	52	16	32
	0.92*[c]	56	13	31
bromobenzene	1.26	51	17	32
benzonitrile	1.80	50	34	16
acetophenone	2.24	46	25	28
nitrobenzene	0.2[b]			
Fenton/toluene[e], [86]	0.05	40	23	37
Fenton/chlorobenzene[e], [86]	0.1	53	12	36

Experimental conditions: [a] **1** (7 mM), 40 % benzene, 20 equiv H_2O_2 vs. iron, added dropwise; [b] **1** (0.5 mM), benzene (300 equiv), H_2O_2 (10 equiv vs. iron); [c] **1** (2 mM), chlorobenzene (280 equiv), H_2O_2 (3 equiv vs. iron), for chlorobenzene ratio of products remains the same as concentration of hydrogen peroxide changes; [d] **1** (5 mM), ethylbenzene (150 equiv), H_2O_2 (3 equiv vs. **1**); [e] Fe^{3+} (50 mM), substrate (10 equiv vs. iron), H_2O_2 (1 equiv vs. iron) in acetonitrile.

*calibrated yield; product of aliphatic chain oxidation is in bold.

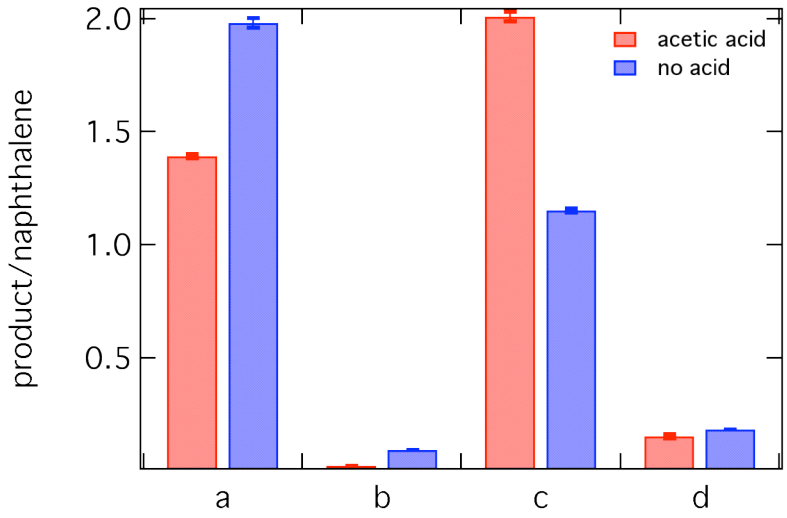

Figure B4. Relative distribution of hydroxylation products for reaction carried out with or without acetic acid; a) oxidation of CH_2, b) oxidation of CH_3, c) aromatic hydroxylation, d) product of radical coupling. Mixture of **1** (5 mM) with ethylbenzene (150 equiv vs. **1**) in acetonitrile was prepared in the glove box, acetic acid (2 equiv) was added immediately prior to addition of H_2O_2 (3 equiv) at room temperature. In 20 min the reaction was quenched by 1-methylimidazole followed by acetylation work up (see experimental section).

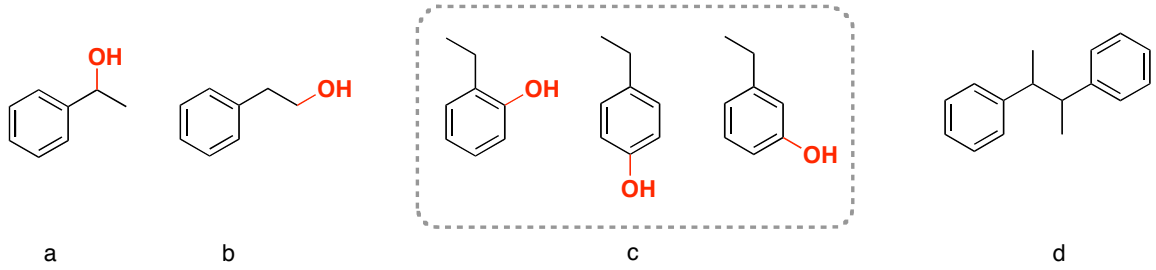

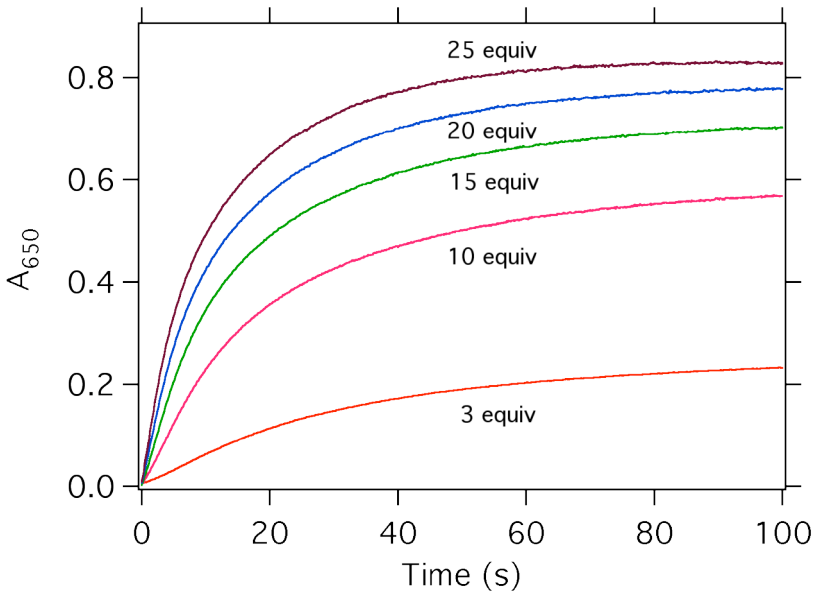

Figure B5. Kinetic traces acquired in stopped-flow showing dependence of phenolate yield on H_2O_2 concentration. Experiment was performed in a single mixing mode in the stopped-flow: **1** (0.5 mM) was mixed with benzene (300 equiv) and variable amounts of hydrogen peroxide in acetonitrile at 20 ˚C.

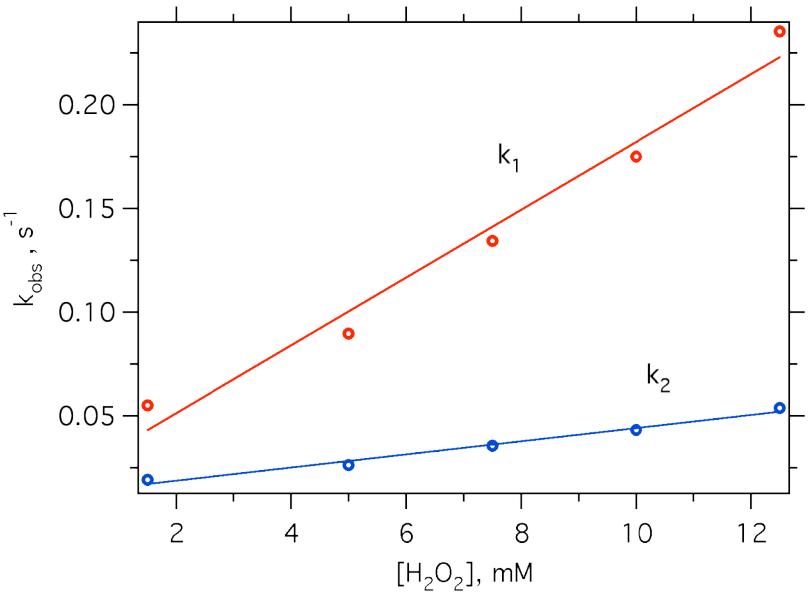

Figure B6. Benzene hydroxylation rates; all kinetic traces at 650 nm were fitted with a double-exponential fit. **1** (0.5 mM) was mixed with H_2O_2/benzene (300 equiv benzene vs. iron) in acetonitrile at 20 ˚C in the stopped-flow.

Table B2. Rate constants of chlorobenzene hydroxylation by hydrogen peroxide in the presence of 1*. Spectral data were fitted in SPECFIT using the A→B→C reaction model.

Chlorobenzene, equiv vs. **1**	k_{1obs}, s^{-1}	k_{2obs}, s^{-1}
50	0.1104	0.0546
100	0.1073	0.0548
150	0.1109±0.0089	0.0561±0.0035
200	0.1213±0.0050	0.0509±0.0012
250	0.1149±0.0014	0.0517±0.0006
560	0.1325±0.0073	0.0495±0.0006
1000	0.1296±0.0051	0.0509±0.0005

Reaction conditions: **1** (1 mM) was mixed with valiable amounts of chlorobenzene in the glove box, hydroxylation reaction was carried out by adding H_2O_2 (3 mM) at 20 °C in acetonitrile. k_{1obs} is the rate of Fe^{III}(OOH) formation, k_{2obs} is the rate of hydroxylation. Each constant represents an average of three trials.

SPECFIT generated constant of Fe^{III}OOH formation (A→B) was additionally confirmed by fitting kinetic trace of the reaction of **1** (1 mM) and hydrogen peroxide (3 mM) at 560 nm. The rate constant was the same (~0.12 s^{-1}).

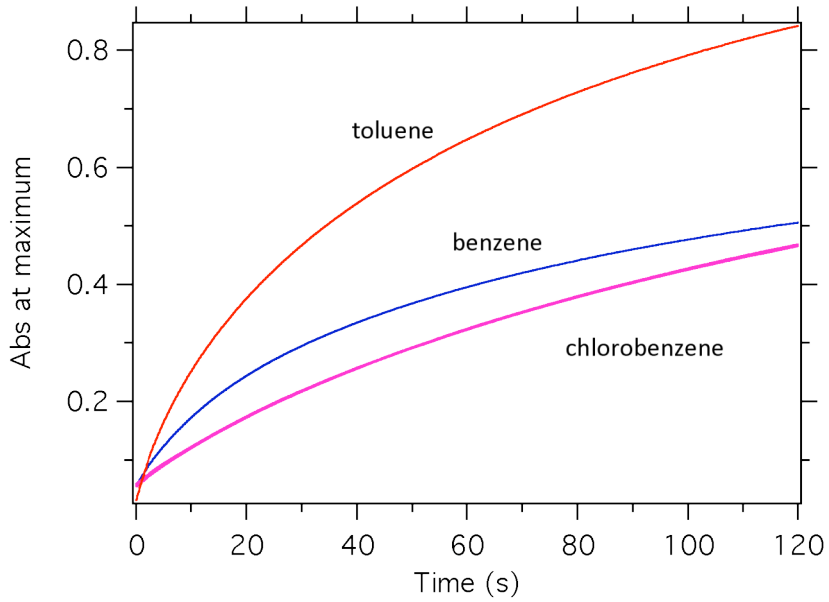

Figure B7**.** Kinetic traces acquired using stopped flow for the reaction of **1a** with benzene, chlorobenzene and toluene ([**1**] = 0.5 mM, [H_2O_2] = 5 mM, 300 equiv of substrate in acetonitrile, 20 ˚C). Spectral data were fitted in IgorPro using A→B→C reaction model.

Table B3. Observed rate constants for hydroxylation with **1** (reaction conditions described above). Constants were determined in IgorPro using a two exponential model.

Substrate	k_{1obs}, s^{-1}	k_{2obs}, s^{-1}
benzene	0.0810	0.0115
chlorobenzene	0.0609	0.0080
toluene	0.0970	0.0133

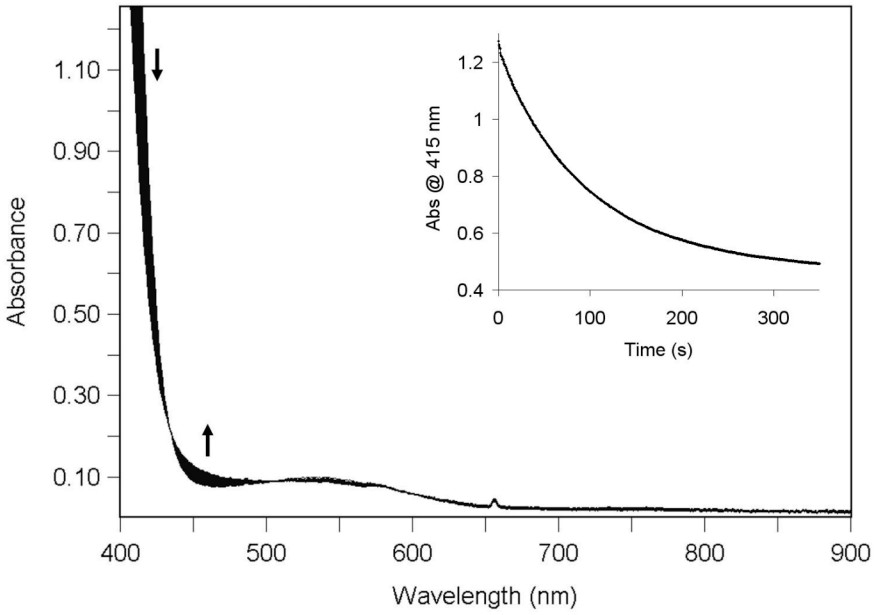

Figure B8. Time resolved UV-vis spectra acquired in the diode array mode using stopped-flow. Fe^{III}(OOH) was generated at -30 °C by mixing **1** and H_2O_2 ([**1**]=1 mM, [H_2O_2]=10 mM).

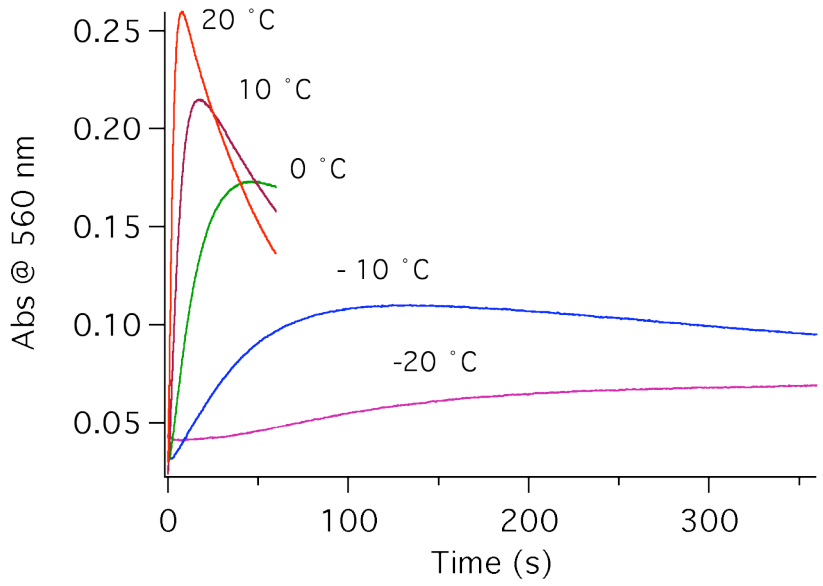

Figure B9. Kinetic traces at 560 nm acquired using stopped-flow for the reaction of **1** with hydrogen peroxide ([**1**] = 1 mM, $[H_2O_2]$ = 10 mM) at different temperatures.

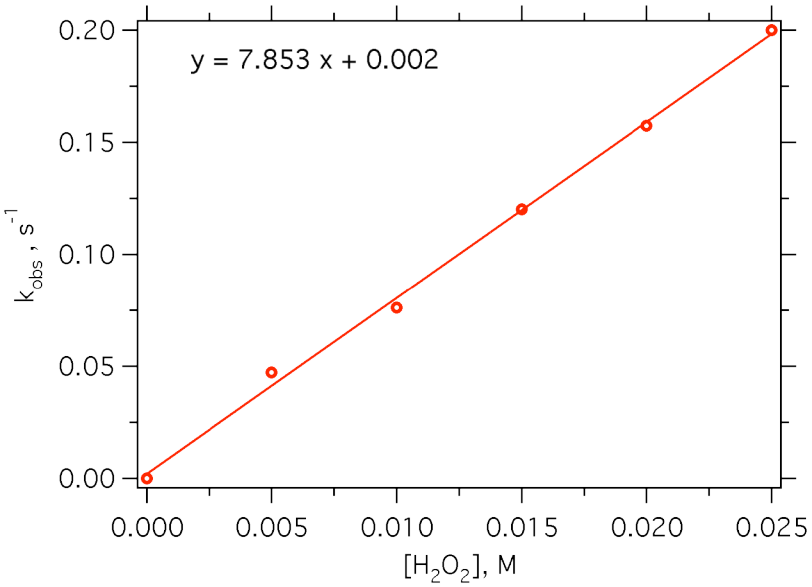

Figure B10. Plot of the observed rate constants versus H_2O_2 concentration for $Fe^{III}(OOH)$ formation in a reaction between **1** and H_2O_2 at 0 ˚C. Data were acquired in the stopped-flow diode array mode and kinetic traces at 560 nm were fitted in Kinetic Studio using single-exponential model.

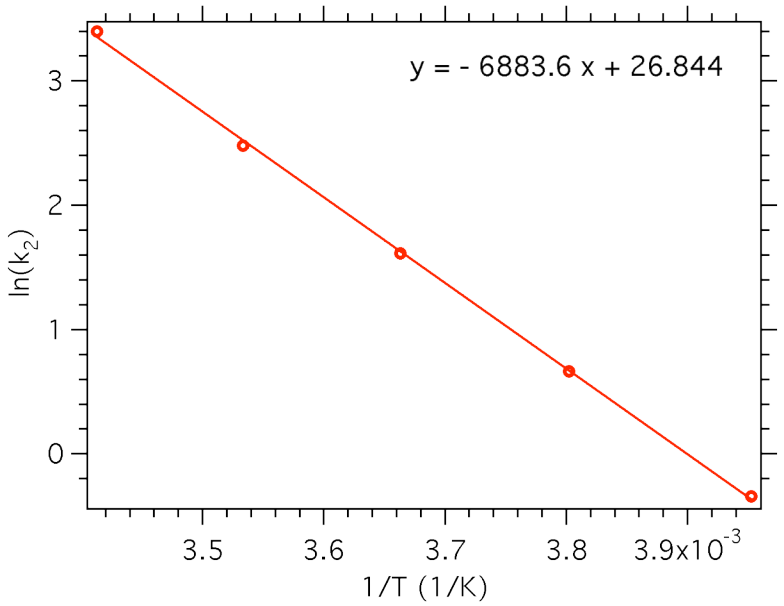

Figure B11. Arrhenius plot for the $Fe^{III}(OOH)$ formation in a reaction between **1** and H_2O_2; $k_2 = k_{obs}/[H_2O_2]$ ($[H_2O_2]$ =0.01 M after mixing in the stopped flow).

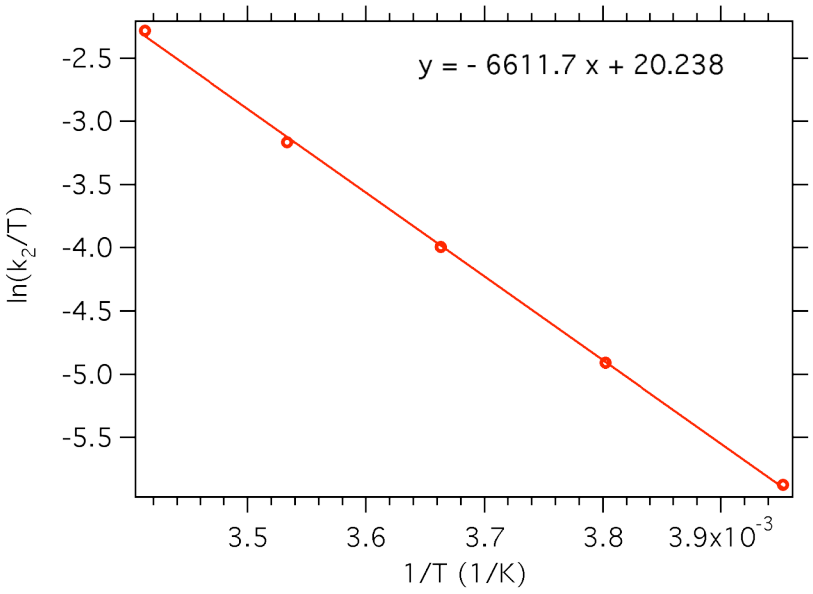

Figure B12. Eyring plot for the $Fe^{III}(OOH)$ formation in a reaction between **1** and H_2O_2; $k_2 = k_{obs}/[H_2O_2]$ ($[H_2O_2]$ =0.01 M after mixing in the stopped flow).

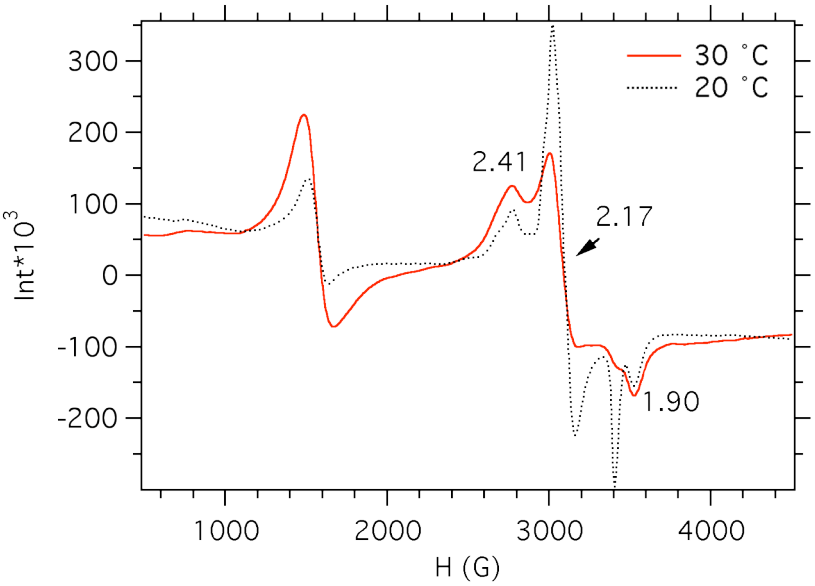

Figure B13. EPR spectra of iron(III) species obtained upon mixing **1** with H_2O_2 at room temperature (dotted line, reaction time 10 s) and at -30 ˚ C (solid line, 5 min). Reaction conditions: [**1**] = 1.5 mM, [H_2O_2] = 15 mM.

Table B4. EPR g_{max}, g_{inter}, g_{min} values for $LFe^{III}(OOH)$ and low-spin LFe^{III} complexes.

Complex	g_{max}	g_{inter}	g_{min}	Ref.
$(BPMEN)Fe^{III}OOH$	2.21	2.14	1.96	this work
$(BPMEN)Fe^{III}$	2.41	2.17	1.90	this work
$L^2Fe^{III}OOH$	2.19	2.12	1.95	[2]
$L^2Fe^{III}X$*	2.30	2.12	1.92	[2]
$(bztpen)Fe^{III}OOH$	2.20	2.16	1.96	[3]
$(bztpen)Fe^{III}X$	2.32	2.14	1.93	[3]
$(PMA)Fe^{III}OOH$	2.21	2.18	1.93	[4]
$(PMA)Fe^{III}Ome$	2.28	2.18	1.93	[4]

* X = Cl, Br, OH, MeO, H_2O or MeOH

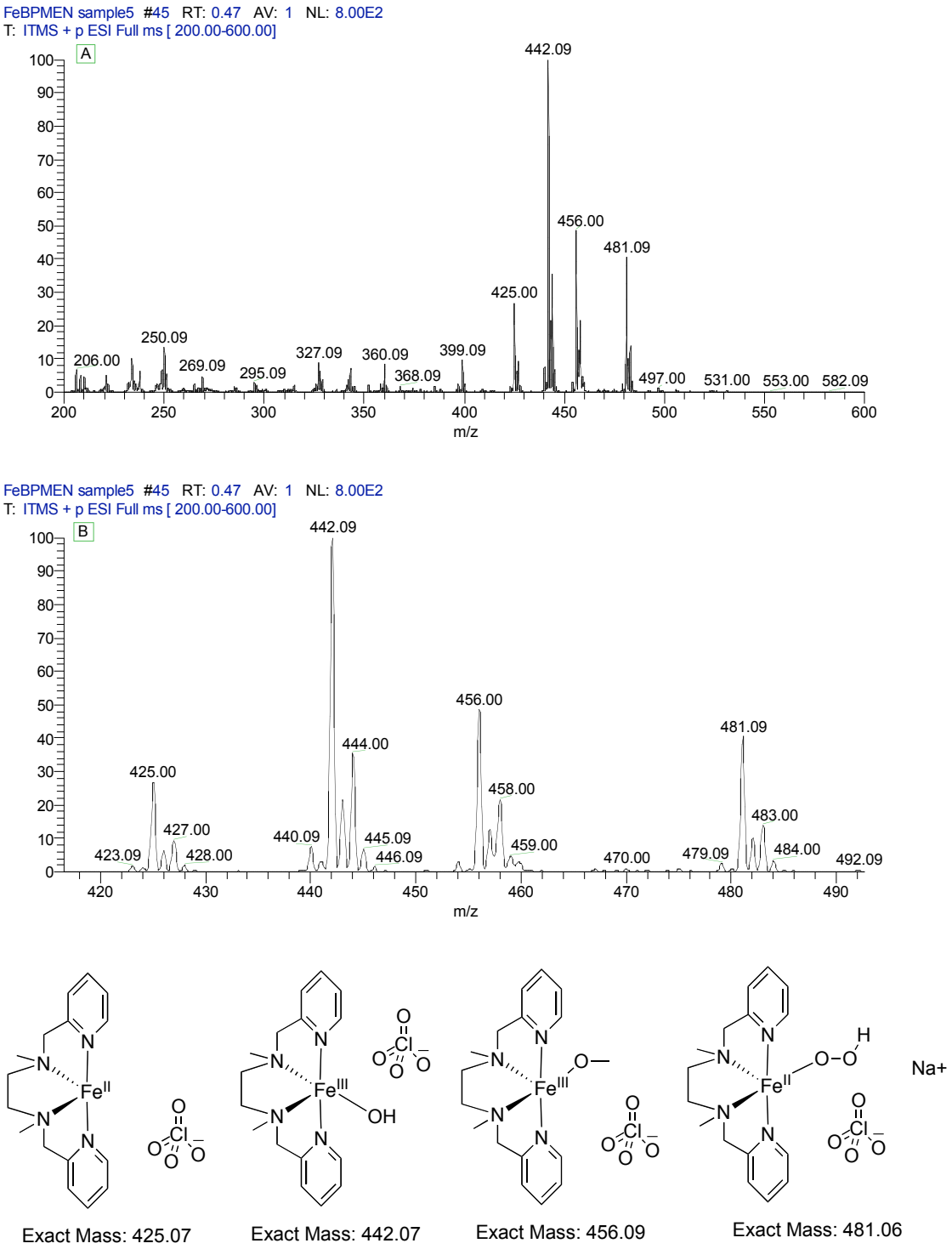

Figure B14. ESI-MS spectrum (A – full spectrum , B- zoomed in region for m/z of 420-490) of the reaction mixture of **1** (1.5 mM) mixed with H_2O_2 (15 mM) at room temperature; peaks at m/z = 425, 442, 456, 481 correspond to $[Fe(BPMEN)](ClO_4)^+$, $[Fe(BPMEN)(OH)](ClO_4)^+$, $[Fe(BPMEN)(OMe)](ClO_4)^+$, $[Fe(BPMEN)(OOH)]Na(ClO_4)^+$ respectively.

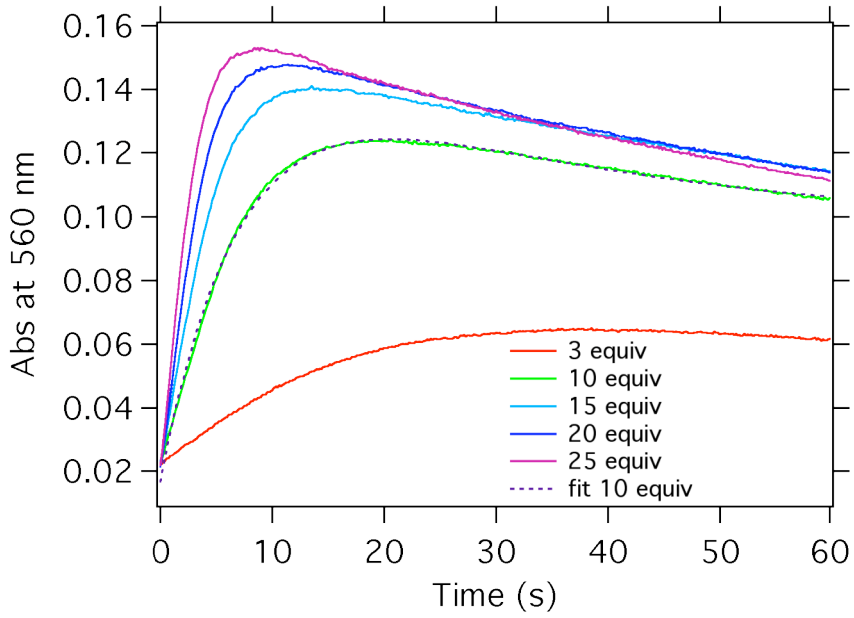

Figure B15. Spectrophotometric yield of $Fe^{III}(OOH)$ depends on [H_2O_2]. **1** (0.5 mM) was mixed with H_2O_2 (variable amounts, 3-25 equiv vs. **1**) in acetonitrile at 20 ˚C.

Table B5. Rate constants of benzene hydroxylation by hydrogen peroxide in the presence of **1**. Spectral data were fitted in kinetic Studio using A→B reaction model.

Benzene, equiv vs. **1**	k_{obs}, s^{-1}
100	0.0270±0.0014
200	0.0278±0.0007
400	0.0289±0.0013
600	0.0278±0.0008

Fe^{III}(OOH) was pre-generated by mixing **1** and H_2O_2 at 20 °C in acetonitrile ([**1**] = 0.5 mM, [H_2O_2] = 5 mM) and then reacted with variable amounts of benzene. Each constant represents an average of at least three trials.

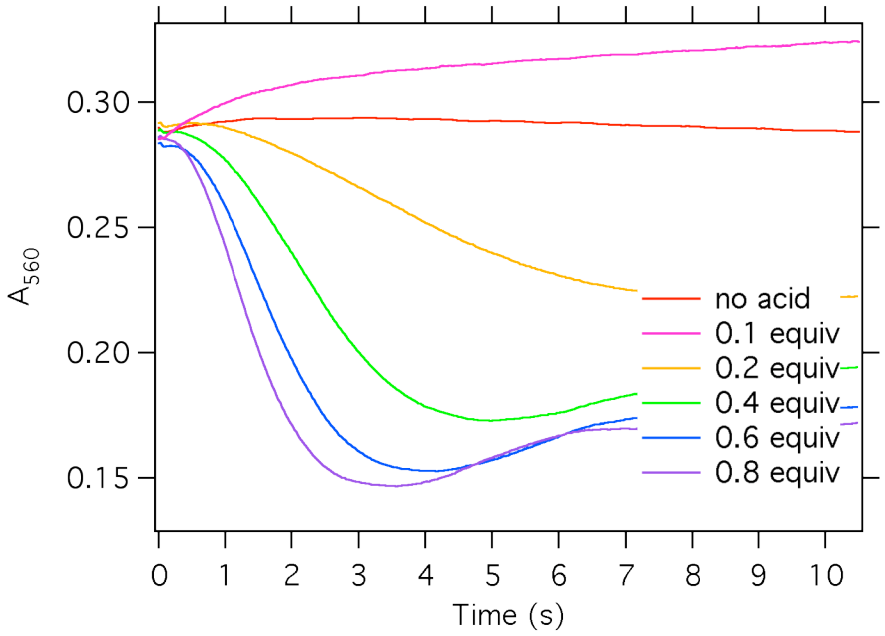

Figure B16**.** Kinetic traces at 560 nm acquired using stopped flow for the reaction of Fe^{III}(OOH) with variable amounts of acetic acid (0.1 – 1 equiv vs. iron) at 10 ˚C in acetonitrile. Fe^{III}(OOH) was pre-generated by mixing **1** (2 mM after mixing) and H_2O_2 (20 mM after mixing), acetic acid was added at the maximal formation of Fe^{III}(OOH) (age time 7 s).

The rate of Fe^{III}(OOH) decay is proportional to the amount of acetic acid added. The observed increase in absorbance at 560 nm upon addition of 0.1 equiv of acetic acid can be explained by change in the spectroscopic signature of Fe^{III}(OOH), upon coordination of acetate.[5] Such small amount of acid does not affect the rate of decay significantly.

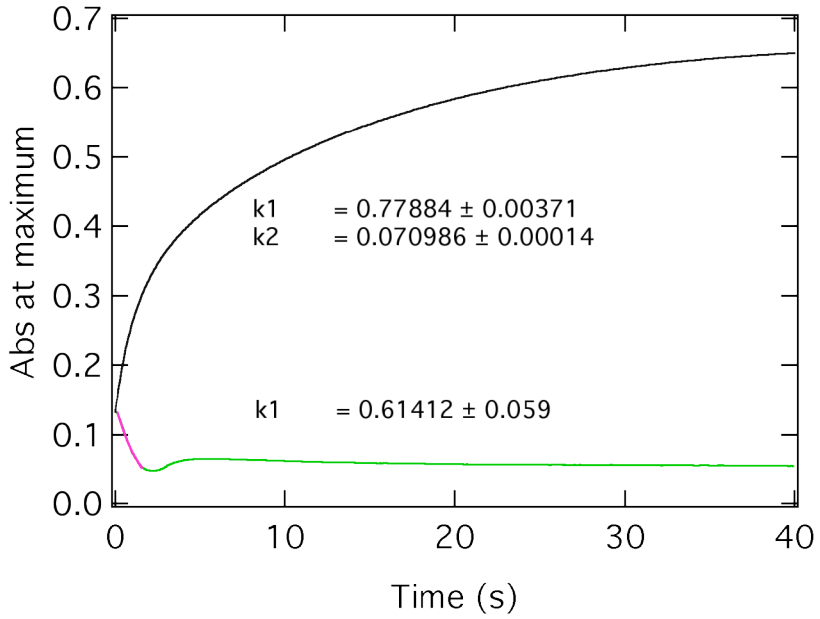

Figure B17. Kinetic traces at 560 nm (decay) and 650 nm (growth) acquired using stopped flow for the reaction of $Fe^{III}(OOH)$ with acetic acid (green trace, [**1**] = 0.5 mM, $[H_2O_2]$ = 5 mM, $[CH_3COOH]$ = 0.5 mM) and $Fe^{III}(OOH)$ with a mixture of acetic acid and benzene (black trace, [**1**] = 0.5 mM, $[H_2O_2]$ = 5 mM, $[CH_3COOH]$ = 0.5 mM, 560 equiv of benzene vs. **1**) in acetonitrile at 20 ˚C. Kinetic trace with acetic acid and benzene was fitted with two exponential fit and corresponding rate constants are shown as k_1 and k_2 on the graph; initial process of kinetic trace with acetic acid only was fitted with a single exponential fit (shown in purple).

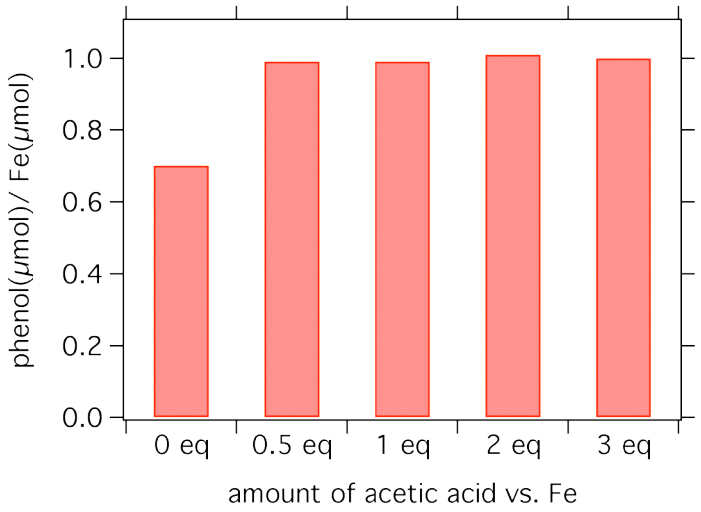

Figure B18. Acetic acid slightly increases yield of phenol. Mixture of **1** (2 mM) with benzene (280 equiv vs. iron) and variable amounts of acetic acid in acetonitrile was prepared in the glove box, H_2O_2 (3 equiv vs. **1**) was injected drop wise at room temperature.

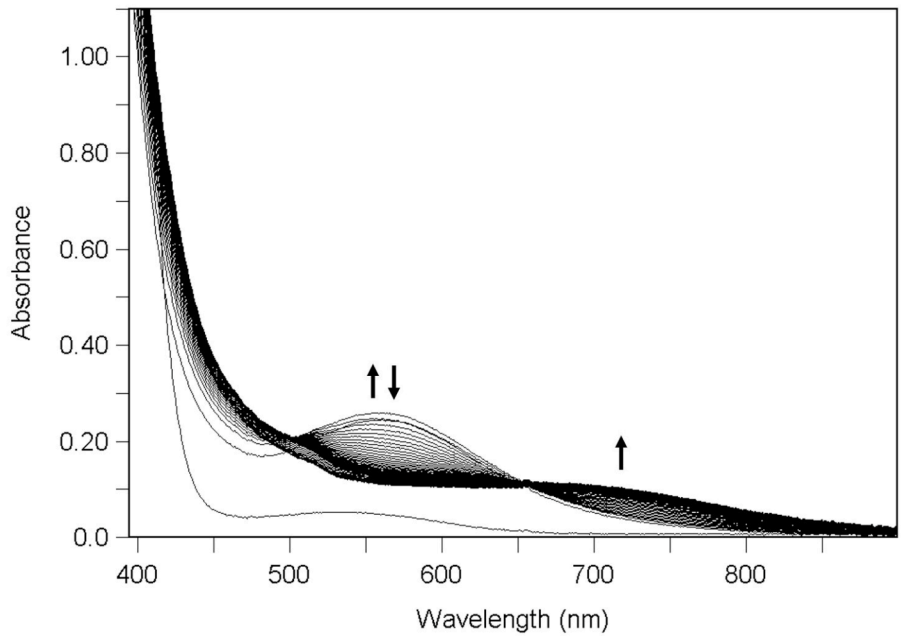

Figure B19**.** Time resolved UV-vis spectra acquired in the diode array mode using stopped-flow. $Fe^{III}(OOH)$ was generated in 10 s at 20 °C by mixing **1** (1 mM) and H_2O_2 (10 mM) and slowly decayed into species **1c** (Fe^{IV}=O).

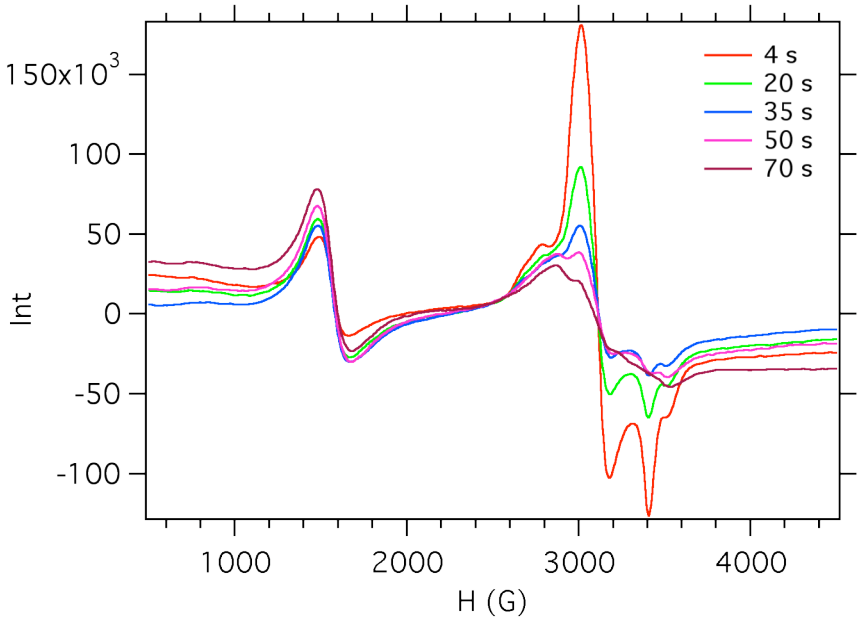

Figure B20. Decay of (BPMEN)Fe^{III}(OOH) at room temperature in acetonitrile. (BPMEN)Fe^{III}(OOH) was generated by mixing **1** (2 mM, 0.2 mL) and H_2O_2 (20 mM, 0.2 mL) directly in EPR tube at room temperature and incubated for different amounts of time (4s, 20s, 35s, 50s, 70s).

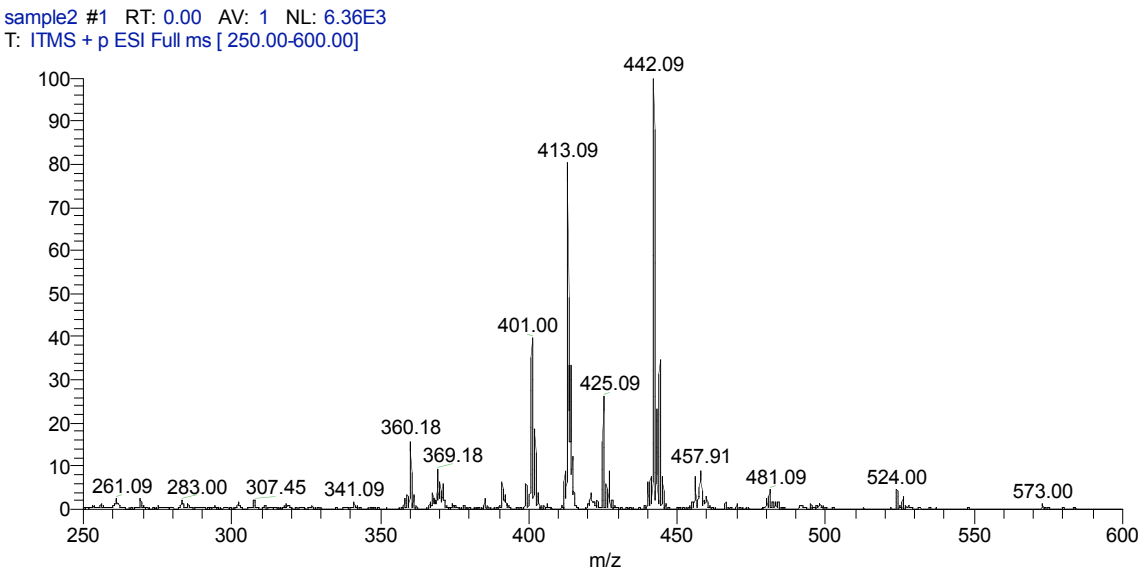

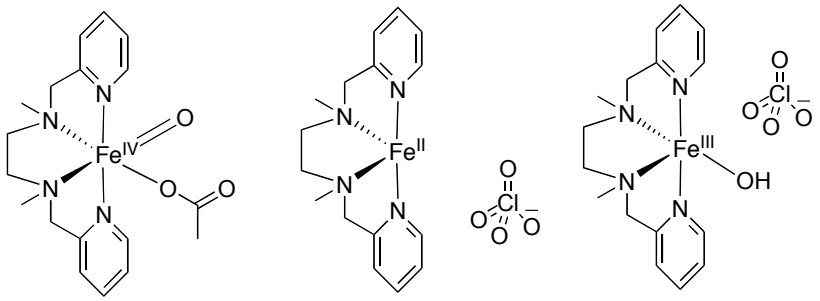

Figure B21. ESI-MS spectrum of the solution: **1** (1.5 mM) + H_2O_2 (15 mM) and acetic acid (1.5 mM) at room temperature; peaks at m/z = 401, 425, 442 correspond to $[Fe(BPMEN)(O)](OAc)^+$, $[Fe(BPMEN)](ClO_4)^+$, $[Fe(BPMEN)(OH)](ClO_4)^+$ respectively.

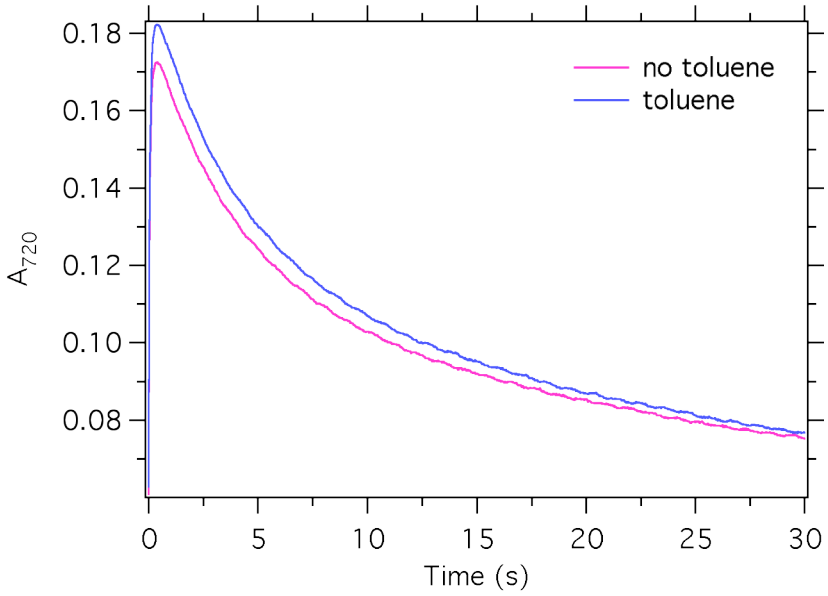

Figure B22. Kinetic traces at 720 nm acquired using stopped-flow for the reaction of **1** with IBX ester show fast accumulation of Fe^{IV}=O and its decay in the presence of toluene and without toluene ([**1**] = 0.5 mM, [IBX-ester] = 2 mM, 150 equiv of toluene in acetonitrile, 20 ˚C).

Table B6. Deterium retention in a competitive isotope effect experiment.

Chlorobenzene substrate	Deuterium retention in chlorophenol products, %*		
	ortho	*meta*	*para*
$^{2}H_0$/3,5-$^{2}H_2$	97.0 (0.5)	11.9 (2.4)	93.6 (0.9)
$^{2}H_0$/2,4,6-$^{2}H_3$	17.1 (1.1)	93.1 (1.5)	32.7 (1.6)

*Average and standard deviation of at least five independent experiments, each sample was analyzed twice. Substrate composition: $^{2}H_0/^{2}H_x$=1; reaction conditions: [**1**] = 2 mM, 280 equiv of chlorobenzenes, 3 equiv of H_2O_2 vs. **1**, 0 ° C.

Substrate synthesis. *3,5-$^{2}H_2$-chlorobenzene and 2,4,6-$^{2}H_3$-chlorobenzene*. Hydrochloride salts of 4-chloroaniline and 3-chloroaniline were prepared by adding DCl to the corresponding aniline (3 g, 23.6 mmol) in D_2O (99 %, 15 mL). Solutions were refluxed in D_2O for 24 hr.[6] The D_2O was removed in vacuo and the procedure was repeated twice with fresh D_2O (15 mL). After three treatments, the solution was neutralized with $NaHCO_3$ and the product was extracted with ethylacetate. To prepare diazonium salt, deuterated aniline was dissolved in 50% HBF_4 (18 mL) and water (18 mL). Cold aqueous solution of $NaNO_2$ (1.725 g, 25 mmol) was added drop wise at 0 °C. After 30 min, pale green crystals of diazonium salt were filtered using cold glass filter, washed with ice cold 50 % HBF_4 (2.5 mL), methanol (3 mL) and ether (3 mL). The resulting product was suspended in cold dichloromethane (150 mL). H_3PO_2 (12.3 mL, aqueous 50%) and trace amount of Cu_2O was added to the stirred suspension at 0 °C.[7] The mixture was stirred for 30 min the neutralized with saturated aqueous $NaHCO_3$. Purity of product was

determined by GCMS to be 97 % for 3,5-$^{2}H_2$-chlorobenzene (3% of single deuterated chlorobenzene) and 98 % for 2,4,6-$^{2}H_3$-chlorobenzene.

Competition experiment. A mixture of **1** with chlorobenzenes was prepared in a glove box (2 mM vs. **1**, 140 equiv of chlorobenzene and 140 equiv of deuterated chlorobenzene). Ratio of chlorobenzenes was determined by GCMS. 3 equiv of H_2O_2 was added dropwise at 0 °C and the mixture was left to react for 30 min. Products were acetylated and subjected to GCMS analysis.

Calculation of deuterium retention. The amounts of the deuterated substrate and the product of NIH shifts were quantified by integrating the intensity of corresponding ions in the GCMS experiment. The deuterium retention for each chlorophenol isomer (*ortho*, *meta* and *para***)** was calculated using $[\mathbf{M}]^+/([\mathbf{M}]^+ + [\mathbf{M\text{-}1}]^+)$, where $[M]^+$ is the total amount of the NIH shifted product (all deuterium retained), corrected for the isotopic purity of the starting substrate. Isotope distribution of chlorine was taken into account to adjust areas of corresponding deuterated products.

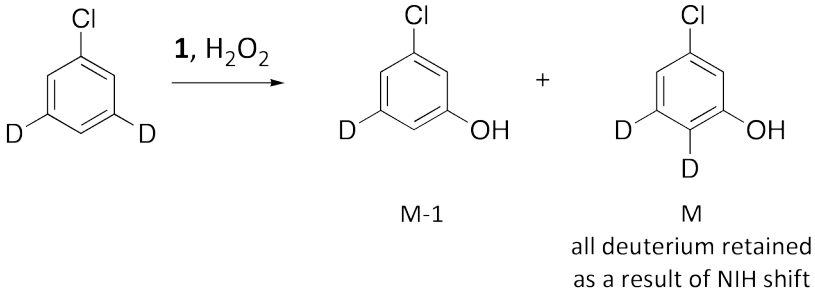

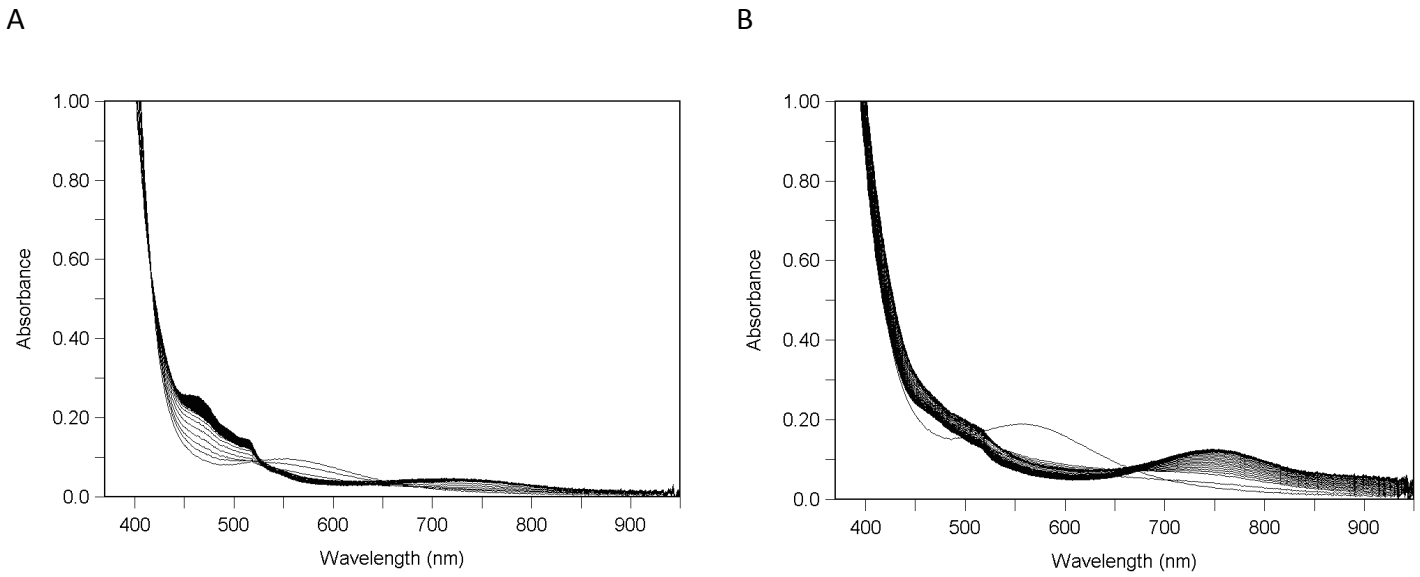

Figure B23. Spectral changes acquired in stopped-flow diode array mode on reaction between pre-generated $Fe^{III}(OOH)$ and acetic acid. (A) Experiment done in double mixing mode: first $Fe^{III}(OOH)$ was generated by mixing solution of **1** (1 mM) and stoichiometric amount of H_2O_2 (1.5 mM) and then 1 equiv of acetic acid was added at the maximum accumulation of $Fe^{III}(OOH)$. Distinct bands at 470 nm and 510 nm and a smaller absorption band at 700 nm indicate formation of $[Fe^{III}_2(\mu\text{-}O)(\mu\text{-}CH_3COO)(BPMEN)_2]$.[8] (B) Alternatively, $Fe^{III}(OOH)$ was generated by mixing **1** (1 mM) and an excess of H_2O_2 (10 mM); subsequent addition of 1 equiv of acetic acid led to formation of Fe^{IV}=O.

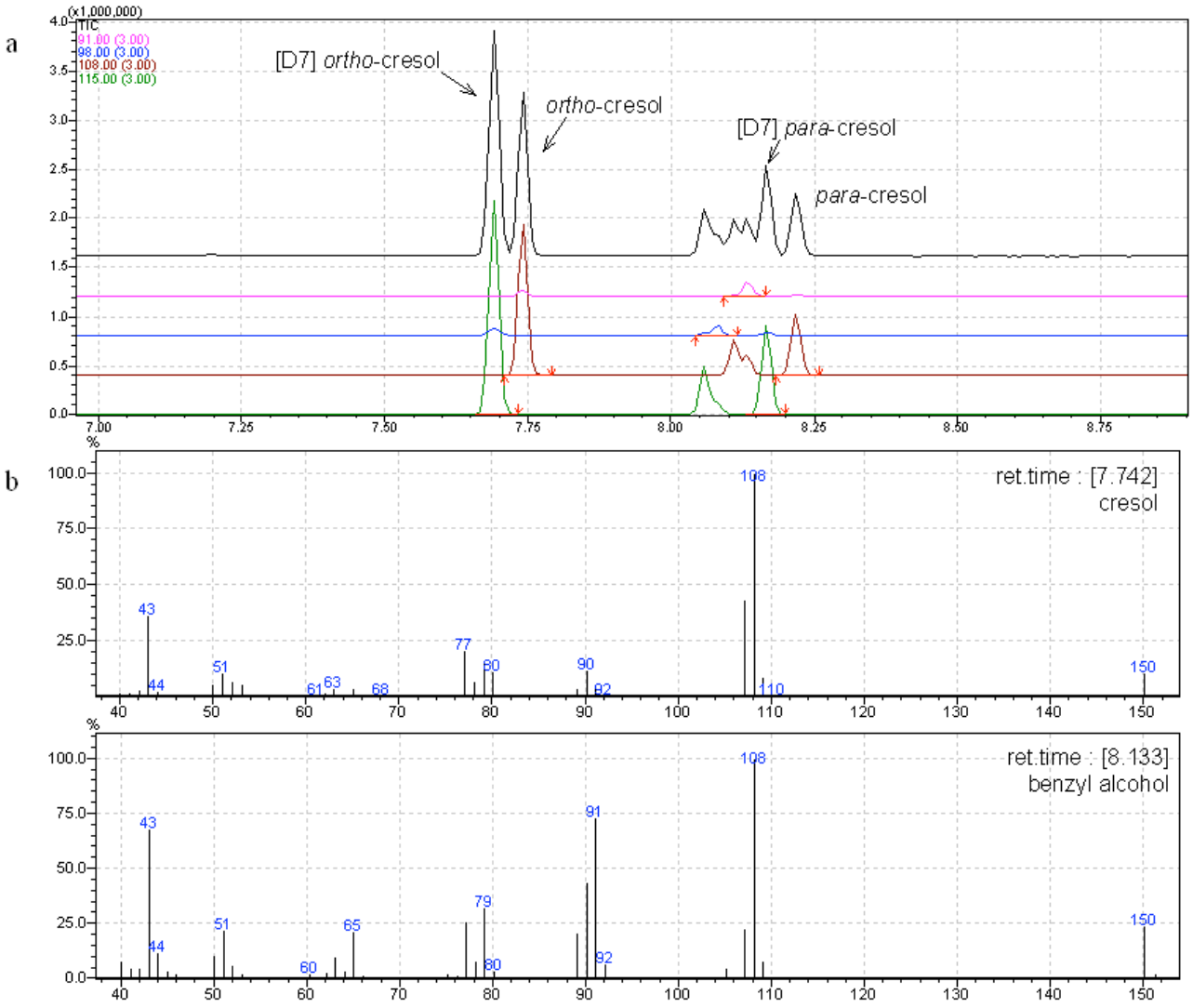

Figure B24. Product analysis by GCMS for hydroxylation of toluene; a) original chromatogram (all ions) and chromatograms based on selected ions that represent cresol (108), [D7]cresol (115), benzyl alcohol (91) and [D7] benzyl alcohol (98); b) mass spectra of cresol and benzyl alcohol show that signal at m/z = 91 is indicative of benzyl alcohol.

8.1 **References:**

[1] W. A. E. McBryde, *Can. J. Chem.* **1968**, *46*, 2385.

[2] B. Bernal, I. M. Jensen, K. B. Jensen, C. J. McKenzie, H. Toftlund, J.-P. Tuchagues, *J. Chem. Soc., Dalton Trans.* **1995**, 3667.

[3] K. B. Jensen, C. J. McKenzie, N. P. Nielsen, J. Z. Pedersen, H. M. Svendsen, *Chem. Commun.* **1999**, 1313.

[4] I. Lippai, R. S. Magliozzo, J. Peisach, *J. Am. Chem. Soc.* **1999**, *121*, 780.

[5] R. Mas-Ballesté, L. Que, Jr., *J. Am. Chem. Soc.* **2007**, *129*, 15964.

[6] G. C. Swain, J. E. Sheats, D. G. Gorenstein, K. G. Harbison, *J. Am. Chem. Soc.* **1975**, *97*, 791.

[7] S. H. Korzeniowski, L. Blum, G. W. Gokel, *J. Org. Chem.* **1977**, *42*, 1469.

[8] R. Hazell, K. B. Jensen, C. J. McKenzie, H. Toflund, *J. Chem. Soc., Dalton Trans.* **1995**,
707

9 Appendix C (chapter 3)

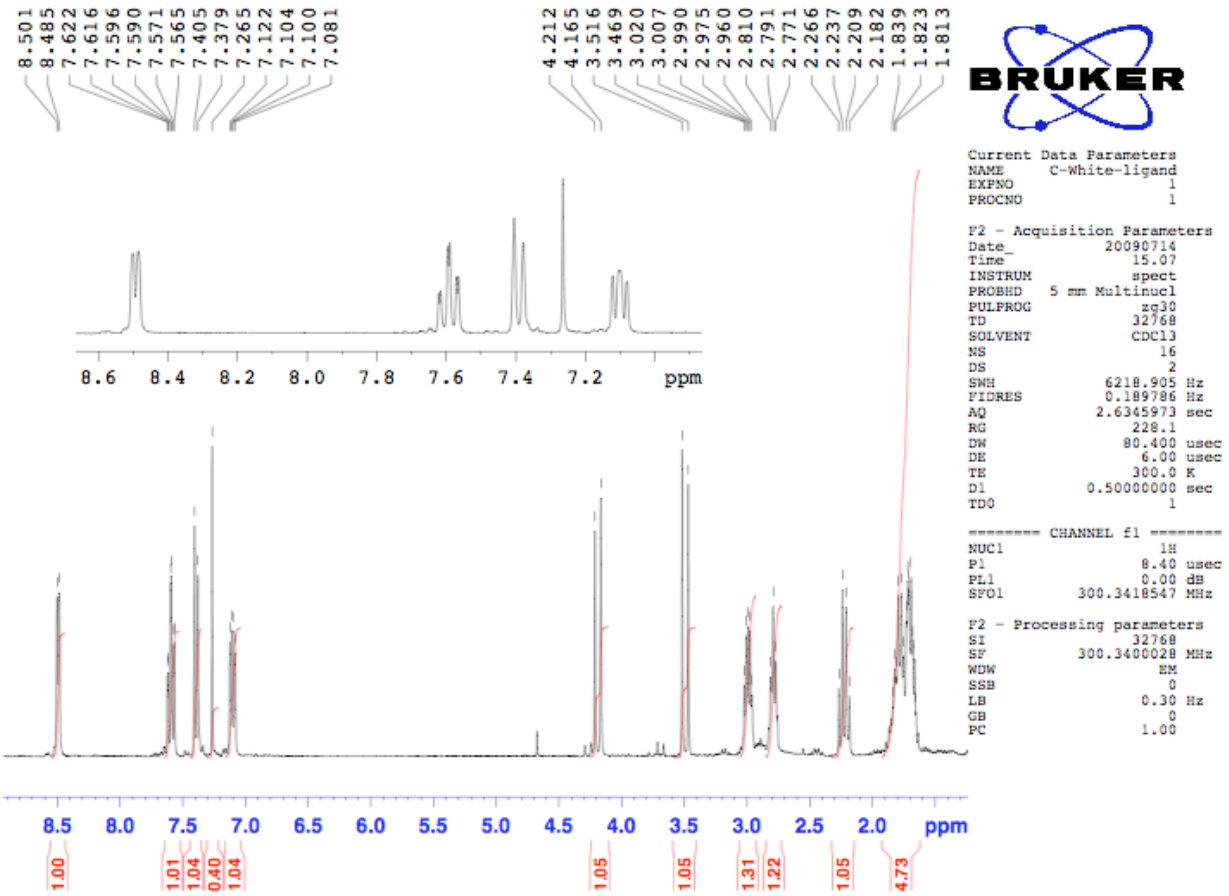

Figure C1. ^{1}H NMR spectrum of BPBP ligand in $CDCl_3$.

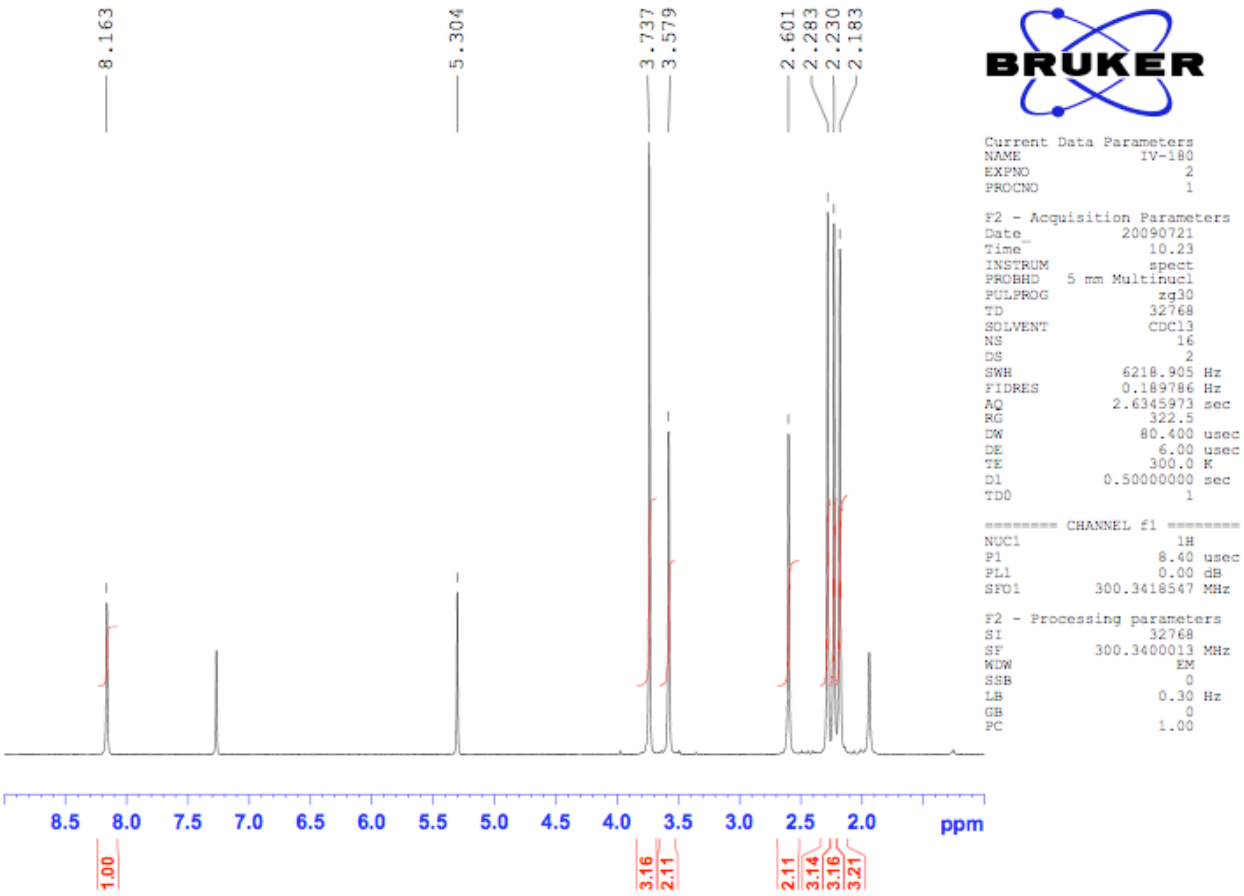

Figure C2. ^{1}H NMR spectrum of purified SR-BPMEN ligand in $CDCl_3$.

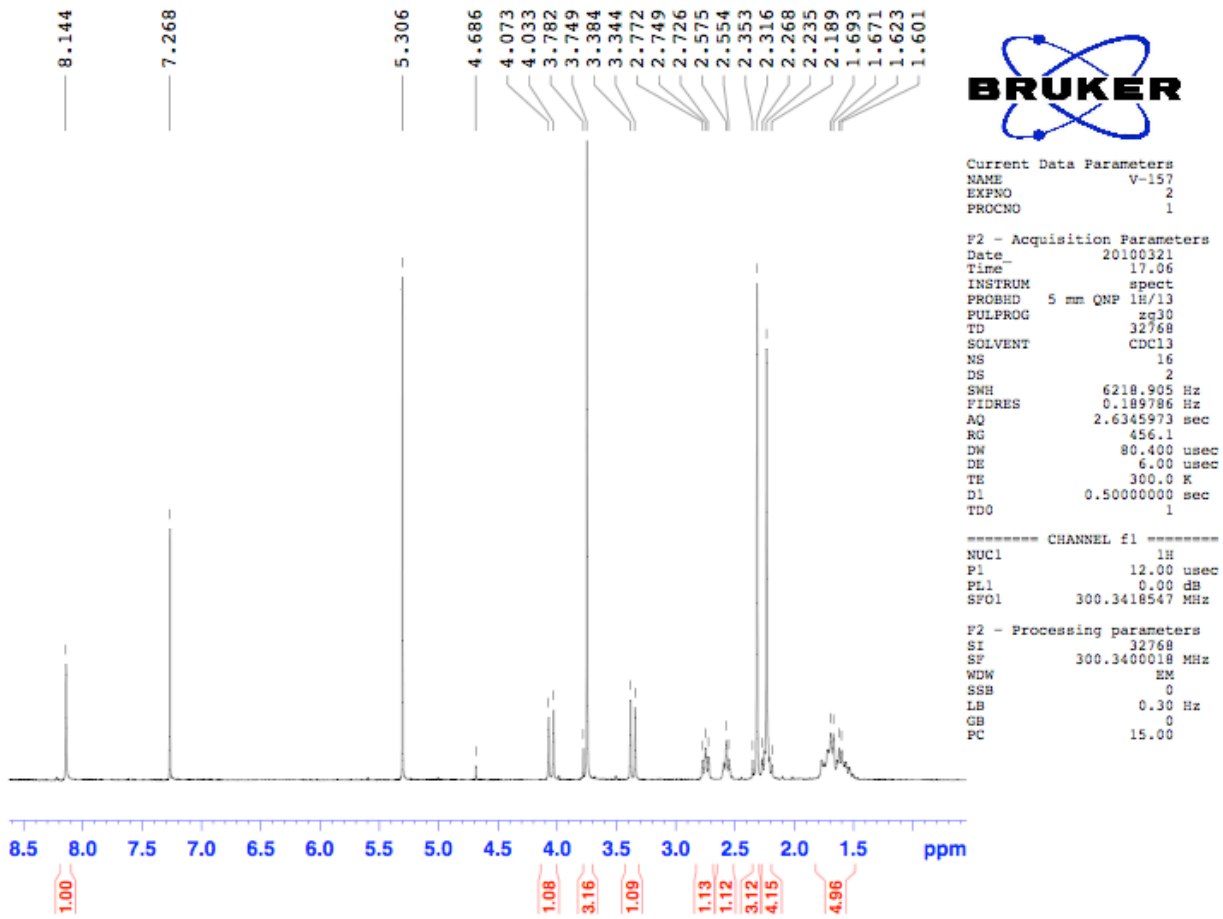

Figure C3. ^{1}H NMR spectrum of recrystallized SR-BPBP ligand in $CDCl_3$.

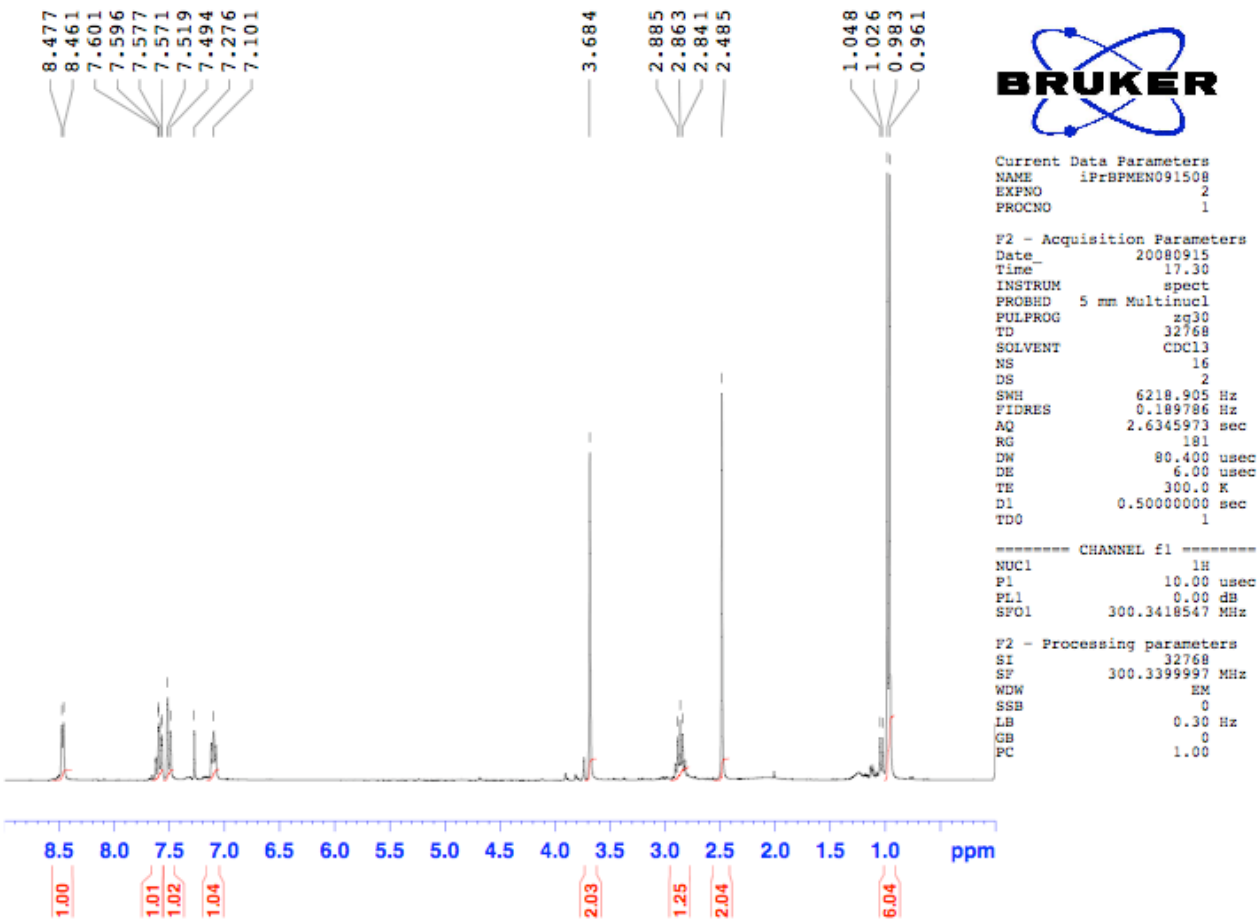

Figure C4. ^{1}H NMR spectrum of iPr-BPMEN ligand in $CDCl_3$.

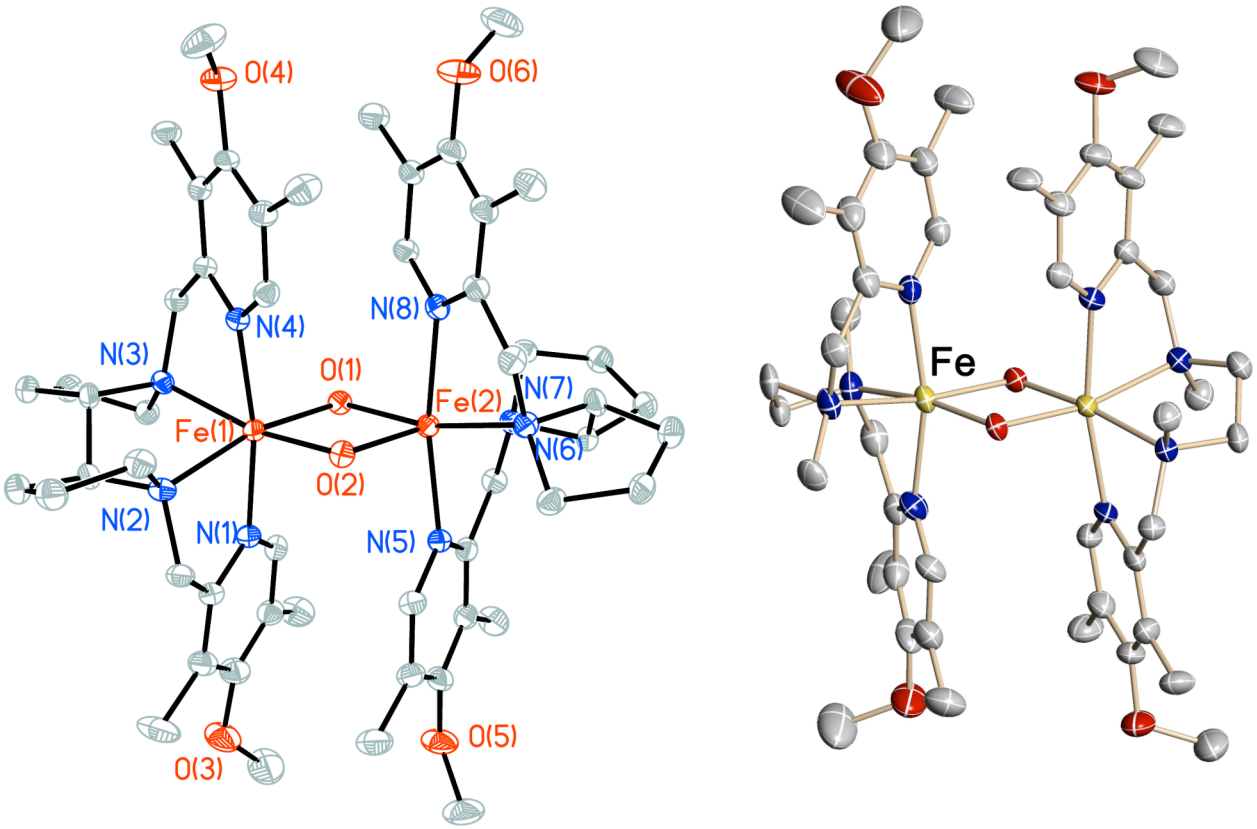

Figure C5. Crystal structure of orange needles that cocrystallize with **SR-3** (left) and **SR-1** (right), crystal structure solved by Dr. Peter Müller (MIT) and Dr. Alexander Filatov (Albany).

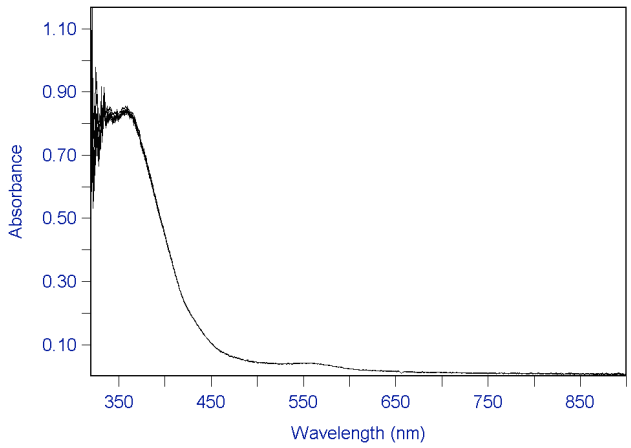

A

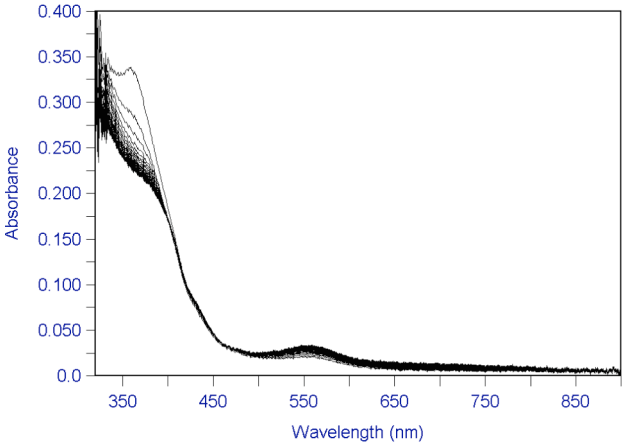

B

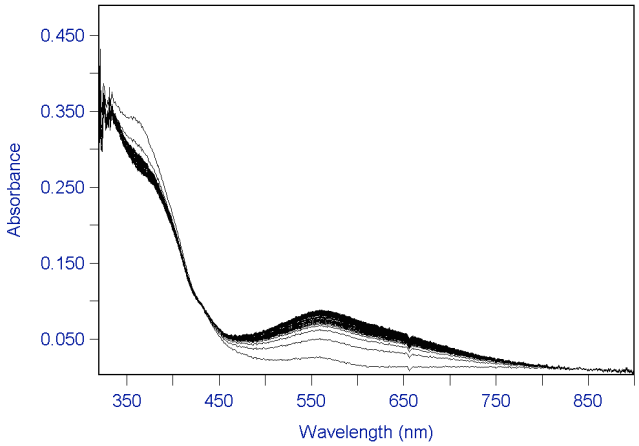

C

Figure C6. Spectrum of orange complex (direrric (μ-O)(μ-OH)) that crystallizes along with **SR-1** (A) and spectral changes when this complex reacts with H_2O_2 (B –decay at 350 nm, growth at 550 nm) and H_2O_2 + benzoic acid (C - decay at 350, growth at 550).

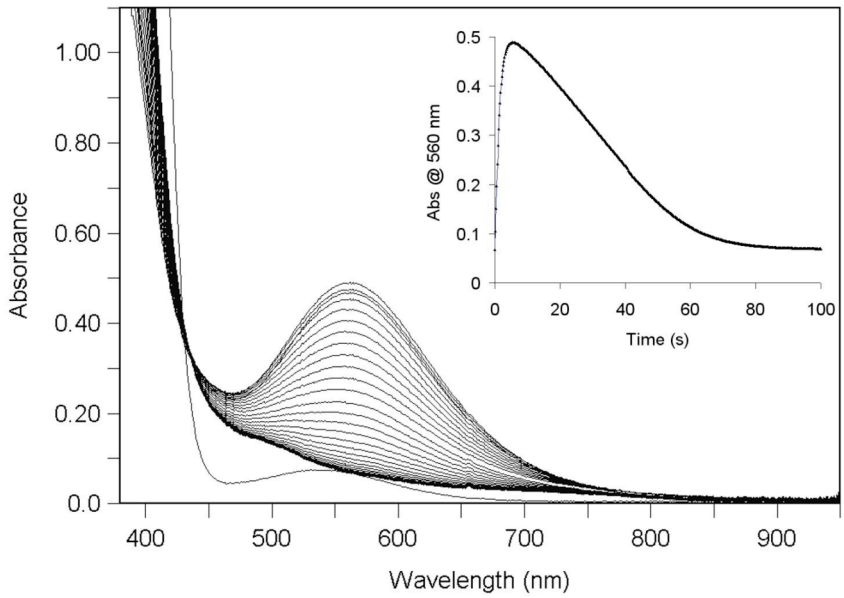

Figure C7. Time resolved UV-vis spectra of the $Fe^{III}(OOH)$ formation at 20 °C in acetonitrile ([**3**] **=** 1 mM, $[H_2O_2]$ = 10 mM). Inset: kinetic trace at 560 nm.

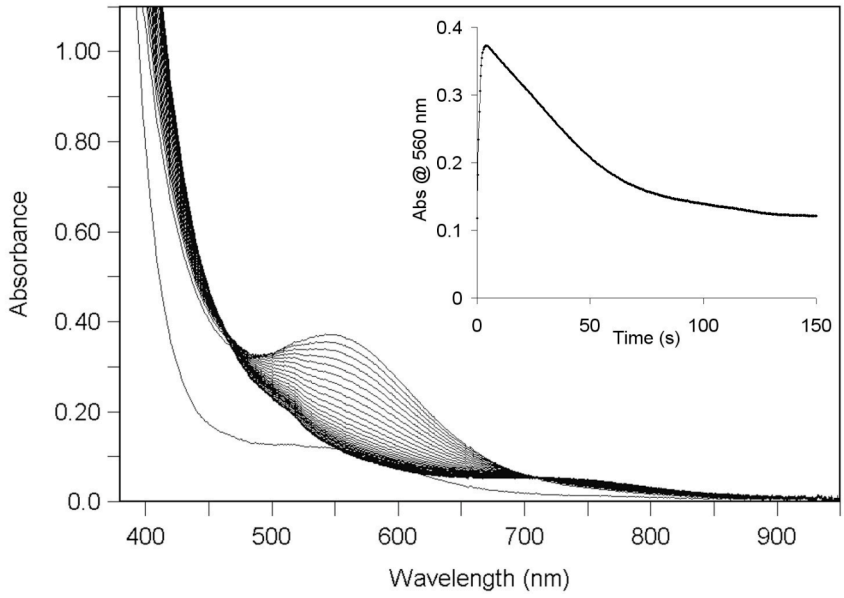

Figure C8. Time resolved UV-vis spectra of the $Fe^{III}(OOH)$ formation at 20 °C in acetonitrile ([**SR-1**] **=** 1 mM, $[H_2O_2]$ = 10 mM). Inset: kinetic trace at 560 nm.

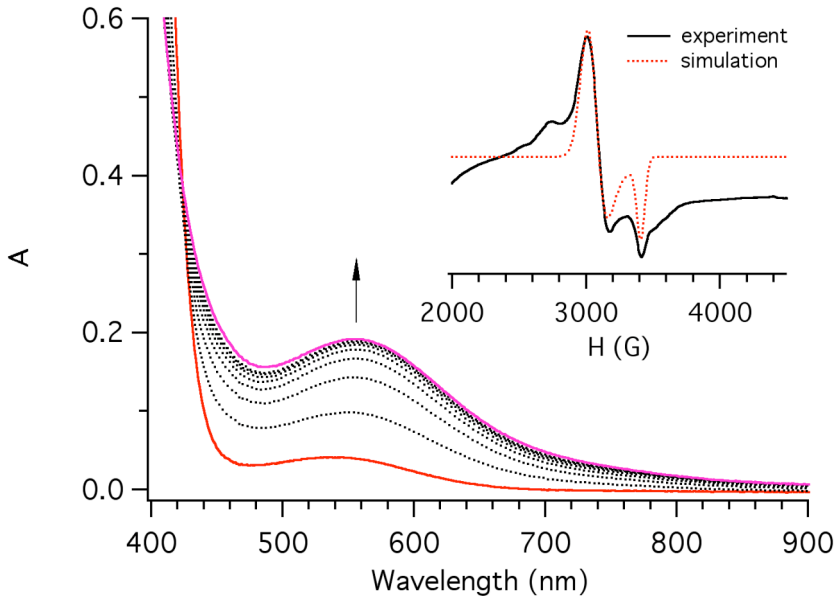

Figure C9. Time resolved UV-vis spectra of the Fe^{III}(OOH) formation at 27 °C in acetonitrile ([**4**] = 1 mM, [H_2O_2] = 30 mM). Maximum accumulation of Fe^{III}(OOH) was seen in 2 s after mixing reagents (red-spectrum of **4**, purple – spectrum of Fe^{III}(OOH)). Inset: EPR spectrum (120 K) of the Fe^{III}OOH, generated by mixing **4** and H_2O_2 in acetonitrile at 0 ˚C and frozen in ~7 s after reagents were mixed ([**4**] = 5 mM, [H_2O_2] = 50 mM after mixing). Spectrum simulated in SimFonia with g values 2.185, 1.98, and 1.955.

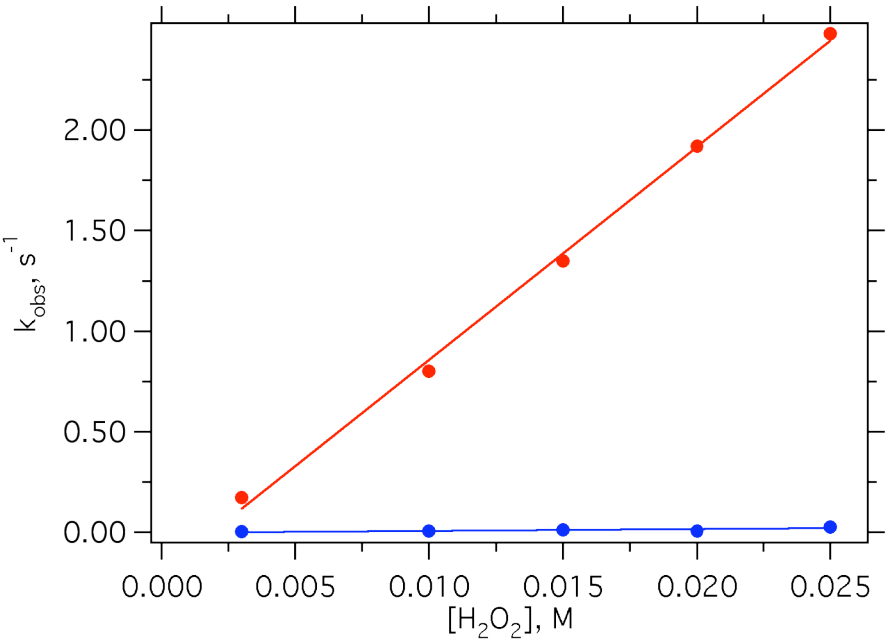

Figure C10. Plot of the observed rate constants versus H_2O_2 concentration for $Fe^{III}(OOH)$ formation (red) and decay (blue) in a reaction between **3** and H_2O_2 at 20 ˚C. Data were acquired in the stopped-flow diode array mode and kinetic traces at 560 nm were fitted in Kinetic Studio using two-exponential model, where first process is $Fe^{III}(OOH)$ formation and second process – its decay.

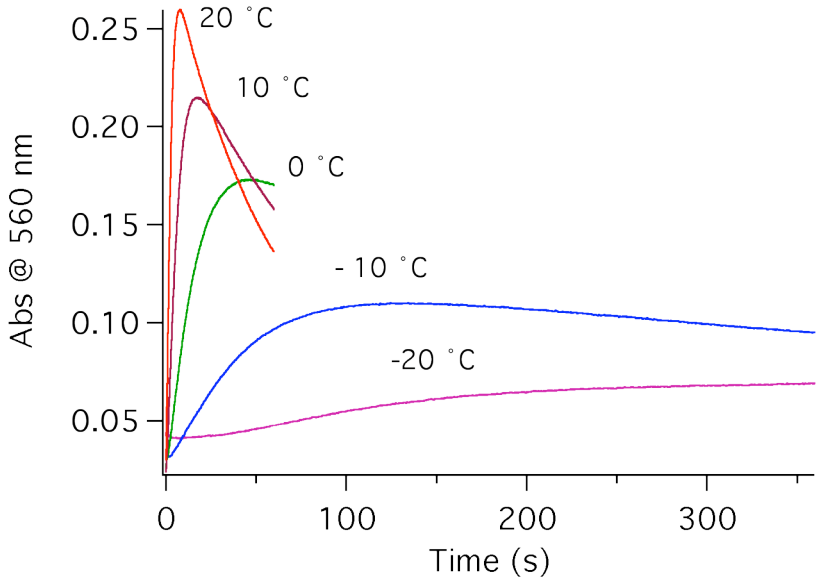

Figure C11. Kinetic traces at 560 nm acquired using stopped-flow for the reaction of **1** with hydrogen peroxide ([**1**] = 1 mM, $[H_2O_2]$ = 10 mM) at different temperatures.

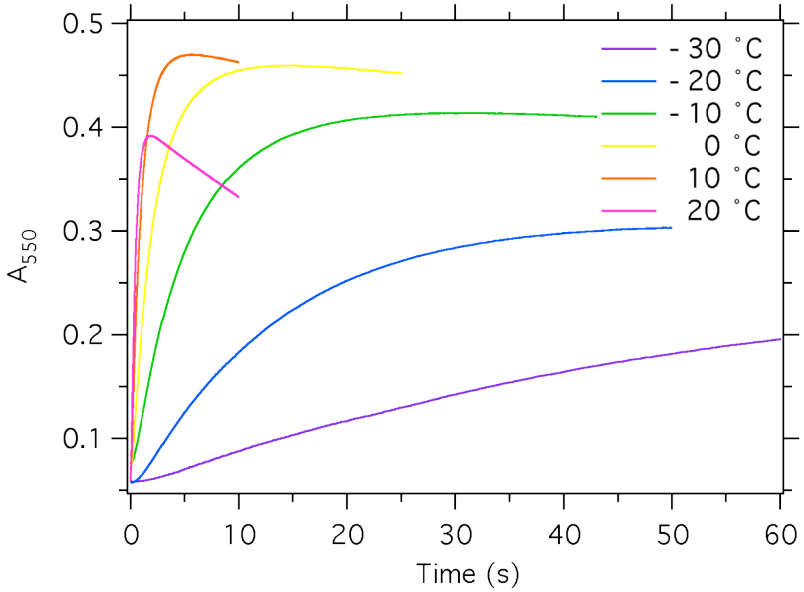

Figure C12. Kinetic traces at 550 nm acquired using stopped-flow for the reaction of **SR-3** with hydrogen peroxide ([**SR-3**] = 1 mM, $[H_2O_2]$ = 10 mM) at different temperatures.

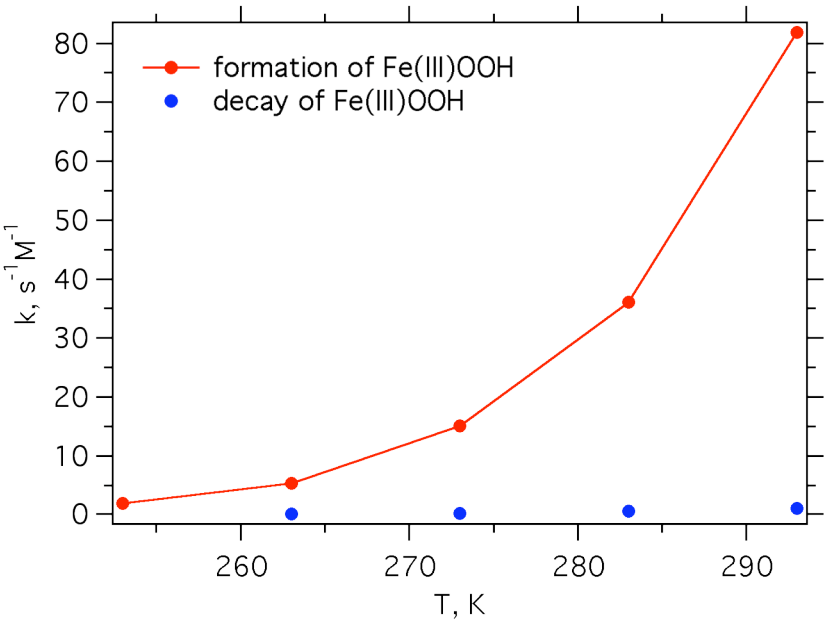

Figure C13. Observed rate constants for $Fe^{III}(OOH)$ formation and decay in a reaction between **3** and H_2O_2; $k_2 = k_{obs}/[H_2O_2]$ ($[H_2O_2]$ =0.01 M after mixing in the stopped flow).

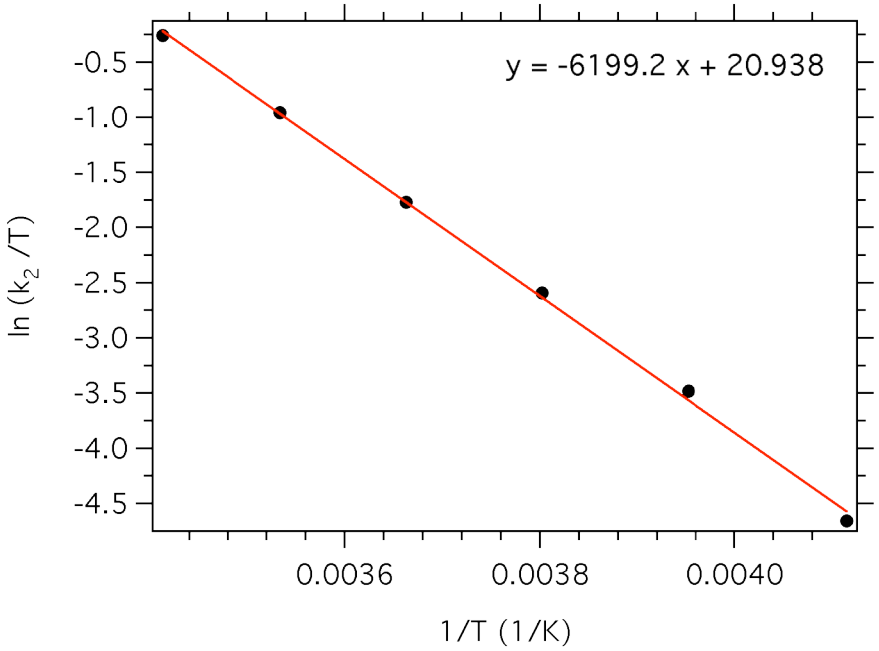

Figure C14. Eyring plot for the $Fe^{III}(OOH)$ formation in a reaction between **SR-3** and H_2O_2; $k_2 = k_{obs}/[H_2O_2]$ ($[H_2O_2]$ =0.01 M after mixing in the stopped flow).

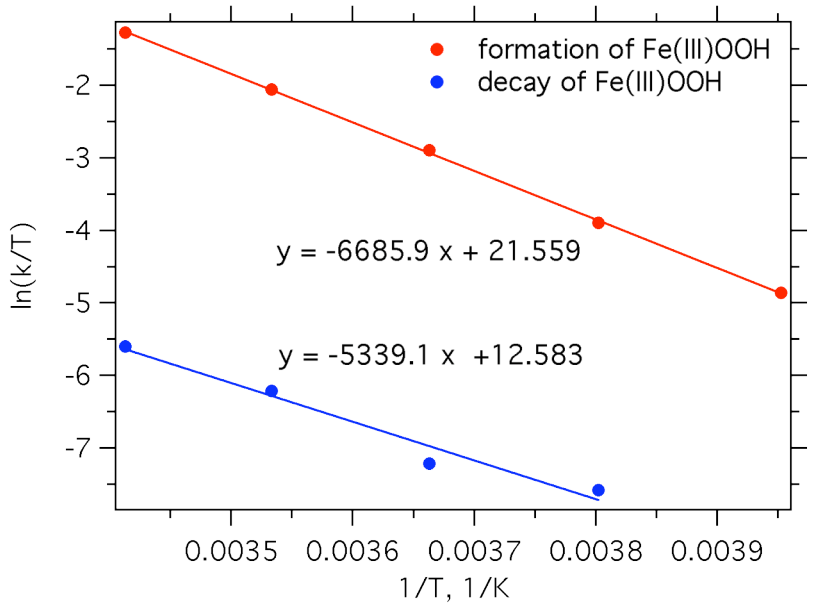

Figure C15. Eyring plot for the $Fe^{III}(OOH)$ formation and decay in a reaction between **3** and H_2O_2; $k_2 = k_{obs}/[H_2O_2]$ ($[H_2O_2]$ =0.01 M after mixing in the stopped flow).

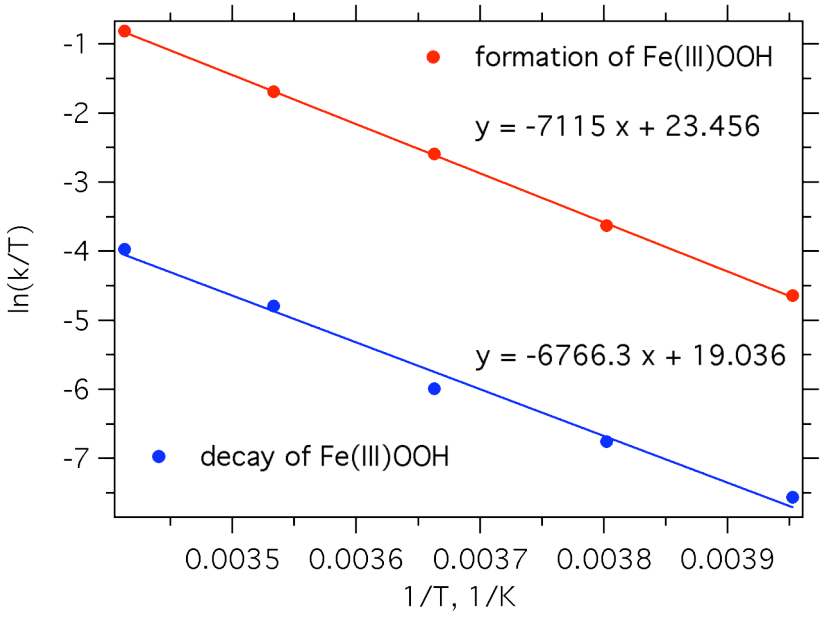

Figure C16. Eyring plot for the $Fe^{III}(OOH)$ formation and decay in a reaction between **SR-1** and H_2O_2; $k_2 = k_{obs}/[H_2O_2]$ ($[H_2O_2]$ = 0.01 M after mixing in the stopped flow).

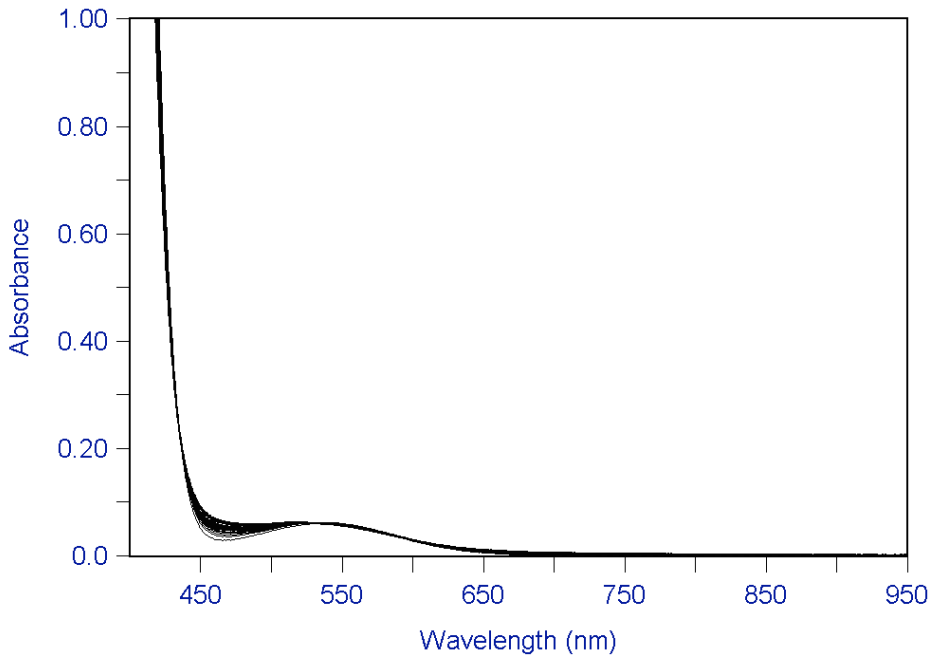

Figure C17. Spectral changes that accompany $Fe^{II} \rightarrow Fe^{III}$ oxidation, reaction was carried out in acetonitrile at 20 ˚C by mixing **3** (1 mM) and H_2O_2 (0.5 equiv), run time 80 s.

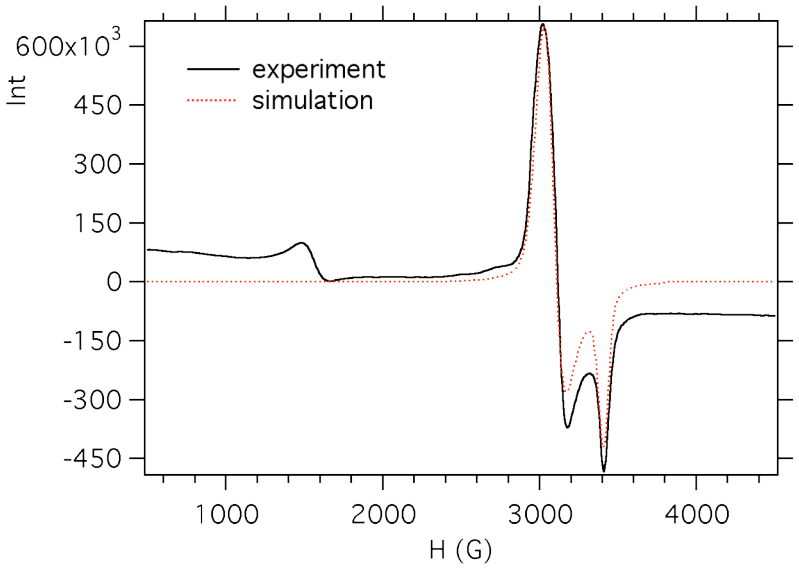

Figure C18. EPR spectrum (120 K) of the $Fe^{III}OOH$, generated by mixing **3** and H_2O_2 in acetonitrile at 0 ˚C and frozen in 30 s after reagents were mixed ([**3**]=1 mM, [H_2O_2]=10 mM after mixing).

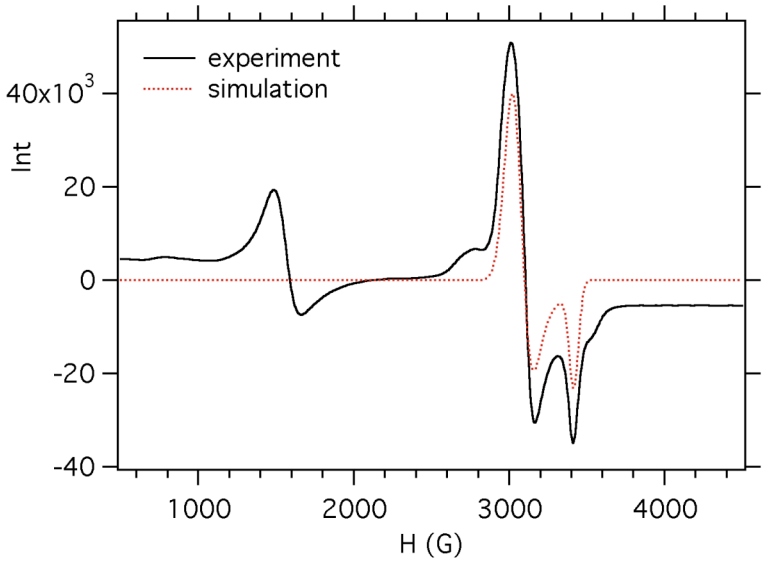

Figure C19. EPR spectrum (120 K) of the $Fe^{III}OOH$, generated by mixing **SR-1** and H_2O_2 in acetonitrile at 0 ˚C and frozen in 10 s after reagents were mixed ([**SR-1**] = 2.5 mM, [H_2O_2] = 25 mM after mixing).

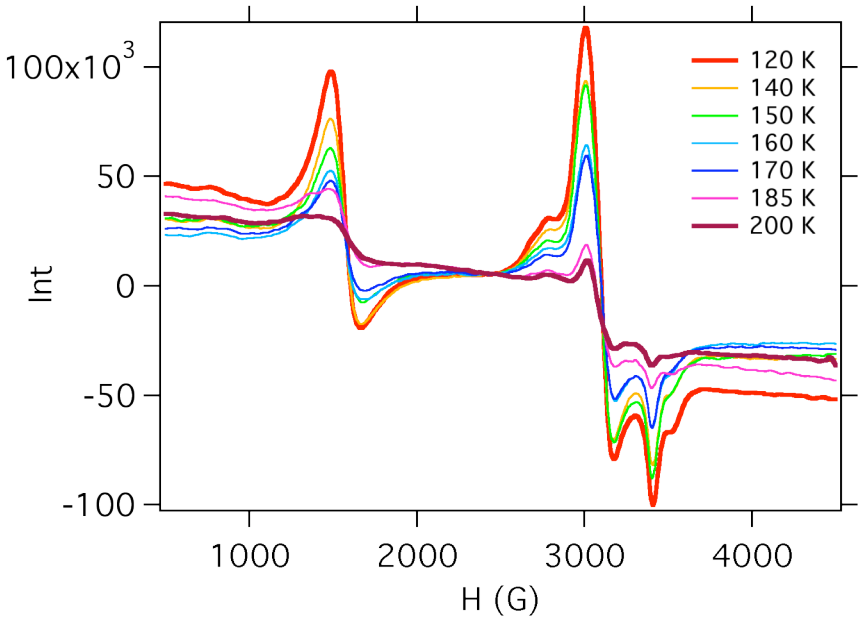

Figure C20. EPR spectra acquired on (BPMEN)Fe^{III}(OOH) (**1a**) at variable temperatures; **1a** was generated by mixing **1** (0.2 mL, 3 mM) and H_2O_2 (0.2 mL, 30 mM) at room temperature and freezing EPR tube immediately after oxidant was added.

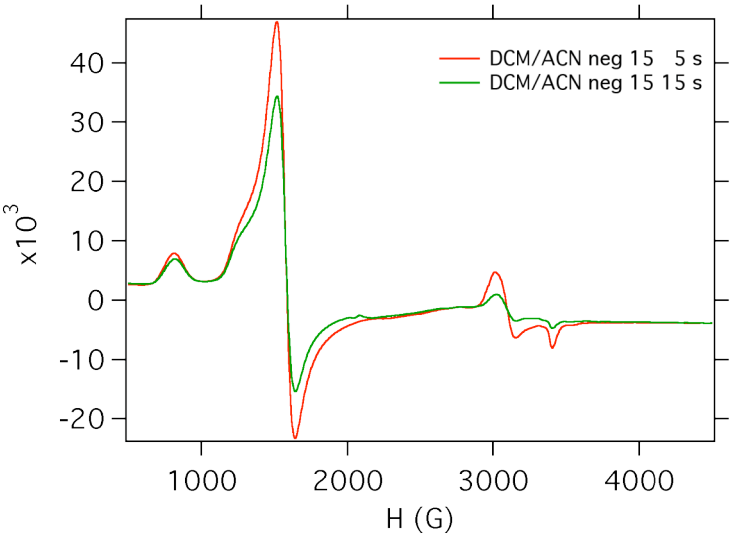

Figure C21. EPR spectra of samples prepared by reacting **SR-3** with H_2O_2 in DCM/acetonitrile mixture. H_2O_2 was delivered at -15 ˚C and then mixture was incubated for 10 s or quenched immediately (5 s).

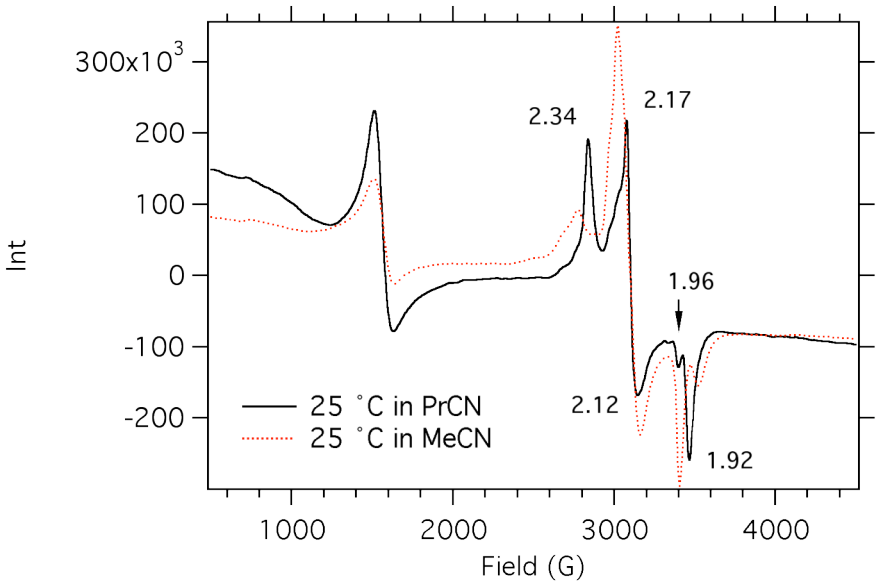

Figure C22. EPR spectra of the low spin iron(III) species generated from **1** and H_2O_2 at 25 ˚C in PrCN and MeCN.

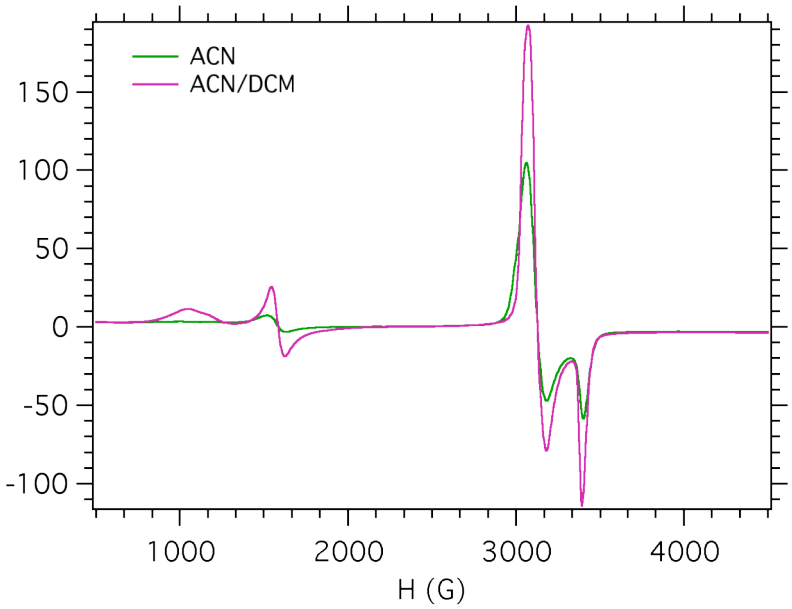

Figure C23. EPR spectra of (TPA)FeIII(OOH) generated in acetonitrile and DCM/acetonitrile mixture; [**2**] = 5 mM, [H_2O_2] = 50 mM, -40 ˚C, reaction time 1 min.

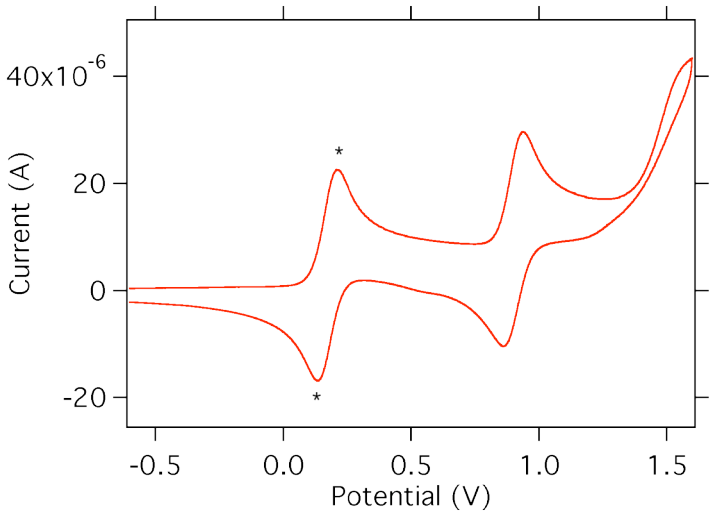

Figure C24. Cyclic voltammogram recorded for $[Fe^{II}BPMEN(CH_3CN)_2]^{2+}$ ([**1**] = 1 mM) in acetonitrile. * denotes Fc/Fc^+ couple. $TBAPF_6$ (0.1 M) was used as electrolyte, scan rate 0.1 V/s.

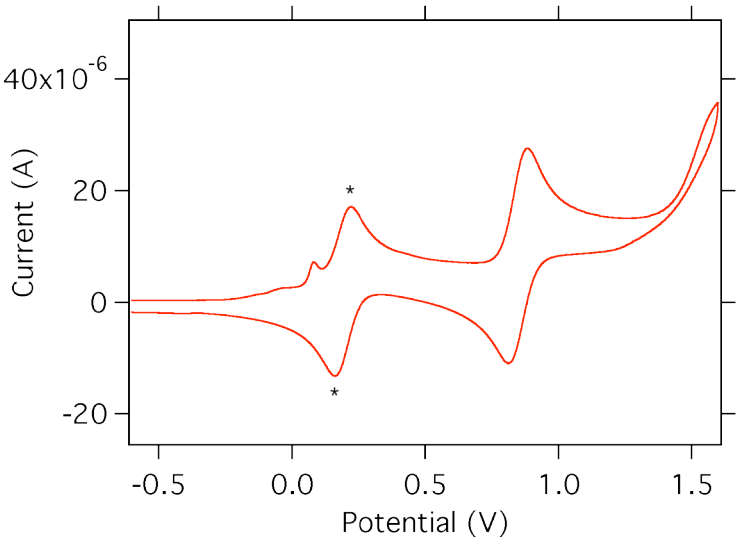

Figure C25. Cyclic voltammogram recorded for $[Fe^{II}BPBP(CH_3CN)_2]^{2+}$ ([**3**] = 1 mM) in acetonitrile. * denotes Fc/Fc^+ couple. $TBAPF_6$ (0.1 M) was used as electrolyte, scan rate 0.1 V/s.

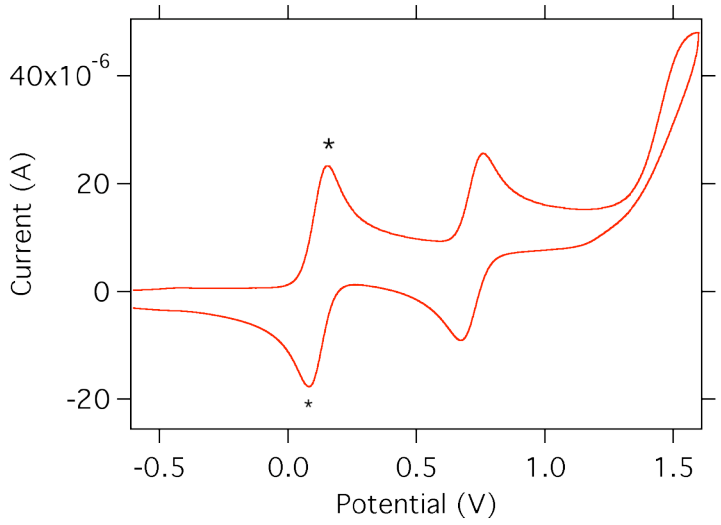

Figure C26. Cyclic voltammogram recorded for $[Fe^{II}MPMEN(CH_3CN)_2]^{2+}$ ([**SR-1**] = 1 mM) in acetonitrile. * denotes Fc/Fc^+ couple. $TBAPF_6$ (0.1 M) was used as electrolyte, scan rate 0.1 V/s.

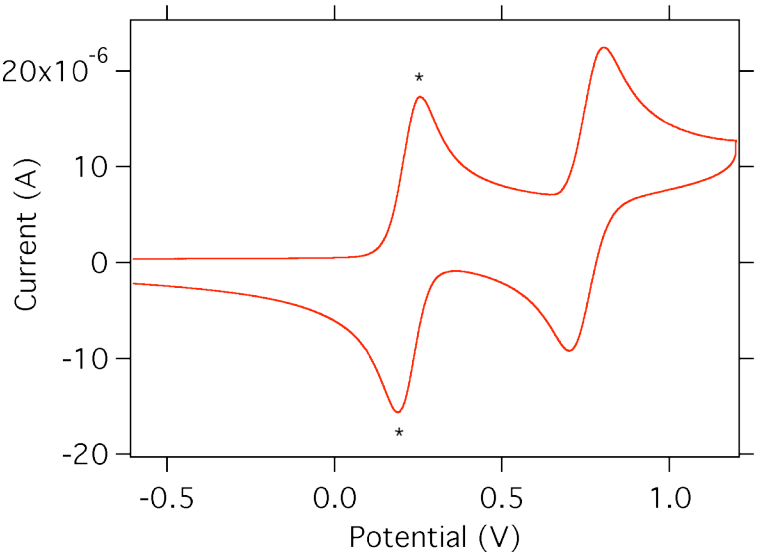

Figure C27. Cyclic voltammogram recorded for $[Fe^{II}SR\text{-}BPBP(CH_3CN)_2]^{2+}$ ([**SR-3**] = 1 mM) in acetonitrile. * denotes Fc/Fc^+ couple. $TBAPF_6$ (0.1 M) was used as electrolyte, scan rate 0.1 V/s.

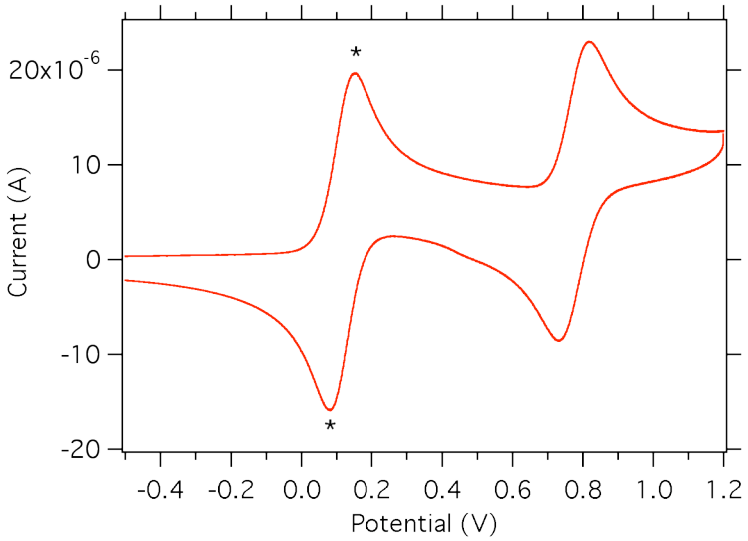

Figure C28. Cyclic voltammogram recorded for $[Fe^{II}PYBP(CH_3CN)_2]^{2+}$ ([**4**] = 1 mM) in acetonitrile. * denotes Fc/Fc^+ couple. $TBAPF_6$ (0.1 M) was used as electrolyte, scan rate 0.1 V/s.

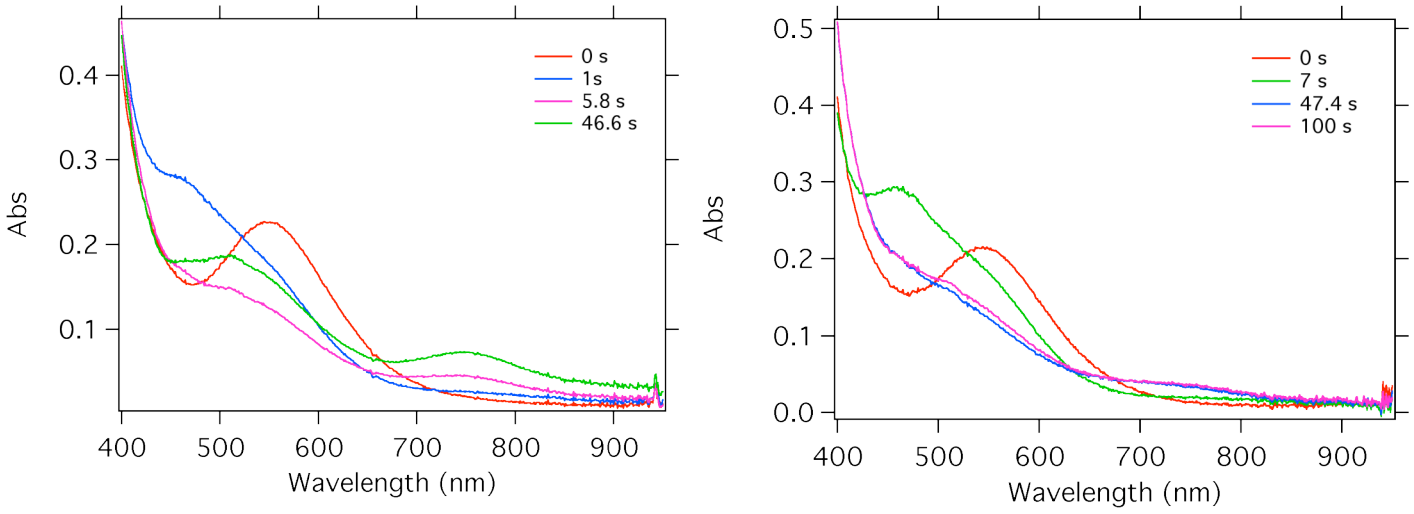

Figure C29. Spectral changes upon addition of acetic acid to (SR-BPBP)Fe^{III}(OOH). Left: data acquired in stopped-flow (diode array mode) at **20 ˚C**, Fe^{III}(OOH) was pregenerated in the first mixing (age time 2s) and then acetic acid was added in the second mixing ([**2**]=0.5 mM, [H_2O_2]=5 mM, [CH_3COOH]=0.5 mM after double mixing); right: same experiment as described above was run at **-10 ˚C**, note: longer time (30 s) was needed to get the highest yield of Fe^{III}(OOH) at – 10 ˚C.

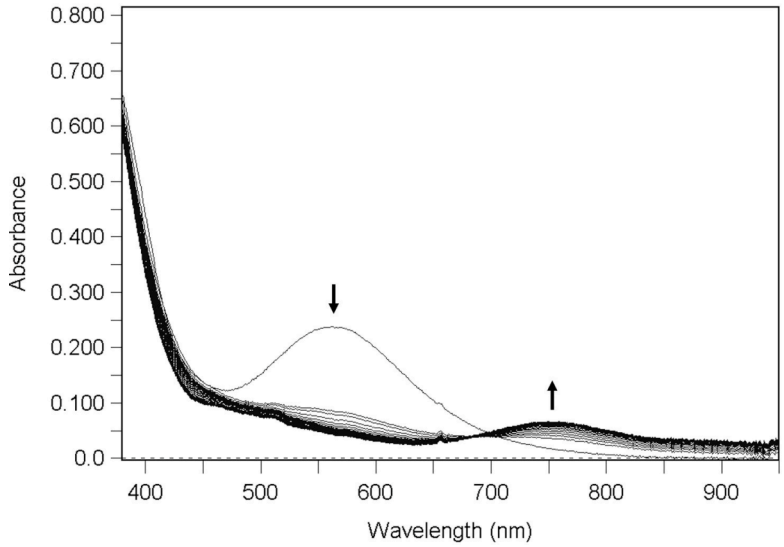

Figure C30. Stopped-flow time resolved UV-vis spectra of the reaction of $Fe^{III}(OOH)$ with 1 equiv of acetic acid. $Fe^{III}(OOH)$ was pre-generated by mixing **3** (0.5 mM) and H_2O_2 (5 mM) at 20 °C in acetonitrile over 6 s. $Fe^{III}(OOH)$ decays quickly (~2 s) upon addition of acetic acid (1 equiv vs. iron) followed by slow (over 80 s) accumulation of $Fe^{IV}=O$ (λ_{max} = 760 nm).

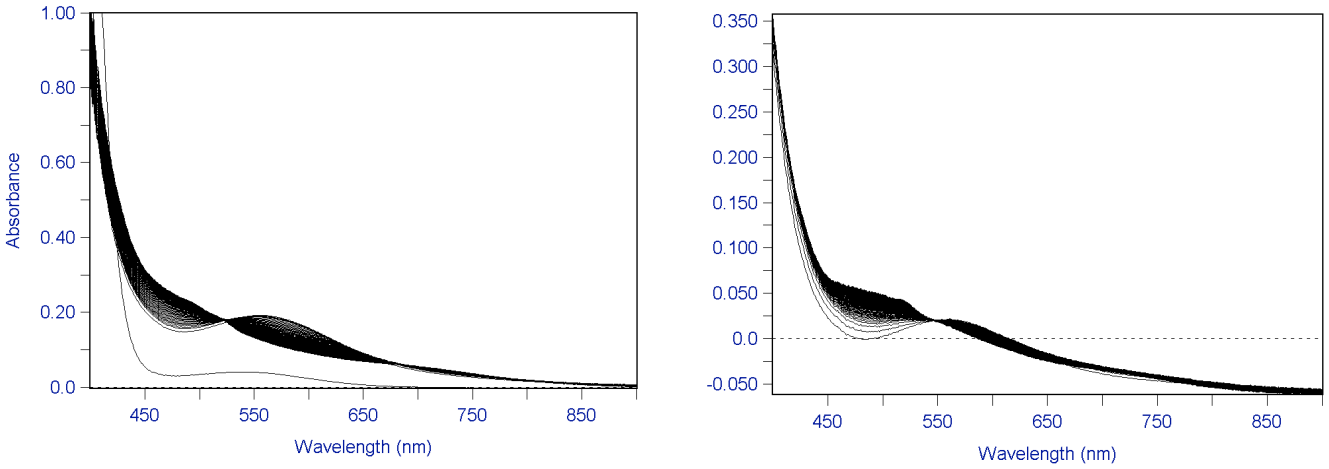

Figure C31. Decay of $Fe^{III}(OOH)$ species that was generated from **4** (1 mM) and H_2O_2 (30 mM) in acetonitrile at 27 ˚C: left – self decay over 40 s; right – 1 equiv of acetic acid was added at the maximum accumulation of $Fe^{III}(OOH)$, run time 40 s (baseline is off).

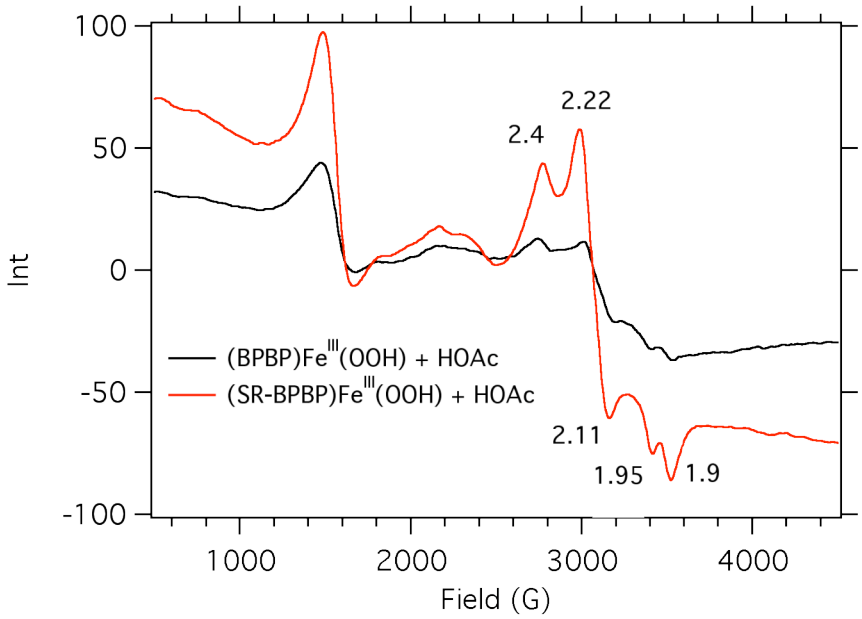

Figure C32. EPR (120 K) spectra of pregenerated $Fe^{III}(OOH)$ with <0.5 equiv of acetic acid. **3**/**1-SR** was mixed with H_2O_2 at 0 ˚C and incubated in acetone/dry ice bath for 30 s and then acetic acid was added and sample frozen immediately in liquid nitrogen ([**3**] = [**1-SR**] = 0.75 mM, [H_2O_2] = 75 mM, [CH_3COOH] = 0.25 mM after mixing).

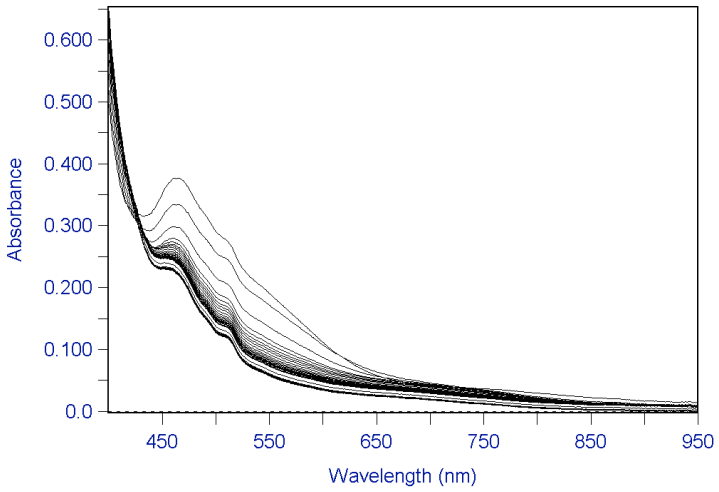

Figure C33. Spectral changes upon mixing **SR-3X** and benzene in acetonitrile at -10 ˚C. **SR-3X** was generated from **SR-3** and H_2O_2/CH_3COOH (1 equiv of H_2O_2 and 1 equiv of CH_3COOH), data acquisition started after benzene (300 equiv) had been added. Age time 15 s, run time 60 s.

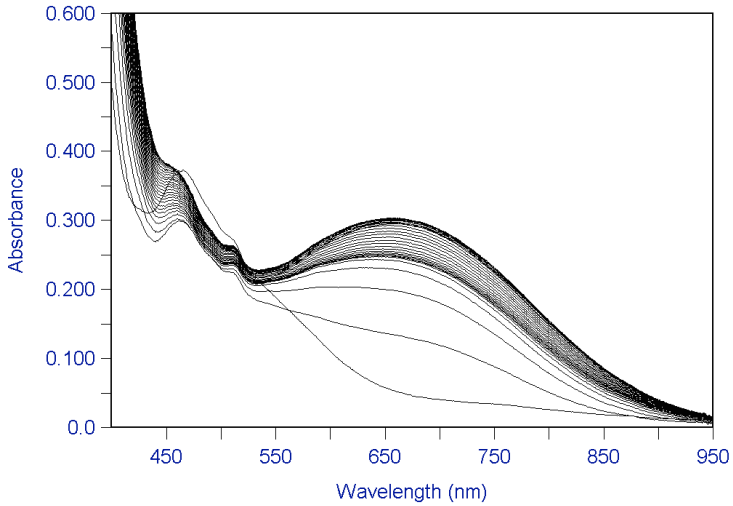

Figure C34. Spectral changes upon mixing **SR-3X** and benzene/H_2O_2 in acetonitrile at -10 ˚C. **SR-3X** was generated from **SR-3** and H_2O_2/CH_3COOH (1 equiv of H_2O_2 and 1 equiv of CH_3COOH), data acquisition started after benzene/H_2O_2 (300 equiv benzene, 4 equiv H_2O_2) had been added. Age time 15 s, run time 60 s.

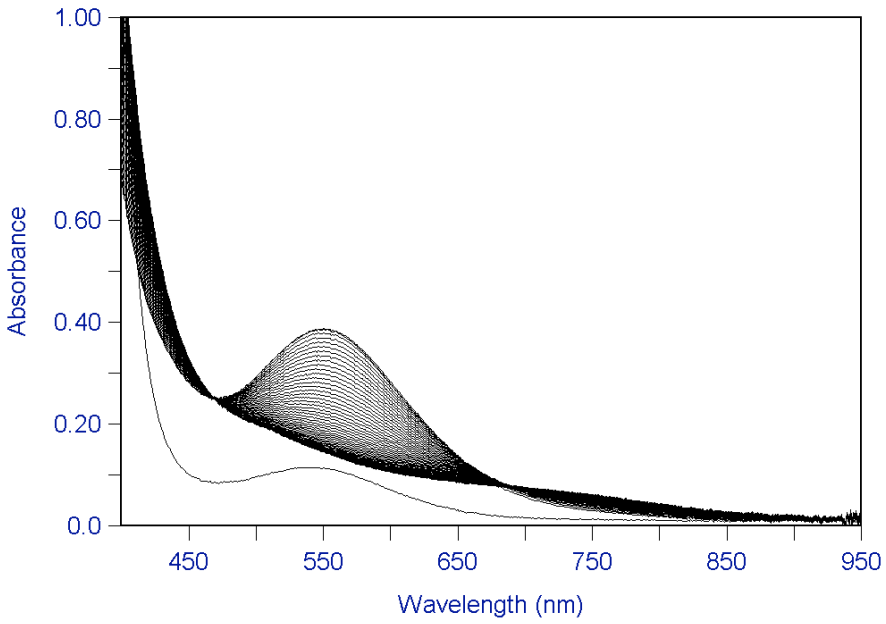

Figure C35**.** Time resolved UV-vis spectra of the Fe^{III}(OOH) formation at 20 °C in acetonitrile ([**SR-3**] **=** 1 mM, [H_2O_2] = 10 mM). Run time shown is 70 s.

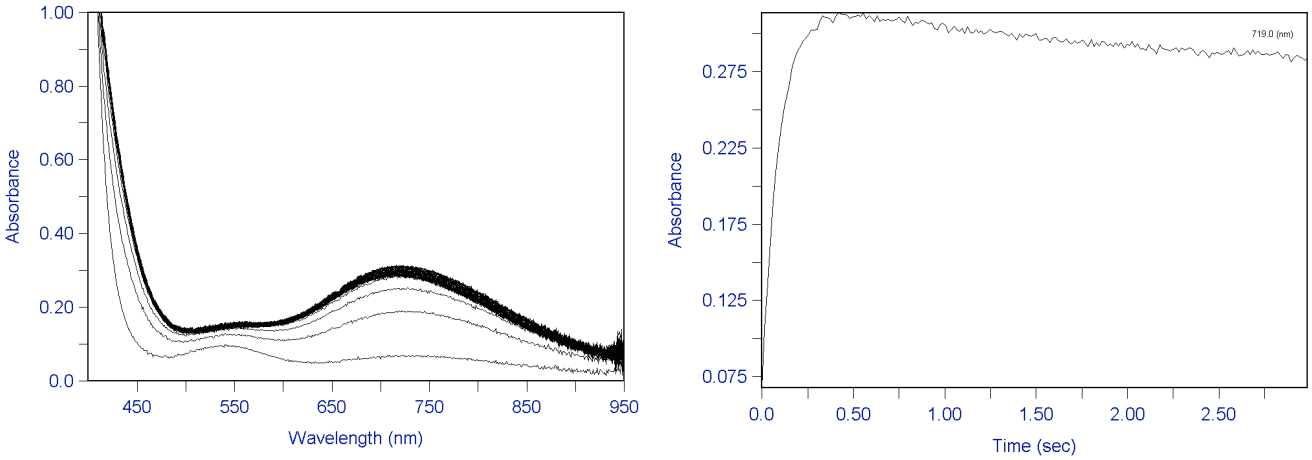

Figure C36. Spectral changes (left) and kinetic trace at 720 nm (right) upon reaction between **SR-3** (1 mM) and IBX-ester (~4 mM) in acetonitrile at -30 ˚C.

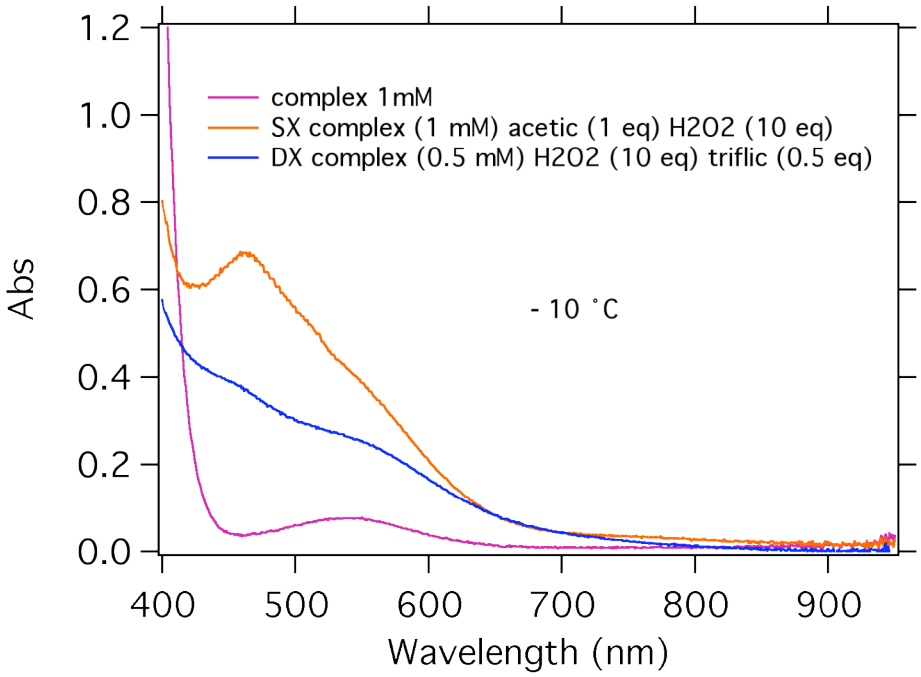

Figure C37. Spectra of the intermediate generated using triflic and acetic acids. Orange spectrum- single mixing experiment with **SR-3** (1 mM) and a mixture of H_2O and acetic acid (10 equiv and 1 equiv respectively). Blue spectrum – $Fe^{III}(OOH)$ was pregenerated by mixing **SR-3** and H_2O_2 (10 equiv) and then triflic acid was added (1 equiv), final concentration of iron is 0.5 mM.

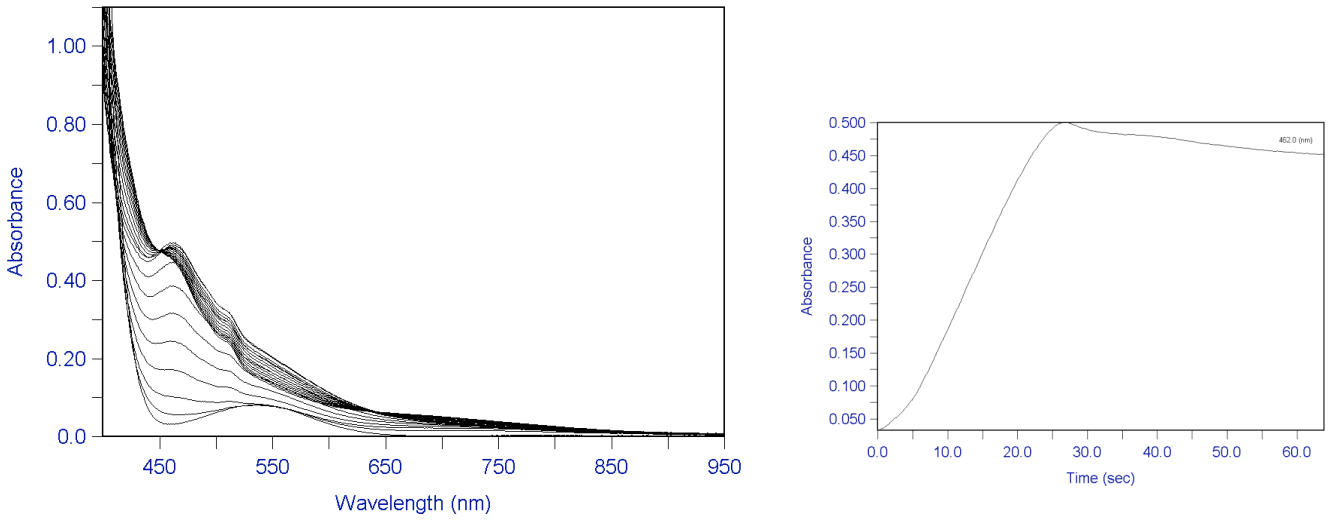

Figure C38. Spectral changes (left) and kinetic trace at 462 nm (right) upon reaction of **SR-3** (1 mM) and H_2O_2 /HOAc in EtCN at -30 ˚C; [**SR-3**] = 1 mM, [H_2O_2] = 5 mM, [HOAc] = 1 mM.

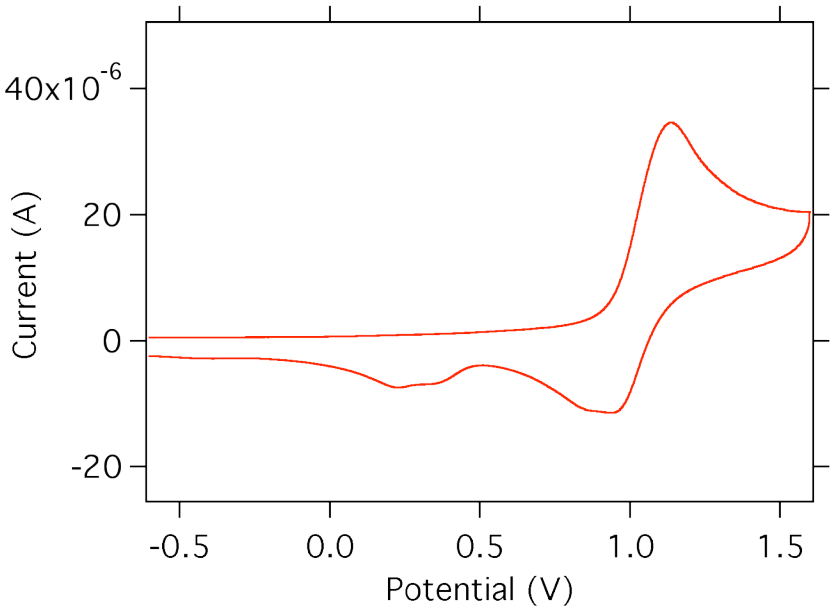

Figure C39. Cyclic voltammogram recorded for Fe^{II}(iPr-BPMEN)$(OTf)_2$ ([**iPr-1**] = 1 mM) in acetonitrile. $TBAPF_6$ (0.1 M) was used as electrolyte, scan rate 0.1 V/s.

10 Appendix D (chapter 4)

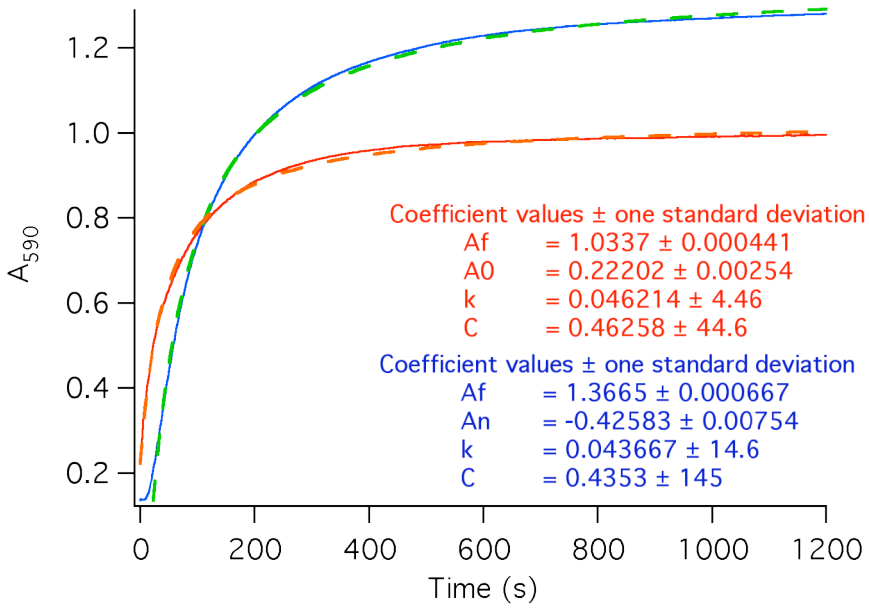

Figure D1. Kinetic traces at 590 nm represent formation of Fe^{III}-salicylate in reaction between dimer (**5**), H_2O_2 and 3,5-dichlorobenzoic acid in the presence (blue) and absence (red) of added water; [**5**] = 0.5 mM, [BA] = 2 mM, [H_2O_2] = 10 mM, [H_2O] = 0.7 M. Kinetic traces were fitted to a second order equation: f(x) = Af-((Af-An)/(1+k*C*x)), this could indicate that reaction is second order in **5** (*additional experiment should be done with constant concentration of H_2O_2 and benzoic acid but variable concentration of dimer, if rate constant does not depend on [**5**] –reaction is first order in **5**).

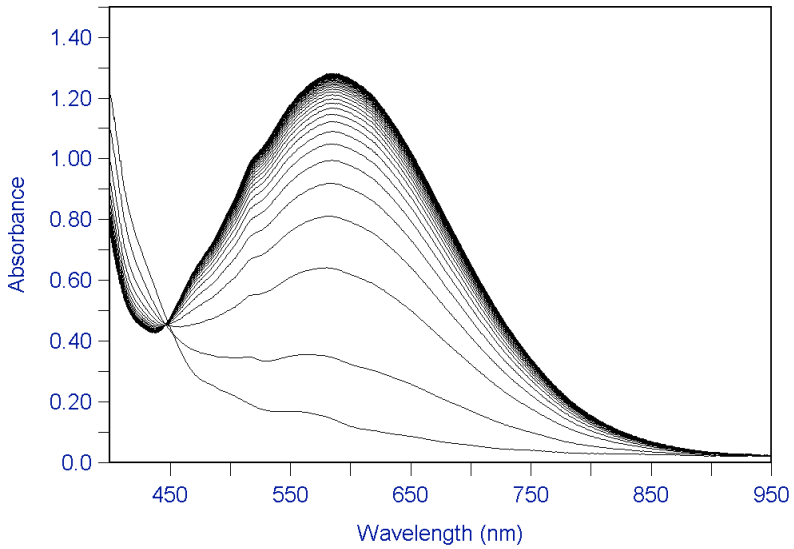

Figure D2. Spectral changes upon reaction of **5**, H_2O_2 and 3,5-dichlorobenzoic acid in acetonitrile at 20°C; [**5**] = 0.5 mM, [3,5-dichlorobenzoic acid] = 2 mM, [H_2O_2] = 10 mM after mixing) indicate formation of Fe(III)-salicylate complex.

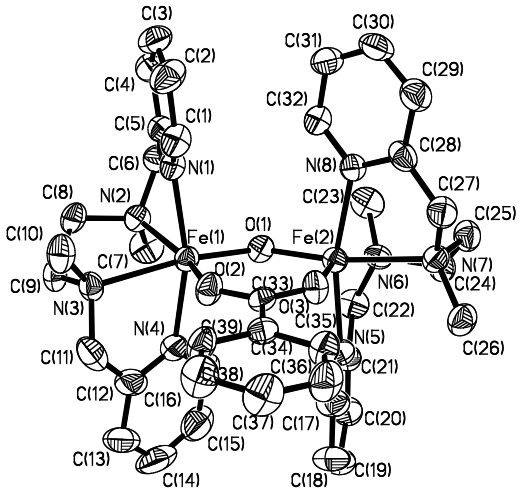

Figure D3. X-ray structure of the complex cation $[Fe^{III}_2(\mu\text{-}O)(\mu\text{-}OOC(C_6H_5))(BPMEN)_2]^{3+}$ (**6**), showing 50% probability thermal ellipsoids. Hydrogen atoms are omitted for clarity.

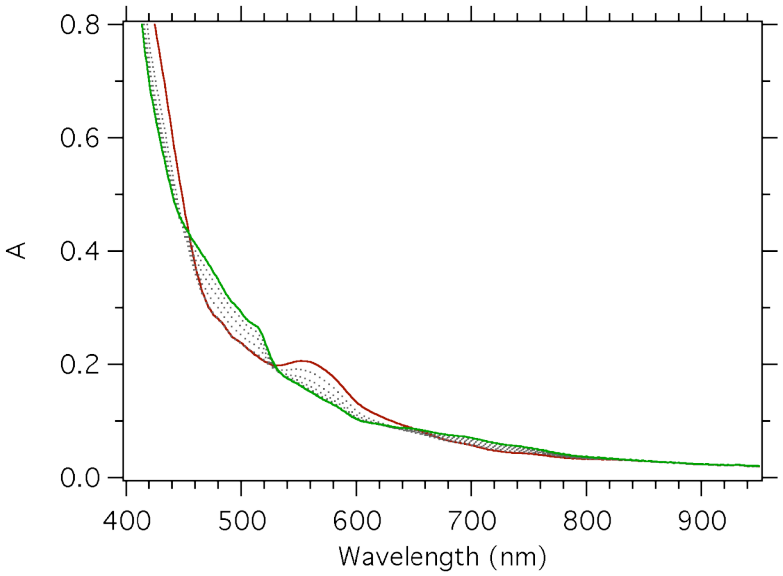

Figure D4. Spectral changes upon reaction of 5 with H_2O_2 in the presence of water in acetonitrile at 20 ˚C; [**5**] = 0.5 mM, [H_2O] = 0.45 M, [H_2O_2] = 10 mM.

11 Appendix E (chapter 5)

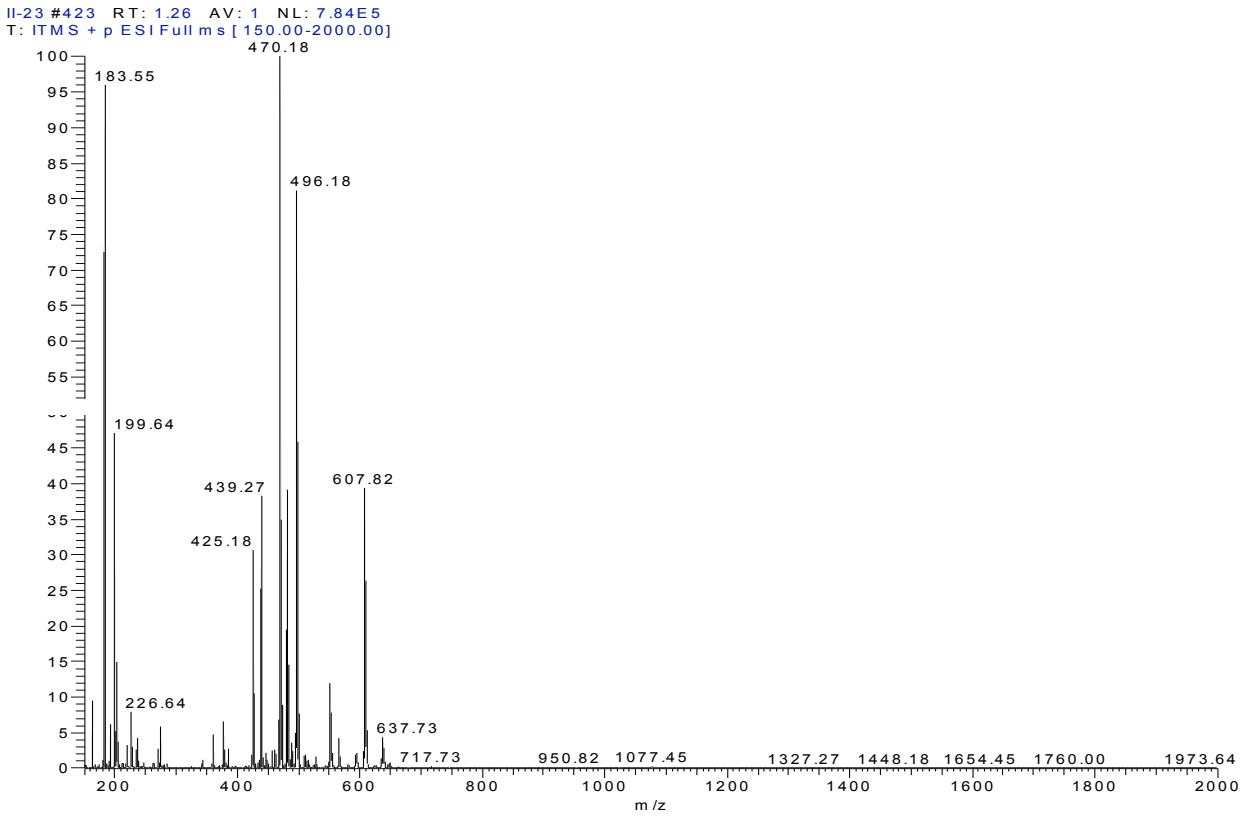

Figure E1. Electrospray mass spectrum of a reacting mixture containing 1, 2-chlorobenzoic acid and hydrogen peroxide (blue solution).

Peaks assignment for spectrum:

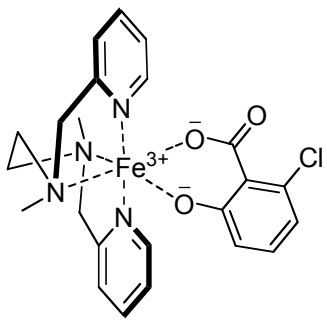

$C_{23}H_{25}ClFeN_4O_3^+$
Exact Mass: 496.0959

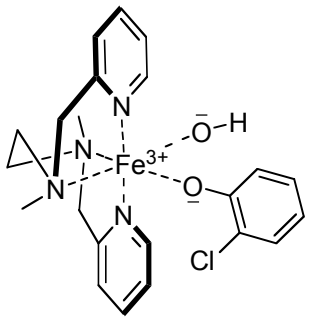

$C_{22}H_{27}ClFeN_4O_2^+$
Exact Mass: 470.1166

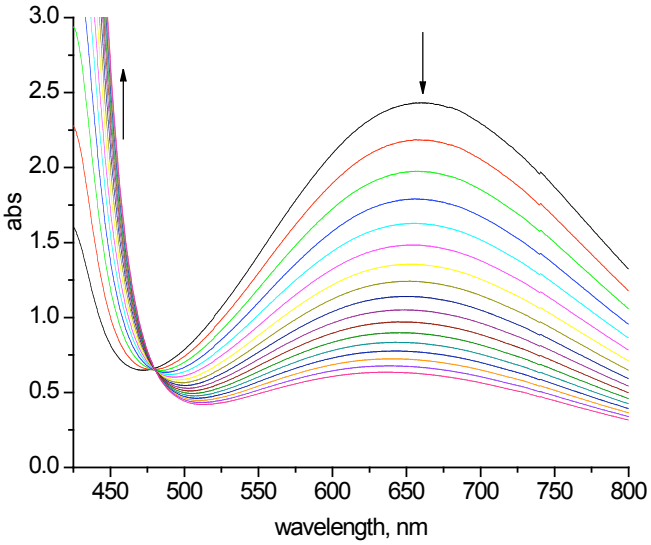

Figure E2. Decomposition of the blue Fe(III)-phenolate product generated upon addition of H_2O_2 (2 equiv) to the mixture of 1 (0.9 mM) and 2,6-dichlorobenzoic acid (2 equiv). Total time of the decay is 30 min.

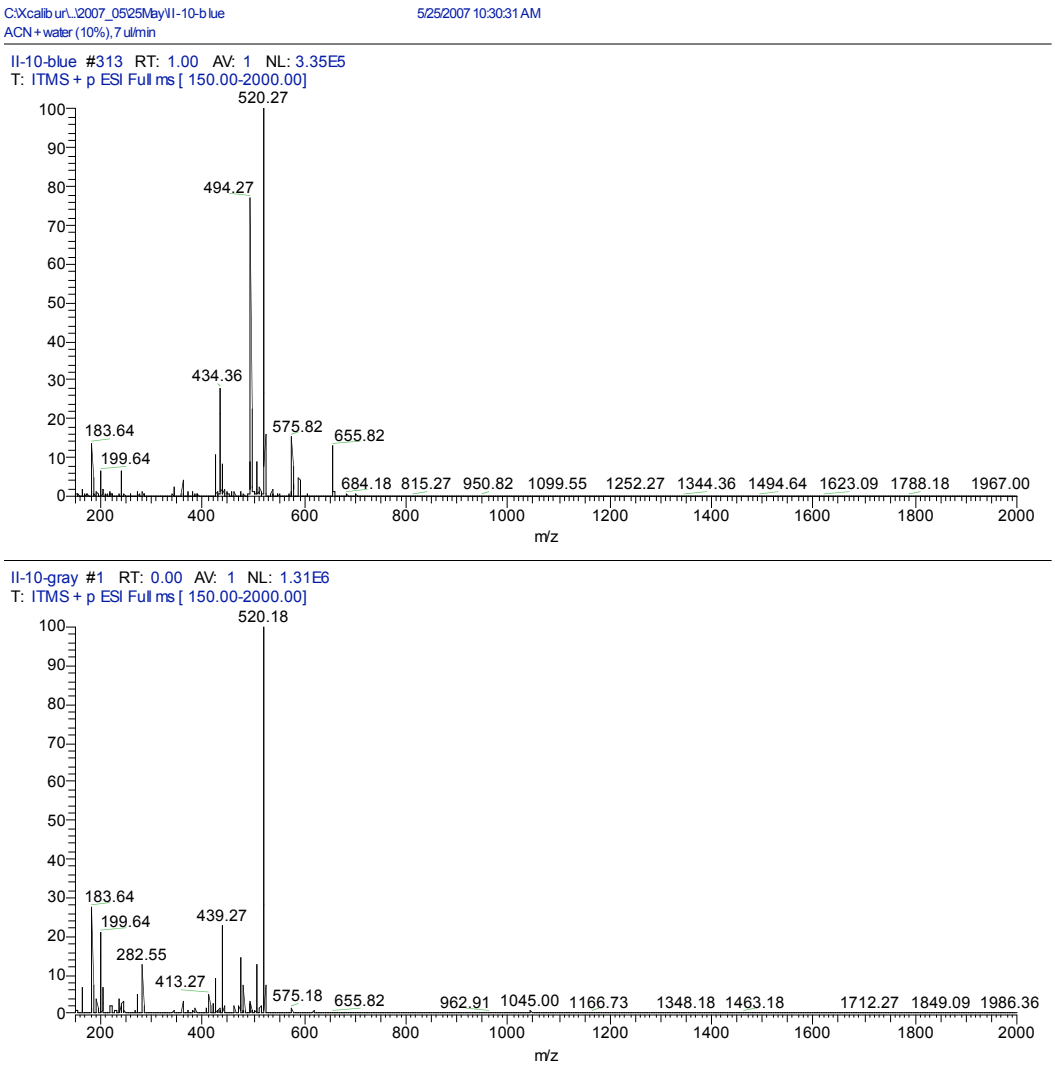

Figure E3. Electrospray mass spectrum of a reaction mixture containing acetylsalicylic acid, hydrogen peroxide and **1** when solution is blue (above) and after it turned gray (below).

Peak assignment for the spectrum:

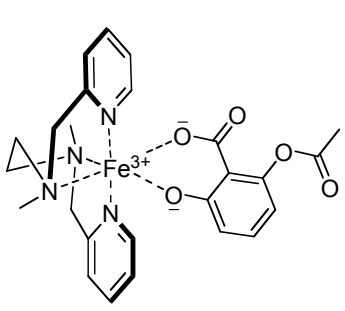

$C_{25}H_{28}FeN_4O_5^+$
Exact Mass: 520.1404

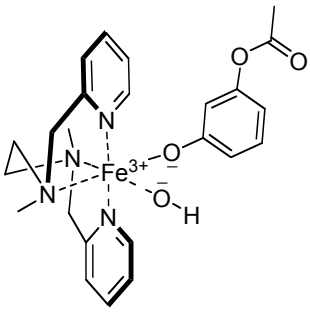

$C_{24}H_{30}FeN_4O_4^+$
Exact Mass: 494.1611

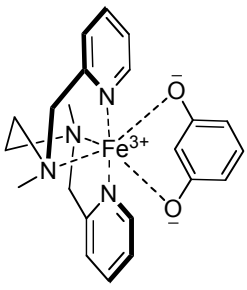

$C_{22}H_{26}FeN_4O_2^+$
Exact Mass: 434.14

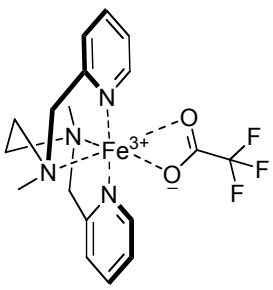

$C_{18}H_{22}F_3FeN_4O_2^{2+}$
Exact Mass: 439.1033

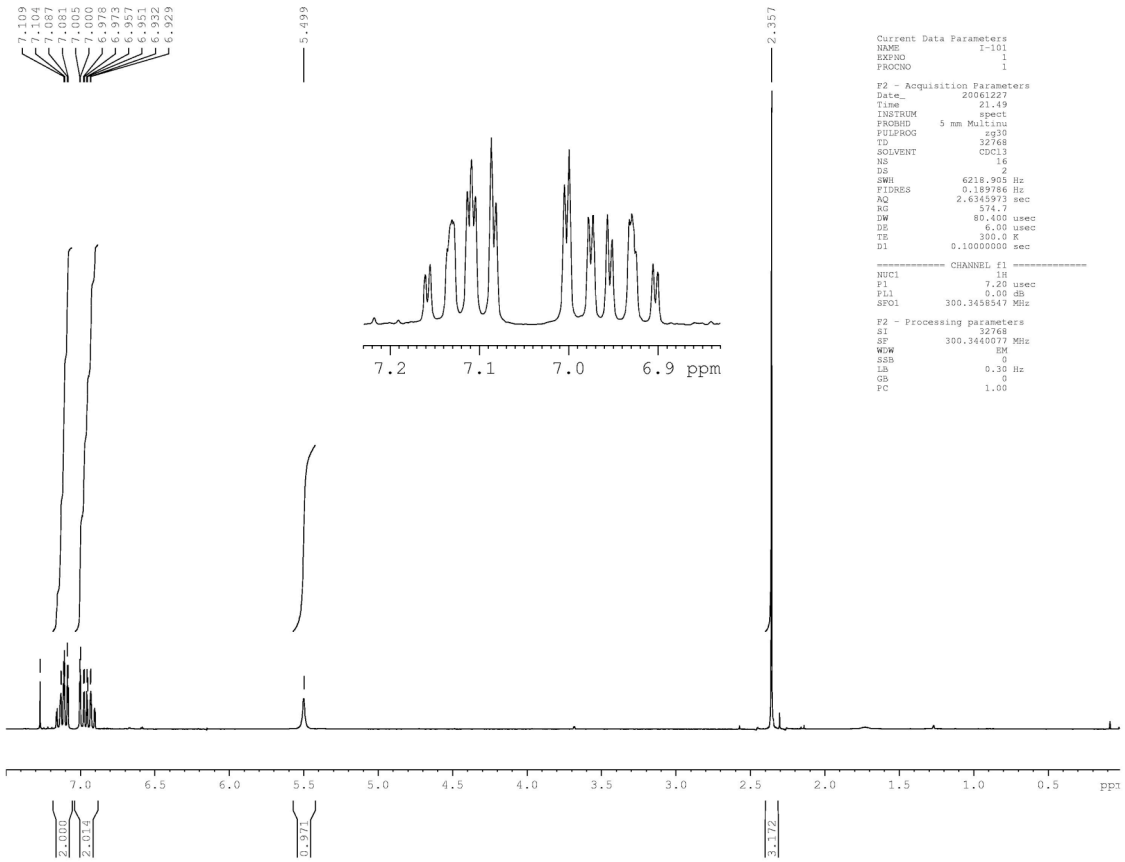

Figure E4. ^{1}NMR spectrum of a product (cetechol monoacetate) of reaction between acetylsalicylic acid and hydrogen peroxide in the presence of **1** (product was isolated).

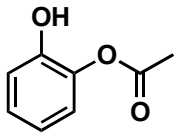

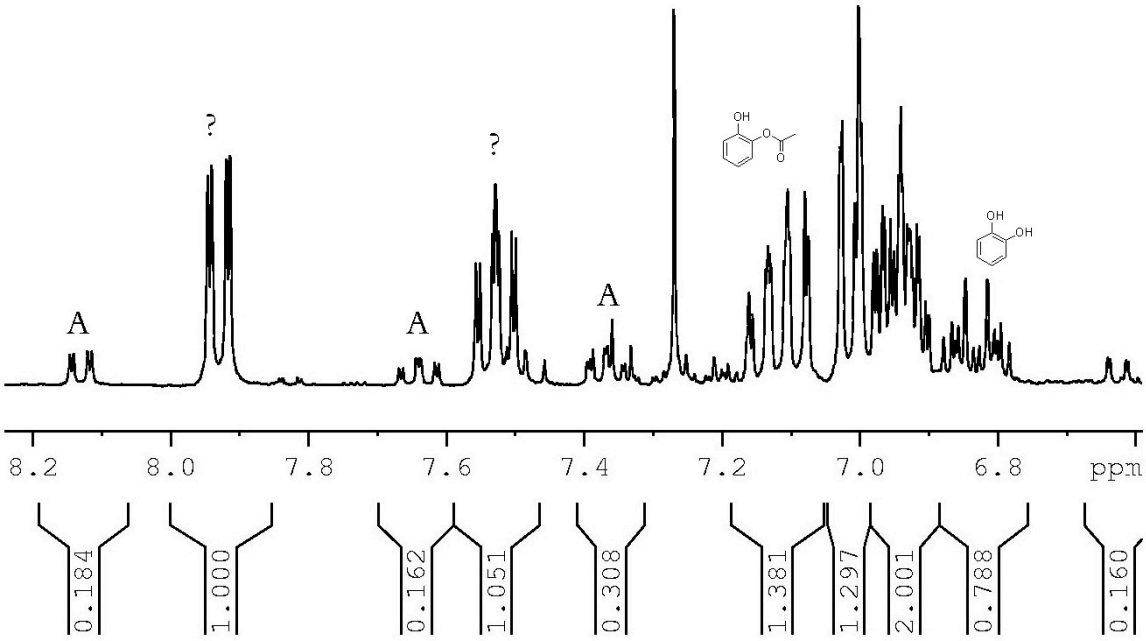

Figure E5. ^{1}H NMR spectrum of a mixture after acetylsalicylic acid reacted with hydrogen peroxide in the presence of **1** (reaction quenched in 5 min). “A” denotes acetylsalicylic acid (starting reactant), question marks indicate signals of 6-hydroxo-acetylsalicylic acid.

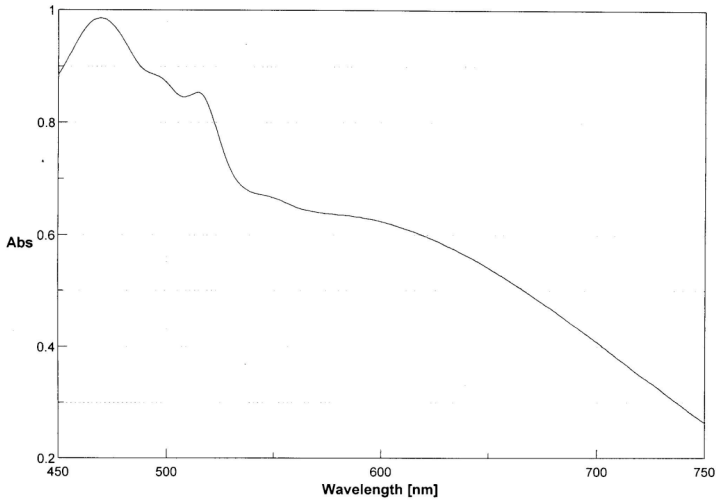

Figure E6. UV-Vis spectrum of reaction mixture containing **1**, acetylsalicylic acid (1.5 equiv) and hydrogen peroxide (3 equiv) after blue color disappeared.

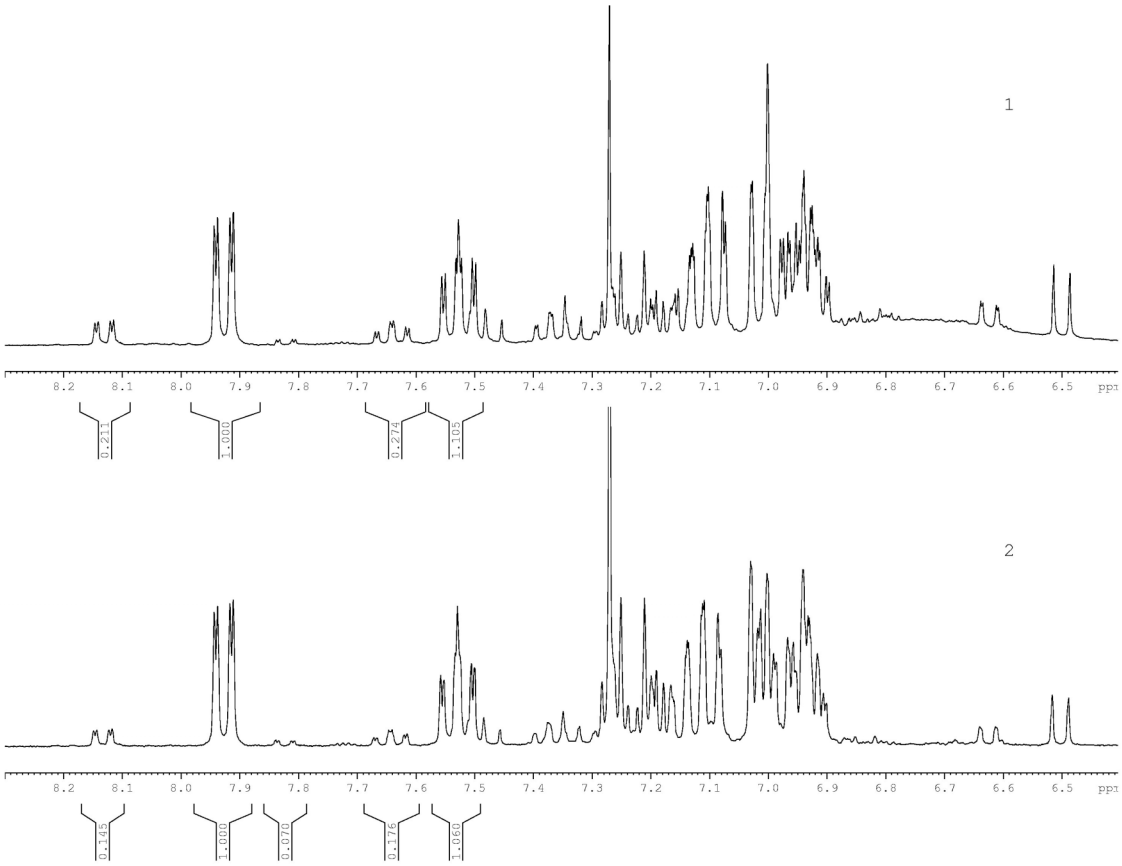

Figure E7. ^{1}H NMR spectra of crude products after reaction between acetylsalicylic acid (1.5 equiv), **1** (6 mM) and hydrogen peroxide (3 equiv). Reaction mixture was split into two parts; one part was quenched in 3 min after addition of hydrogen peroxide and products extracted (1), another was left in the fridge overnight and products were extracted next day (2).

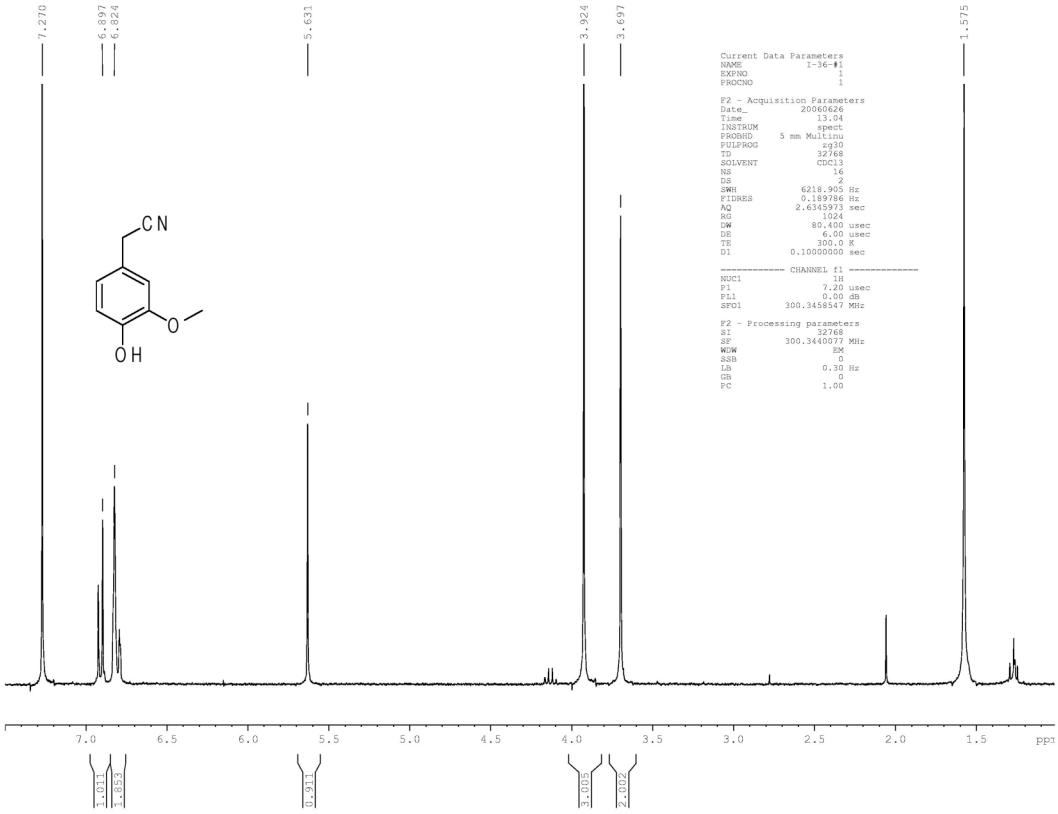

Figure E8**.** ^{1}H NMR spectrum of a product (4-hydroxy-3-methoxyphenylacetonitrile) of the reaction between 2-methoxybenzoic acid and hydrogen peroxide in the presence of **1.** Solvent $CDCl_3$.

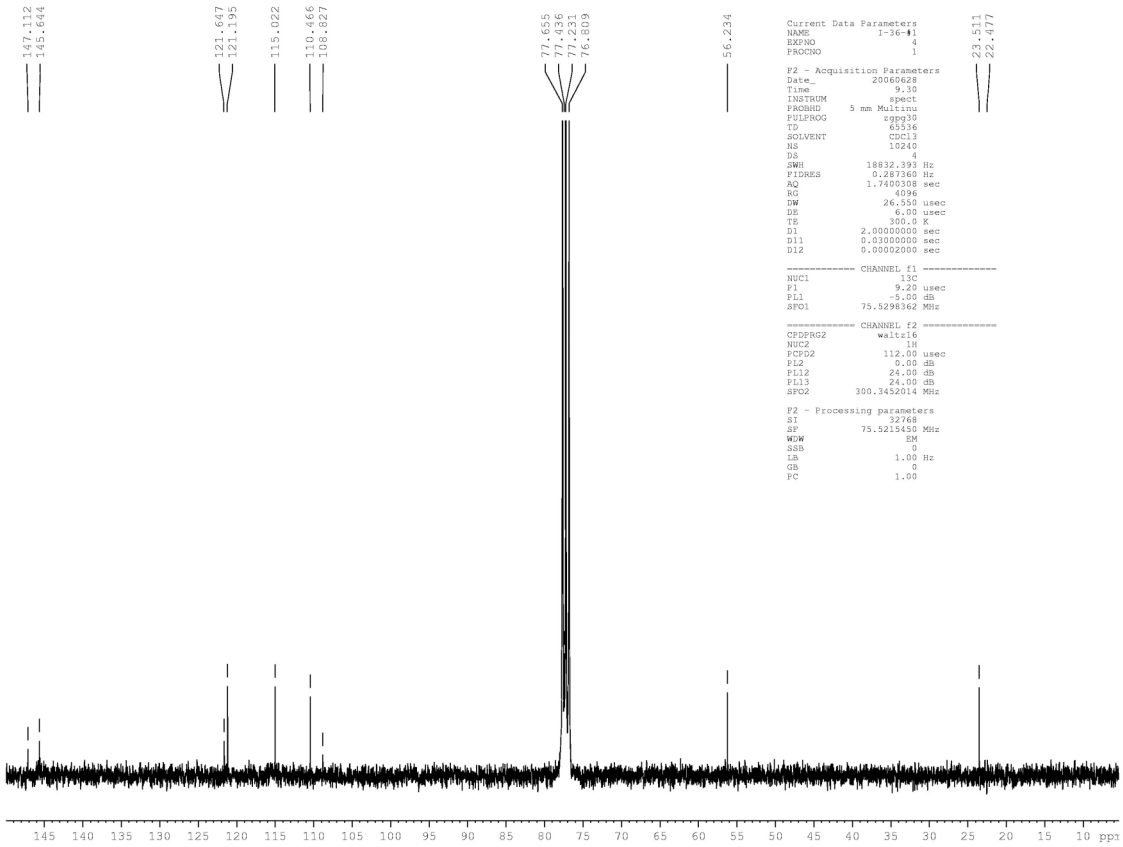

Figure E9. ^{13}C NMR spectrum of a product (4-hydroxy-3-methoxyphenylacetonitrile) of the reaction between 2-methoxybenzoic acid with hydrogen peroxide in the presence of **1.** Solvent $CDCl_3$.

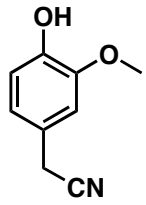

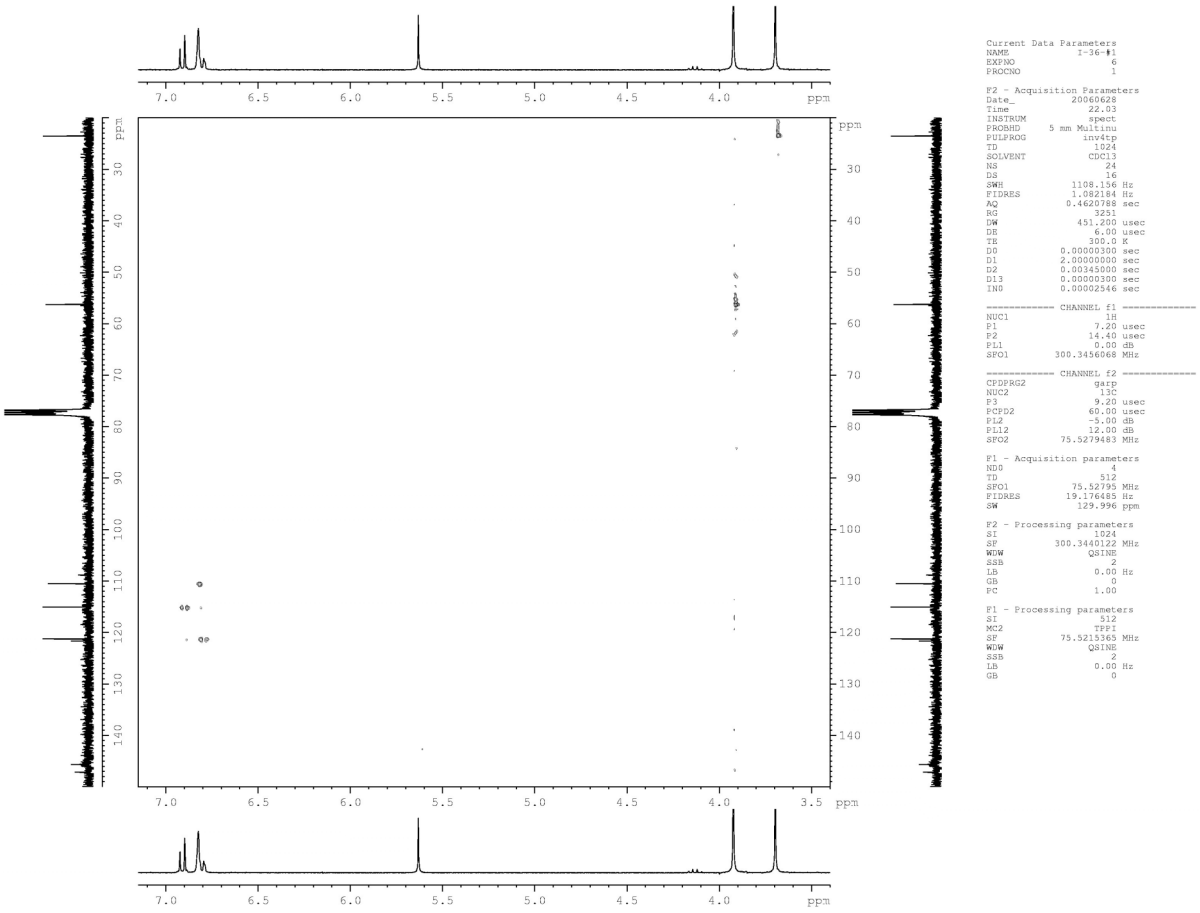

Figure E10**.** HMQC spectrum of a product (4-hydroxy-3-methoxyphenylacetonitrile) of the reaction between 2-methoxybenzoic acid with hydrogen peroxide in the presence of **1.** Solvent $CDCl_3$.

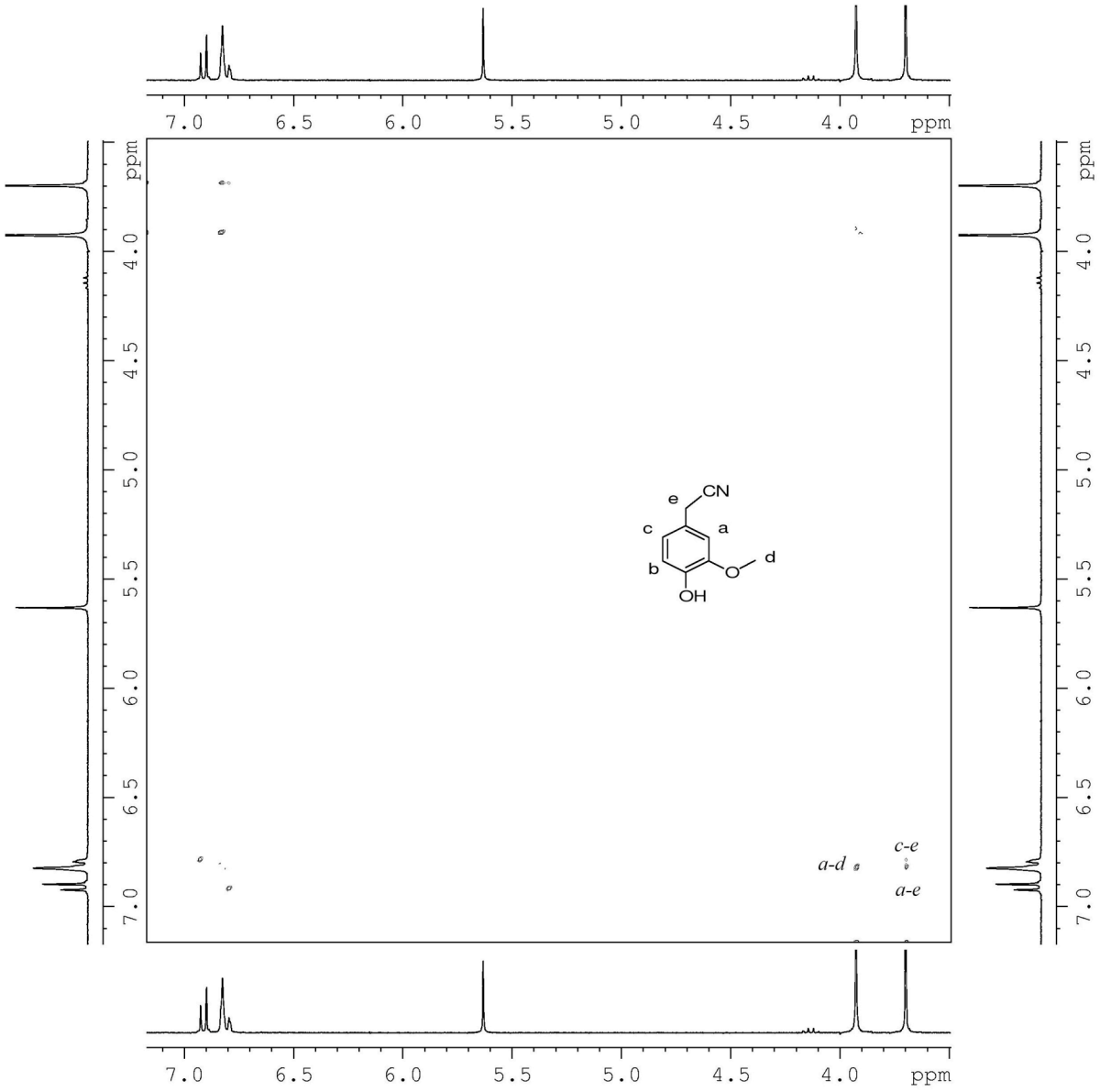

Figure E11. NOESY spectrum of a product (4-hydroxy-3-methoxyphenylacetonitrile) of the reaction of 2-methoxybenzoic acid with hydrogen peroxide in the presence of **1.** Solvent $CDCl_3$.

Table E1. ^{1}H NMR ($CDCl_3$) chemical shifts (ppm) of 3,5,3,5'-tetramethyl-biphenyl-4,4'-diol (tmbd)[2] and biphenyl product obtained in oxidation reaction

	Ph-	Ph-O-**H**	Ph-C**H**$_3$
tmbd	7.14 (s, 4 H)	4.62 (s, 2 H)	2.29 (s, 12 H)
this work	7.16 (s, 4H)	4.62 (s, 2 H)	2.31 (s, 12 H)

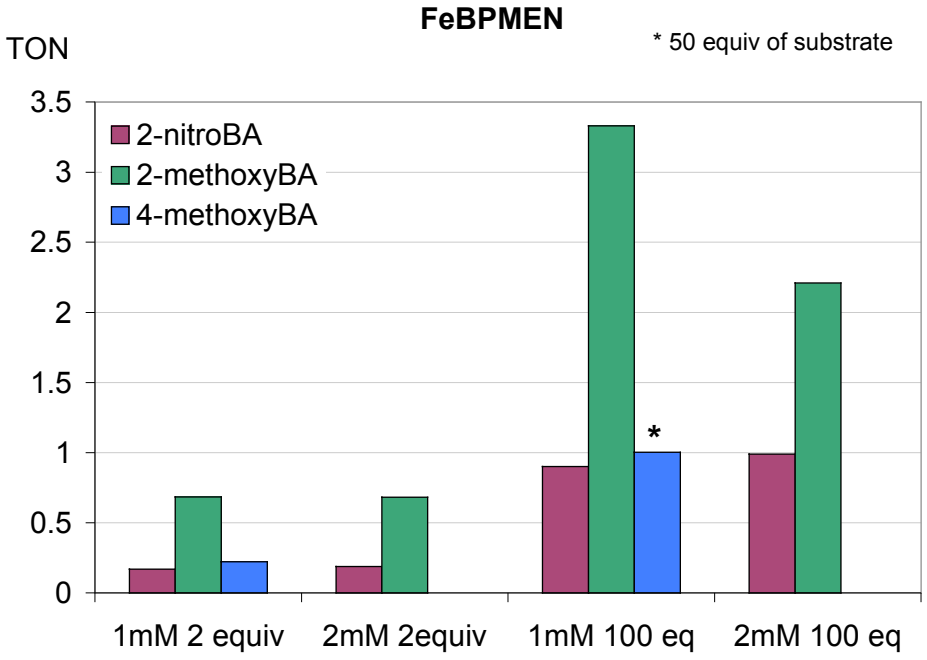

Reaction conditions: the reaction has been performed with 1 equivalent of complex (1mM or 2 mM), 100 equivalents of acid and 10 equivalents of H_2O_2 or with 1 equiv of complex (1mM or 2 mM), 2 equiv of acid and 3 equiv of H_2O_2 at 25 °C and stirred for 30 minutes. Each number represents an average of at least three trials. Due to solubility problems only 50 equiv of 4-methoxybenzoic acid were added.

Figure E12. Yield of *ipso*-hydroxylation products using **1**.

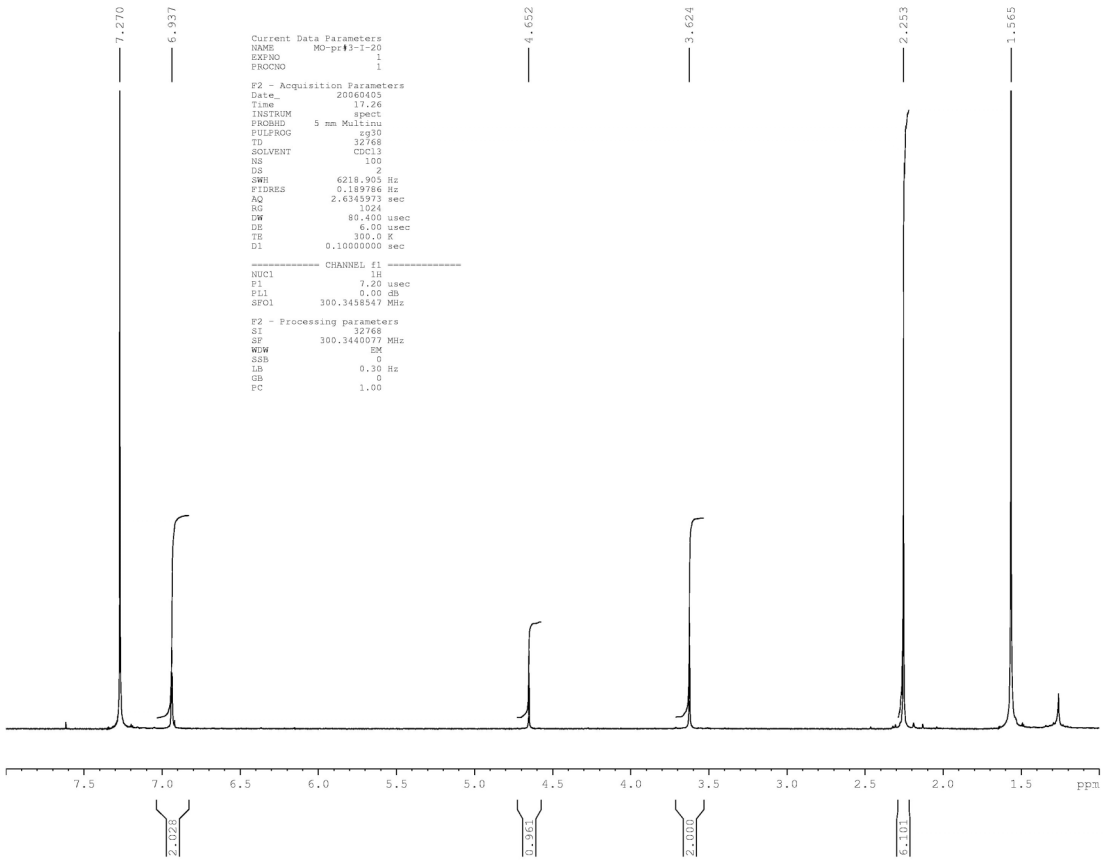

Figure E13. ^{1}H NMR spectrum of product (4-hydroxy-3,5-dimethylphenylacetonitrile) of the reaction between 2,6-dimethylbenzoic acid and hydrogen peroxide in the presence of **1**.

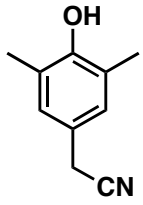

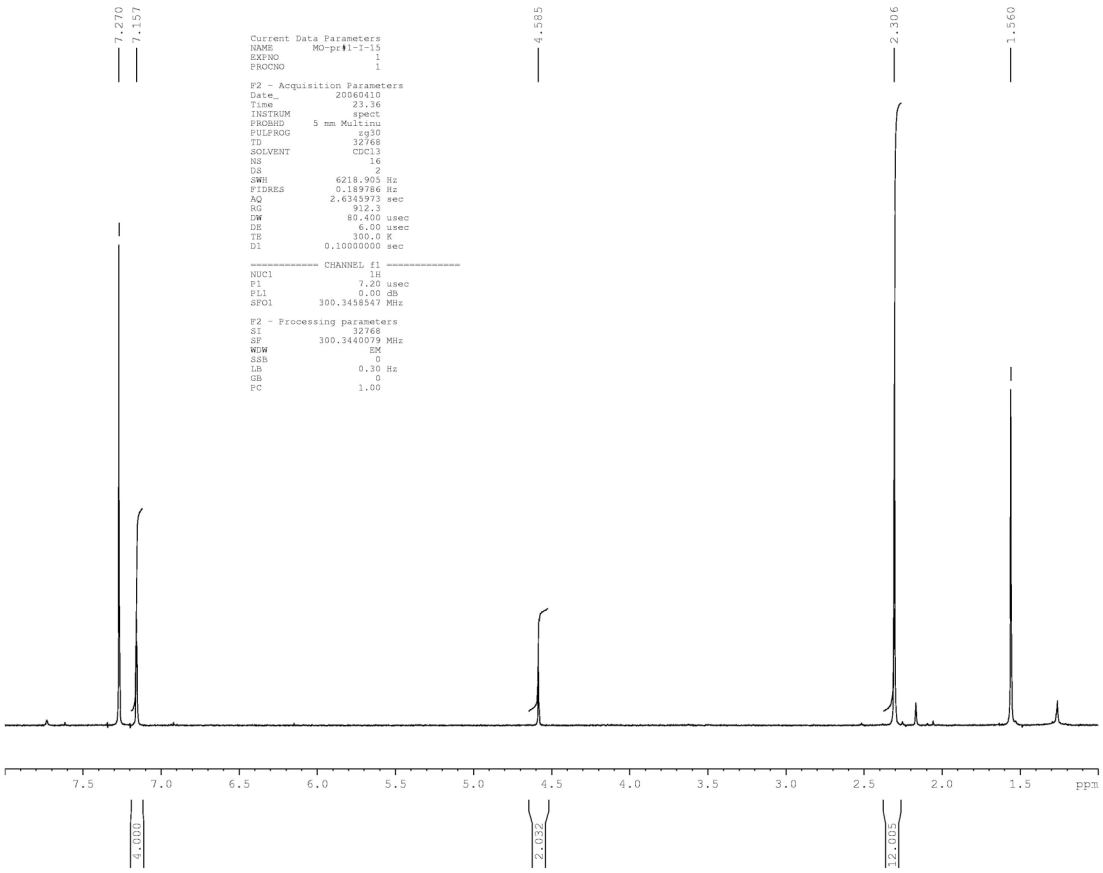

Figure E14. ^{1}H NMR spectrum of product (3,5,3’,5’-tetramethyl- biphenyl-4,4’-diol) of the reaction between 2,6-dimethylbenzoic acid with hydrogen peroxide in the presence of **1**.

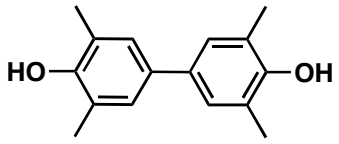

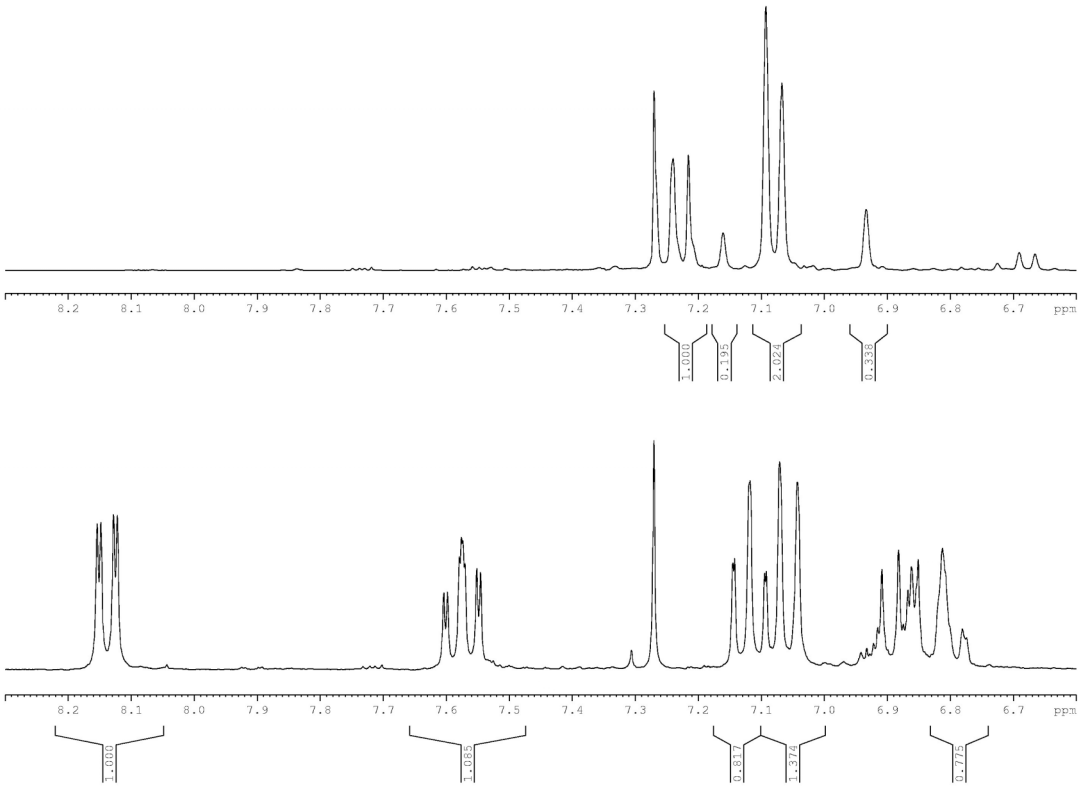

Figure E15. ^{1}H NMR spectra of reaction mixtures after 2,6-dimethylbenzoic acid (above) and 2-methoxybenzoic acid reacted with hydrogen peroxide in the presence of **1.**

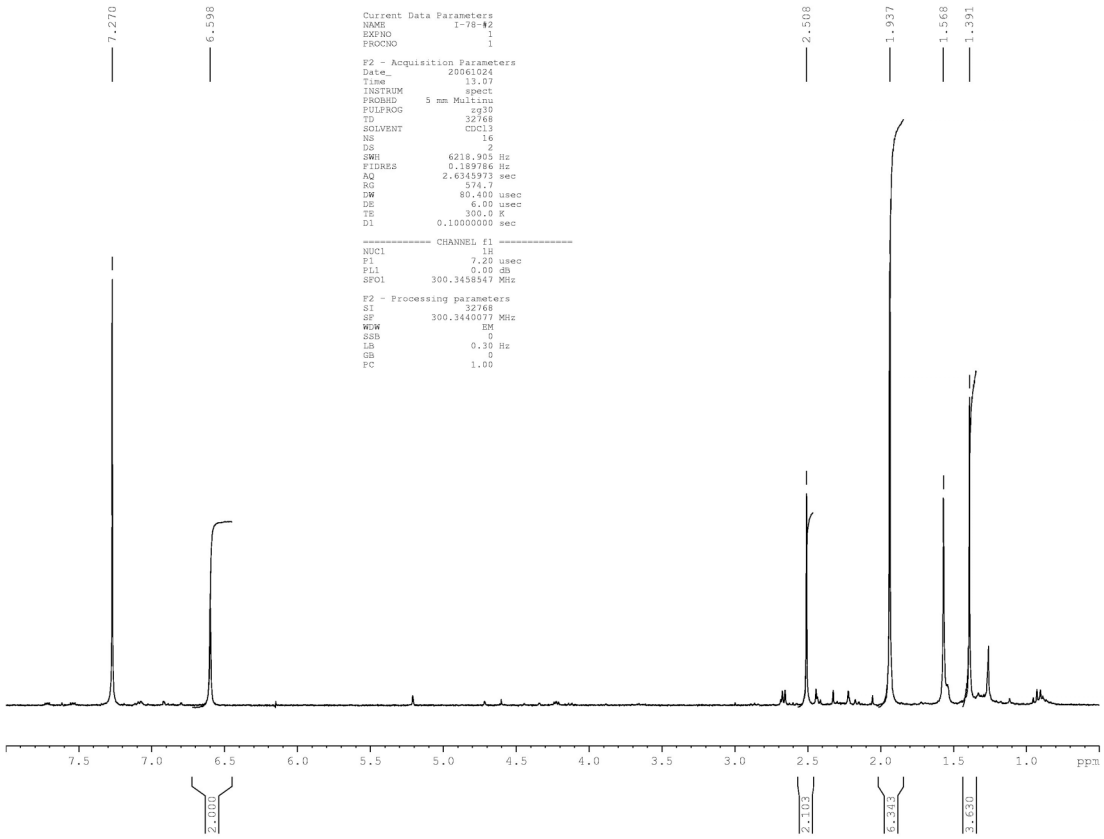

Figure E16. ^{1}H NMR spectrum of product (2,5-cyclohexadien-1-one, 2,4,6-trimethyl-4-acetonitrile) of the reaction of 2,4,6-trimethylbenzoic acid with hydrogen peroxide in the presence of **1**. Solvent $CDCl_3$.

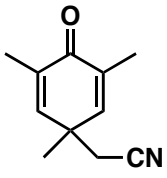

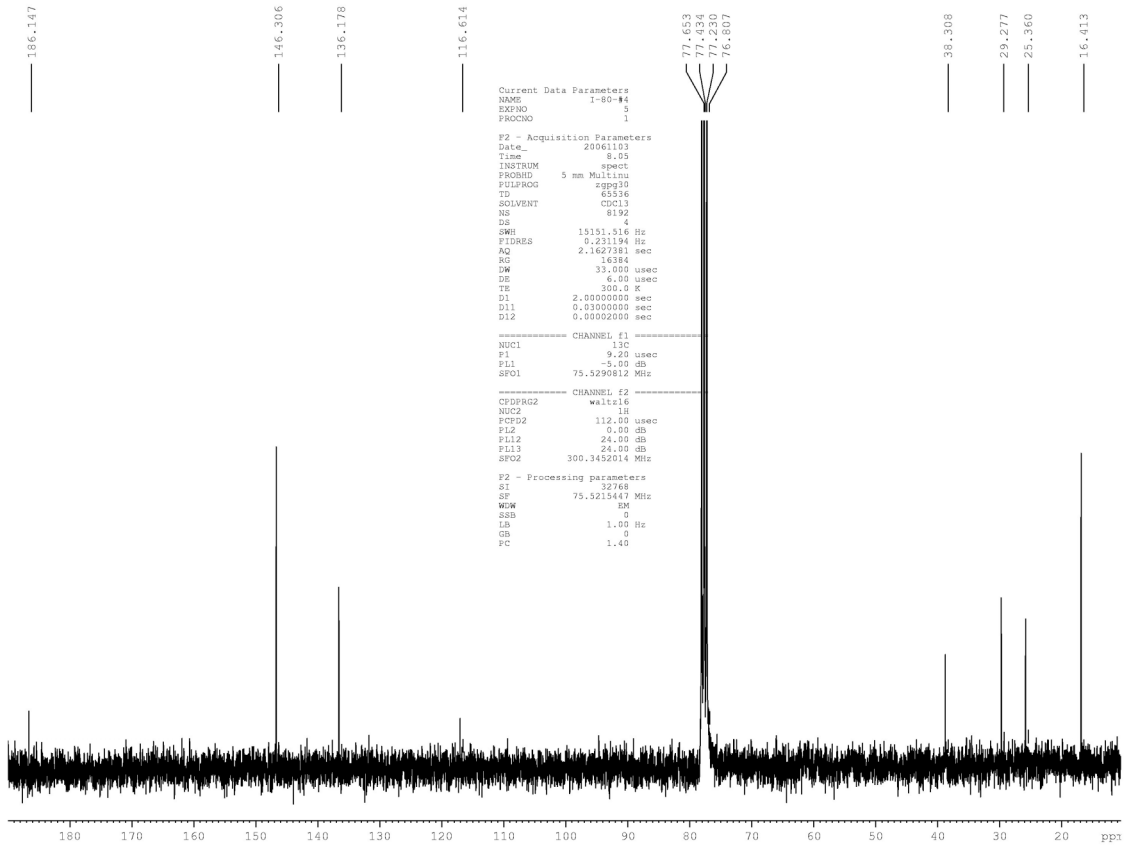

Figure E17. ^{13}C NMR spectrum of product (2,5-cyclohexadien-1-one, 2,4,6-trimethyl-4-acetonitrile) of the reaction between 2,4,6-trimethylbenzoic acid and hydrogen peroxide in the presence of **1**.

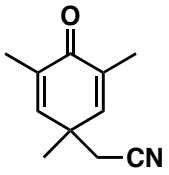

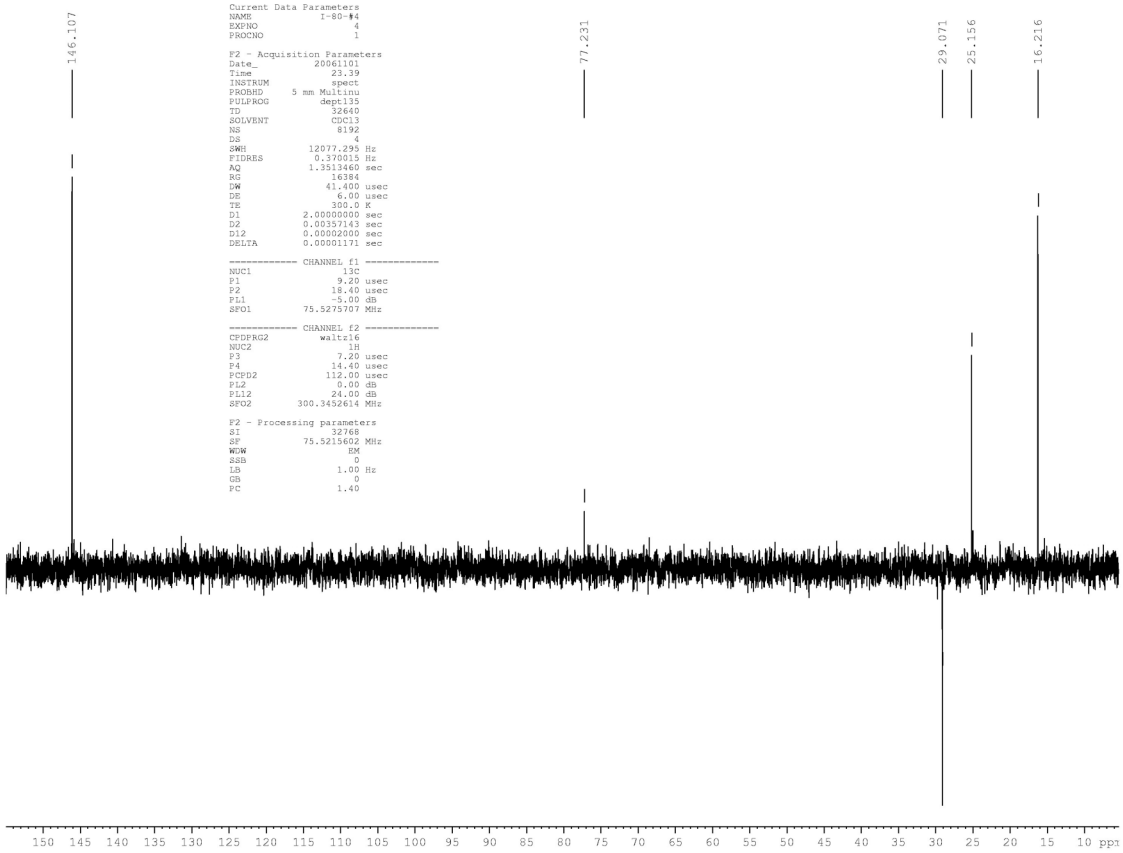

Figure E18**.** DEPT 135 spectrum of product (2,5-cyclohexadien-1-one, 2,4,6-trimethyl-4-acetonitrile) of the reaction between 2,4,6-trimethylbenzoic acid and hydrogen peroxide in the presence of **1**.

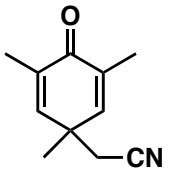

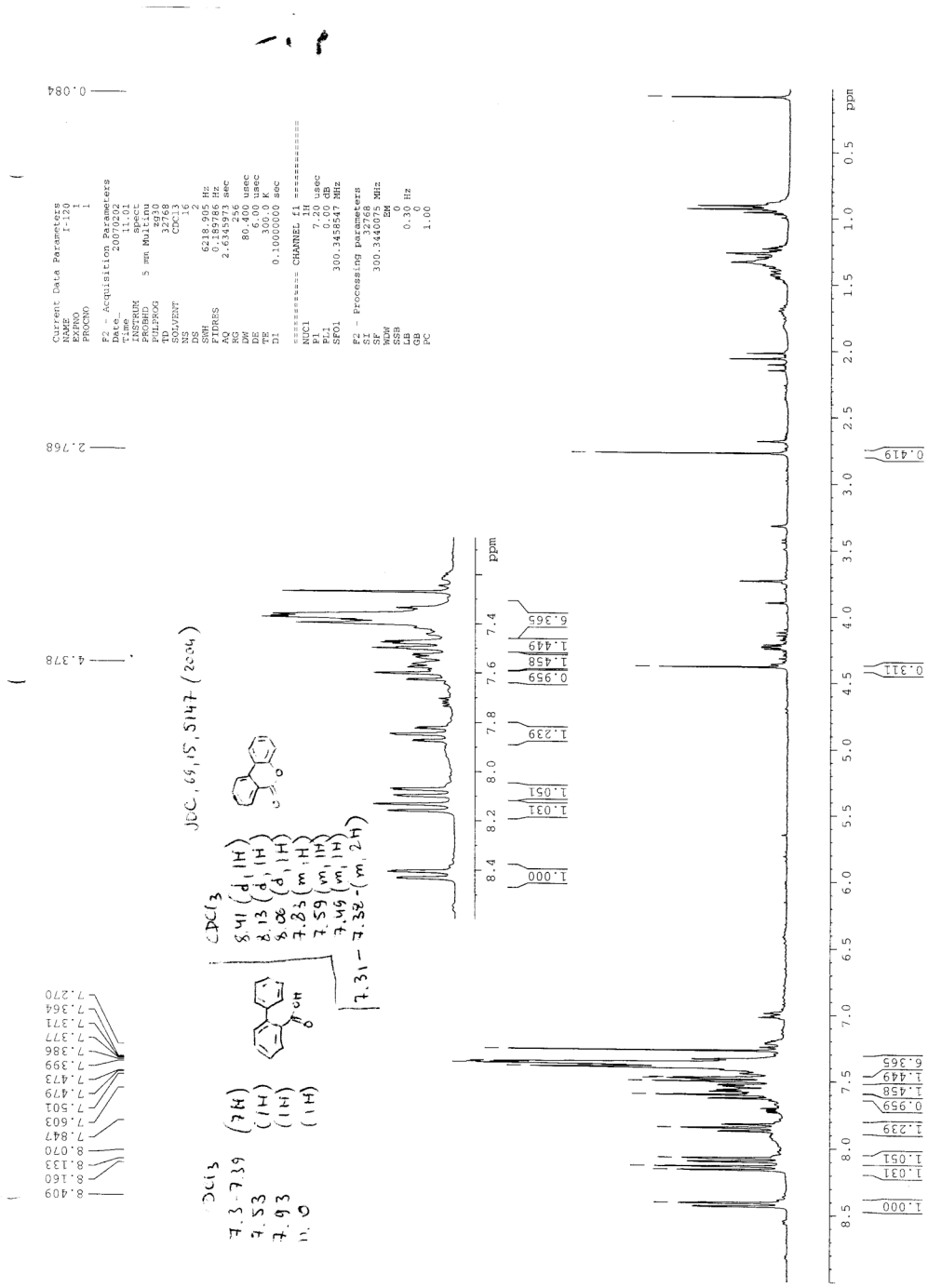

Figure E19. ^{1}H NMR spectrum of the crude reaction mixture after diphenyl-2 carboxylic acid reacted with H_2O_2 in the presence of **1**; diphenyl-2 carboxylic acid in $CDCl_3$ 7.3-7.39 (7H), 7.53 (1H), 7.93 (1H), 11.0 (1H), 3,4-benzocoumarin in $CDCl_3$ 8.41 (d, 1H), 8.13 (d, 1H), 8.06 (d, 1H), 7.83 (m, 1H), 7.59 (m, 1H), 7.49 (m, 1H), 7.31-7.38 (m, 2H).[8]

12 Appendix F (chapter 6)

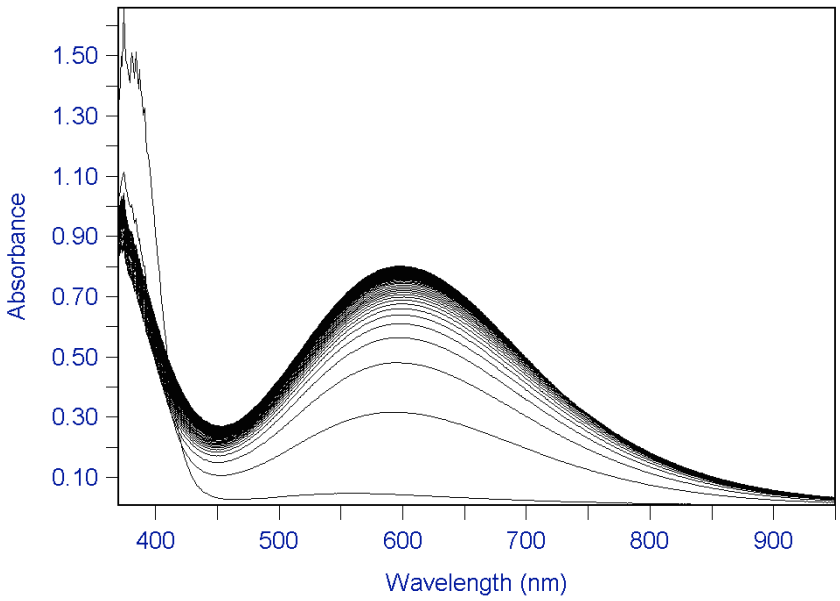

Figure F1. Spectral changes upon reaction of **1** (0.5 mM), H_2O_2 (10 mM) and benzoic acid (1 mM) at 20 ˚C in acetonitrile.

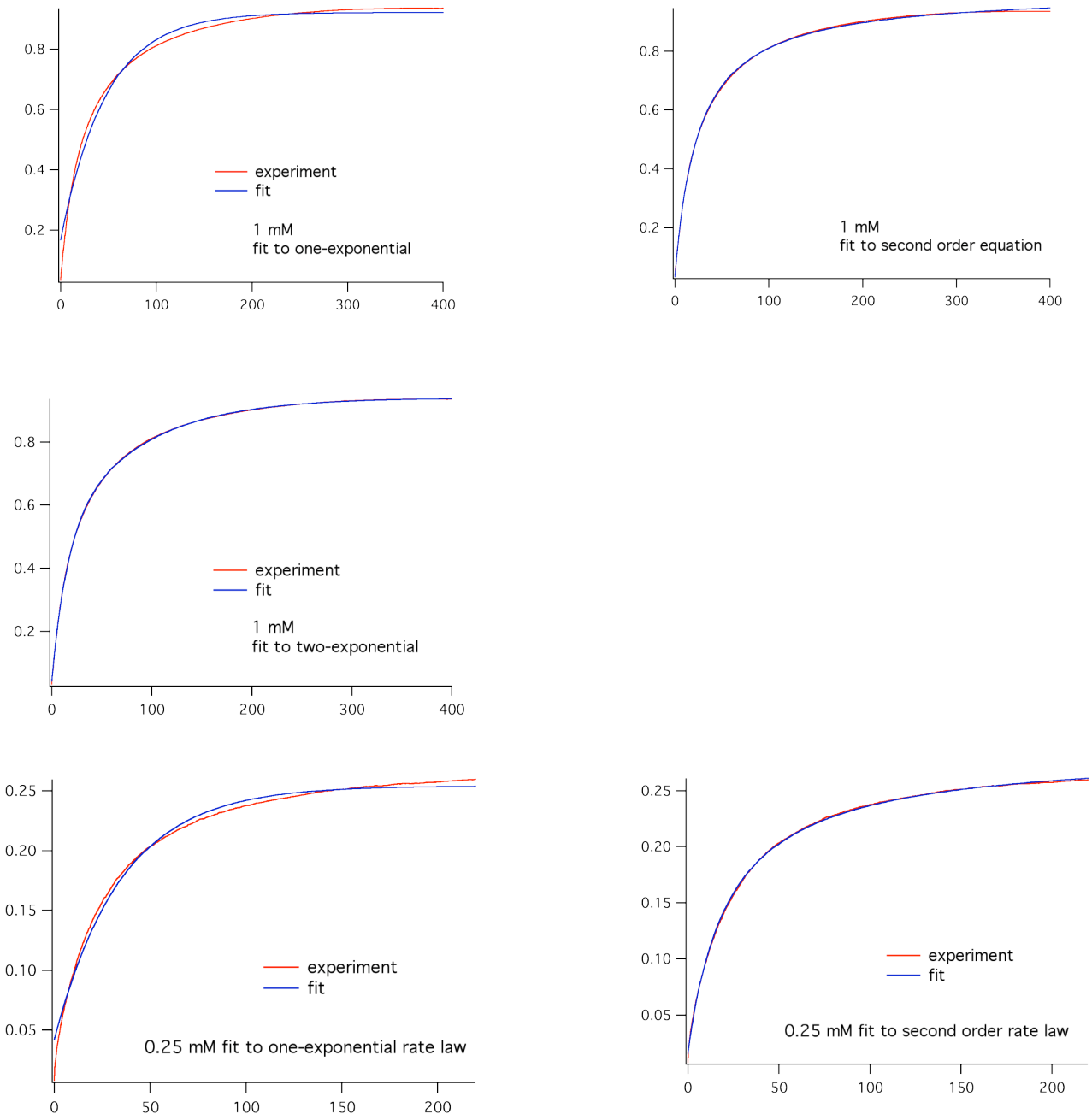

Figure F2. Kinetic traces at 600 nm for the reaction between **1,** benzoic acid and H_2O_2 and fits to one-exponential, double-exponential, and second rate order law. 1 mM and 0.25 mM represent the higher and lowest initial concentration of iron used; [BA] = 1 mM, [H_2O_2] = 1.5 mM in all experiments.

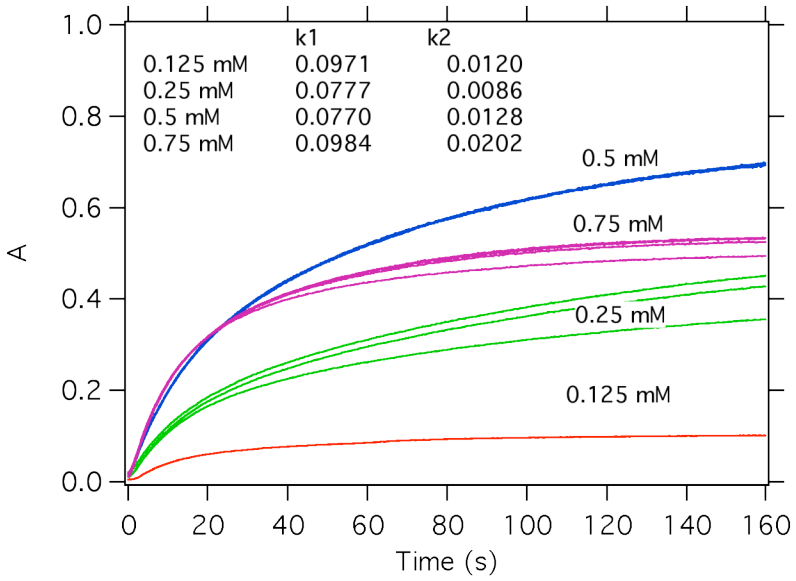

Figure F3. Kinetic traces at 635 nm represent formation of Fe(III)-phenolate at 20 ˚C in acetonitrile. Concentration of **1** was varied (0.125-0.75 mM after mixing) while concentration of hydrogen peroxide and benzene remained constant ($[H_2O_2]$ = 5 mM, [benzene] = 300 equiv vs. 1 mM iron). Each constant on the graph is an average of at least 3 runs. (VI-32)

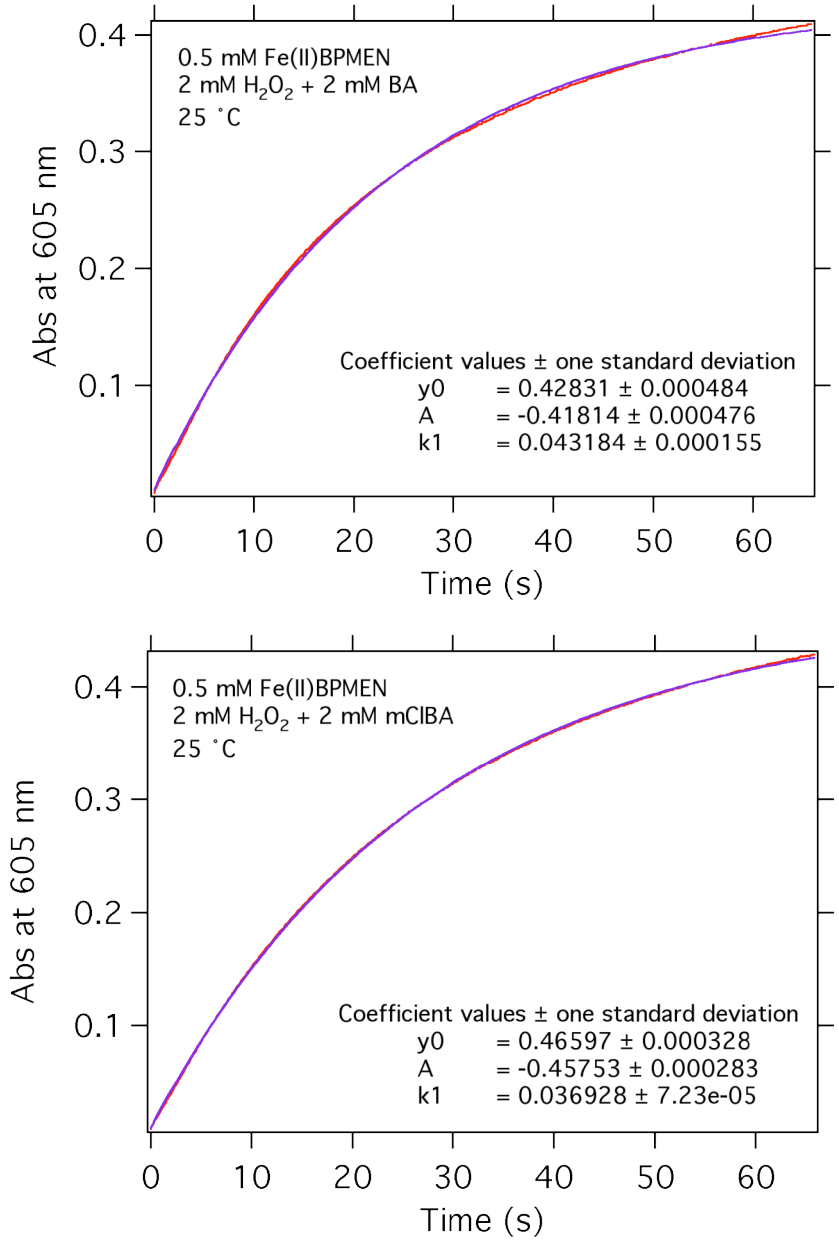

Figure F4. Kinetic traces at 605 nm for the reaction between **1**, benzoic acid (or 3-chlorobenzic acid) and H_2O_2 in acetonitrile at 25 ˚C; concentrations after mixing: [**1**] = 0.25 mM, [H_2O_2] = [BA] = 1 mM.

Table F1. Rate constants for the hydroxylation of benzoic acids with H_2O_2 in the presence of **1**. k_1 – observed rate constant determined from single exponential fit of kinetic traces at 400 nm (first rapid process); k_2- rate of salicylate formation; k_3- rate of salicylate decay

mM before mixing 25º C			Rate constants y = -dy exp(-kx) + mx + yinf		
Fe	H_2O_2	substrate	k_1	k_2	k_3
1	34	BA	**1.2**	**0.5**	-
1	34	3,5-dichlorobenzoic acid	**1.6**	**0.3**	-
1	15	2-methoxybenzoic acid	**0.9**	**0.3**	**0.03**
	5			**0.1**	
1	10	aspirin	-	**0.12**	**0.004**
	20			**0.2**	**0.007**
	30			**0.3**	**0.008**

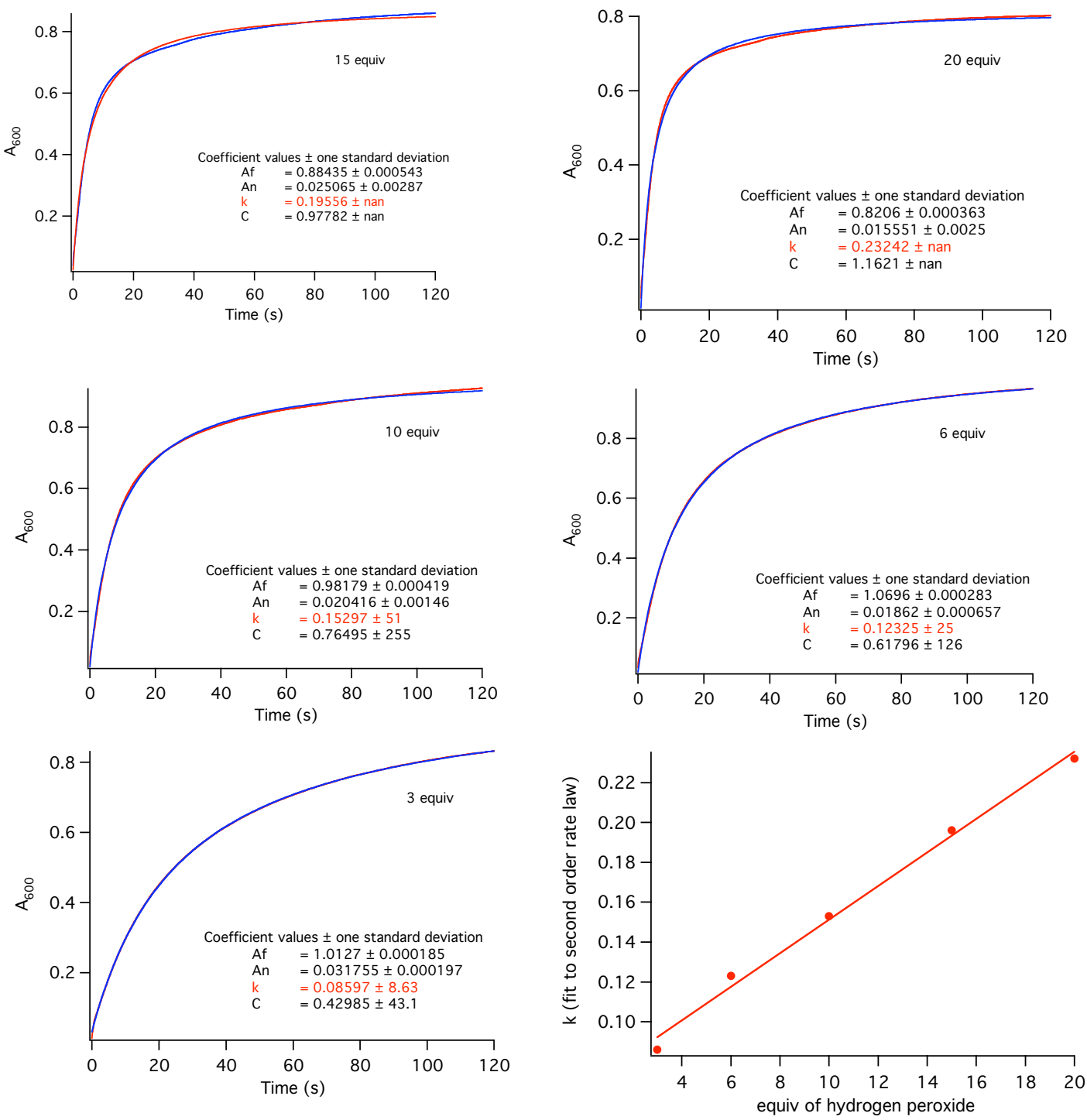

Figure F5. Kinetic traces at 600 nm were acquired for the reaction of **1** (0.5 mM), H_2O_2 (variable) and benzoic acid (1 mM) at 20 ˚C in acetonitrile. Kinetic traces are in red and their corresponding fits to f(x) = Af-((Af-An)/(1+k*C*x)) equation are in blue.